Impact of Wind Power Plants with Full Converter Wind Turbines on Power System Small-Signal Stability

Inherent Characteristics and Potential for Power Oscillation Damping Control

Knüppel, Thyge; Nygaard Nielsen, Jørgen; Dixon, Andrew

Publication date:
2012

Document Version
Publisher's PDF, also known as Version of record

Technical University of Denmark

Thyge Knüppel

Impact of Wind Power Plants with Full Converter Wind Turbines on Power System Small-Signal Stability

Inherent Characteristics and Potential for Power Oscillation Damping Control

PhD Thesis, May 2012

DTU Electrical Engineering
Department of Electrical Engineering

Thyge Knüppel

Impact of Wind Power Plants with Full Converter Wind Turbines on Power System Small-Signal Stability

Inherent Characteristics and Potential for Power Oscillation Damping Control

PhD Thesis, May 2012

Impact of Wind Power Plants with Full Converter Wind Turbines on Power System Small-Signal Stability, Inherent Characteristics and Potential for Power Oscillation Damping Control

This report was prepared by
Thyge Knüppel

Supervisors
Prof. Jacob Østergaard, Technical University of Denmark
PhD Kim Høj Jensen, Siemens Wind Power A/S
PhD Jørgen Nygaard Nielsen, Siemens Wind Power A/S
Dr. Andrew Dixon, National Grid Electricity Transmission, UK

Department of Electrical Engineering
Centre for Electric Technology (CET)
Technical University of Denmark
Elektrovej building 325
DK-2800 Kgs. Lyngby
Denmark

www.elektro.dtu.dk/cet
Tel: (+45) 45 25 35 00
Fax: (+45) 45 88 61 11
E-mail: cet@elektro.dtu.dk

Release date:	2012-05-26
Category:	1 (public)
Edition:	Second
Comments:	This report is part of the requirements to achieve the PhD Degree at the Technical University of Denmark.
Rights:	©Thyge Knüppel, 2012
ISBN:	978-87-92465-79-5

Preface

This report is part of the requirements to achieve the PhD Degree at the Technical University of Denmark. The work has been completed within the framework of the Danish Industrial PhD Programme, which is administrated by the Danish Agency for Science, Technology and Innovation, and is co-funded by Siemens Wind Power A/S.

The project has been conducted at the Centre for Electric Technology, Department of Electrical Engineering at the Technical University of Denmark.

The work has been carried out in a collaboration between Siemens Wind Power A/S, Centre for Electric Technology at the Technical University of Denmark, and National Grid Electricity Transmission, UK.

Thyge Knüppel

Kgs. Lyngby, 2012-05-26

Acknowledgment

First of all, I would like to thank my supervisors Prof. Jacob Østergaard from Centre for Electric Technology at the Technical University of Denmark, Kim Høj Jensen, Jørgen Nygaard Nielsen, and, for the first part of the project, Vladislav Akhmatov from Siemens Wind Power A/S, and Dr. Andrew Dixon from National Grid Electricity Transmission for their continued guidance, support, and inspiration throughout the project.

I would like to acknowledge the work of past and present colleagues at Siemens Wind Power A/S and Siemens AG that have contributed to the development of the wind turbine (WT) simulation models on which a large part of this work has been based. It has been a privilege to have had access to validated models of commercially available WTs across a range of software platforms. Without the hard, dedicated work and the large number of man hours that has gone into model development and benchmarking with high-order EMT models and field test results, the WT model that has been used for these studies would not have had the same trustworthiness, and, hence, the credibility of the findings would be less.

A special thanks is directed to the Wind Farm Control group and the Software Team at Siemens Wind Power A/S for the close collaboration with preparation and execution of the conducted field tests.

Finally, I want to extend a warm thanks to my friends and family for their support, good advice, and not least, for their patience during the project.

Summary

Wind power is being developed in power systems all around the world, and already today wind power covers more than 20 % of the electricity consumption in some countries. As the size of each wind power plant (WPP) increases and as the levels of penetration reaches certain magnitudes, the inclusion of the dynamic properties of the WPPs in the power system stability studies become important.

The work presented in this report deal with the impact of WPPs based on full converter wind turbines (WTs) on the power system small-signal rotor angle stability. During small disturbances in the power system, the rotor speed of the synchronous machines will eventually return to its steady state if the power system is small-signal stable. The dynamic properties of a WPP are fundamentally different from those of a synchronous machine, and the interaction of WPPs with the synchronous machines in power system oscillations has not yet been fully clarified.

The participation of the WPP in the power system oscillations was investigated for a number of WPP penetration levels and for different WPP modes of operation. It was generally found that the inter-area modes were largely unaffected by the WPP penetration level and mode of operation. The participation of the WT mechanical system in the inter-area modes were found to be orders of magnitudes smaller than the participation of the synchronous generators. The reactive power controller of the WPP and the WT were found have the highest participation among the WPP and WT states.

WPPs based on converter interfaced WTs offer a high degree of controllability due to the rapid response of the converter and the ability

to control both the active and the reactive power output. During this project, it has been explored how these properties could be utilized to actively contribute to the modal damping of weakly damped power oscillations through WPP power oscillation damping control (POD). Emphasis has been put on WPP level PODs due to its simplicity as compared to individual WT PODs, and since this offers a single point of access if the operation of the POD is to be controlled by a wide-area measurement system. The findings encourage that a WPP level POD is feasible, since the WTs in a 150 WT WPP required very similar control signals to optimally contribute to an increased modal damping, and since time domain simulations showed that the interaction between the WTs did not adversely effect the ability of the WTs to generate an aligned WPP response.

The theoretical findings are supported with field test results on a small 13 WT WPP that has been subject to open-loop tests of both active and reactive power modulations in the frequency range of 0.1 to 1.0 Hz. With the field tests it has been shown that it was possible to control the WTs to deliver a common WPP response that was consistent in both frequency and phase. This was achieved for both active and reactive power modulation.

Dansk Resumé

Vindkraft udvikles og udbygges i elforsyningssystemer over hele verden og udgør allerede i dag over 20 % af det samlede elforbrug i nogle lande. Som kapaciteten af de enkelte vindkraftværker øges, og som den samlede andel af vindkraft i elsystemet stiger, øges også vigtigheden af at inkludere de dynamiske egenskaber for vindkraftværkerne i stabilitetsstudier af elforsyningssystemer.

Arbejdet, der præsenteres i denne rapport, omhandler indvirkningen af vindkraftværker baseret på vindmøller med fuld last konvertere på småsignals stabiliteten af synkronmaskinernes rotorvinkel svingninger. De rotorvinkel svingninger der induceres af små forstyrrelser vil i et elforsyningssystem der er småsignals stabilt efterhånden forsvinde, hvorefter synkromaskinerne returnerer til deres ligevægtstilstand. De dynamiske egenskaber for vindkraftværker er fundamentalt forskellige fra synkronmaskinens, og samspillet mellem vindkraftværker og synkronmaskiner under effektpendlinger er endnu ikke fuldt belyst.

Deltagelsen af vindkraftværker i effektpendlinger er blevet undersøgt for en række udbygningsniveauer og for en række af vindkraftværkets forskellige driftstilstande. Resultaterne viste, at egenværdierne for pendlinger mellem større dele af elsystemet var nærmest upåvirket vindkraftværkets størrelse og driftstilstand. Deltagelsen af vindmøllernes mekaniske system i svingningerne var størrelsesordener mindre end for synkronmaskinerne. Regulatorerne i vindkraftværket og i vindmøllerne for reaktiv effekt regulering viste sig at være de delsystemer i vindkraftværket det havde den største indflydelse på egenværdierne for effekt pendlingerne.

Vindkraftværker baseret på fuld last konverter vindmøller er meget regulerbare på grund af konverterens hurtige respons og idet både den aktive og den reaktive effekt kan reguleres. Det er igennem dette projekt blevet undersøgt, hvorledes disse positive egenskaber kunne udnyttes til styre vindkraftværkerne for aktivt at bidrage til dæmpningen af svagt dæmpede effektpendlinger. Fokus har været på en central regulator for vindkraftværket, idet den vil være simplere sammenlignet med regulatorer for hver enkelt vindmølle, og idet en sådan vil fungere som et samlet interface, hvis regulatoren skal forbindes til eksterne styresignaler. De opnåede resultater er positive i forhold til en sådan central regulator, idet de optimale styresignaler for vindmøllerne i en undersøgt 150 vindmølle vindkraftværk kun havde små variationer i forhold til at opnå en øget dæmpning af effektpendlingerne. Tidsdomæne simuleringer viste desuden, at vindmøllernes indbyrdedes interaktion ikke i negativ grad påvirkede deres evne til at bidrage til et kollektivt respons for vindkraftværket.

Resultaterne fra de teoretiske undersøgelser understøttes af feltmålinger fra et mindre vindkraftværk med 13 vindmøller, hvor der blev foretaget åbensløjfe tests med både aktiv og reaktiv effektmodulering i frekvensintervallet 0.1 til 1.0 Hz. Feltmålingerne viste, at det var muligt at styre vindmøllerne og få dem til at levere et kollektivt respons for vindkraftværket, der var konsistent i både frekvens og fase. Dette sås i responset for både aktiv og reaktiv effektmodelering.

Contents

Contents I

List of Figures V

List of Tables XI

List of Abbreviations XIII

1 Introduction 1
- 1.1 Mechanical Equivalents . . . 3
- 1.2 State of the Art . . . 5
  - 1.2.1 Impact of WTs and WPPs on Rotor Angle Small-Signal Stability . . . 5
  - 1.2.2 Control of Variable Speed WTs for Power Oscillation Damping . . . 6
- 1.3 Objectives and Contributions . . . 9
- 1.4 List of Publications . . . 12
  - 1.4.1 Primary Papers . . . 12
  - 1.4.2 Secondary Papers . . . 13
  - 1.4.3 Published Patent Applications . . . 14
- 1.5 Thesis Organization . . . 14

2 Overview of Models and Linear Analysis Methods 17
- 2.1 Power System Modeling . . . 17
  - 2.1.1 Applied Power System Models . . . 19
  - 2.1.2 Wind Turbine Modeling . . . 22
- 2.2 Eigenvalue Analysis . . . 24
  - 2.2.1 Eigenvalue Analysis of ODE System . . . 24
  - 2.2.2 Eigenvalue Analysis of DAE System . . . 27
  - 2.2.3 Numerical Example . . . 28
- 2.3 Residues for Controller Tuning . . . 32

2.4 Synchronizing and Damping Torques 33
2.5 Induced Torque Coefficient 36
2.6 Alternative Means of Analysis 38
2.6.1 Theory of Normal Form 38
2.6.2 Bifurcation Analysis 39

3 Analysis of Present Normal Operation of WPPs 41
3.1 Participation of WPPs in Power System Oscillations . . 43
3.1.1 Considered Strategies to Accommodate an Increased Penetration of Wind Power 43
3.1.2 Impact of Increased WPP Penetration on the Small-Signal Stability 44
3.1.3 Discussion 46
3.2 Effect of Park Level Voltage and Frequency Control on the Small-Signal Stability 49
3.2.1 Investigated WPP Controllers 49
3.2.2 Torques Induced on the Synchronous Generators from the WPP Controllers 50
3.2.3 Discussion 51

4 Control of WPPs for Improvement of Power Oscillation Damping 55
4.1 Induced Damping Torques from ΔP and ΔQ POD at WPPs 56
4.1.1 Frequency Domain Evaluation with Constant PQ Model 57
4.1.2 Frequency Domain Evaluation with Dynamic WT Model 61
4.1.3 Time Domain Evaluation with Dynamic WT Model 63
4.1.4 Discussion 65
4.2 ΔP POD that Utilizes the WT Inertia as Energy Storage 67
4.2.1 Frequency Domain Analysis 69
4.2.2 Time Domain Analysis 70
4.2.3 Discussion 72

5 Evaluation of Park Level POD Considering WPP as Modular and Distributed Unit 77
5.1 Phase Compensation Requirements for WPP ΔQ POD 78
5.1.1 Evaluation on Single Machine Infinite Bus System 80
5.1.2 Discussion 82
5.2 Potential Use of Common Park Level POD 83
5.2.1 Residue Sensitivity Towards Individual WTs and Internal WPP State of Operation 85

5.2.2 Time Domain Evaluation of ΔP and ΔQ POD . 88
5.2.3 Interaction between WPP Voltage Controller and ΔQ POD 89
5.2.4 Discussion 92
5.3 Impact of WPP Model Complexity on Computed Damping Contribution 95
5.3.1 Aggregation Method and Controllability Estimation 95
5.3.2 Results for Aggregated WPP Representations . . 96
5.3.3 Discussion 97

6 Field Test **101**
6.1 Test Setup 102
6.2 Reactive Power Modulation 103
6.2.1 WPP Level 103
6.2.2 WT Level 107
6.3 Active Power Modulation 111
6.3.1 WPP Level 111
6.3.2 WT Level 115
6.4 ΔQ POD Frequency Response 119
6.5 Discussion 120

7 Conclusion **123**
7.1 Summary of Results 123
7.2 Future Research 126

Bibliography **129**

Appendices **147**

A Selected Publications **149**
A.1 "Small-signal stability of wind power system with full-load converter interfaced wind turbines" 149
A.2 "Induced torques on synchronous generators from operation of wind power plant based on full-load converter interfaced wind turbines" 175
A.3 "Power oscillation damping control of inter-area oscillation through active and reactive power modulation from wind power plants with full converter wind turbines" 183
A.4 "Power oscillation damping controller for wind power plant utilizing wind turbine inertia as energy storage" . 205

A.5 "Power oscillation damping capabilities of wind power plant with full converter wind turbines considering its distributed and modular characteristics" 215
A.6 "Towards a reactive power oscillation damping controller for wind power plant based on full converter wind turbines" 239

List of Figures

1.1 Two mass mechanical equivalent to inter-area oscillations . 4

2.1 Single-line diagram of the two generator network. 19
2.2 Single-line diagram of the four generator network. 19
2.3 Single-line diagram of the developed seven generator network. 20
2.4 Single-line diagram of the 68 generator power system [41]. . 21
2.5 Wind turbine concept used in the analysis, that is, a full converter WT. 23
2.6 Overall block diagram of the WT model. 23
2.7 Eigenvalue location in complex plane and its stability properties in the linear sense. 26
2.8 Generator speed change response to a square pulse perturbation in exciter reference voltage. Stable case. 29
2.9 Generator speed change response to a square pulse perturbation in exciter reference voltage. Unstable case. 30
2.10 Generator speed change response to a square pulse perturbation in exciter reference voltage. Marginally stable case. . 30
2.11 Mode-shape for the three electromechanical modes. λ_1: inter-area mode, λ_2: area 1 local mode, and λ_3: area 2 local mode. 31
2.12 Effect of controller tuning on modal damping. 34
2.13 Schematic illustration of machine interactions in a multimachine power system. 35

3.1 Overview of the complex plane with the system eigenvalues for both case 1 and 2 with 1 000 MW of wind power. 45
3.2 Comparison of eigenvalue trajectories for the dominant inter-area mode, λ_1, for integration strategy case 1. The arrows show the movement with increasing WPP penetration. . . 46

3.3 Comparison of selected, normalized participation factors for the dominant inter-area mode, λ_1, for case 1. For the WPP, participation factors are shown for mechanical shaft-, generator-, and rotor-angle states, as well as the maximum participation over all WPP states. 47
3.4 Sensitivity of the dominant inter-area mode, λ_1, to perturbations of ± 40 % on selected WT and WPP control parameters. The arrows show increasing parameter values. Sensitivities are evaluated for a case 1 high wind scenario with a 1 000 MW of wind power. 48
3.5 Block diagrams of generic voltage and frequency controllers. 50
3.6 Effect of feedback controller between bus frequency and active power set point. The capacity of the WPP is 108 MW. 51
3.7 Comparison of predicted, $\hat{\lambda}_{cl}$, and actual closed-loop inter-area eigenvalue, λ_{cl}, for a WPP voltage and frequency controller when the PCC is traversing from the sending end of an inter-tie to the receiving end. The capacity of the WPP is 108 MW. 52

4.1 Open-loop residues as a function of the location r for a damping controller based on ΔP_3 (top row) or ΔQ_3 (bottom row) modulation. Results are for the two generator system without shunt loads. 58
4.2 Open-loop residues and closed-loop eigenvalues as a function of the location r for a damping controller based on ΔP_3 modulation. Arrow shows increasing r. Results are for the two generator system with shunt loads. 59
4.3 Open-loop residues and closed-loop eigenvalues as a function of the location r for a damping controller based on ΔQ_3 modulation. Arrow shows increasing r. Results are for the two generator system with shunt loads. 60
4.4 Contribution of ΔV and $\Delta\theta$ to the damping torque as a function of the location r for a damping controller based on ΔP_3 (upper plots) or ΔQ_3 (lower plots) modulation. The left hand side graphs show the induced damping torques on G_1 and the right hand side graphs the induced torques on G_2. $\eta_V \hat{B}_V$: solid, $\eta_\theta \hat{B}_\theta$: dashed. 61
4.5 Open-loop residues and closed-loop eigenvalues and damping as a function of the location r for the ΔP POD. Results are for the inter-area mode in the four generator system. Dashed curve in residue plots are with PCC frequency as POD input and the magnitude is scaled with 10^{-1}. 62

4.6 Open-loop residues and closed-loop eigenvalues and damping as a function of the location r for the ΔQ POD. Results are for the inter-area mode in for four generator system. Dashed curve in residue plots are with PCC frequency as input and the magnitude is scaled with 10^{-1}. 63

4.7 Top: Generator speed difference between area 1 and 2, that is $\Delta\omega_1 - \Delta\omega_3$. Bottom: Output reference of WPP POD where solid is the active power reference, and dashed is the voltage reference. Synchronous machine PSSs are in service and the WPP PODs are driven by the generator speed difference between G_1 and G_3. 65

4.8 Induced mechanical oscillations when active power is exchanged with the rotational system of a single-mass, single machine swing system. 68

4.9 Residues from generator speed difference, $\Delta u_{d\omega}$, and PCC bus frequency, Δu_f, to WPP active power set-point. 70

4.10 Comparison of predicted and actual shift in inter-area and local-area modes as a function of POD gain. 72

4.11 WPP active power output, rotor speed, and ΔP POD input and output following a 1 second, 5 % step on the voltage reference of G_3 in medium wind conditions. Solid: no WPP ΔP POD, dashed: $\Delta u_{d\omega}$ input, dotted: Δu_f input. 73

4.12 Generator speed and active power output following a 1 second, 5 % step on the voltage reference of G_3 in medium wind conditions. Solid: no WPP ΔP POD, dashed: $\Delta u_{d\omega}$ input, dotted: Δu_f input. 74

5.1 Single-line diagram of a single WT infinite bus system that show the feedback path through the WPP control. 79

5.2 Block diagram of the utilized WPP voltage controller with two possible input points for the ΔQ POD. 80

5.3 Dependency of phase shift induced by the WT voltage controller to the strength of the grid. Solid lines: detailed model, dashed lines: simplified model. 81

5.4 Induced phase shift in the WT voltage reference signal by WPP voltage, reactive power, or power factor control for an input at V_{POD1}. Solid: voltage control, dashed: reactive power control, dash dotted: power factor control. Note that the curves for reactive power and power factor control overlap. 82

5.5 Induced phase shift in the WT voltage reference signal by WPP voltage, reactive power, or power factor control for an input at V_{POD2}. Solid: voltage control, dashed: reactive power control, dash dotted: power factor control. Note that the curves for reactive power and power factor control overlap. 83
5.6 Single-line diagram showing the layout of the 150 WT WPP and the connection to the 68 generator system shown in Figure 2.4. 84
5.7 Complex plane with the system eigenvalues. 86
5.8 Residue magnitudes and angles for WT active power modulation for λ_1. 87
5.9 Residue magnitudes and angles for WT reactive power modulation for λ_1. 87
5.10 Comparison of selected WT power outputs with the corresponding WPP power output at the PCC. 89
5.11 Speed of selected generators. Solid: no WPP POD, dashed: WPP ΔP POD, dotted: WPP ΔQ POD. 90
5.12 Impact of ΔQ POD operation during a distant three-phase short-circuit on the PCC voltage and reactive power transfer. 91
5.13 Input and output signals of the WPP control during a distant treephase short-circuit. 92
5.14 Selected WT reactive power outputs during a distant three-phase short-circuit with and without the ΔQ POD in operation. Dashed: no ΔQ POD, solid: ΔQ POD. 93
5.15 Long distance transfer function for a ΔQ POD and the active power measured at one inter-tie of bus 309. 97
5.16 Controllability factors evaluated from the long distance transfer function to active power variation at one inter-tie of bus 309 for both a ΔP POD (left side plots) and a ΔQ POD (right side plots). 98
5.17 Change in active power between the system areas as measured at a single inter-tie of the respective busses. The WPP is equipped with a ΔQ POD. 99

6.1 ΔQ POD signal and measurements of the PCC reactive power with reactive power modulation at a subset of the tested frequencies 104
6.2 Detrended measurements of the PCC active power with reactive power modulation at a subset of the tested frequencies 104
6.3 FFT of ΔQ POD signal and PCC reactive power with reactive power modulation at a subset of the tested frequencies 105
6.4 PSD of ΔQ POD signal and PCC reactive power with reactive power modulation at a subset of the tested frequencies 105

6.5 FFT of PCC active power with reactive power modulation at a subset of the tested frequencies 106
6.6 Measurements of the WT active and reactive power with reactive power modulation for a full test period with an applied frequency of oscillation of 0.3 Hz. 107
6.7 Detrended measurements of the WT reactive power with reactive power modulation at a subset of the tested frequencies 108
6.8 FFT of WT reactive power with reactive power modulation at a subset of the tested frequencies. 109
6.9 WVD of the reactive power output of a single WT and of the PCC reactive power output with reactive power modulation at a subset of the tested frequencies. 110
6.10 ΔP POD signal and measurements of the PCC active power with active power modulation. 111
6.11 Measurements of the PCC reactive power with active power modulation. 112
6.12 FFT of ΔP POD signal and PCC active power with active power modulation. 113
6.13 PSD of ΔP POD signal and PCC active power with active power modulation. 113
6.14 FFT of PCC reactive power with active power modulation. 114
6.15 Measurements of the WT active and reactive power with reactive power modulation for a full test period with an applied frequency of oscillation of 0.5 Hz. 115
6.16 Detrended measurements of the WT active power with active power modulation. 116
6.17 FFT of WT active power with active power modulation. . . 117
6.18 WVD of the active power output of a single WT and of the PCC active power output with active power modulation. . . 118
6.19 Enlarged plot of Figure 6.18 with a frequency of oscillation of 0.2 Hz. 118
6.20 Frequency response from WPP ΔQ POD to reactive power flow measured at the PCC in test where a high filter time constant in the reactive power measurement reduces the impact from the feedback. 119
6.21 Frequency response from WPP ΔQ POD to reactive power flow measured at the PCC with nominal time constant in the reactive power measurement filter. 120

List of Tables

2.1 Speed mode participation factors. λ_1: inter-area mode, λ_2: area 1 local mode, and λ_3: area 2 local mode. 32

3.1 Overview of analyzed case studies. 44

4.1 Generator output in generator convention for the investigated power outputs a bus 3. The column "No loads" corresponds to $P_{L1,2} = Q_{L1,2} = 0$ in Figure 2.1 on page 19. . . . 57
4.2 Modal characteristics for the inter-area mode as computed from both eigenvalue analysis and as extracted from time domain simulations with synchronous generator PSSs in service. 64
4.3 Induced torques on G_{1-4} from WPP ΔP POD at the modal frequencies of the inter-area mode, D^1, local-area mode for area 1, D^2, and area 2, D^3. Results are shown for the ΔP POD using both speed difference, $\Delta u_{d\omega}$, and PCC frequency as input, Δu_f. 71

5.1 List of studied scenarios with the WPP being in different internal states. 85

List of Abbreviations

DAE	Differential Algebraic Equations
DD	Direct Drive
DFIG	Doubly Fed Induction Generator
DMC	Decentralized Modal Control
EMT	Electromagnetic Transient
FACTS	Flexible AC Transmission System
FFT	Fast Fourier Transform
FRT	Fault Ride Through
FSIG	Fixed Speed Induction Generator
GDRG	Generalized Dynamic Relative Gain
HVDC	High-Voltage Direct Current
ITC	Induced Torque Coefficient, cf. section 2.5
LMI	Linear Matrix Inequality
ODE	Ordinary Differential Equations
OPF	Optimal Power Flow
PCC	Point of Common Connection
PMSG	Permanent Magnet Synchronous Generator
PMU	Phasor Measurement Unit
POD	Power Oscillation Damping Controller
ΔP POD	Active power POD
ΔQ POD	Reactive power POD
PSD	Power Spectral Density
PSS	Power System Stabilizers
RGA	Relative Gain Array
RMS	Root Mean Square
SCR	Short Circuit Ratio

Continued on next page

Continued from previous page

SVC	Static Var Compensator
TCSC	Thyristor Controlled Series Compensation
VSC	Voltage Source Converter
WAMS	Wide Area Measurement System
WF	Wind Farm
WPP	Wind Power Plant
WT	Wind Turbine
WVD	Wigner-Ville Distribution

Chapter 1

Introduction

In an interconnected power system, the speed of the synchronous generators will constantly adjust according to the imbalance between generation and demand, where a production surplus will cause overspeeding of the generators; and vice versa. It must be noted that the applied governor control is to keep the synchronous speed, that is, the nominal grid frequency, within a required narrow range of operation. If a power oscillation between two areas of a power system is excited, the rotor angles of the synchronous machines in one area will start to oscillate in counter phase with the synchronous machines in the other area and thereby force a flow of active power back and forth between the areas. If the oscillation is sufficiently damped, the oscillation will die out and the rotor angles return to a steady state. However, if there is insufficient damping in the power system for this particular oscillation, an ever increasing amount of active power is exchanged between the two areas until other security devices, for example synchronous machine or transmission line safety equipment, trip the unit or the component. A cascading effect of equipment tripping and ultimately system blackout can be the consequence.

Power system oscillations are discussed by Pourbeik et al. [93], Rogers [99], Wilson et al. [128] in terms of the nature of their origin, possible means of mitigation, possible impact of renewable and non-synchronous generation, and its potential as a root cause to system blackout.

The described rotor angle oscillations and the associated oscillations of active power is a variant of rotor angle stability, since the exchange of active power is primarily caused by the acceleration and deceleration of the synchronous machines in the system. Rotor angle oscillations are often divided into

- large disturbances (transient stability), and
- small disturbances (small-signal stability),

where only the latter is treated here. Generally, a disturbance is considered small if the dynamic response following the event can be represented with sufficient accuracy by a linear model. Small-signal rotor angle stability (for simplicity, hereinafter termed small-signal stability) is often defined as [66, p.23]

> "the ability of the power system to maintain synchronism under small disturbances".

The inability of a power system to maintain synchronism can manifest itself in two ways, *1)* an aperiodic drift of the rotor angles, or *2)* as rotor angle oscillations with an increasing amplitude. The first corresponds to insufficient synchronizing torque and the latter to insufficient damping torque. These terms are further elaborated in section 2.4.

Power system oscillations are inherent in interconnected power systems based on synchronous generators [50]. Power oscillations where one part of the system oscillates against another part, often occur in large interconnected power systems, where two or more areas are interconnected through relatively weak AC transmission lines, hence also referred to as inter-area oscillations. Whether or not an oscillation is stable or unstable is a system property. This means that it is not the contingency initiating the oscillation that determine the level of damping, instead it is the state of the power system, that is, operating condition, controller tuning, transmission lines and generators in service, etc. A small-signal unstable power system can be simulated in steady state without the presence of rotor angle oscillations, since these need an event to be excited by. Once excited, however, the oscillations will built up until the power system is restored to a stable state or until the simulation breaks down. It should be mentioned that steady state is a theoretical condition and that a power system in reality is *never* in steady state due to

- load variations,
- variability in production,
- discrete changes in the system,
- etc.,

and small-signal instability can, thus, not be tolerated in an actual power system.

Power system oscillations are typically divided into three groups depending on the global (or local) scale of the participation of the synchronous machines in the oscillation [66].

- Inter-area oscillations where a group of machines in one area oscillates against a group of machines in another area, typically $f \in [0.1\ 0.3]$ Hz
- Intra-area oscillations where a group of machines in one area oscillates against a group of machines in the same area, typically $f \in [0.4\ 0.7]$ Hz
- Local-area or inter-machine oscillations involve machines which are located close to each other, typically $f \in [0.7\ 2.0]$ Hz. This includes adverse interaction between equipment control systems.

Many factors beside the frequency of oscillation, do, however, determine the nature of the oscillations, and the concepts of mode-shape and participation factor are used to correctly identify the source, nature, and significance of a mode.

In [124] it is shown analytically that low frequency inter-area oscillations are fundamental properties of large longitudinal systems and that the presence of weak inter-ties between groups of generators is not a necessary condition.

1.1 Mechanical Equivalents

To understand the phenomena that result in small-signal stability problems in electrical power systems, it is illustrative to convert the problem into an equivalent spring mass system. An excellent derivation and explanation is found in Samuelsson [105] where the mechanical equivalents are extensively used. Here, only a brief summary is presented for illustration.

The spring mass equivalent for an inter-area oscillation is shown in Figure 1.1, where M_i is the inertia of the ith machine, k_i represents the transmission line reactance, and F_C is a controlled active source.

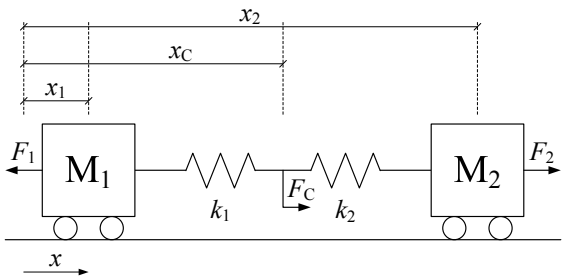

Figure 1.1: Two mass mechanical equivalent to inter-area oscillations

Newtons second law of motion used for the system in Figure 1.1 yields

$$M_1\ddot{x}_1 = (x_C - x_1)k_1 - F_1 \tag{1.1a}$$
$$M_2\ddot{x}_2 = (x_C - x_2)k_2 + F_2 \tag{1.1b}$$
$$0 = (x_1 - x_C)k_1 + (x_2 - x_C)k_2 + F_C \tag{1.1c}$$

where M_i is the mass, k_i the spring constant, x_i the location, and where F_i is an external force. If the speed state variable is introduced, $v_i = \dot{x}_i$, (1.1) may be put into a system of differential and algebraic equations (DAE) as

$$\begin{bmatrix} \dot{v}_1 \\ \dot{v}_2 \\ \dot{x}_1 \\ \dot{x}_2 \\ 0 \end{bmatrix} = \left[\begin{array}{cccc|c} 0 & 0 & \frac{-k_1}{M_1} & 0 & \frac{k_1}{M_1} \\ 0 & 0 & 0 & \frac{-k_2}{M_2} & \frac{k_2}{M_2} \\ 1 & 0 & 0 & 0 & 0 \\ 0 & 1 & 0 & 0 & 0 \\ \hline 0 & 0 & k_1 & k_2 & -(k_1+k_2) \end{array}\right] \begin{bmatrix} v_1 \\ v_2 \\ x_1 \\ x_2 \\ x_C \end{bmatrix} + \ldots$$
$$\begin{bmatrix} \frac{-1}{M_1} & 0 & 0 \\ 0 & \frac{1}{M_2} & 0 \\ 0 & 0 & 0 \\ 0 & 0 & 0 \\ 0 & 0 & 1 \end{bmatrix} \begin{bmatrix} F_1 \\ F_2 \\ F_C \end{bmatrix} \tag{1.2}$$

The system in (1.2) has the exact same structure as is found for linearized power system models where the dynamic states, that is, x and v, are replaced by, respectively, the rotor angle and the rotor speed [105, 112], as will also be shown later in (2.32).

The local area oscillation, where a single machine or a group of machines oscillate against a much larger group of machines, whose speed can be considered constant during the oscillation, is a special case of (1.1). Consider the case where $M_2 \gg M_1$ or even $M_2 = \infty$, then the dynamic response of the area that is represented by M_2 vanishes and M_1 is oscillating against a fixed source, that is, a single machine infinite source system. If the rows and columns of (1.2) that correspond to x_2 and v_2 are removed, the DAE for a local area system is obtained.

1.2 State of the Art

1.2.1 Impact of WTs and WPPs on Rotor Angle Small-Signal Stability

The damping of critical inter-area oscillations is affected by a number of factors such as network topography, generator excitation control, HVDC control, transmission line power flows, etc. [99, 128]. Also, the presence of non-synchronous generation units can have an impact on the damping of inter-area oscillations. In [12, 111] comparisons are presented of the influence on power system oscillations of wind turbines (WTs) and wind power plants (WPPs) based on fixed speed induction generators (FSIGs) and doubly fed induction generators (DFIGs). Slootweg and Kling [111] find that particularly FSIG WPPs tend to improve the damping of inter-area oscillations, while no significant effect is observed for intra-area oscillation. It is, however, noticed that the results become ambiguous when a large part of the synchronous generation in an oscillatory node is replaced with wind power. Chaudhuri and Chaudhuri [18] study several operating scenarios for DFIG integration into a small two area system and find that the DFIG integration mostly contributes positively to the damping of the inter-area mode, although a negative impact is found for certain scenarios. In [12] it is found that both FSIG and DFIG WPPs improve the damping of inter-area oscillations; although to a lesser extend for the DFIG WPP. In [43, 104] also full converter interfaced WPPs are included in the comparison. Hagstrom et al. [43] note that the DFIG does not have any significant effect on the damping while the full-load converter type WPP, here modeled as a negative load, decreases the damping. In [104] it is concluded that the characteristics of the variable speed WPPs, that is, WPPs based on either DFIGs or full converter WTs, are practically identical, while the FSIG WPPs result in slightly better system damping. A study of increased DFIG penetration on a five area system is presented in [84] where it is concluded that the influence on the modal

damping is highly dependent on which synchronous generators that are displaced. That is, the changed power flow in the system as well as the potential disconnection of synchronous generators that are dominant in the stabilization of certain modes, will significantly impact the modal damping. A WT based on a direct drive (DD) permanent magnet synchronous generator (PMSG) is analyzed in [47] where a small-signal model is derived and used in a single machine infinite bus system for tuning of the control parameters.

In [122] the influence is analysed of the voltage/VAR control mode of DFIG based WPPs on inter-area oscillations. The study finds that increasing the penetration of wind power generally has a favorable effect, with increased frequency and damping of the inter-area mode between a weak and a stronger system. With the WPP in voltage control mode, Tsourakis et al. [122] find an adverse interaction for some parameter-set. It is, however, noted that these interactions can be avoided with appropriate tuning of the voltage controller. The influence of the WPP voltage and reactive power control on rotor angle stability is studied by Vittal et al. [125], here it is found that voltage control, when compared to power factor control at the WPP, increases the rotor angle stability and the subsequent damping of rotor angle oscillations following the loss of a power plant. In Modi et al. [84], it is found that the modal damping can be marginally improved through modulation of the DFIG voltage controller gain.

In [116, 117] a generic small-signal stability model is developed for fixed and variable speed WTs with corresponding collector and utility grid to which the units are connected. The approach is based on sensitivity analysis and singular value decomposition.

1.2.2 Control of Variable Speed WTs for Power Oscillation Damping

The idea of contributing to the modal damping of power systems through modulations of the active or reactive power output of converter interfaced units is not new in the academic community. This has been conceptually treated by, for example, Smed and Andersson [112] in 1993 for both active and reactive power modulation and by Cresap and Mittelstadt [21] in 1976 for active power modulation.

The introduction of converter interfaced WTs inspired researchers to look into the possibility of modulation of their active or reactive power output to give a positive contribution to the modal damping. The results have been published in a number of recent publications where

it has been proposed to equip WTs or WPPs with a power oscillation damping controller (POD) for active power modulation (ΔP POD) [24, 30, 32, 48, 65, 80, 110, 121, 123], reactive power modulation (ΔQ POD) [3, 24, 32, 38], or using a combination of both [18, 24, 33, 35, 74]. Gautam et al. [37] study how to mitigate the impact of reduced power system inertia through control of the DFIG torque reference and find that also the small-signal stability is improved from this control.

It is generally found in the studies that the WPP PODs contribute positively to the modal damping of the power system under investigation. The level of added damping as well as the magnitude of the modulated output power varies from study to study. Also the complexity of the applied WT model varies from a controllable load, for example [74] to rather detailed representations, for example [38]. The bulk of the published studies have dealt with conceptual aspects of equipping WTs or WPPs with POD(s) and have all used aggregated WPP models and, generally, small benchmark power systems. An exception is the studies by Gautam et al. [37, 38] where aggregated WPPs are used in a large power system model having over 22 000 buses and 3 104 synchronous generators.

The dual problem of designing a DFIG damping controller for torsional shaft oscillations and a ΔP POD for power system oscillations is considered by Kshatriya et al. [65] that formulates a non-linear optimization problem around a partial eigenstructure assignment method to achieve this goal. The optimization results in a number of controller candidates from which the designer can select the most suitable and robust controller.

It is generally recognized that FACTS PODs are less robust than synchronous machine power system stabilizers (PSSs) against changes in the operating conditions of the power system [99]. Due to the similarity in the grid connection of full converter WTs and FACTS devices, this characteristic might also apply for a WPP POD. This means that it might be advantageous to resort to the various techniques that have been developed for FACTS PODs if similar characteristics are found for a WPP POD. The use of robust control theory for FACTS PODs is treated in [132] to accommodate the issue of insufficient robustness, while Fan [31] presents a review of robust control methods, which have been applied for power system applications.

The residue is the first order sensitivity to an eigenvalue for the feedback between a system output and a system input. The residue angle is, thus, a measure of the necessary phase compensation to achieve a positive damping contribution, while the residue magnitude indicates

the shift of the eigenvalue in the complex plane. This approach is used by Adamczyk et al. [3], Sigrist and Rouco [110] to design WPP PODs with the appropriate amount of phase compensation. Residue based approaches are often combined with a screening of appropriate input and output signals to find the pair that yields the best compromise between performance and robustness across different system operating conditions. Often this task is combined with the subproblem of optimal siting. A number of studies have dealt with this optimization task for damping studies with FACTS devices, for example [68, 72, 83, 98, 127]. A particle swarm optimization approach for robust tuning of a WPP POD based on phase compensation filters is investigated by Mendonca and Lopes [78]. Here, the optimization seeks to achieve adequate levels of damping performance, while considering a large number of operating conditions.

A different approach that is known from non-linear control and that is based on Lyapunov theory is to use energy function analysis. Lyapunov's second method describes that a system is asymptotically stable if the Lyapunov function is positive definite and if and only if the time derivative of the Lyapunov function is negative [44, p.134]. An example of a Lyapunov function is the energy function for the system and stability is assured if energy is dissipated from the system. This approach is used by Fernández et al. [33, 34] for a WPP ΔQ and ΔP POD where control signals are derived that increase the rate of diminution of energy in the system. A similar approach is used by Ruan et al. [101] for a generic converter interfaced power station. Martinez et al. [74] uses the derived control functions from [101] for a study of the performance of WPP PODs, but where the WPP is simply represented as a controllable load.

A seemingly attractive approach towards managing the inherently changing and essentially unknown operating conditions for the power system, that make controller design and evaluation difficult, is to design an adaptive controller that automatically adapts to the changing conditions. Sadikovic et al. [103] proposes an adaptive POD for a thyristor controlled series compensator (TCSC) where the swing dynamics are detected with the Kalman filtering approach from [64]. In each time step, the POD parameters are updated from a pole placement technique where the operational limits of the POD signal is considered. Time domain simulations are shown in Sadikovic et al. [103] where a TCSC equipped with a fixed parameter POD fail to stabilize an off-nominal operating condition that the adaptive POD do stabilize. The adaptive POD proposed by Korba et al. [64] is in [19] used for a static var compensator (SVC) POD and is compared to a model based POD

in a number of contingencies. Remote measurements based on phasor measurement units (PMUs) are in the study utilized for both PODs. Chaudhuri et al. [19] find that similar damping performance is achieved from the two designs, although a slightly higher control effort is found for the adaptive POD. When adaptive controllers are considered, it is however, clear that the performance of such control will depend on the ability of the system identification to fast and accurately detect the governing dynamics that the POD should respond to.

In [69, 89] it is for a FACTS POD proposed to use a combination of bang-bang control and a low gain continuous controller to avoid interactions with other damping controllers. Regarding WPP PODs, this approach might be interesting for a ΔQ POD whereas the bang-bang control would be problematic for a ΔP POD, due to both the time constants of the active power system as well as the added stress that such control signal would inflict on the mechanical system.

Coordinated tuning of POD controllers is another way to limit any adverse impact from control interactions. An approach based on induced torques is proposed by Gibbard et al. [42], Pourbeik and Gibbard [95] where the mutually induced torque coefficients (ITCs) reveal the interaction between the stabilizing controllers in the system, cf. section 2.5. A coordinated design of decentralized PODs through the solution of linear matrix inequalities (LMIs) is presented by Ramos et al. [97] where multiple operating conditions are considered simultaneously in the LMI formulation. Messina et al. [79] propose to use generalized dynamic relative gain (GDRG), which is an extension to the static relative gain array (RGA) calculation, as a tool for selection of input and output variables for the PODs that minimize the control interaction between the PODs. In [36], a method based on pole placement is proposed for coordinated tuning of several synchronous generator PSSs and FACTS PODs where the method of decentralized modal control (DMC) [17] is utilized for calculation of the filter parameters for the PSSs and the PODs. In [1], a method of wide-area supervisory control is patented, which aims at coordinated POD control of multiple WPPs in a power system, although the details of the supervisory control are not presented.

1.3 Objectives and Contributions

Throughout the project and in the conducted studies, emphasis has been put on capturing and including as many WT and WPP characteristics as possible to be able to show a fair and balanced picture that

reflects the characteristics of contemporary WPPs in commercial operation. This is reflected in the detailed WT models used, the selection of transformer and collector grid parameters, and in the WT and WPP operating conditions that have been investigated.

It is the hope that the presented work will contribute to fill in and close the gap between the early and more conceptual studies and the knowledge necessary for practical use.

The response of full converter WTs in the presence of power system oscillations was analyzed with detailed simulation models of a commercially available WT.

- Studies were conducted that revealed a very low participation of the WT states in the power oscillations. The participation was orders of magnitude smaller than those found for the synchronous generators. It was found that the WT reactive power controller had the largest participation, whereas a negligible participation was found for the WT mechanical states. Sensitivity studies of the control parameters for active and reactive power regulation supported this finding. The hypothesis that the WT mechanical states would interact through the WT control system with the power oscillations in the system, could therefore not be confirmed.

Variable speed WTs offer control of both the active and reactive power output, which in the literature has been proposed utilized to have the WPPs contribute to the modal damping.

- On a simple two machine network, the path from WT active and reactive power output to modal damping was shown analytically.

  When repeated with an actual WT model on a more detailed network, a cross coupling was observed between the idealized active and reactive power responses. That is, an applied reactive power modulation induces an active power modulation and similarly for an applied active power modulation. The cross coupling was found to originate from a combination of converter control and induced network response.

- Regarding active power modulation, it has, from an energy perspective, been demonstrated that the stored kinetic energy in the rotational mechanical system can be used to supply a modulated active power output to induce a damping torque onto the synchronous generators in the system.

- WPPs are routinely equipped with park level voltage or reactive power controllers that function to coordinate the response of the WTs to a achieve a certain condition at a certain bus. With the requirements of today, the bandwidth of such controllers overlap with the frequency range in which a ΔQ POD would be expected to operate. It has been shown that this interaction has to be considered when a ΔQ POD is designed, in order to achieve the required phase shift through the system.

Large WPPs are modular and can be distributed over a large geographical area, which are characteristics that have not been captured in the previously published studies where aggregated, single WT representations have been used.

- With residue analysis it was shown that very similar residue angles were found for the individual WT terminal busses for both active and reactive power modulation. This means that very similar control should be applied to each WT to achieve the maximum contribution to the modal damping.

  These findings encourage that a park level POD is feasible, which for practical matters would be highly beneficial compared to individually tuned WT PODs.

- The capabilities of WPPs based on full converter WTs to contribute to the modal damping through modulation of active or reactive power was demonstrated with a 150 WT WPP and it was shown that the WTs within the WPP could be controlled to appear as a single unit.

- Through controllability factor estimation and time domain simulations, it was shown that a high degree of WT aggregation was possible without affecting the impact and performance of the WPP POD.

Field tests were conducted on a small WPP where the response to both an active and a reactive power modulation was tested. Park level PODs were considered in both cases that transmitted continuous reference signals to all the WTs. Response tests for both the ΔQ and the ΔP PODs were conducted in the frequency range from 0.1 to 1.0 Hz, while the frequency response estimations for the ΔQ POD were conducted in the range from 0.1 to 2.0 Hz.

- Both for the tested ΔP and ΔQ POD responses, the WTs were capable of tracking the received reference to produce an aligned response at the PCC.

- On WT level, the tightest tracking was found for the tested ΔQ POD where an aligned output was seen across the WTs. For the ΔP POD, a slight variation was found in the frequency of the active power modulation at WT level. This variation was not observed in the combined WPP response, which is most likely caused by the averaging effect over the WTs.

- The field tests verified the cross coupling between active and reactive power modulations that was identified theoretically from residue analysis. Distinct magnitude peaks was found in the PCC reactive power when an active power modulation was applied to the WTs. Similarly for the PCC active power when a reactive power modulation was applied, although this effect was found to be less pronounced.

- The frequency response was estimated for a ΔQ POD that was interfaced to a WPP level reactive power controller to analyze the interaction between the controllers. The field tests demonstrated previous theoretical evaluations that found that the interaction between the controllers had to be considered when a ΔQ POD was designed, since the interaction had a significant influence on the phase of the response.

1.4 List of Publications

During the course of the PhD project, the papers listed in sections 1.4.1 and 1.4.2 were composed as part of the dissemination requirements. The work has, furthermore, resulted in two published patent applications that are shown in section 1.4.3.

The papers given in section 1.4.1 contain the main results from the project and are included as appendix A, whereas the contributions of those in section 1.4.2 are at least partially covered by the papers in section 1.4.1.

1.4.1 Primary Papers

- T. Knüppel, J. N. Nielsen, K. H. Jensen, A. Dixon, and J. Østergaard. Small-signal stability of wind power system with full-load

converter interfaced wind turbines. *IET Renewable Power Generation*, 6(2):79–91, 2012. doi: 10.1049/iet-rpg.2010.0186. ISSN 1752-1416. [61], included on page 149.

- T. Knüppel, J. N. Nielsen, K. H. Jensen, A. Dixon, and J. Østergaard. Induced torques on synchronous generators from operation of wind power plant based on full-load converter interfaced wind turbines. In F. A. Aranda, editor, *Scientific Proceedings of the European Wind Energy Conference & Exhibition*, pages 68–71. The European Wind Energy Association, March 2011. [55], included on page 175.

- T. Knüppel, J. N. Nielsen, K. H. Jensen, A. Dixon, and J. Østergaard. Power oscillation damping control of inter-area oscillation through active and reactive power modulation from wind power plants with full converter wind turbines. *Unsubmitted manuscript*. [62], included on page 183.

- T. Knüppel, J. N. Nielsen, K. H. Jensen, A. Dixon, and J. Østergaard. Power oscillation damping controller for wind power plant utilizing wind turbine inertia as energy storage. In *2011 IEEE PES General Meeting, Wind & Solar Super Session*, pages 1–8, Detroit, MI, USA, July 2011. IEEE Power & Energy Society. doi: 10.1109/PES.2011.6038908. ISBN: 978-1-4577-1001-8. [54], included on page 205.

- T. Knüppel, J. N. Nielsen, K. H. Jensen, A. Dixon, and J. Østergaard. Power oscillation damping capabilities of wind power plant with full converter wind turbines considering its distributed and modular characteristics. *Accepted for publication in IET Renewable Power Generation Special Issue*, 2012. [63], included on page 215.

- T. Knüppel, S. Kumar, P. Thuring, M. Støttrup, and J. Friman. Towards a reactive power oscillation damping controller for wind power plant based on full converter wind turbines. In *Accepted for panel presentation at 2012 IEEE PES General Meeting*, pages 1 – 8, San Diego, CA, USA, July 2012. IEEE Power & Energy Society. [60], included on page 239.

1.4.2 Secondary Papers

- T. Knüppel, V. Akhmatov, J. N. Nielsen, K. H. Jensen, A. Dixon, and J. Østergaard. Small-signal stability analysis of full-load converter interfaced wind turbines. In *8th International Workshop*

on Large-Scale Integration of Wind Power into Power Systems as well as on Transmission Networks for Offshore Wind Farms, 2009. [51].

- T. Knüppel, V. Akhmatov, J. N. Nielsen, K. H. Jensen, A. Dixon, and J. Østergaard. On small-signal stability of wind power system with full-load converter interfaced wind turbines. In *WINDPOWER 2010 Conference & Exhibition, Dallas, TX, USA*. American Wind Energy Association, 2010. [52].

- T. Knüppel, J. Thisted, B. Andresen, M. N. Frydensbjerg, V. Akhmatov, and J. N. Nielsen. Grid support capabilities of full-load converter interfaced wind turbines. In *POWER-GEN India & Central Asia*. PennWell Corporation, April 2010. [53].

- T. Knüppel, J. N. Nielsen, K. H. Jensen, A. Dixon, and J. Østergaard. Power oscillation damping capabilities of wind power plant with full converter wind turbines considering its distributed and modular characteristics. In *Proceedings of IET Renewable Power Generation Conference 2011*, Radisson Blu, Edinburgh, UK, September 2011. The Institution of Engineering and Technology, IET RPG. doi: 10.1049/cp.2011.0130. [56].

- J. Mehmedalic, T. Knüppel, and Jacob Østergaard. Using H_∞ to design robust POD controllers for wind power plants. In *47th International Universities' Power Engineering Conference*, Brunel University, London, UK, September 2012. [77].

1.4.3 Published Patent Applications

- T. Knüppel, B. Andresen, and M. N. Frydensbjerg. Power oscillation damping by a converter-based power generation device. World Intellectual Property Organization, International Publication No.: WO 2012/041527 A1, April 2012. International Filing Date: 2011-01-19. Siemens AG. [58].

- T. Knüppel, S. Kumar, and P. Thuring. Power oscillation damping controller. World Intellectual Property Organization, International Publication No.: WO 2012/041543 A1, April 2012. International Filing Date: 2011-06-10. Siemens AG. [59].

1.5 Thesis Organization

The thesis is based on the papers listed in section 1.4.1. As such, the main results will appear from the papers and only summarized in the

main body of the thesis. The topics covered by the papers are naturally divided into three parts, which are here given as chapter 3, 4, and 5, whereas the field tests are covered in chapter 6. A short description of each chapter is given as:

- Chapter 2: Summaries are presented of the applied models, that is, the power system models and the employed WT model, and the linear analysis methods used throughout the thesis.
- Chapter 3: The interaction between a WPP based on full converter WTs and power system oscillations is analyzed for the present standard configuration where the WPP does not actively contribute to power oscillation damping.
- Chapter 4: The possibility to actively control the WPP to enhance the modal damping is investigated for both a ΔP and a ΔQ POD, and it is analyzed how the location of the WPP within the oscillation affects the ability of the WPP to contribute to the modal damping.
- Chapter 5: A WPP is not a single unit but instead distributed and may consist of more than hundred units. These characteristics of a WPP are treated for both a ΔP and a ΔQ POD to analyze the potential for a park level POD.
- Chapter 6: Measurement results from field tests with a small WPP where the response of the WPP to a park level ΔP or ΔQ POD signal has been investigated.
- Chapter 7: Conclusions and outlook.

Chapter 2

Overview of Models and Linear Analysis Methods

Power system oscillations and the application of eigenvalue analysis as means of analysis are well described in the literature, as for example [66, 99]. Another approach is to base the analysis on signal processing of measured data [119, 120]. When analyzing very large systems this measurement based approach has the advantage that it is not dependent on the accuracy of a large dynamic model.

2.1 Power System Modeling

A power system is in general terms described by a set of non-linear dynamic equations and a set of algebraic relations [66]

$$\dot{x} = \tilde{f}(x, v, u, t) \quad 0 = \tilde{h}(x, v, u, t) \quad y = \tilde{g}(x, v, u, t), \tag{2.1}$$

where $\dot{x} = \frac{\mathrm{d}x}{\mathrm{d}t}$, $x^{n\times 1}$ is the state vector, $v^{o\times 1}$ is a vector with algebraic variables, $u^{r\times 1}$ the input vector, $y^{m\times 1}$ the output vector, t is time dependency, and where $\tilde{f}$, $\tilde{h}$, and $\tilde{g}$ are non-linear functions. When the derivatives in (2.1) are not explicit functions of t, (2.1) is said to be autonomous and is reduced to

$$\dot{x} = f(x, v, u) \quad 0 = h(x, v, u) \quad y = g(x, v, u). \tag{2.2}$$

While the format in (2.2) is suitable for time domain simulations it is often desirable to simplify the expression to do other types of analysis. A common approach is to Taylor expand (2.2) around an operating point, (x_0, v_0, u_0), that is found by solving $\dot{x} = 0$. Let the partial derivatives be defined as

$$A_{11} = \frac{\partial f}{\partial x} \quad A_{12} = \frac{\partial f}{\partial v} \quad B_1 = \frac{\partial f}{\partial u} \tag{2.3a}$$

$$A_{21} = \frac{\partial h}{\partial x} \quad A_{22} = \frac{\partial h}{\partial v} \quad B_2 = \frac{\partial h}{\partial u} \tag{2.3b}$$

$$C_1 = \frac{\partial g}{\partial x} \quad C_2 = \frac{\partial g}{\partial v} \quad D_1 = \frac{\partial g}{\partial u}, \tag{2.3c}$$

equation (2.2) is then represented by the linear DAE [105]

$$\begin{aligned} \begin{bmatrix} \Delta\dot{x} \\ 0 \end{bmatrix} &= \begin{bmatrix} A_{11} & A_{12} \\ A_{21} & A_{22} \end{bmatrix} \begin{bmatrix} \Delta x \\ \Delta v \end{bmatrix} + \begin{bmatrix} B_1 \\ B_2 \end{bmatrix} \Delta u \\ \Delta y &= \begin{bmatrix} C_1 & C_2 \end{bmatrix} \begin{bmatrix} \Delta x \\ \Delta v \end{bmatrix} + D_1 \Delta u. \end{aligned} \tag{2.4}$$

The system description in (2.4) gives the linear behavior in a small neighborhood around the operating point (x_0, v_0, u_0), hence the Δ-notation. The deviation variables are defined as

$$\begin{aligned} \Delta x &= x - x_0 \quad \Delta v = v - v_0 \\ \Delta u &= u - u_0 \quad \Delta y = y - y_0. \end{aligned}$$

For simplicity, the Δ-notation is dropped in the following.

The algebraic variables, v, are eliminated using the algebraic subsystem of (2.4) to give v in terms of x and u. Performing these matrix manipulations yield

$$A = A_{11} - A_{12}A_{22}^{-1}A_{21} \quad B = B_1 - A_{12}A_{22}^{-1}B_2 \tag{2.5a}$$

$$C = C_1 - C_2A_{22}^{-1}A_{21} \quad D = D_1 - C_2A_{22}^{-1}B_2. \tag{2.5b}$$

With (2.4) described purely by ordinary differential equations (ODE), the system is in the classical state space form

$$\begin{aligned} \dot{x} &= Ax + Bu \\ y &= Cx + Du \end{aligned} \tag{2.6}$$

where $x^{n\times 1}$ is the state vector, $u^{r\times 1}$ the input vector, $y^{m\times 1}$ the output vector, $A^{n\times n}$ is the system state matrix, $B^{n\times r}$ the input matrix, $C^{m\times n}$ the output matrix, and $D^{m\times r}$ the feed forward matrix.

2.1.1 Applied Power System Models

2.1.1.1 Two Generator System

The two generator network shown in Figure 2.1 was introduced in [112] to study the impact of HVDC on system damping and later used in [100] to study power system damping by power modulation of a voltage-source-converter (VSC) power station.

The network in Figure 2.1, with its purely reactive network and the generators modeled with the classical model, that is, a voltage source behind the transient reactance of the generator, is sufficiently simple to allow for analytical evaluations. The parameters are available in the paper in appendix A.3.

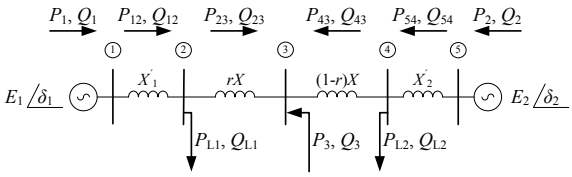

Figure 2.1: Single-line diagram of the two generator network.

The two generator system can be considered as a simplified representation of the linearized swing dynamics of two areas in a power system; similar to the mechanical equivalent shown in Figure 1.1.

2.1.1.2 Four Generator System

The network shown in Figure 2.2 is based on the four generator system in [115], which is a modified version of the two area system originally defined in [50]. This system possesses many of the same properties as the two generator equivalent in section 2.1.1.1 but where also the dynamics of the generator and WT controls are considered.

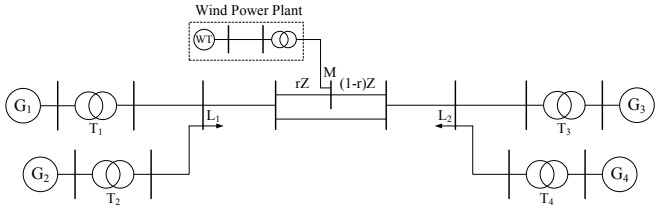

Figure 2.2: Single-line diagram of the four generator network.

2.1.1.3 Seven Generator System

The seven generator system in Figure 2.3 was developed in collaboration with National Grid as an extension to the three generator system described in Anaya-Lara et al. [11] to improve the numerical properties of the system.

The developed model may assist in the understanding of power oscillations between major areas of the UK power system, although the model does not accurately represent particular aspects of the UK network, and hence, should not be used to draw conclusions regarding the performance of this network.

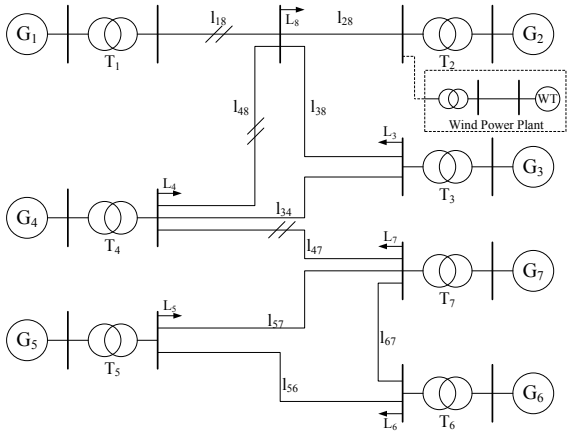

Figure 2.3: Single-line diagram of the developed seven generator network.

The system is further described in Knüppel et al. [61] where also the parameters for the network and for the synchronous generators are available, cf. appendix A.1.

2.1.1.4 68 Generator System

The system was originally developed by Gibbard and Vowles [41] to provide a benchmark system for analyzing power system oscillations and the single-line diagram of the network is depicted in Figure 2.4. The original system has 59 busses and fourteen power stations and data is provided for six different operating conditions, ranging from “heavy load” to “light load” to be able to test the performance of damping controllers to changing operating conditions. The system parameters

and the distribution of load and generation for the provided operating conditions are available from Gibbard and Vowles [41].

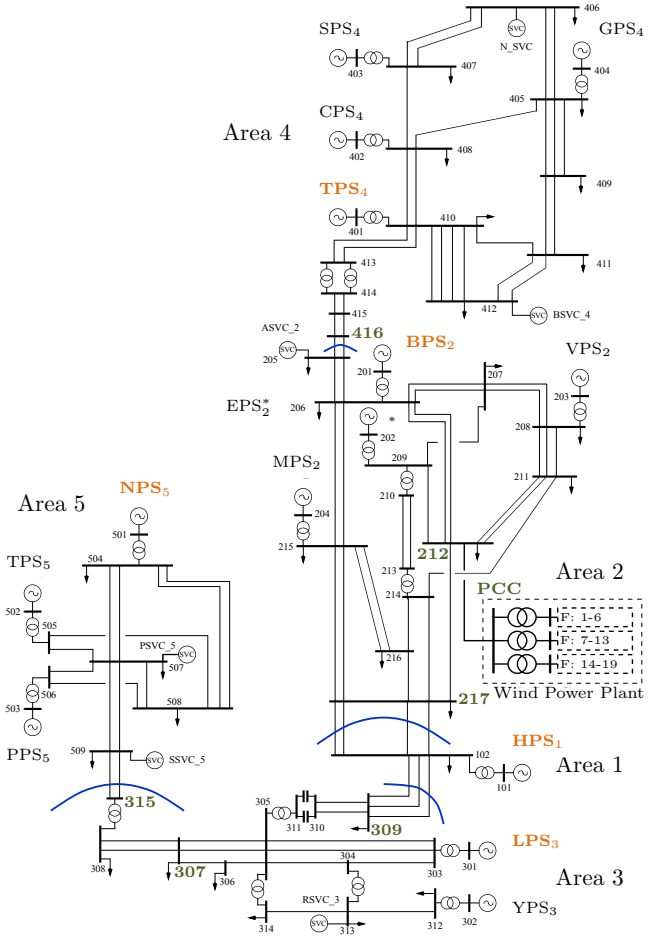

Figure 2.4: Single-line diagram of the 68 generator power system [41].

For the studies conducted in this thesis the generators within the fourteen power stations are represented individually, which in total corresponds 62 on-line synchronous generators for the heavy load scenario. All the generators are equipped with standard IEEE STAB1 PSSs, which have been tuned to obtain weakly damped oscillations between the areas. A plot of the complex plane with the eigenvalues that capture the power oscillations in the system is shown in Figure 5.7 on page 86.

2.1.2 Wind Turbine Modeling

An overview of contemporary WT concepts is presented and discussed in [70, 71] where especially the different concepts for generator and drive train are discussed in [70], while [71] also discusses different converter concepts, grid connection issues, and present and discuss future concepts for connection of off-shore WPPs. As discussed by Li and Chen [70], WTs are often classified into fixed speed, limited variable speed, and variable speed WTs according to their ability to vary the speed of the WT rotor. The variable speed WTs are, furthermore, often subdivided into WTs with a partial scale and a full scale converter, and according to drive train and generator type.

WT modeling is a topic that has received a lot of attention in the scientific literature. The FSIG is described in a number of textbooks as for example [2, 8]. For variable speed WTs, especially the modeling and control of the DFIG concept have been widely described in the literature, as for example [5, 6, 8, 20, 27, 28, 81, 82, 118]. In [7, 8] the modeling and control are presented of a full converter WT with an induction generator. Huang et al. [47], Strachan and Jovcic [114], Wu et al. [129] present the modeling and control of a DD PMSG where [47] also includes a number of references to the modeling and control of PMSGs and where [114] has a detailed description of the process employed for tuning of the WT controllers.

For power system studies, the WTs within a WPP are often aggregated into equivalent WT generators that consist of one of more upscaled WTs [9, 16, 86, 108].

The WT concept for this study has an induction generator and is interfaced through a full-load converter system as illustrated in Figure 2.5. The WT is pitch controlled and has variable speed operation to maximize the active power output. The dynamic model represents a 3.6 MW Siemens Wind Power WT and the dynamic fault-ride-through (FRT) response of the model has been validated from field tests [90]. The WT is represented with a reduced order, positive sequence, RMS model that is suitable for dynamic power system studies. The model includes a variable wind speed aerodynamic model, a two-mass model of rotor, gearbox, and generator, machine and grid side converter, DC-link, and a generic reduced order control scheme. For the different studies the WT model is used for both an aggregated representation of a WPP as well as to represent the individual WTs in a WPP.

A block diagram showing the overall connections is shown in Figure 2.6 and the individual blocks are further described in Knüppel et al. [61],

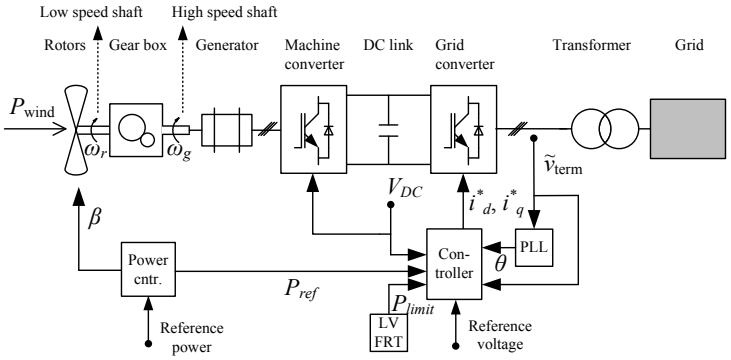

Figure 2.5: Wind turbine concept used in the analysis, that is, a full converter WT.

cf. appendix A.1.

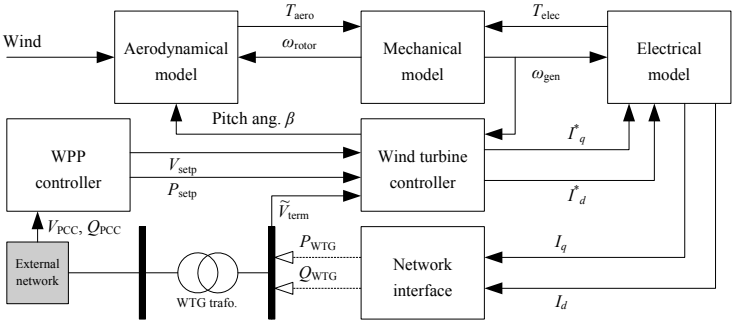

Figure 2.6: Overall block diagram of the WT model.

For the studies where POD operation of the WPP is investigated, only continuous PODs are considered. The general structure for the investigated PODs are

$$G_{\mathrm{POD}}(s) = K \frac{s\,T_{wo}}{s\,T_{wo}+1} \frac{1}{s\,T_{lp}+1} G_{pc}(s) \tag{2.7}$$

where K is the gain, T_{wo} the wash-out filter time constant, T_{lp} the low-pass filter time constant, and where $G_{pc}(s)$ is the transfer function for the phase compensation. The POD is driven by a power system signal with good observability of the oscillation in question, and its output is added to a WT or WPP signal with control of either the active or the reactive power output of the WT(s). The phase compensation

is determined from residue analysis using the approach presented in section 2.3 and the magnitude of the gain, K, from root-locus analysis and time domain simulations.

2.2 Eigenvalue Analysis

2.2.1 Eigenvalue Analysis of ODE System

To analyze the dynamic performance of the system in (2.6) it is often useful to perform a similarity transformation to diagonalize A, that is, decouple the system dynamics [66, 99]. It should be remembered that this is only possible given that A has an eigenbasis, that is, given that A is not defective.

$$A\phi_i = \lambda_i \phi_i, \quad \text{for } i = 1, 2, \ldots, n \tag{2.8}$$

where the ith eigenvalue, λ_i, is found as the solution of

$$\det(A - \lambda_i I) = 0 \tag{2.9}$$

and where $I^{n\times n}$ is the identity matrix and $\phi_i^{n\times 1}$ the right eigenvector for the ith eigenvalue, also commonly referred to as the mode-shape for the ith mode. Similar to the formulation in (2.8), the left eigenvector is defined as

$$\psi_i A = \lambda_i \psi_i, \quad \text{for } i = 1, 2, \ldots, n \tag{2.10}$$

where $\psi_i^{1\times n}$ is the left eigenvector for the ith eigenvalue.

In compact notation for all n eigenvalues, the right and left eigenvector matrices are defined as

$$\Phi = [\phi_1 \ \phi_2 \ \cdots \ \phi_n] \quad \Psi = \left[\psi_1^T \ \psi_2^T \ \cdots \ \psi_n^T\right]^T \tag{2.11}$$

Further, for power system studies the eigenvector matrices are usually scaled to satisfy $\Psi\Phi = I$. When the indicated similarity transformation is performed, first define a new state vector, z, in the transformed coordinates

$$x = \Phi z. \tag{2.12}$$

Then substitute (2.12) into (2.6)

$$\begin{aligned} \Phi\dot{z} &= A\Phi z + Bu \\ y &= C\Phi z + Du \end{aligned} \tag{2.13}$$

and premultiply by Φ^{-1}

$$\begin{aligned} \dot{z} &= \Lambda z + B'u \\ y &= C'z + Du \end{aligned} \tag{2.14}$$

to obtain the ODE system in the transformed and decoupled coordinate set, z. Using (2.14) and the inverse of the (2.12) transformation, the time domain response for the ith state vector, given in terms of the modal eigenvector matrices and the initial conditions for the state vector, $x(0)$, is given by

$$x_i(t) = \phi_{i1}\psi_1 x(0)e^{\lambda_1 t} + \phi_{i2}\psi_2 x(0)e^{\lambda_2 t} + \cdots + \phi_{in}\psi_n x(0)e^{\lambda_n t} \tag{2.15}$$

The right eigenvector, ϕ_i, describes how the activity of the ith mode is distributed on the n state variables, while the left eigenvector, ψ_i, weighs the contribution of the n state variables on the ith mode. The entrywise product of ϕ_i and ψ_i^T is thus a measure of the importance of the states within the individual modes and is referred to as the participation factors

$$p_i = [\phi_{1i}\psi_{i1} \ \phi_{2i}\psi_{i2} \ \cdots \ \phi_{ni}\psi_{in}]^T , \tag{2.16}$$

or in compact notation

$$P = \Phi \otimes \Psi^T \tag{2.17}$$

where $\otimes$ denotes the entrywise product of two equal sized matrices. Of special interest is the speed participation factors, since these indicate the sensitivity of the eigenvalue to the addition of mechanical damping at the shaft [99].

The eigenvalues provide important information on the dynamics of the system in terms of the frequency and damping of any oscillations. If the ith eigenvalue is given as $\lambda_i = a \pm jb$, the natural frequency, ω_n, the damped frequency, ω_d, and the damping ratio, ζ, are defined as

$$\omega_n = \sqrt{a^2 + b^2} \quad \left[\frac{\text{rad}}{\text{sec}}\right], \quad \omega_d = b \quad \left[\frac{\text{rad}}{\text{sec}}\right], \quad \zeta = \frac{-a}{\omega_n} \quad [-]$$

From classical control theory of continuous and time invariant systems, it is given that mode λ_i is asymptotically stable only if $a < 0$ [44, p.123]. The stability properties of an eigenvalue is schematically depicted in Figure 2.7. If the eigenvalue has only a real part, $\lambda = a$, its time response is monotonically decreasing if the eigenvalue is stable, or increasing if unstable. For a pair of complex eigenvalues, $\lambda = a \pm jb$,

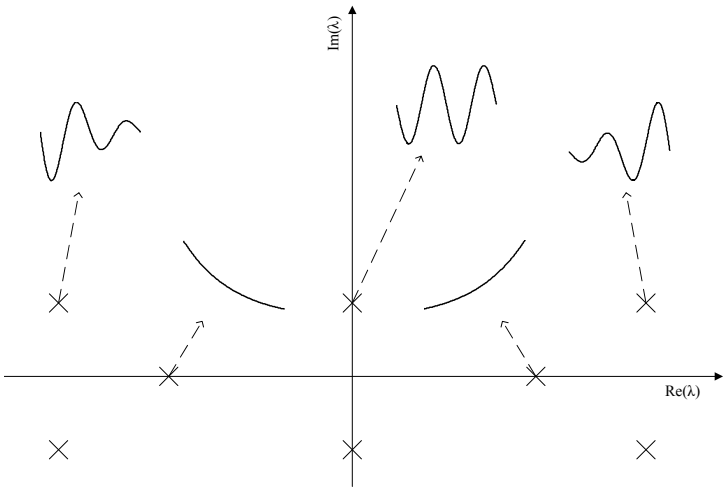

Figure 2.7: Eigenvalue location in complex plane and its stability properties in the linear sense.

an oscillatory time response is obtained where the value of its real part, a, determines whether the amplitude is decreasing, increasing, or constant.

It should be remembered that power systems in general are non-linear while the modal analysis is based on a linear approach. Thus, the results from the modal analysis are only valid in proximity of the linearization point and should be perceived as a snapshot of the dynamic system behavior.

For highly non-linear systems, the results from the linear analysis should be interpreted with care, since the dynamics of the system might not be represented very accurately by the linear approximation. The method of normal forms offers a framework for extending the modal analysis to include higher order terms and thereby capture dynamics not captured by a linear model, cf. section 2.6.1. Bifurcation analysis offers another framework for analysis of non-linear systems where the dependency of qualitative changes of the system to system parameters and initial conditions are explored, cf. section 2.6.2. These methods are especially important for stressed, highly non-linear power systems which are not accurately described by the linear approximation in (2.6). Linear analysis is often complemented with non-linear time domain simulations, where the time domain results are used for assessment of the valid-

ity of the linear analysis. That is, have the important dynamics been captured by the linear approximation with sufficient accuracy.

To gain deeper insight into the dynamic behavior of the system, a series of modal analysis are often conducted where certain system parameter(s) are gradually changed. Analyzing the movement of the eigenvalues in the complex plane, reveals the influence of the varied parameter to overall system dynamics and small-signal stability.

2.2.2 Eigenvalue Analysis of DAE System

Eigenvalue analysis is often conducted on the ODE description in (2.6) as described in section 2.2.1. A disadvantage with this approach is, however, that it removes part of the inherent structure of the power system model in (2.4). The system matrices in (2.4) are generally sparse whereas the equivalent ODE description is dense, which is caused by the elimination of the algebraic variables as shown in (2.5a).

In the following let the complete DAE system in (2.4) be described with the $\tilde{\cdot}$ notation such that (2.4) is given as

$$\begin{aligned} E\dot{\tilde{x}} &= \widetilde{A}\tilde{x} + \widetilde{B}u \\ y &= \widetilde{C}\tilde{x} + \widetilde{D}u \end{aligned} \tag{2.18}$$

where

$$E = \begin{bmatrix} I^{n\times n} & 0^{n\times o} \\ 0^{o\times n} & 0^{o\times o} \end{bmatrix} \tag{2.19}$$

is defining the differential and the algebraic part of $\dot{\tilde{x}}$.

The similarity transformations performed with the left and right eigenvectors, as defined in (2.8) and (2.10) for the ODE system, can for the DAE description be defined as

$$\widetilde{A}\widetilde{\Phi} = E\widetilde{\Phi}\widetilde{\Lambda} \qquad \widetilde{\Psi}\widetilde{A} = \widetilde{\Lambda}\widetilde{\Psi}E \tag{2.20}$$

where the compact notation in (2.11) has been used for the right and the left eigenvectors. Consider the similarity transformation using the right eigenvector matrix in (2.20) and expand the matrices into the corresponding differential and algebraic subsystems

$$\begin{bmatrix} A_{11} & A_{12} \\ A_{21} & A_{22} \end{bmatrix} \begin{bmatrix} \widetilde{\Phi}_d \\ \widetilde{\Phi}_a \end{bmatrix} = \begin{bmatrix} I & 0 \\ 0 & 0 \end{bmatrix} \begin{bmatrix} \widetilde{\Phi}_d \\ \widetilde{\Phi}_a \end{bmatrix} \widetilde{\Lambda}. \tag{2.21}$$

If secondly, the algebraic eigenvector matrix, $\widetilde{\Phi}_a$, is eliminated, (2.21) is given as

$$\underbrace{(A_{11} - A_{12}A_{22}^{-1}A_{21})}_{A}\widetilde{\Phi}_d = \widetilde{\Phi}_d\widetilde{\Lambda}. \tag{2.22}$$

Comparing the first term in (2.22) with (2.5a), it is clear that this is exactly the ODE A matrix. Uniqueness of the eigenvalue decomposition gives that $\widetilde{\Lambda} = \Lambda$, and $\widetilde{\Phi}_d = \Phi$. This result is intuitively correct since the transformation from DAE to ODE preserves the dynamical behavior of the system.

A similar result is obtained from the similarity transformation with the left eigenvector matrix.

The algebraic part of the eigenvectors, $\widetilde{\Phi}_a$ and $\widetilde{\Psi}_a$, are then obtained from

$$\widetilde{\Phi}_a = -A_{22}^{-1}A_{21}\widetilde{\Phi}_d \qquad \widetilde{\Psi}_a = -\widetilde{\Psi}_d A_{12}A_{22}^{-1}. \tag{2.23}$$

2.2.3 Numerical Example

The benchmark system presented in section 2.1.1.2 displays some fundamental properties with respect to power system oscillations. The four generator, two area system has a total of three electromechanical modes, two local modes between G_1 and G_2, and between G_3 and G_4, and an inter-area mode with G_{1-2} oscillating against G_{3-4}. Let the inter-area mode be named λ_1, the area 1 local mode λ_2, and the area 2 local mode λ_3.

Power system oscillations are a system property and not related to the event that excites the oscillations. In an unstable power system, oscillations with increasing amplitudes thus occur regardless of the activating event, be it a short-circuit, a transformer tap-change, a generator set-point change, naturally occurring load changes, etc.

In sections 2.2.3.1 to 2.2.3.3 the three theoretical possibilities are illustrated, that is, stable, unstable, and marginally stable. The rotor speed of the four generators are plotted following a 0.2 second, 5 % square pulse to the voltage set-point of one exciter. The exercise is repeated for an exciter in both area 1 and 2.

2.2.3.1 Stable Case

In the stable system all eigenvalues have negative real parts and any dynamic response described by the linear model approximation will

return to the steady state operating point. This is shown in Figure 2.8 for a square pulse input to the reference voltage to the exciter of G_1 and G_3.

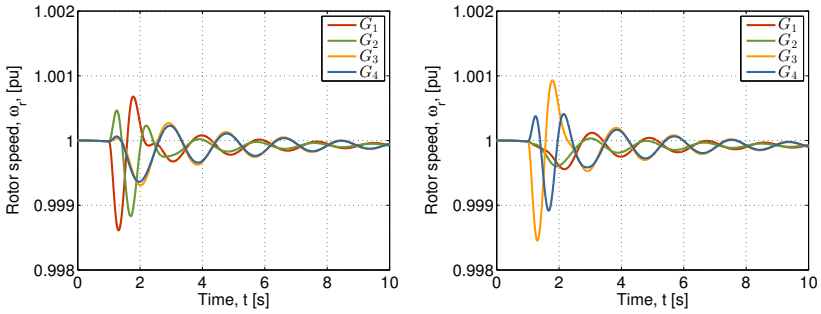

(a) Perturbation on G_1 **(b)** Perturbation on G_3

Figure 2.8: Generator speed change response to a square pulse perturbation in exciter reference voltage. Stable case.

The dynamic responses after applying the perturbation in area 1 and 2 are shown in Figure 2.8a and 2.8b, respectively. In both plots it is initially the local-area mode in the area with the perturbation that is excited, after which the inter-area oscillation takes over and dominates the response. As expected, the oscillations have a decreasing amplitude.

2.2.3.2 Unstable Case

A system is small-signal unstable if one or more eigenvalues have a positive real part. Any event that excites an unstable mode will lead to oscillations of increasing amplitude unless system protection is operated to return the system to a stable operating point. The response to the voltage reference perturbation is depicted in Figure 2.9 where the increasing amplitudes of the oscillations are noticed. Note how the rotor speeds are constant before the perturbation is applied. This illustrates that the system will in fact remain in the steady state operating point until the unstable mode is excited[1].

[1]Notice that this is a rather theoretical observation since actual power systems, as previously discussed, have a stochastic nature and therefore do not *have* a steady state.

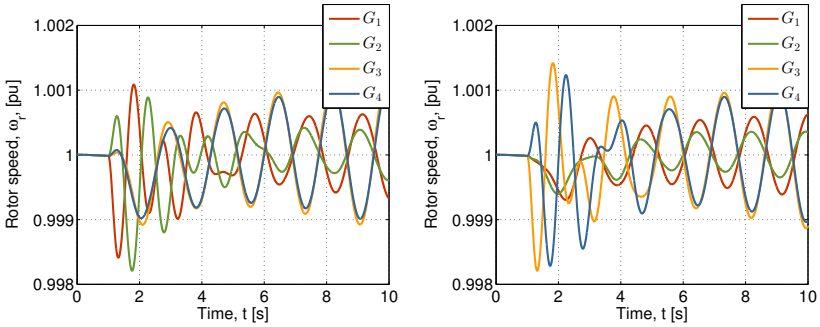

(a) Perturbation on G_1 **(b)** Perturbation on G_3

Figure 2.9: Generator speed change response to a square pulse perturbation in exciter reference voltage. Unstable case.

2.2.3.3 Marginally Stable Case

The marginally stable power system describes the situation where sustained oscillations occur. In Figure 2.10, the speed deviations are plotted for this special case. The time responses are dominated by the local-area modes for the first couple of cycles, after which the response is dominated by the undamped inter-area mode.

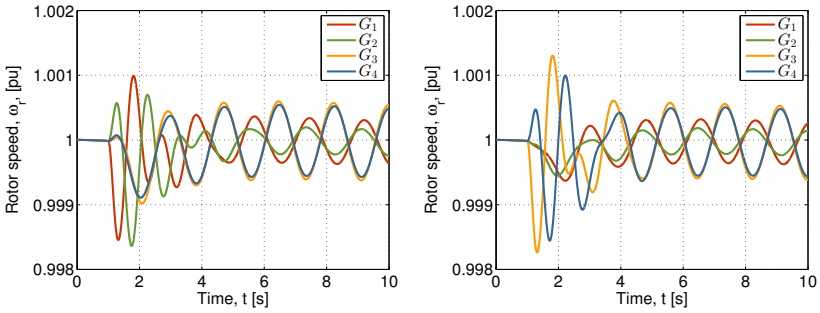

(a) Perturbation on G_1 **(b)** Perturbation on G_3

Figure 2.10: Generator speed change response to a square pulse perturbation in exciter reference voltage. Marginally stable case.

2.2.3.4 Oscillating Groups of Generators

As shown from the time domain simulations in Figure 2.8 to 2.10, the generators in each area have a tendency of swinging against each other in a local-area mode. Just as the two areas have an inherent oscillation which involves all four generators.

The time domain response for the ith state variable is as discussed in section 2.2.1 and shown in (2.15) shaped by the ith right eigenvector, ϕ_i. This is utilized in the mode-shape plot to identify groups of oscillating generators. The mode-shape plot is basically the right eigenvector plotted for the speed states for the inter-area and the two local-area modes. The scaled mode-shapes for the system in Figure 2.2 is plotted in Figure 2.11. The grouping is noted by the approximate 180° separation between the vectors.

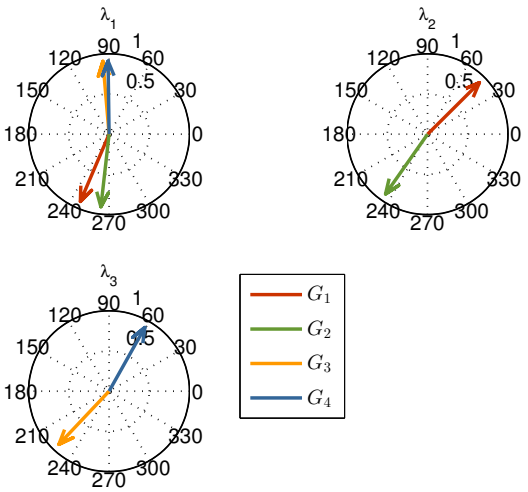

Figure 2.11: Mode-shape for the three electromechanical modes. λ_1: inter-area mode, λ_2: area 1 local mode, and λ_3: area 2 local mode.

The right eigenvector contains information on the grouping of the generators within the oscillation but not on the participation in the oscillation. For this end the participation factors are computed as the product between the right and the left eigenvector, cf. (2.16). For the inter-area and the two local area oscillations, the scaled speed participation factors are shown in Table 2.1. The participation factors reveal that all generators have a high participation in the inter-area mode, while only the generators in area 1 have high participation in the local-area mode

for this area, and vice versa for the local mode for area 2.

Table 2.1: Speed mode participation factors. λ_1: inter-area mode, λ_2: area 1 local mode, and λ_3: area 2 local mode.

State variable	$\lvert p_{\lambda_1}\rvert$	$\lvert p_{\lambda_2}\rvert$	$\lvert p_{\lambda_3}\rvert$
ω_1	0.6186	0.8145	0.0197
ω_2	0.3387	1.000	0.0514
ω_3	1.000	0.0489	0.7052
ω_4	0.8005	0.0299	1.000

2.3 Residues for Controller Tuning

The mapping of input u to output y in the state space description of (2.6) can be expressed in terms of the transfer function [66, 99]

$$G(s) = \frac{y(s)}{u(s)} \tag{2.24a}$$

$$= C_y(sI - A)^{-1}B_u + D_{yu} \tag{2.24b}$$

$$= K\frac{N(s)}{D(s)} + D_{yu} = K\frac{(s-z_1)(s-z_2)\cdots(s-z_n)}{(s-\lambda_1)(s-\lambda_2)\cdots(s-\lambda_n)} + D_{yu}. \tag{2.24c}$$

Provided that the eigenvalues of the system are distinct it is possible to do the partial fraction expansion

$$G(s) = \frac{R_1}{s-\lambda_1} + \frac{R_2}{s-\lambda_2} + \cdots + \frac{R_n}{s-\lambda_n} + D_{yu}. \tag{2.25}$$

Here, R_h is the residue for the hth eigenvalue for the transfer function (2.24a). The residues may also be computed directly from the state space description

$$R_{yu}^h = C_y\psi_h\phi_h B_u. \tag{2.26}$$

From (2.26) it is seen that the residue is the product between the observability and controllability of the hth mode in the input, output pair, u, y. Consider the feedback $u(s) = kC(s)y(s)$; the transfer function is then given as

$$y(s) = \left[\sum_{i=1}^{n}\frac{R_i}{s-\lambda_i} + D\right]kC(s)y(s) \tag{2.27}$$

where the eigenvalues of the controlled system are computed as the roots of

$$0 = 1 - \left[\sum_{i=1}^{n} \frac{R_i}{s - \lambda_i} + D\right] kC(s). \tag{2.28}$$

Next, consider the mode shift of the hth eigenvalue, $\lambda_{h,\text{new}} = \lambda_h + \Delta\lambda_h$ by evaluating the limit of (2.28) at the complex frequency $s = \lambda_{h,\text{new}}$ as k and $\Delta\lambda_h$ approaches zero.

$$\lim_{\substack{k=0 \\ \Delta\lambda_h=0}} \left(1 - \left[\frac{R_h}{\lambda_h + \Delta\lambda_h - \lambda_h} + \sum_{\substack{i=1 \\ i\neq h}}^{n} \frac{R_i}{\lambda_h + \Delta\lambda_h - \lambda_i} + D\right] kC(\lambda_h + \Delta\lambda_h)\right)$$

$$= 1 - \frac{R_h}{\Delta\lambda_h} kC(\lambda_h) = 0 \tag{2.29}$$

hence

$$\Delta\lambda_h = R_h kC(\lambda_h). \tag{2.30}$$

From (2.30) it is given that the residue for an eigenvalue for the transfer function between output, y, and input, u, is the sensitivity of this eigenvalue to a scalar feedback control. The magnitude of the residue is thus a measure of the impact of the control gain on the eigenvalue while the angle indicates the direction of the eigenvalue movement. This is schematically illustrated in Figure 2.12a where $G(s)$ is the uncontrolled system, that is, the power system model without the additional control, $C(s)$ the proposed control, and k the control gain. The concept of residue angle and required phase compensation of $C(s)$ to achieve pure damping is illustrated in Figure 2.12b.

2.4 Synchronizing and Damping Torques

The synchronizing and damping torques for a synchronous machine are defined from the swing equation of this machine. That is, the relation between the rate of change of speed and the torque imbalance on the shaft [99]

$$\begin{aligned} \Delta\dot{\omega} &= \tfrac{1}{2H}\left(\Delta T_m - \Delta T_e\right) \\ &= \tfrac{1}{2H}\left(\Delta T_m - K_s\Delta\delta - K_d\Delta\omega\right) \end{aligned} \tag{2.31}$$

where H is the inertia constant, and K_s and K_d are known as the synchronizing and the damping torque coefficient, respectively [66]. The

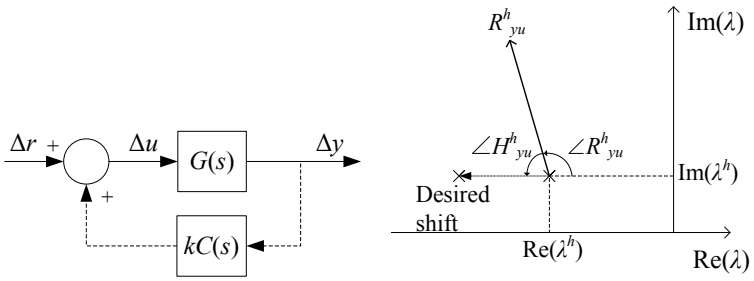

(a) Feedback control. **(b)** Eigenvalue sensitivity.

Figure 2.12: Effect of controller tuning on modal damping.

synchronizing and damping torques are hence the component of electromagnetic torque, ΔT_e, in phase with rotor angle, $\Delta\delta$, and rotor speed, $\Delta\omega$, respectively.

Figure 2.13 provides an overview of the machine interactions in a multimachine system with N synchronous machines, and a machine j that is interfaced through a full-load converter. Although greatly simplified, the figure shows how the rotational mechanical system of the synchronous machines is directly coupled to the network, since the injected currents are a function of $\Delta\delta$ and $\Delta\psi_{fd}$. Recently an increasing number of non-synchronous units are being connected to the grid, including converter interfaced power production units, FACTS devices, etc. For such units, here illustrated with a WT, the only connection between the network and the rotational system, if such exist for the particular unit, is through the controller with the generator side converter controlling the rotational speed of the generator, ω_g. As a result, the terms synchronizing and damping torques of the rotational mechanical system of a WT has little meaning in the conventional sense of (2.31).

In a single machine infinite bus system, the synchronizing and damping torques are given directly when the generator equations are put together with the stiff voltage source at the infinite bus. In a multimachine system, however, the multiple paths, the number of equations, and the mutual interaction between the machines complicate matters. To compute the synchronizing and the damping torque for a multimachine system, first consider a power system modeled with the standard state space description in (2.6). Then consider a partitioning that separates

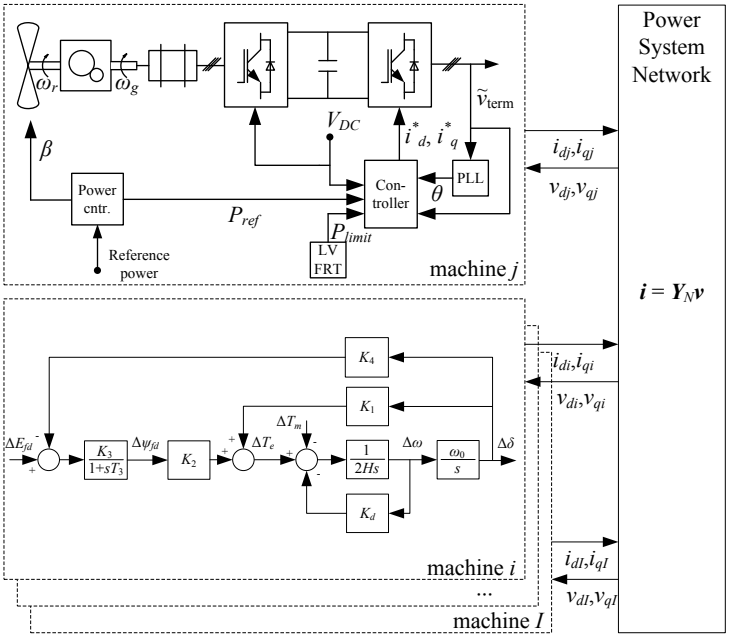

Figure 2.13: Schematic illustration of machine interactions in a multimachine power system.

the subsystem which contains the generator rotor dynamics [99]

$$\begin{bmatrix} \dot{\delta} \\ \dot{\omega} \\ \dot{x}_o \end{bmatrix} = \left[\begin{array}{cc|c} A_{\delta\delta} & A_{\delta\omega} & A_{\delta x_o} \\ A_{\omega\delta} & A_{\omega\omega} & A_{\omega x_o} \\ \hline A_{x_o\delta} & A_{x_o\omega} & A_{x_o x_o} \end{array}\right] \begin{bmatrix} \delta \\ \omega \\ x_o \end{bmatrix} + \left[\begin{array}{c} B_\delta \\ B_\omega \\ \hline B_{x_o} \end{array}\right] u$$
$$\begin{bmatrix} T_e \\ T_m \end{bmatrix} = \left[\begin{array}{cc|c} C_{T_e\delta} & C_{T_e\omega} & C_{T_e x_o} \\ C_{T_m\delta} & C_{T_m\omega} & C_{T_m x_o} \end{array}\right] \begin{bmatrix} \delta \\ \omega \\ x_o \end{bmatrix} + Du \tag{2.32}$$

here indicated in the expanded state space matrices by dividing lines. In (2.32), δ is a vector with the rotor angle states for all the generators in the system and ω is similarly a vector with all the speed states. If δ and ω are considered input to the subsystem described by x_o, the state equations for this subsystem is given by

$$\dot{x}_o = A_{xx}x_o + A_{x\delta}\delta + A_{x\omega}\omega. \tag{2.33}$$

Replacing $\dot{x}_o$ by sx_o and using that $s\delta = \omega$, the transfer functions from

δ to electrical, T_e, and mechanical torque, T_m, are given as

$$x_o(s) = (sI - A_{xx})^{-1} (A_{x\delta} + sA_{x\omega})\,\delta \tag{2.34a}$$
$$T_e(s) = C_{T_e x_o} x_o(s) + (C_{T_e \delta} + sC_{T_e \omega})\delta \tag{2.34b}$$
$$T_m(s) = C_{T_m x_o} x_o(s) + (C_{T_m \delta} + sC_{T_m \omega})\delta. \tag{2.34c}$$

If (2.34b) and (2.34c) are substituted into (2.31), a transfer function is obtained that is suitable for calculation of the frequency dependent synchronizing and damping torques in a multimachine system

$$\begin{aligned} s\omega(s) &= \tfrac{1}{2H} (T_m(s) - T_e(s)) \\ &= -\tfrac{1}{2H} (K_s(s) + sK_d(s))\,\delta(s) \end{aligned} \tag{2.35}$$

When evaluating the synchronizing and damping torques as in (2.35), it should be remembered that only the diagonal terms of $K_s(s)$ and $K_d(s)$ relate the speed deviation of machine j with the swing equation of the jth machine. The off-diagonal terms are relating the speed deviation of the other synchronous generators with the jth swing equation, and the impact in terms of stability depends on the phase of the oscillations of these machines with respect to machine j. For a two machine, two area system as analyzed in [100, 112], the generators oscillate in counter phase and any positive or negative effects are readily identified, where positive diagonal elements and negative off-diagonal elements represent a positive damping contribution. Although the generators in a multimachine system will group in an oscillation and have similar phase of oscillation within the group, it may be a challenge to compute the net impact using the approach outlined with (2.35). From a system stability perspective, it should be mentioned that the outlined approach gives the contribution to $K_s(s)$ and $K_d(s)$ that are induced on the machines from the network side when the machines are oscillating at a certain frequency. The ijth component is thus the torque induced on the ith generator when the jth generator is oscillating with a frequency of $j\omega$, where the oscillation of generator j is considered input to the model and $K_s(s)$, $K_d(s)$ output. This means that the internal feedback in the generators is not considered and that the computed synchronizing and damping torques do not represent the overall system stability, but are components of the overall torques in the machines.

2.5 Induced Torque Coefficient

Eigenvalue analysis is commonly used to analyze systems for small-signal stability and provides valuable information about the inherent stability properties of the system. A challenge with the method is to

identify the root cause of a an observed shift in the stability properties. In [42, 94], induced torque coefficients (ITC) are introduced as a means to analyze the damping impact from FACTS stabilizers in multimachine systems. The framework for ITC is an extension to the analysis of the synchronizing and damping torques, where the challenge about relating an induced torque on machine j from machine i is considered directly.

The calculation of the ITCs is based on the PVr transfer function, which is the transfer function from exciter reference voltage to the active power output of the synchronous generators and it is computed with all shaft dynamics disabled [39, 40]. The rationale behind ITC is that although a FACTS stabilizer, or in this case a WT, does not have a mass, which is synchronously connected to the network, there is still a path from the currents, i_{dj}, i_{qj}, of machine j through the network to the electromagnetic torque of machine i. From machine j it is thus possible to induce an electromagnetic torque on machine i and that torque may be decomposed into torques in phase with $\Delta\delta_i$ and $\Delta\omega_i$.

For the ith machine, the damping torque induced by the jth stabilizing unit, D_{ij}, is thus the component of torque in phase with $\Delta\omega_i$, where it is utilized that the per unit air-gap power, ΔP_e, equals the per unit air-gap torque, ΔT_e, [66]. The transfer function is then given as [94]

$$D_{ij} = \frac{\Delta T_{e,ij}}{\Delta\omega_i} = \frac{\Delta P_{e,ij}}{\Delta\omega_i} \tag{2.36a}$$

$$= \underbrace{\frac{\Delta P_{e,ij}}{\Delta u_j}}_{H_{\mathrm{PVr}}} \underbrace{\frac{\Delta u_j}{\Delta y_j}}_{j\text{th PSS}} \frac{\Delta y_j}{\Delta\omega_i} \tag{2.36b}$$

where Δu_j is the input signal to the jth unit from the stabilizer and Δy_j is the signal from which the oscillation is observed. In (2.36b), the last expression relates the speed deviation on machine i to the stabilizing input signal of the jth stabilizing unit, that is, PSS, FACTS device, etc. If only the hth mode, λ_h, is excited, then the state vector is described as $\Delta x = \phi_h \mathrm{e}^{\lambda_h t}$ [66]. Any output Δy_j is then given by $C_j\phi_h$, where C_j is the row of the output matrix in (2.6) that corresponds to Δy_j. Equation (2.36b) is then given as

$$D_{ij}^h = \frac{\Delta P_{e,ij}}{\Delta u_j}(\lambda_h)\frac{\Delta u_j}{\Delta y_j}(\lambda_h)\frac{C_j\phi_h}{C_i\phi_h} \tag{2.37a}$$

$$= \chi_{ij}^h \frac{\Delta u_j}{\Delta y_j}(\lambda_h) \tag{2.37b}$$

where each transfer function is evaluated at $s = \lambda_h$, where C_i is the row in the output matrix that corresponds to $\Delta\omega_i$, and where χ_{ij}^h is a

complex number, which is independent of the applied control and which represents the impact of stabilizer j on the ITC of the ith synchronous generator for the hth mode. From the ITC for the hth mode, D^h, a first order approximation of the mode shift of the hth mode is given as [94]

$$\Delta\lambda_{h,ij} = -\frac{p_{ih}}{2H_i} D^h_{ij} \tag{2.38a}$$

$$= -\frac{p_{ih}}{2H_i} \chi^h_{ij} \frac{\Delta u_j}{\Delta y_j}(\lambda_h) \tag{2.38b}$$

where H_i is the inertia constant of the ith synchronous generator and p_{ih} is the participation factor of the speed state of the ith synchronous generator for the hth mode. Let

$$\xi^h_{ij} = -\frac{p_{ih}}{2H_i} \chi^h_{ij} \tag{2.39}$$

and denote $\xi^h_j = \sum_{\forall i} \xi^h_{ij}$. It can then be proved that ξ^h_j is equivalent to the residue between output Δy_j and input Δu_j [96], and examining the elements of ξ^h_{ij} thus reveals the contribution of each synchronous generator to the residue of the hth system mode.

Summing over all i in (2.38) then gives the predicted mode shift when the controller $\frac{\Delta u_j}{\Delta y_j}$ is inserted into the loop

$$\Delta\lambda_{h,j} = \frac{\Delta u_j}{\Delta y_j}(\lambda_h) \sum_{\forall i} \xi^h_{ij}. \tag{2.40}$$

Using (2.40) it is possible to predict the mode shift of the hth eigenvalue due to the presence of the jth controller, $\frac{\Delta u_j}{\Delta y_j}$. Similarly, summing over all j gives the total mode shift due to the stabilizing action of all the stabilizing units. The prediction of the hth closed-loop eigenvalue, $\hat{\lambda}_{h,cl}$, is then given from the open-loop eigenvalue, $\lambda_{h,ol} = \lambda_h$, and the predicted mode shift as calculated in (2.40)

$$\hat{\lambda}_{h,cl} = \lambda_{h,ol} + \Delta\lambda_{h,j} \tag{2.41}$$

2.6 Alternative Means of Analysis

2.6.1 Theory of Normal Form

For highly non-linear systems, the accuracy provided by a linear approach may be insufficient to accurately determine the dynamic characteristics of the system [126], which has led to inclusion of higher order

terms using the theory of normal forms. The theory of normal forms has developed as a method to simplify the analysis of complex non-linear dynamics [13, 87]. The method is based on a sequel of non-linear coordinate transformations in which the non-linear terms successively are transformed to their simplest form, that is, their normal form. In [75, 106] the fundamental framework are presented for power system analysis using normal forms.

2.6.2 Bifurcation Analysis

Bifurcation analysis originates from the analysis of complex and highly non-linear dynamic systems, and is the study of qualitative or structural changes in the system as one or more system parameters are slowly varied [107, 113]. Using continuation methods, the dependency of the system dynamic properties to the continuation parameter is traced to form a bifurcation or branching diagram.

Bifurcation theory and continuation methods are extensively used in the PhD thesis by Dong [25] to study power system stability and security boundaries. As detailed in [25], different power system stability phenomena are closely related to system bifurcations. Where, for example, voltage collapse may origin as a saddle-node bifurcation, emergence of undamped power system oscillations as a Hopf bifurcation, or instability caused by limiters in the control or in the components as a limit-induced bifurcation. The general use of bifurcation theory for power system studies is presented in [4], whereas a study of damping controllers for power system oscillations in the view of Hopf bifurcations is presented in [83]. Yang et al. [130] perform a continuation analysis on different machine and external parameters of a DFIG infinite bus system, and shows that Hopf bifurcations may arise if the DFIG controllers are not properly tuned. In [73], bifurcation theory is used for the calculation of parameter changes that are critical with respect to saddle-node or Hopf bifurcations. Based on the solution of this critical distance problem in the parameter space, Makarov et al. [73] suggest that a stability proximity index can be based on the length of the solution vector. The impact of the exciter voltage limit on the power system small-signal stability is studied in [45] where it is concluded that the presence of non-differential elements such as limiters has great impact on the small-signal stability region. It is concluded that such non-differential components should be included in future small-signal stability studies.

Chapter 3

Analysis of Present Normal Operation of WPPs

The impact of increased penetration of wind power on the power system small-signal stability has been analyzed in a number of publications for the different available WT technologies. A large scale integration of wind power clearly has the potential to change the modal characteristics of the system by

1. significantly change the dispatch of the existing power units,
2. significantly alter the power flows in the system, and
3. interacting with the synchronous machines through the transmission network to change the synchronizing and damping torques induced on their shafts.

Here, *1)* and *2)* are the consequence of a changed power in-feed pattern and of which synchronous generators and stabilizing units that are disconnected, and as such not related to any specific power production technology. A more elaborate discussion is carried out in [128]. Case *3)*, on the other hand, does depend on the power conversion technology and the utilized control.

A number of small-signal stability studies that involve different WT concepts have been reported in the literature. An overview of published studies was presented in section 1.2.1.

Although complicated in practice, it is advantageous to attempt to isolate the factors that drive the changes in the modal characteristics when the impact of WPPs on the small-signal stability of power systems is analyzed, such that cause and effect are more clearly drawn up. This is advisable for clarity and to facilitate the comparison between studies from different researchers on the impact on small-signal stability of increased penetration of wind power. When country specific penetration studies are conducted, this isolation of the factors makes less sense, since it is here the changed stability picture that is in focus. This, on the other hand, means that it might be difficult to attribute any changes in the small-signal stability to a specific factor, that is, power flow changes, power production technology, etc.

If it is found that the output of the WPP(s) has significant impact on the modal characteristics, it could be relevant to consider stochastic methods due to the intermittent power output of a WPP, which is caused by the stochastic and uneven wind conditions on the WPPs in the system and on the WTs within a WPP. Monte Carlo simulations are proposed in [46, 88, 102, 109] for stochastic power system analysis, while a probabilistic collocation method is proposed in [133], which may provide an approximation with less computational effort compared to the Monte Carlo approach. In [109], the use of Monte Carlo simulations is demonstrated for the analysis of the impact of stochastic wind conditions on the damping of power system oscillations.

The interaction between market operation and security assessment is studied by Zarate-Minano et al. [131]. Here, an optimal power flow (OPF) approach is proposed that explicitly considers the security limits of voltage and small-signal stability of the power system. When the market dispatch violates a security limit, a computation of the optimal generator redispatch and amount of load shedding is conducted.

The results presented in section 3.1 focus on the impact of the WT technology, that is case *3)*, and the study has, thus, been conducted to limit the impact of changed power flow patterns, while gradually increasing the penetration of the WPP.

The results presented in this chapter are detailed in the papers

- "Small-Signal Stability of Wind Power System With Full-Load Converter Interfaced Wind Turbines" [61], and

- "Induced Torques on Synchronous Generators from Operation of Wind Power Plant based on Full-Load Converter Interfaced Wind Turbines" [55].

3.1 Participation of WPPs in Power System Oscillations

The full converter between the WT generator and the grid has the effect of decoupling the generator dynamics from the grid dynamics, and extending this argumentation the WT generators cannot contribute to power system oscillations. However, as the WTs and the WPPs are equipped with various controllers to provide system services, it is possible that the controllers can interact with system dynamics and impact the small-signal stability. Such interaction may be investigated with aid of participation factors to identify states that play a dominant part in the oscillatory modes.

The study is based on the seven generator power system described in section 2.1.1.3, which has a dominant inter-area mode, λ_1, that separates generator G_1 and G_2 from the remaining generators. Only selected results are presented here while the full paper [61] is found in appendix A.1.

3.1.1 Considered Strategies to Accommodate an Increased Penetration of Wind Power

To accommodate new production capacity, part of the existing power production units must either reduce their power production or disconnect from the power system, if there is not an equivalent increase in the demand. Two cases are here considered to capture these two fundamentally different approaches to accommodate an increased penetration of wind power.

1. The active power output of the nearby generator, G_2, is reduced to accommodate the increased power in-feed from the WPP while the MVA rating is maintained. That is, all synchronous generators remain connected but G_2 operate at a reduced set-point.

2. The MVA rating of the nearby generator, G_2, is reduced as the penetration of wind power increases while the loading is maintained. In other words, the WPP displaces synchronous generators, which are disconnected.

It should be noted that the power production is only shifted from G_2 to the WPP, which are connected to the same high voltage bus, and that the power flow in the system is unchanged for all the investigated wind power penetration levels and for both cases. The capacity of the WPP is increased linearly from 36 to 1 000 MW in ten steps. The study is repeated as shown in Table 3.1 to capture different modes of operation of the WTs and the WPP in terms of wind conditions, curtailed operation, and the presence of park level voltage control.

Table 3.1: Overview of analyzed case studies.

	Case	Active power production [pu]	Park level voltage control
High wind	1, 2	1	with/without
Medium wind	1, 2	0.69	with/without
Low wind	1, 2	0.14	with/without
Medium production	1, 2	0.69	without
Low production	1, 2	0.14	without

3.1.2 Impact of Increased WPP Penetration on the Small-Signal Stability

An overview of the system eigenvalues in the last step with a 1 000 MW of wind power is shown in Figure 3.1 for both accommodation strategies. Only results from case 1 will be shown in the following but similar results are found for the case 2 accommodation strategy.

The trajectories of the dominant inter-area mode, λ_1, for increasing WPP capacities are shown in Figure 3.2 for the investigated WPP operating conditions for case 1. The eigenvalue trajectories are grouped in terms of the active power output of the WPP. A minor increase in the damping ratio is noted when the WPP output is below rated power, while a slowly decreasing trend is found for top half of WPP capacities when the WPP outputs rated power.

Compared to the base case without wind power, the relative increase in the damping ratio of λ_1 when the WPP capacity is 1 000 MW is between -0.80 and 5.5 % and a similar impact is found for the other inter-area modes.

Selected participation factors are shown in Figure 3.3 for a WPP capacity of 1 000 MW where it is shown that the participation of the WT mechanical system is orders of magnitude smaller, $\simeq 10^{-5}$, than the participation of the synchronous machine mechanical system. The

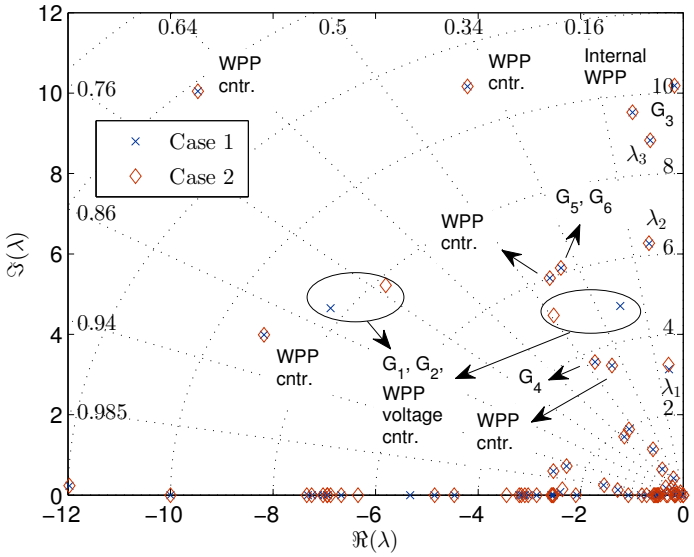

Figure 3.1: Overview of the complex plane with the system eigenvalues for both case 1 and 2 with 1 000 MW of wind power.

maximum WPP participation is found in either the WT voltage controller or in the WPP voltage controller. It is, furthermore, seen that the power output of the WPP does not significantly impact the participation of the synchronous generators in the eigenvalue, since uniform ratios appear in the participation factors irrespective of the WPP power output.

To evaluate the sensitivity of the WT and WPP control tuning on the modal characteristics of the dominant inter-area mode, λ_1, selected control parameters are in turn varied from their nominal value with ± 40 %. A case 1 high wind scenario with a WPP capacity of 1 000 MW is used for the sensitivity evaluation. The considered controllers are WT voltage control, WT active power control, park level WPP voltage control, and WT pitch control. For all controllers, parameters that affect both the speed and the gain of each controller are analyzed within the specified parameter range. The sensitivities are shown in Figure 3.4 where the arrows show increasing values of the control parameters, that is, from -40 % to $+40$ % of the nominal value. The largest sensitivity is found for the speed of the WT voltage controller followed by the speed and gain of the WPP voltage controller. The controllers for active

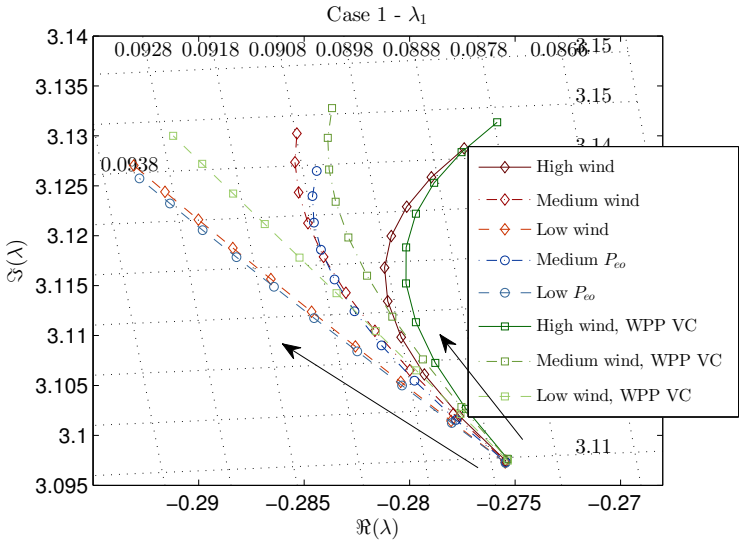

Figure 3.2: Comparison of eigenvalue trajectories for the dominant inter-area mode, λ_1, for integration strategy case 1. The arrows show the movement with increasing WPP penetration.

power control, that is, WT active power control and WT pitch control, only have a limited impact on the dominant inter-area mode, λ_1.

3.1.3 Discussion

The case study was designed to keep the power flow in the system unchanged irrespective of the WPP capacity by balancing the output of the WPP with an adjacent synchronous generator. This design was chosen to be able to isolate the impact of the WPP and not consider derived effects from changed power production and power flow patterns, or from changes to the voltage profile of the system. For both accommodation strategies and for all the investigated operating scenarios, the study found that the modal characteristics of the inter-area modes were largely unaffected by the increased penetration of the WPP. However, a more complex picture might be found for actual integration studies, since the derived effects from the changed production patterns should also be included. Regarding the accommodation strategy, a ranking index of the synchronous generators is proposed by Alhasawi and Milanovic [10] in order to find an integration strategy for WPPs that does not leave the power system with detrimental dynamic properties, be-

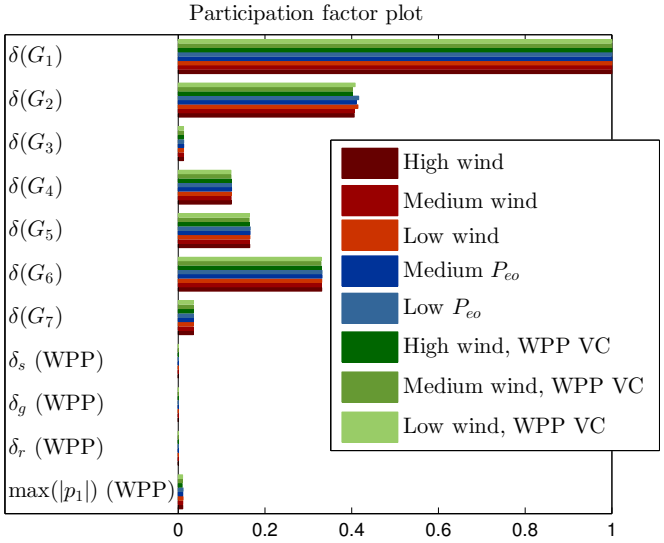

Figure 3.3: Comparison of selected, normalized participation factors for the dominant inter-area mode, λ_1, for case 1. For the WPP, participation factors are shown for mechanical shaft-, generator-, and rotor-angle states, as well as the maximum participation over all WPP states.

cause synchronous generators with a stabilizing effect on the system are disconnected to accommodate the power in-feed from the WPP. A case study based on the generator ranking index is presented in [10] and it is recommended to de-load the most influential synchronous generators to do a large scale wind power integration. The conclusion that the synchronous generator displacement strategy is very important with respect to the resulting modal properties of the power system, is also reported by Modi et al. [84] in a case study on an Australian equivalent network.

The results in Figure 3.3 support that there is a general decoupling between the WT mechanical system and the grid dynamics when the WTs are in a state of operation where the conditions for the linear representation are satisfied. The same conclusion is found by Strachan and Jovcic [114] in a study on voltage controller design for weak power grids.

The linear model that is used to calculate the eigenvalues and the participation factors are computed from a first order Taylor expansion of the

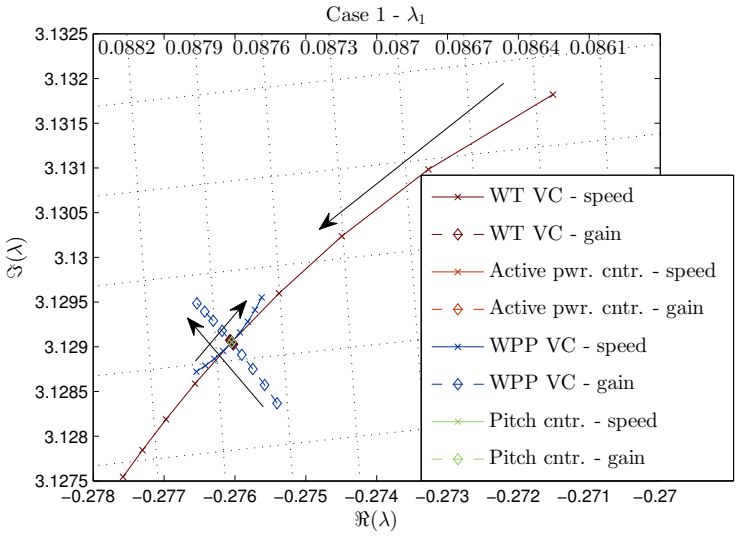

Figure 3.4: Sensitivity of the dominant inter-area mode, λ_1, to perturbations of ± 40 % on selected WT and WPP control parameters. The arrows show increasing parameter values. Sensitivities are evaluated for a case 1 high wind scenario with a 1 000 MW of wind power.

non-linear WT model. In this representation, the system is described in terms of deviations from the steady state and it is implicitly given that all the state variables can move freely in all directions. This means that for example limiters have no representation and that other highly non-linear behaviors are not accurately represented in the linear model. An important difference between a synchronous machine and a power converter, is that the latter has more sharply drawn operational limits and are often controlled much tighter than the synchronous machine. To optimize the power extraction from the wind, a full converter WT uses different control regimes in different modes of operation, which means that the WT can be put in an operating condition where only a small perturbation causes a change in the control regime. These power converter and variable speed WT characteristics may challenge the accuracy of the linear representation from certain operating conditions and, hence, of the findings obtained from eigenvalue analysis. From a practical perspective, the dynamic properties in very specific operating conditions, or in narrow bands around these, might be of limited importance, since a WT is operating under fluctuating wind conditions

and consequently, under changing operating conditions. The validity of the linear approximation in these regime changing operating conditions, hence might be of mostly theoretical interest.

The finding that the WT and WPP voltage controllers have the most significant, although still small compared to the synchronous generators, participation in the rotor angle oscillations is supported by the results from Tsourakis et al. [122], Vittal et al. [125]. A study on the impact of dynamic voltage support on the small-signal stability is presented in [29] where a large scale system study on the Nordic interconnected system is conducted. Here it is found that a SVC used for voltage control had a positive impact on the modal damping when located in an export area, where a detrimental effect was found when located in an import area.

3.2 Effect of Park Level Voltage and Frequency Control on the Small-Signal Stability

A trend in wind power is that more functionalities and system services are expected delivered from the WPPs, and to this end the WPPs are fitted with auxiliary controllers to deliver the service in question. As discussed in section 2.3 and shown in Figure 2.12, any feedback control will affect the closed-loop performance of the power system.

In this study the framework of induced torque coefficients (ITC), cf. section 2.5, is introduced for analysis of two commonly used auxiliary WPP controllers, that is, voltage and frequency droop controllers. An advantage with ITC is that the eigenvalue sensitivity to a planned controller is evaluated and assessed directly on the open-loop system, which means that important information on the impact on the small-signal stability is revealed early in the design process of the planned controller.

The full study is found in [55] which is included as appendix A.2.

3.2.1 Investigated WPP Controllers

The WPP is equipped with generic droop controllers for PCC voltage and frequency control. The block diagrams for the droop controllers are depicted in Figure 3.5 where d is the droop characteristic, LP a low-pass filter, and PI a proportional and integral controller. The dead band in Figure 3.5b is used for time domain simulation and can be omitted for small-signal analysis.

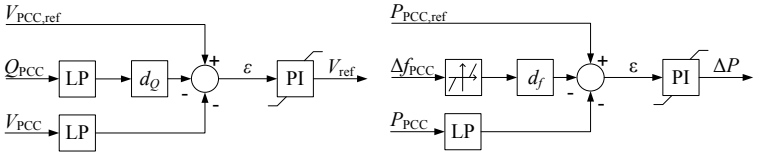

(a) Park level voltage controller. **(b)** Park level frequency controller.

Figure 3.5: Block diagrams of generic voltage and frequency controllers.

For the voltage control a droop factor of 4 % is used, whereas a droop factor of 0.6 $\frac{\text{pu}}{\text{Hz}}$ is used for the frequency control.

The study is based on the four generator system presented in section 2.1.1.2 and is repeated where the in-feed location of the WPP is transversing the length between the two groups of oscillating machines.

3.2.2 Torques Induced on the Synchronous Generators from the WPP Controllers

The induced torques on each synchronous generator in the system due to a feedback between bus frequency and active power output is shown in Figure 3.6 for a WPP capacity of 108 MW. From the calculated ITCs, it can be seen that a positive damping torque is induced onto the synchronous generators in the nearby area, $G_{1,2}$, while a smaller negative damping torque is induced onto the synchronous generators in the distant area. As the WPP is moved along the inter-tie towards the center point of the oscillation, the positive damping torque on $G_{1,2}$ reduces while the negative damping torque on $G_{3,4}$ increases. When the WPP is moved beyond the center of the oscillation, the roles of $G_{1,2}$ and $G_{3,4}$ are interchanged. Similar curves are computed for the frequency controller and a WPP capacity of 324 MW and for a WPP voltage controller for both WPP capacities. These plots are found in appendix A.2. For the voltage control, a far more complex picture of ITCs is found from which the impact of the controller cannot be readily identified without information on the design of the WPP voltage controller itself.

In Figure 3.7, the predicted mode shift is compared to the actual mode shift that is obtained when the controllers are inserted and the feedback closed. The direction of the arrow shows the movement of the WPP from the sending end side towards the receiving end of the inter-tie. First of all it is noted that the predicted mode shifts have good

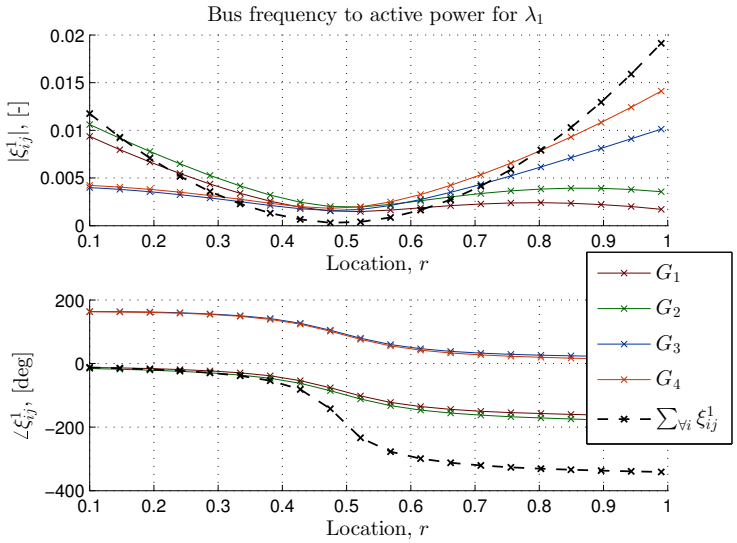

Figure 3.6: Effect of feedback controller between bus frequency and active power set point. The capacity of the WPP is 108 MW.

resemblance with the actual closed-loop eigenvalues. Secondly, it is noted that the impact of the frequency controller is as predicted from Figure 3.6, with the largest positive contribution when the WPP is located towards either of the two oscillating groups of generators. While very limited impact is found when the WPP is located midway between the oscillating groups. The impact of the voltage control is less pronounced than that of the frequency control and the trajectory of the closed-loop eigenvalue resembles that of the open-loop system.

3.2.3 Discussion

Generally it is found that both in-feed location, WPP size, and the auxiliary control affect the modal characteristics of the investigated inter-area mode.

The ITCs show that the largest effect of the frequency droop controller is achieved when the WPP is located close to a group of synchronous generators, while a very low effect is found when the WPP is located midway between the two oscillating groups of synchronous generators. The same conclusions are reported in [100, 112] and also shown in [62], which is included as appendix A.3.

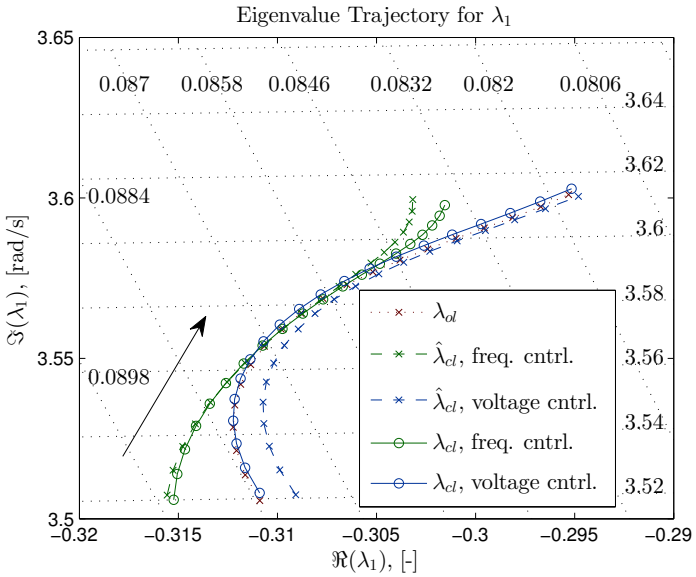

Figure 3.7: Comparison of predicted, $\hat{\lambda}_{cl}$, and actual closed-loop inter-area eigenvalue, λ_{cl}, for a WPP voltage and frequency controller when the PCC is traversing from the sending end of an inter-tie to the receiving end. The capacity of the WPP is 108 MW.

The finding that the feedback between bus frequency and active power output has a positive effect on the damping ratio is in line with Samuelsson [105, p.66], where it is proofed that for small control gains the active power controlled by the local bus frequency will add damping to all modes simultaneously. Similar results are reported by Gautam et al. [37] where an improved modal damping is found when the WTs are equipped with a controller, which is designed to mitigate the impact of reduced inertia in the power system, that changes the torque reference with a signal that is proportional to the frequency deviation. Ruan et al. [101] study the control of active and reactive power for VSC power stations using energy function analysis, and report that control of active power proportional to the frequency increases the rate of energy diminution and, hence, increases the damping.

It is shown and discussed that only a limited impact is found for the WPP voltage control, which might seem to contradict the referenced studies in section 3.1.3 where voltage control is highlighted as a significant subsystem with respect to small-signal stability. Here it should

be remembered that the WT is operating in local voltage control mode even when the WPP voltage control is disabled and that the results therefore are not contradictory. The study presented in section 3.1 that included a similar WPP voltage controller as the one analyzed here also found a limited impact from the WPP voltage control, cf. Figure 3.2.

A somewhat idealized representation of the interaction between the WPP controllers and WTs have been used in presented study, since the WPP controllers are represented without consideration of the processing and transmission delays that inevitably will be present. A fixed and regular delay will add a pure phase lag to the controller transfer function and, hence, from (2.37a) also to the phase of the ITCs. If a total delay associated with processing and transmission of 50 ms is considered, it would for the studied inter-area mode correspond to a phase lag of around 10°, which would not change the main conclusions from the paper.

Chapter 4

Control of WPPs for Improvement of Power Oscillation Damping

It is well established that the small-signal stability of a power system can be improved through proper reactive power modulation of FACTS devices [99] and this is in practice used by transmission system operators, as for example reported in [67]. For active power modulation, it has similarly been established that HVDC links may be utilized for power oscillation damping [112], which is also utilized in practice as illustrated in [22].

The ability to control both the active and the reactive power output of variable speed WTs, has inspired researchers to look into the possible use of WPPs based on variable speed WTs to actively contribute to the small-signal stability of rotor angle oscillations. The use of active power modulation is reported in [24, 30, 32, 48, 65, 80, 110, 121, 123], reactive power modulation in [3, 24, 32, 38], while the combination of both active and reactive power modulation is treated in [18, 24, 33, 35, 74], cf. section 1.2.2.

This chapter is based on the papers

- "Power Oscillation Damping Control of Inter-Area Oscillation Through

Active and Reactive Power Modulation from Wind Power Plants With Full Converter Wind Turbines" [62], cf. page 183, and

- "Power Oscillation Damping Controller for Wind Power Plant Utilizing Wind Turbine Inertia as Energy Storage" [54], cf. page 205.

4.1 Induced Damping Torques from ΔP and ΔQ POD at WPPs

As discussed in sections 2.4 and 2.5, the rotational masses of a full converter WT are not directly connected to the grid, but have a rotational speed that is determined by the machine side converter. In section 3.1 it was shown that the WT mechanical system has a very low participation in low frequency power system oscillations. This, however, does not imply that the control of WPPs and WTs cannot affect the modal characteristics of such power system oscillations. Both for active and reactive power modulation, this has been shown in the academic literature [99, 112] and has been demonstrated in practice [22, 67].

The framework for ITCs, as introduced in section 2.5, propose a means to calculate the component of damping torque that is induced on each synchronous generator as a consequence of an applied feedback control. The ITCs are closely related to residues [96], which give the modal sensitivity to a feedback control. Residues are here used to analyze the possibility and effectiveness of using WPPs for the delivery of damping torque to the synchronous machines to improve the modal damping of the power system. As shown by Ruan et al. [100], Smed and Andersson [112], the effectiveness, on the damping ratio of an inter-area mode of an active or a reactive power modulating damping control, is highly dependent on the in-feed location of the unit and the type of power modulation.

The setup from Ruan et al. [100], Smed and Andersson [112] with a two area system where the in-feed location of the WPP in traversing the length of the connecting inter-tie is adopted for this study. For each in-feed location, the residue is calculated for both a ΔP and a ΔQ POD to evaluate the impact of the distance to each of the oscillating areas. The residue is, cf. (2.26), the product of the mode observability and the mode controllability where both a good observability and a good controllability are needed in order to design an effective POD. To leave out the influence of a changing observability as the in-feed location changes, but only study the ability of the WPP to affect the modal characteristics of the inter-area mode, the generator speed difference across the inter-tie is used as input to the PODs. The generator speed

difference is independent of the location of the WPP and the residues calculated at the different in-feed locations may thus be compared in terms of ability of the WPP to affect the modal characteristics. Three WPP penetration levels are considered which are given from Table 4.1.

Table 4.1: Generator output in generator convention for the investigated power outputs a bus 3. The column "No loads" corresponds to $P_{L1,2} = Q_{L1,2} = 0$ in Figure 2.1 on page 19.

		No loads		Shunt loads	
Case #	P_{30} [MW]	P_{10} [MW]	P_{20} [MW]	P_{10} [MW]	P_{20} [MW]
C1	108	325	−433	1 292	1 334
C2	216	217	−433	1 184	1 334
C3	324	109	−433	1 076	1 334

First in section 4.1.1, an idealized system is considered with perfect decoupling of the active and reactive power control. Secondly in section 4.1.2, the study is repeated with a dynamic WPP model and considering the control of the synchronous generators. The results presented here are primarily based on the content of Knüppel et al. [62]

4.1.1 Frequency Domain Evaluation with Constant PQ Model

The study of the idealized system is based on the two area, two machine equivalent network given in section 2.1.1.1 where a constant PQ model represents the WPP. Initially the loads are neglected, that is, $P_{L1} = P_{L2} = Q_{L1} = Q_{L2} = 0$, and the system simplifies to the one studied in [100, 112] with one synchronous machine equivalent describing the sending end area and one that describes the receiving end area. The only source of damping in the system is a controllable component of active or reactive power at the WPP and the system is undamped when these are disabled. The derivation of the equations that describe the system is given in [62], which is found in appendix A.3.

The residues for both a ΔP and a ΔQ POD are given in Figure 4.1. The ΔP POD residues show that an active power modulation is most effective when close to one of the oscillating areas and that it should be in phase with the speed deviation of the synchronous generators in the nearby area. The ΔQ POD is most effective when located in between the two areas and the ability to affect the damping ratio of the inter-area mode depends on the production at the WPP and thereby on the

power flow on the inter-tie. These findings are similar to the results previously presented by Ruan et al. [100], Smed and Andersson [112]

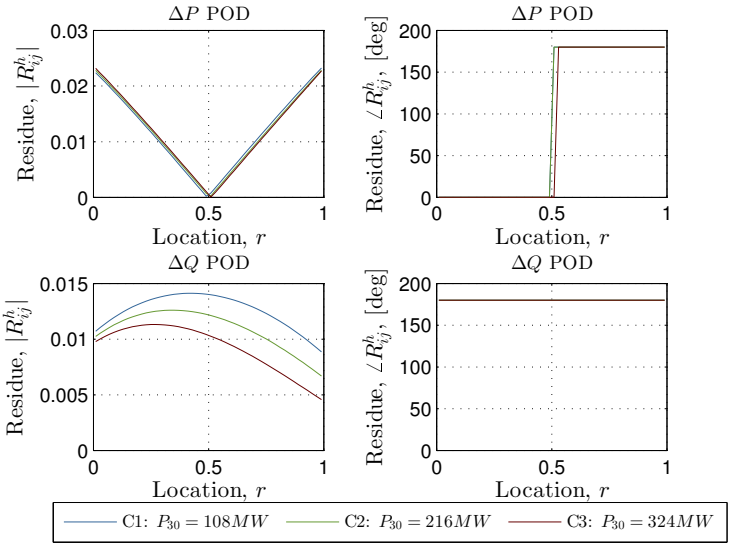

Figure 4.1: Open-loop residues as a function of the location r for a damping controller based on ΔP_3 (top row) or ΔQ_3 (bottom row) modulation. Results are for the two generator system without shunt loads.

If a constant PQ shunt load[1] is connected on both ends of the inter-tie such that both machines are operating as generators, some notable differences are seen in the residue characteristics. For the ΔP and the ΔQ POD these are seen in Figure 4.2 and 4.3, respectively, where also the closed-loop eigenvalues are shown for the resulting system with the POD enabled. First, it is for the ΔP POD seen that the center of the oscillation changes with the active power output of the WPP. Secondly, for the ΔQ POD it is seen in Figure 4.3 that, depending on the active power output from the WPP, the feedback changes sign.

To understand the mechanisms that cause the change of sign in the feedback, it is illustrative to take a closer look at how the modulated active or reactive power lead to changes in the modal damping. For the analyzed two machine system, this is can be done directly by inspection of the generator speed subsystem, $A_{\omega\omega}$, of its the state space

[1] It should be noted that the constant PQ load representation means that induced active load response has not been considered here.

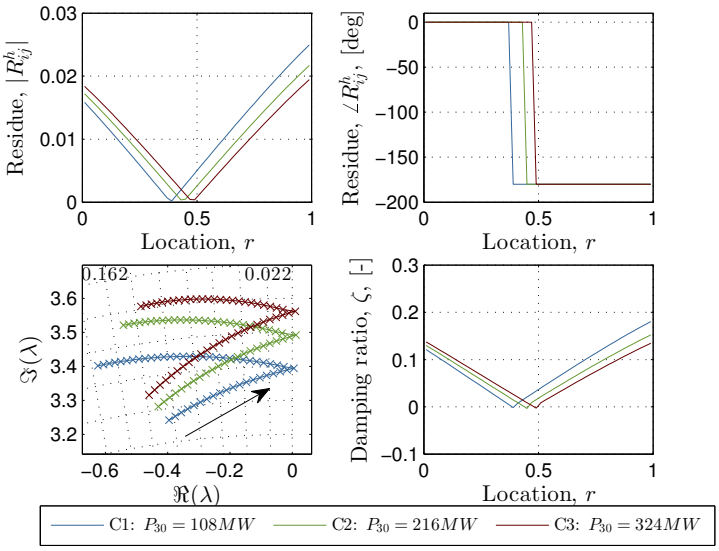

Figure 4.2: Open-loop residues and closed-loop eigenvalues as a function of the location r for a damping controller based on ΔP_3 modulation. Arrow shows increasing r. Results are for the two generator system with shunt loads.

representation. As discussed in section 2.4, the damping torque on a synchronous machine is the torque component in phase with the speed deviation of the machine. Since the only source of damping stem from the modulated output of the WPP PODs, the output of the WPP can be traced to a torque component in phase with the generator speed deviation of each generator. For a proportional feedback controller, the closed-loop state space system is calculated with $A_{cl} = A - BKC$, where K is the gain of the feedback control and where A, B, and C are as defined in (2.6). Both K and C are constant matrices that do not depend on the location r and any change in damping torque must therefore derive from B. Expanding the matrix manipulations in the DAE to ODE conversion, as shown in (2.5a), with $\hat{B} = A_{22}^{-1} B_2$ yield

$$\Delta\dot{\omega}_1 : \quad \eta_{V_1} \hat{B}_{V_1} + \eta_{\theta_1} \hat{B}_{\theta_1} \tag{4.1a}$$

$$\Delta\dot{\omega}_2 : \quad \eta_{V_2} \hat{B}_{V_2} + \eta_{\theta_2} \hat{B}_{\theta_2}, \tag{4.1b}$$

where the η's are the non-zero elements of A_{12}, where $\Delta\dot{\omega}_i$ is the differential equation that is affected by the control, and where the subscript of $\hat{B}$ corresponds to the algebraic variable mapped through this ele-

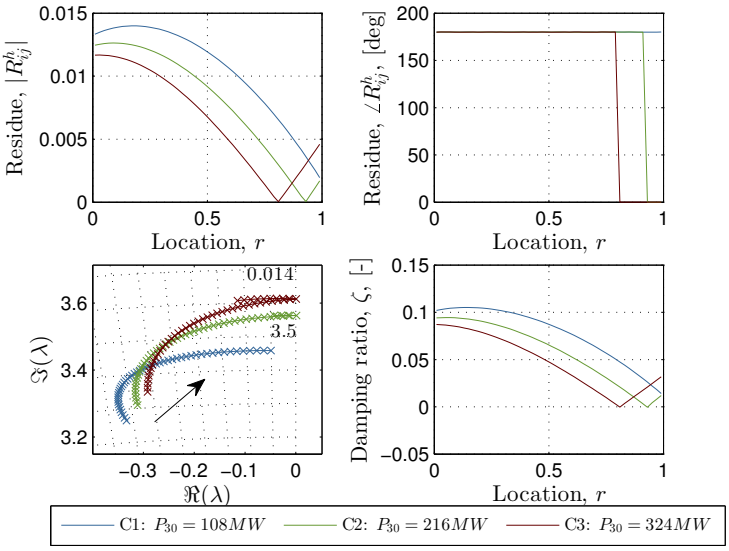

Figure 4.3: Open-loop residues and closed-loop eigenvalues as a function of the location r for a damping controller based on ΔQ_3 modulation. Arrow shows increasing r. Results are for the two generator system with shunt loads.

ment. In other terms, $\hat{B}_{V_1}$ is a mapping from ΔP_3 and ΔQ_3 to ΔV_1. From (4.1) the effect of the damping controllers can be decomposed into a perturbation of the generator terminal voltage magnitude, ΔV_i, and angle, $\Delta\theta_i$. The terminal conditions of G_1 and G_2 are mapped through A_{12} to a perturbation of $A_{\omega\omega}$, which describes the damping torques of G_1 and G_2. In other words, $\eta_{V_i}\hat{B}_{V_i}$ is the component of induced damping torque on machine i that derive from changes in the terminal voltage magnitude, while $\eta_{\theta_i}\hat{B}_{\theta_i}$ is the component that derive from changes in the terminal voltage angle.

The decomposition shown in (4.1) is in Figure 4.4 plotted for the ΔP and ΔQ PODs from, respectively, Figure 4.2 and 4.3. Intuitively, one would expect that an active power modulation would primarily affect the voltage angle while a reactive power modulation would primarily affect the voltage magnitude. From Figure 4.4 it is seen that the dominant contribution follows this pattern, but also that there is an impact from both the voltage magnitude and angle from both the ΔP and especially from the ΔQ POD. The ΔP POD effectively adds a positive damping torque to only one synchronous generator, while an amount of negative

damping torque is added to the other. At the center point of the oscillation, these cancel each other and the oscillation is undamped. For the ΔQ POD, it is seen that the contribution to the damping torque from modifying ΔV_i at some location, r, is completely countered by a negative damping torque contribution from $\Delta\theta_i$, thereby effectively changing the sign of the feedback. This location is marked in Figure 4.4 with dash-dotted vertical lines.

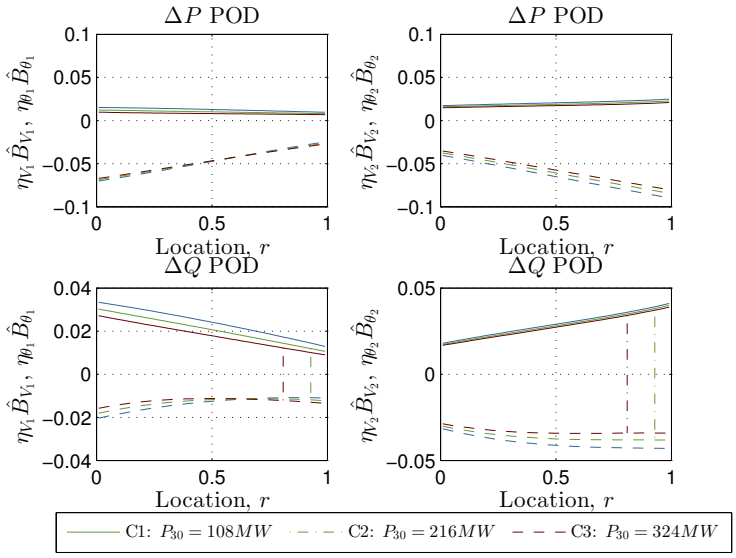

Figure 4.4: Contribution of ΔV and $\Delta\theta$ to the damping torque as a function of the location r for a damping controller based on ΔP_3 (upper plots) or ΔQ_3 (lower plots) modulation. The left hand side graphs show the induced damping torques on G_1 and the right hand side graphs the induced torques on G_2. $\eta_V \hat{B}_V$: solid, $\eta_\theta \hat{B}_\theta$: dashed.

4.1.2 Frequency Domain Evaluation with Dynamic WT Model

The system that was treated in section 4.1.1 is, as mentioned, highly idealized with, for instance, a perfect decoupling of the active and reactive power control for the WPP and with a simplified representation of the WPP and generator dynamics. To extend the study to a more complex, although still quite simple, system, the study was repeated

on the four machine system from section 2.1.1.2 to which a dynamic, aggregated WT model was connected.

The open-loop system residues and the closed-loop system eigenvalues are for the ΔP POD shown in Figure 4.5. The closed-loop eigenvalues are at each location computed with the ΔP POD inserted in the feedback, where the phase characteristic of the ΔP POD is computed according to the complement of the residue phase at this location, and with a constant loop gain at the inter-area mode frequency. The dashed curves show the residue characteristic for a damping control that uses the PCC frequency as input and it is seen that its residue characteristic is similar to the one with generator speed difference input. When comparing to the idealized characteristic in Figure 4.1, a good resemblance is found, although a closer inspection of especially the $P_{30} = 108$ MW case reveals that it has a softer curvature in the residue magnitude characteristic around the center of oscillation.

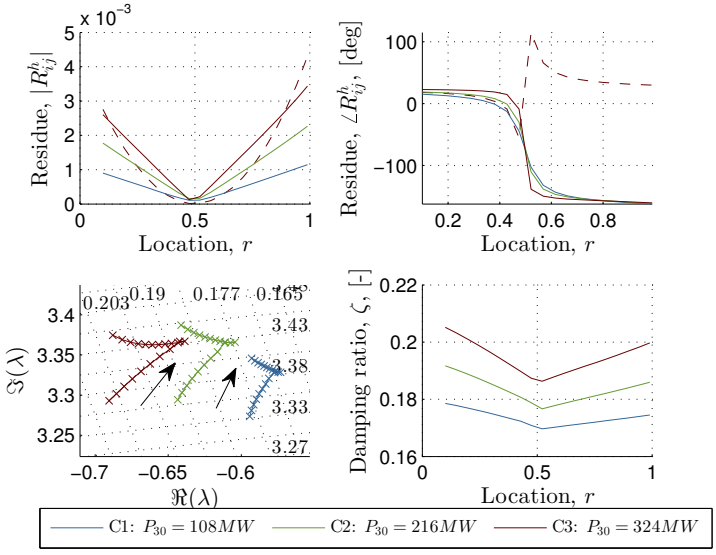

Figure 4.5: Open-loop residues and closed-loop eigenvalues and damping as a function of the location r for the ΔP POD. Results are for the inter-area mode in the four generator system. Dashed curve in residue plots are with PCC frequency as POD input and the magnitude is scaled with 10^{-1}.

The residue characteristic for the ΔQ POD and the closed-loop eigenvalues are given in Figure 4.6, and when compared to the idealized

characteristic in Figure 4.1 it appears that the residue characteristics have been turned upside down. With increasing active power outputs from the WPP, the magnitude of the residues approach the V-shape that is seen in the response from the ΔP POD. Similar findings are made for the residue phase characteristics that for increasing size of the WPP show increasing resemblance with the characteristic of the ΔP POD.

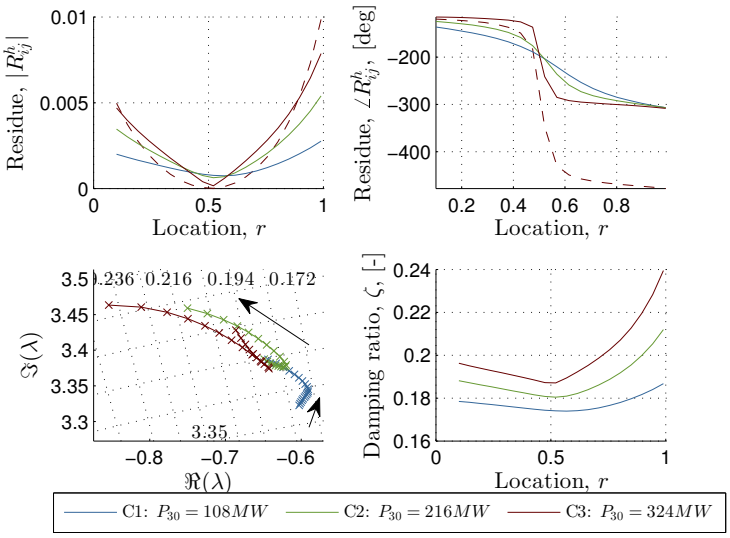

Figure 4.6: Open-loop residues and closed-loop eigenvalues and damping as a function of the location r for the ΔQ POD. Results are for the inter-area mode in for four generator system. Dashed curve in residue plots are with PCC frequency as input and the magnitude is scaled with 10^{-1}.

4.1.3 Time Domain Evaluation with Dynamic WT Model

To assess the accurateness of the linear model for the eigenvalue analysis where limiters and other highly non-linear phenomena are not accurately represented, time domain simulations have been performed on the non-linear system. In the time domain simulations, the system is excited with a 0.2 second, 5 % step change to the voltage reference of the exciter at G_1 in area 1. Investigated WPP POD configurations are

- $P, Q \in \{0, 0\}$: no WPP POD
- $P, Q \in \{1, 0\}$: ΔP WPP POD
- $P, Q \in \{0, 1\}$: ΔQ WPP POD
- $P, Q \in \{1, 1\}$: both ΔP and ΔQ WPP POD.

A comparison between the analytical modal characteristics for the inter-area mode and those computed from the time domain responses are shown in Table 4.2. First it is noted that very similar results are obtained, which show that the linear approximation in this case does not significantly affect the findings. Secondly, it is noted that the best performance is achieved with the combined use of ΔP and ΔQ PODs, while a pure ΔP POD performs second best, and the pure ΔQ POD shows the least improvement to the damping ratio. Although it is also clear from Table 4.2 that only small improvements are found for this well damped system. A plot of the time domain simulations is available in the paper in appendix A.3.

Table 4.2: Modal characteristics for the inter-area mode as computed from both eigenvalue analysis and as extracted from time domain simulations with synchronous generator PSSs in service.

	Modal analysis		Time domain	
	ζ	ω_d	ζ	ω_d
Configuration	[-]	[Hz]	[-]	[Hz]
$P, Q \in \{0, 0\}$	0.186	0.529	0.186	0.527
$P, Q \in \{1, 0\}$	0.205	0.524	0.210	0.537
$P, Q \in \{0, 1\}$	0.196	0.546	0.200	0.543
$P, Q \in \{1, 1\}$	-	-	0.223	0.539

The dynamic response of the inter-area mode and the control action from the WPP PODs are shown in Figure 4.7 for the case where the PSSs of the synchronous generators are disabled. The difference in the generator speed between area 1 and 2, that is, between G_1 and G_3, is plotted to show the impact of the applied POD control on the inter-area oscillation. In this situation the system is small-signal unstable, but the system is stabilized with either of the WPP POD combinations. The improved performance from the combined use of a ΔP and a ΔQ POD is clearly noted from Figure 4.7 with a faster decay of the oscillation. It is also interesting to note that similar performance is achieved with the ΔP and the ΔQ PODs, although the location of the WPP close

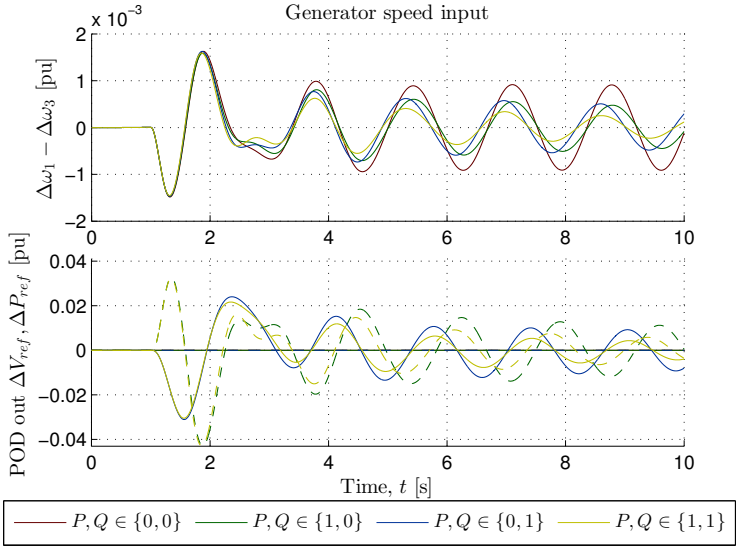

Figure 4.7: Top: Generator speed difference between area 1 and 2, that is $\Delta\omega_1 - \Delta\omega_3$. Bottom: Output reference of WPP POD where solid is the active power reference, and dashed is the voltage reference. Synchronous machine PSSs are in service and the WPP PODs are driven by the generator speed difference between G_1 and G_3.

to area 1 would favor the ΔP POD according to the idealized residue characteristics.

A time domain simulation with the PCC frequency input is shown in appendix A.3 and shows similar damping performance with a similar control effort.

4.1.4 Discussion

The decomposition of the contribution to the damping torque in terms perturbations of the terminal voltage magnitude and angle, that was calculated for the two machine system and shown in Figure 4.4, reveals how the modulated power output of the WPP propagates into a damping torque component. The presented decomposition confirms the intuitive result that an active power modulation would predominantly affect the voltage angle while the reactive power modulation impacts through both the voltage magnitude and angle. But the results also show an example where a positive contribution from voltage magni-

tude at some location is countered by a negative contribution from the voltage angle. This means that in general, both components need to be considered. For more complex systems it is generally not possible to make the simple connection that was made here between the phase of the generator speed deviation of the different generators, which is necessary in order to evaluate whether an induced torque results in increased or decreased damping torque. This is further discussed in section 2.4. The presented decomposition is, nevertheless, illustrative for the understanding of the mechanisms in which a WPP may affect the inter-area mode damping.

The study on the two machine system was repeated on a four machine system where generator and WPP dynamics were considered. Here it was found that the residue characteristics from the idealized two machine system in general could not be transferred to more complicated systems. On the four machine system, a cross coupling was observed between the residue characteristics for active and reactive power modulation. The shape of the residue characteristics appear by superposition of the residues for the ΔP and the ΔQ POD, and is caused by a combination of converter control and induced network response. The cross coupling was most dominant in the reactive power modulation. Here, the induced network response means that the applied reactive power modulation will induce an active power modulation of the nearby impedance load of $P(t) = P_0 \left(\frac{V(t)}{V_0}\right)^2$. An active power modulation will, on the other hand, change the reactive power consumption of the WPP collector grid, which will impact the WT terminal voltage and result in control action from the WT voltage controller. A similar aspect is also treated in [112], where it for a HVDC system is shown that the implicit reactive power modulation following an applied active power modulation can have a detrimental effect on the modal damping.

From Figure 4.6 with the ΔQ POD, it is seen that the cross coupling results in a far more complex residue phase characteristic, since the residue phase is highly dependent on the WPP output. This could increase the challenge of finding a robust tuning for the ΔQ POD, since the power output of a WPP is highly variable and since its modular nature means that the power rating cannot be considered fixed. This is treated further in section 5.2.1 where the residue sensitivity towards the internal state of a 150 WT WPP is investigated.

The observed cross coupling between the residue characteristics for active and the reactive power modulation is treated further in chapter 6 where field tests are presented that show the same cross coupling.

The main body of the study was conducted using the generator speed difference across the inter-tie as input to the PODs. This is, however, an input signal, which from a practical perspective poses significant challenges, since it must be transmitted from remote locations. Its use is here justified with the previously discussed properties of the signal and since the study is not a POD design study but a study conducted to show some fundamental characteristics of active and reactive power modulations from WPPs. To have a locally available signal to compare against, the study was repeated with the PCC frequency measurement as input and with very similar results. This supports that the applicability of the findings is not limited to the generator speed difference input.

4.2 ΔP POD that Utilizes the WT Inertia as Energy Storage

Generally, when WPPs are utilized for power system services based on the delivery of active power, the WTs need to be curtailed to reserve a certain amount of active power production, since the unmanaged output at any given time is subject to the current wind conditions. Since the fuel for a WT cannot be stored and saved for later use, power curtailment equals lost production from the WPP, which means that there are economic considerations associated with this mode of operation.

The ability of variable speed WTs to utilize part of the kinetic energy stored in the rotational mechanical system for power system services has for immediate frequency support been shown in the literature, as for example [26, 49, 57, 76, 85]. For power oscillation damping, the oscillatory nature of the modulated active power output means that the net energy content in the signal is low or even negative. Here, a ΔP POD is investigated that utilizes the WT rotational mechanical system as an energy storage from which damping power is exchanged. When positive active power is required, energy is drawn from the rotational system hence decreasing its rotational speed, while the rotational speed of the mechanical system is increased in the half cycle where negative damping power is delivered. The response of a single-mass swing system to a damped sinusoidal power reference is shown in Figure 4.8 for a sweep of inertia constants that are typical for contemporary WTs in the MW class.

The power exchange with the stored kinetic energy in the rotational mechanical system that is utilized in the investigated ΔP POD, may for a full converter WT be achieved through control of the active power

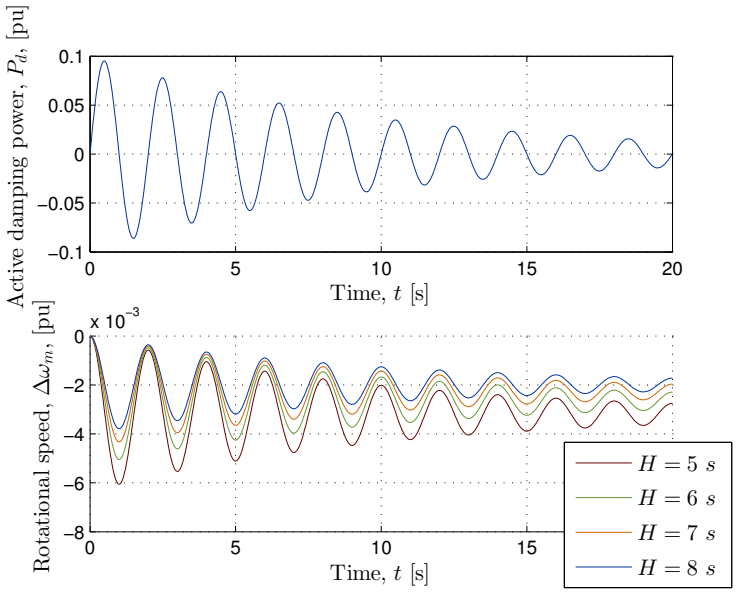

Figure 4.8: Induced mechanical oscillations when active power is exchanged with the rotational system of a single-mass, single machine swing system.

reference of the grid side converter. In the following it is assumed that the grid side converter responds to the power reference, while the machine side converter manages the power balance. The power balance for the DC link dictates that the machine side converter must increase the amount of power that is drawn from the generator when the grid side converter increases the active power output in order to maintain the DC link voltage. And when the electrical torque on the generator exceeds the mechanical torque from the WT rotor, the mechanical system is decelerated. The overlaid oscillating power reference from the ΔP POD can from the WT power control essentially be considered as a disturbance.

The study is based on the benchmark system described in section 2.1.1.2, but where the WPP is represented by three aggregate WTs that, respectively, consist of 50, 35, and 25 3.6 MW WTs. The three WTs are used as a simple multi WT representation of a WPP to do an initial assessment on the possibility of using a common WPP ΔP POD. A more detailed evaluation is conducted in chapter 5 where a WPP is represented with 150 WTs.

Two candidates are considered for input signal to the ΔP POD; namely *1)* the speed difference between a synchronous generator in each area, that is, between G_1 and G_3, $\Delta u_{d\omega}$, and *2)* the bus frequency at the PCC, Δu_f. The former being the reference signal for the inter-area oscillation between the areas, while the latter is a measurement obtained locally. Residue analysis is conducted at each in-feed location as the WPP is traversing the length of the transmission line from the sending end area to the receiving end area, to study the impact of the WPP location within the oscillation.

ΔP PODs for both input candidates are implemented and tested with time domain simulations for both high wind conditions at 12 $\frac{\text{m}}{\text{s}}$, where the WPP is delivering rated output power, and for medium wind conditions at 10 $\frac{\text{m}}{\text{s}}$, where the WT is delivering around 0.69 pu. In the time domain simulations, the oscillations are excited by a 1 second, 5 % step to the voltage reference of the exciter at G_3.

The results presented here are part of the paper [54], which is also attached as appendix A.4.

4.2.1 Frequency Domain Analysis

To assess the feasibility of a WPP ΔP POD, the residues are calculated both for the aggregated WTs individually and for a common WPP POD as shown in Figure 4.9. The results are seen to be similar to those in section 4.1.2. The residue magnitude is seen to align with the capacity involved with the active power modulation, that is, the larger the unit the higher the residue magnitude. This is intuitively understandable because the residue is the eigenvalue sensitivity to the feedback control where a larger unit has a higher leverage on the properties of the eigenvalue than the smaller unit.

The phase characteristics for the speed difference input, $\Delta u_{d\omega}$, and the PCC frequency input, Δu_f, are shown in Figure 4.9, where the similarities to the results in section 4.1.2 are evident. The residue phase characteristics of the ΔP PODs for the feeder aggregate WTs are very similar to the residue phase characteristic for the central WPP ΔP POD, which implies that the same phase compensation can be used for all the WTs within the WPP.

The ITCs on the synchronous generators, G_{1-4}, are shown in Table 4.3 for the WPP connected close to area 1 at $r = 0.1$. Both input candidates add damping to the inter-area mode and have limited effect on the local area mode in area 2, that is, the distant area. The ΔP POD with PCC frequency input also increases the damping ratio for the area 1 local

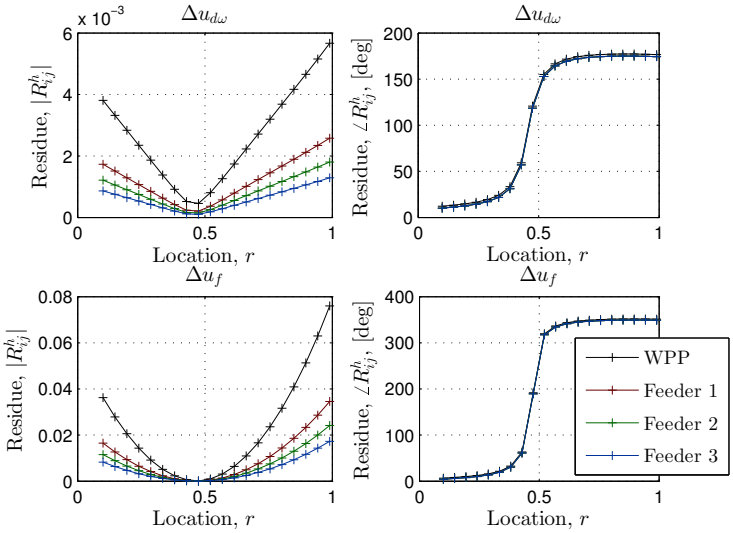

Figure 4.9: Residues from generator speed difference, $\Delta u_{d\omega}$, and PCC bus frequency, Δu_f, to WPP active power set-point.

mode, while the damping ratio for this mode is decreases with the $\Delta u_{d\omega}$ input.

A comparison between the predicted and the actual shift of the inter-area and the two local area eigenvalues for a sweep of POD gains is shown in Figure 4.10. For the POD with PCC frequency input the gain is varied in the range [0.5; 3], while the gain is varied in the range [5; 30] for the $\Delta u_{d\omega}$ input due to a lower amplitude in the input signal.

4.2.2 Time Domain Analysis

Time domain simulations are presented in Figure 4.11 and 4.12 for WPP and synchronous machine quantities, respectively. Only time domain results for the medium wind condition are shown but similar dynamic responses are found for the high wind conditions, which are available in appendix A.4. A gain of 20 is used for the $\Delta u_{d\omega}$ input while a gain of 1.5 is used for the Δu_f input to account for the different amplitudes in the two signals following the disturbance.

When no ΔP POD is installed, each feeder has an almost constant power output, whereas a superimposed oscillation is noted when the ΔP POD is enabled. The PCC frequency driven ΔP POD has a larger

Table 4.3: Induced torques on G_{1-4} from WPP ΔP POD at the modal frequencies of the inter-area mode, D^1, local-area mode for area 1, D^2, and area 2, D^3. Results are shown for the ΔP POD using both speed difference, $\Delta u_{d\omega}$, and PCC frequency as input, Δu_f.

(a) Input: speed difference between G_1 and G_3, $\Delta u_{d\omega}$.

	D^1	D^2	D^3
G_1	$0.07\angle\ 177°$	$0.08\angle\ 165°$	$0.004\angle -65°$
G_2	$0.07\angle\ 179°$	$0.10\angle -10°$	$0.008\angle\ \ 35°$
G_3	$0.03\angle -12°$	$0.003\angle\ 147°$	$0.03\angle -27°$
G_4	$0.04\angle -13°$	$0.004\angle\ \ 73°$	$0.04\angle\ 162°$

(b) Input: PCC frequency, Δu_f.

	D^1	D^2	D^3
G_1	$0.05\angle\ 163°$	$0.04\angle\ \ 21°$	$10^{-4}\angle\ \ 75°$
G_2	$0.05\angle\ 165°$	$0.06\angle -154°$	$3 \cdot 10^{-4}\angle\ 171°$
G_3	$0.02\angle -26°$	$0.002\angle\ \ 4°$	$0.001\angle\ 110°$
G_4	$0.03\angle -26°$	$0.002\angle\ -71°$	$0.002\angle -61°$

initial response, since it tries to counteract the common decrease in generator speed that is seen from Figure 4.12. After around 2 seconds, a similar response is seen for both ΔP PODs.

A slightly dropping rotor speed is noticed in Figure 4.12 for the simulation without ΔP POD, which shows the more complex dynamics of the WT when it is operating for optimal power extraction. Here, the output of the WT depends not only on the wind speed but also on the actual speed of the rotor, which influences the aerodynamic efficiency of the rotor and thereby the power extracted from the wind. With the ΔP PODs in operation, clearly visible oscillations are imposed onto the WT mechanical system. The $\Delta u_{d\omega}$ input imposes rather uniform oscillations around the nominal speed, whereas for the Δu_f input the main rotor oscillation is slower and has a superimposed oscillation at the inter-area mode frequency.

The synchronous machine response is shown in Figure 4.12 in terms of the rotor speeds and the active power output. With the ΔP PODs in operation an increased damping is observed.

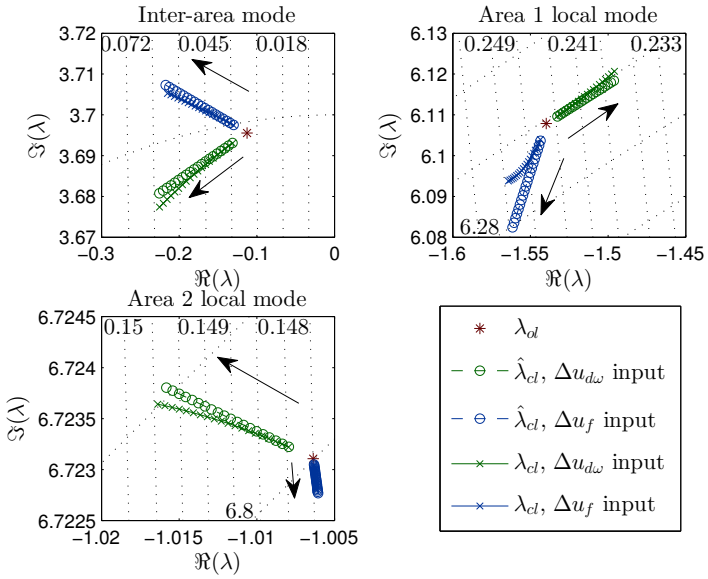

Figure 4.10: Comparison of predicted and actual shift in inter-area and local-area modes as a function of POD gain.

4.2.3 Discussion

The ability to exchange damping power with the rotational mechanical system of the WT is demonstrated with time domain simulations in both high and medium wind speed conditions. When the WPP is equipped with a ΔP POD, the damping of the rotor angle oscillations increases, cf. Figure 4.12. The ΔP PODs were tuned for a light contribution, which is noted from a first swing power amplitude below 0.06 pu and a second swing power amplitude below 0.02 pu, cf. Figure 4.11, as well as from the resulting synchronous machine speed responses shown in Figure 4.12. The damping ratio could have been increased by increasing the controller gain, which is also given from the small-signal analysis, cf. Figure 4.10, but here the small disturbance should also be considered and that the ΔP POD should not be tuned specifically to the simulated scenario, since this would result in a saturated response for more severe disturbances with associated larger mechanical loads on the WT.

A closer inspection of the responses for the Δu_f driven ΔP POD in Figure 4.12, reveals that the pre-disturbance operating point is slightly

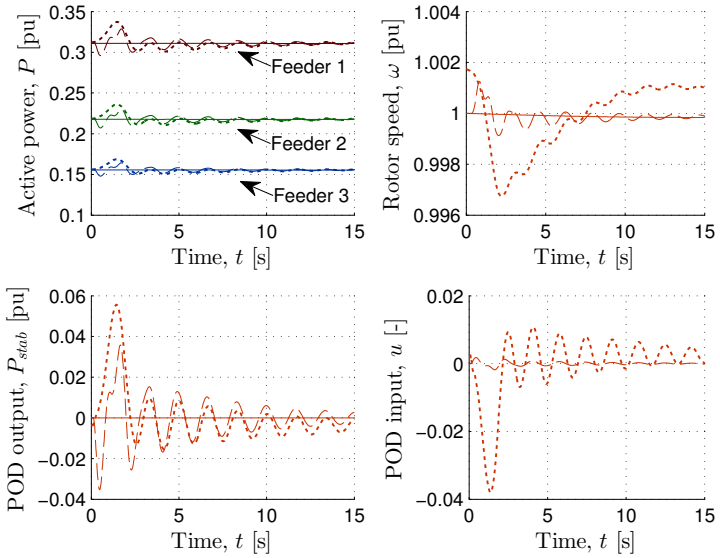

Figure 4.11: WPP active power output, rotor speed, and ΔP POD input and output following a 1 second, 5 % step on the voltage reference of G_3 in medium wind conditions. Solid: no WPP ΔP POD, dashed: $\Delta u_{d\omega}$ input, dotted: Δu_f input.

different from the two other scenarios. This behavior is not seen in the simulations for high wind speed, cf. appendix A.4. It is caused by the more complex dynamics of the WT mechanical system when in optimum power extraction and the synthesized frequency measurement in a power system software with a floating reference angle. In Figure 4.12, it manifests itself in the nonzero output of the ΔP POD at $t = 0$. For an actual design task, such characteristic is of course not acceptable. Here, however, the main purpose is to demonstrate the response of the WT mechanical system to the oscillating power reference from the ΔP POD. An objective that the conducted simulations nevertheless aid to clarify.

The presented results show that from an energy perspective a limited amount of active power for the ΔP POD could be supplied for by the kinetic energy in the WT mechanical system. Initial simulation results were presented based on the WT model described in section 2.1.2 that indicate that the commanded active power modulation does not adversely affect the operation of the WT. Although suitable for power

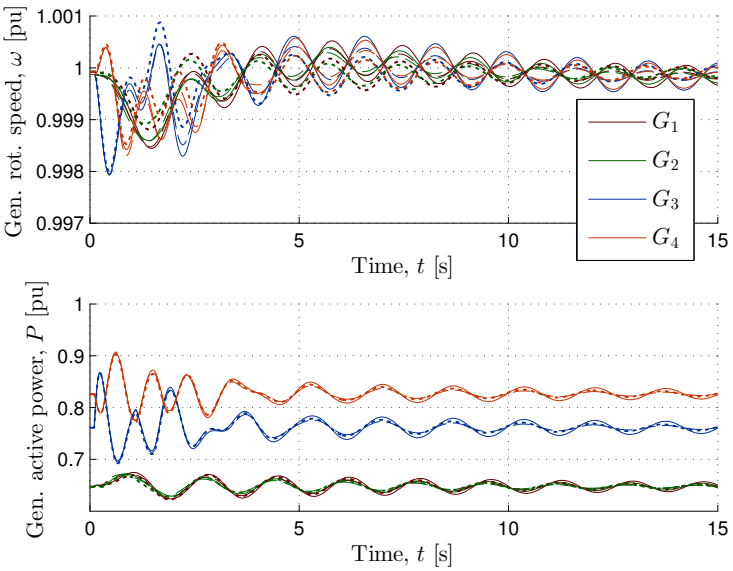

Figure 4.12: Generator speed and active power output following a 1 second, 5 % step on the voltage reference of G_3 in medium wind conditions. Solid: no WPP ΔP POD, dashed: $\Delta u_{d\omega}$ input, dotted: Δu_f input.

system stability studies, the level of details of the mechanical system does not allow for an assessment of the feasibility of the analyzed ΔP POD. A ΔP POD modulates the active power output of the WT, which has an immediate effect on the torques that are experienced by both the mechanical parts of the WT, for example generator, gearbox, drive train, and blades, as well as on the mechanical support structures, for example tower and nacelle. The maximum allowable rate of change of the active power must also be considered, since the required active power gradient to track the reference depends on both the amplitude, A, and the frequency of the oscillation, f, with the maximum gradient given as $\Delta \dot{P}_{d,max} = A\, 2\pi f$. A POD is expected to operate within the frequency range of power system oscillations but if WT mechanical resonance frequencies are present within this frequency range, it may exclude the WT from participating in a frequency range around the resonance frequencies. Generally, the feasibility of a ΔP POD necessitate that any additional loads are within the design criteria for the WT, or that the ΔP POD service is valuable enough to justify reinforcement of any limiting mechanical structures. In [32], it is for a DFIG ana-

lyzed that the use of a ΔP POD can have a destabilizing effect on the torsional drive train mode, while a similar effect was not found when a ΔQ POD was used.

Certain reservations should, thus, be made with regards to the presented results, since the complex dynamics of the mechanical structures within and surrounding a WT are not captured by the power system stability model that was used for the studies in this thesis. To evaluate the impact of active power modulation on the WT mechanical system it would be necessary to make use of detailed mechanical simulation models. And although such study could aid to make the cost in terms of reduced lifetime and the general feasibility of a ΔP POD visible, such evaluation has been considered out of the scope of this thesis.

Chapter 5

Evaluation of Park Level POD Considering WPP as Modular and Distributed Unit

Converter interfaced units have a long tradition for being equipped with auxiliary PODs to improve the small-signal rotor angle stability, as was also discussed in chapter 4. Although the controllability of full converter WTs may be comparable to that of other converter interfaced units, there are also distinct differences that must be considered when the potential use of WPPs for power oscillation damping is studied. A WPP is, as previously discussed, a modular and distributed unit that may consist of more than a hundred individual units, which are spread over a large geographical area. Denholm et al. [23] estimate that the minimum geographical footprint for modern WTs is $5 - 8$ MW/km^2.

In previously published studies, an aggregate WPP using only a single WT model has been considered, cf. section 1.2.2 for a listing of these. Therefore only the conceptual use of WPPs for power oscillation damping has been demonstrated, while the distributed and modular characteristics of an actual WPP has not yet been studied.

The performance of a WPP POD depends on that each WT modulates its output such that a common WPP response is seen at the PCC. For voltage and frequency control, WPP supervisory control is routinely applied that, respectively, regulate the reactive and the active power

output of the individual WTs to have a common WPP response. Although proven successful for a number of commissioned WPPs, the control objectives and performance criteria of these WPP controllers are different from that of a WPP POD. This means that the operating experiences with WPP voltage and frequency controllers cannot be directly transferred to a WPP POD.

The phase compensation requirements for a ΔQ POD is analyzed in section 5.1. Both grid strength and the interaction with WPP voltage and reactive power controllers influence the resulting phase of the modulated WPP reactive power output and must be considered when a ΔQ POD is designed. In section 5.2, the potential use of WPP PODs for both active and reactive power modulation is analyzed with a 150 WT WPP. For power system stability studies, the WTs within a WPP are often aggregated into simpler equivalents to reduce model complexity and the computational burden of the study. The impact of such model simplification on the controllability of low frequency power oscillations is assessed in section 5.3 where the 150 WTs are aggregated into larger equivalents.

The results presented in this chapter are primarily based on the content of the papers:

- "Power Oscillation Damping Capabilities of Wind Power Plant with Full Converter Wind Turbines Considering its Distributed and Modular Characteristics" [63], cf. page 215, and
- "Towards a Reactive Power Oscillation Damping Controller for Wind Power Plant Based on Full Converter Wind Turbines" [60], cf. page 239.

5.1 Phase Compensation Requirements for WPP ΔQ POD

For a continuous ΔQ POD that operates by modulating the reactive power output at a certain phase with respect to the POD input signal from which the oscillation is observed, it is important to have an understanding of the factors that affect the phase shift for the system. The ability of a WPP to track an oscillating voltage reference depends among other things on *1)* the interaction between the ΔQ POD and WPP level voltage, reactive power, and power factor controllers, *2)* the strength of the grid, and *3)* the bandwidth of WT and WPP controllers. Here, only *1)* and *2)* will be considered, while a single parameter set is

used for both the WPP and the WT controllers. But it is clear that the tuning of the involved controllers will also have an impact on the resulting phase shifts.

To evaluate the need for phase compensation for a common WPP POD, the system in Figure 5.1 is considered. The aggregated representation of the WT means that it is only the interactions between the WPP and the grid, and between the WT controller and the WPP controller that are considered.

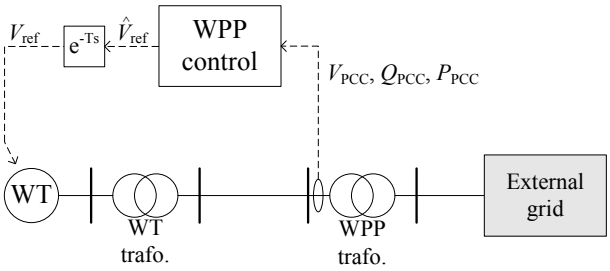

Figure 5.1: Single-line diagram of a single WT infinite bus system that show the feedback path through the WPP control.

Three WPP controllers for reactive power control are considered, namely *1)* voltage control, *2)* reactive power control, and *3)* power factor control, which operate in parallel with the ΔQ POD inside the "WPP control" block of Figure 5.1. The output delay is assumed to cover both the actual transmission time between the WPP control and the WTs as well as processing time at both WPP and WT level. An output delay of 50 ms has been considered and it has been represented with an exact delay model, $e^{-T_s s}$. The WPP controllers are based on the same structure, which is shown in Figure 5.2 for the voltage controller. The error calculation has for the other considered controllers been appropriately modified. Two input candidates are considered for the ΔQ POD reference signal as indicated on Figure 5.2, where input 1, V_{POD1}, corresponds to a tracking problem whereas input 2, V_{POD2}, corresponds to a disturbance rejection problem.

The WPP voltage, reactive power, and power factor control aim at coordinating the response of the WTs to achieve a certain condition at the PCC. To achieve this condition, a subset of the PCC quantities voltage, reactive power, and active power are measured and fed to the WPP controllers. For the ΔQ POD, this adds an additional feedback path from the modulated reactive power output of the WTs, through the collector grid, the WPP voltage, reactive power, or power factor control, to an

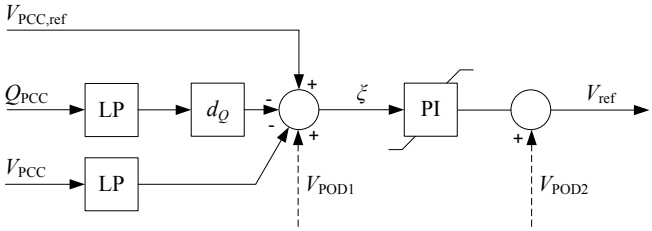

Figure 5.2: Block diagram of the utilized WPP voltage controller with two possible input points for the ΔQ POD.

updated voltage reference signal. Clearly, this can potentially affect the phase of the ΔQ POD response if the bandwidth of the controllers overlap. The speed of a WPP voltage control is determined by various grid code requirements where, for instance, the UK grid code requires that 90 % of the pre-disturbed value is delivered within 1 second [92]. Clearly, such response time is within the range of low frequency power system oscillations and some degree of interaction must be expected.

The presented results are based on [60] which is included as appendix A.6.

5.1.1 Evaluation on Single Machine Infinite Bus System

The grid inverter at the WTs tracks the received voltage reference by control of the reactive current. Intuitively this means that a larger change in the reactive current is necessary for a strong grid when compared to a weaker grid, since the voltage in the strong grid is more difficult to change. When commanded to track an oscillating voltage reference, the inability of the WT voltage controller to tightly follow the reference will result in a terminal voltage that is lagging the reference.

In Figure 5.3, the frequency response is shown for the transfer function between the voltage reference received at the WT to its terminal voltage. Frequency responses are shown for a sweep of short-circuit ratios (SCRs) for both the detailed WT representation, cf. section 2.1.2, and a simplified analytical expression. The simplified expression shown in Figure 5.3 is based on a reduced representation of the WT voltage controller and a Thévenin representation of the network. The transfer function derived for this representation is available in the paper in appendix A.6.

The results in Figure 5.3 are seen to follow what was reasoned, and

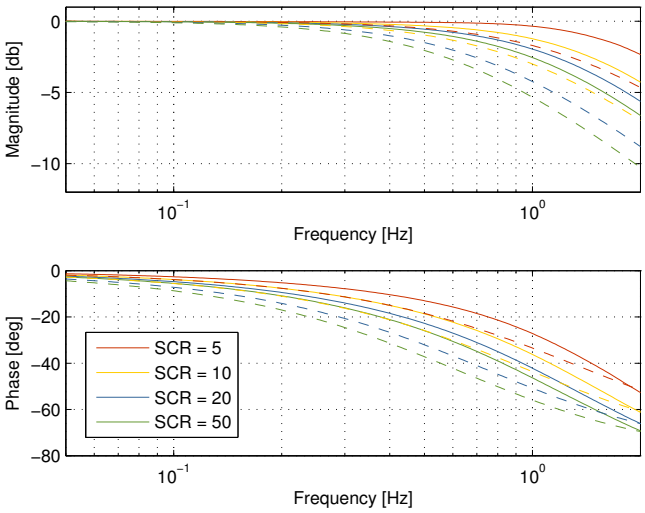

Figure 5.3: Dependency of phase shift induced by the WT voltage controller to the strength of the grid. Solid lines: detailed model, dashed lines: simplified model.

the simplified expression is seen to capture the dominant dynamics, although more conservative than the detailed model.

As shown in Figure 5.2, two input candidates are considered for the ΔQ POD signal. To evaluate the impact of the WPP controllers on the resulting ΔQ POD phase characteristic, the frequency response of the transfer function between the output of the ΔQ POD and the voltage reference received at the WT is shown in Figure 5.4 and 5.5 for input V_{POD1} and V_{POD2}, respectively. In both Figure 5.4 and 5.5, the frequency responses for reactive power and power factor control overlap and it is not possible to distinguish between the curves for these controllers, while the frequency response for the voltage controller is fundamentally different. For the reactive power and the power factor control, the feedback gain at low frequencies is seen to increase with decreasing SCRs, whereas less impact of the SCR is noted for the voltage control. For the reactive power and the power factor control, a variation is noted in the phase response across the investigated SCRs, while a more uniform phase response is found for the voltage controller. For frequencies above 1 Hz, the time delay is seen to dominate the response with increasing phase lag.

Figure 5.4 shows the frequency response for input V_{POD1}. For the volt-

age controller, the phase response has a variation of ±15° around 0° for frequencies below 1 Hz, whereas the reactive power and power factor control for the same frequencies show a variation between −5° to −35°. The offset in the magnitudes shown in Figure 5.4 is caused by the different units used for the different WPP controllers.

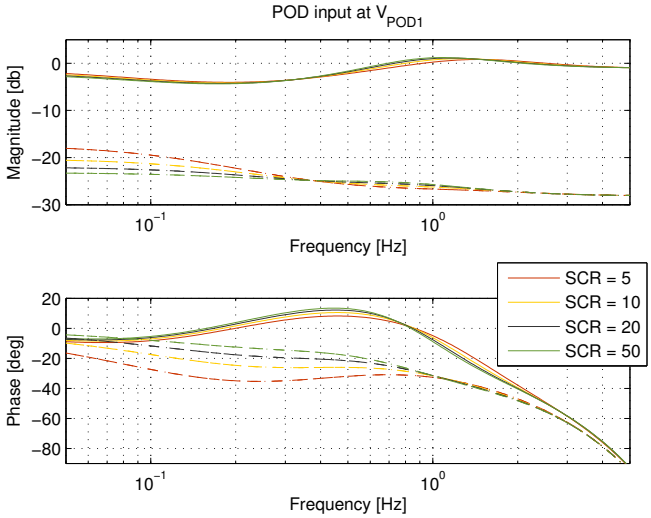

Figure 5.4: Induced phase shift in the WT voltage reference signal by WPP voltage, reactive power, or power factor control for an input at V_{POD1}. Solid: voltage control, dashed: reactive power control, dash dotted: power factor control. Note that the curves for reactive power and power factor control overlap.

For input V_{POD2}, a similar frequency response is found for all three controllers as shown in Figure 5.5. For low frequencies, the WPP control is sufficiently fast to cancel most of the response commanded by the ΔQ POD with a resulting low gain.

5.1.2 Discussion

The SCR at the PCC is important with respect to the stiffness of the voltage, and hence, to the ability of the WT voltage controller to track a given oscillating voltage reference. The study showed that for the frequency range of interest for power oscillating damping, the SCR at the PCC could have a not insignificant impact on the resulting phase shift through the WT voltage controller.

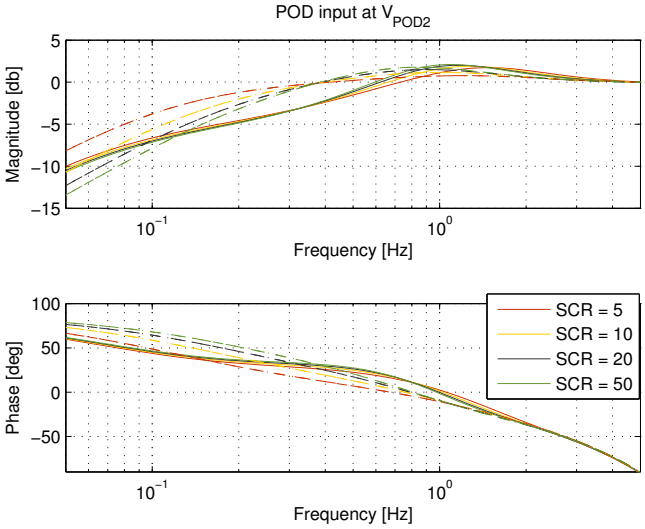

Figure 5.5: Induced phase shift in the WT voltage reference signal by WPP voltage, reactive power, or power factor control for an input at V_{POD2}. Solid: voltage control, dashed: reactive power control, dash dotted: power factor control. Note that the curves for reactive power and power factor control overlap.

The impact of the SCR was found to be small for the WPP voltage controller, whereas a larger impact was found for the analyzed reactive power and power factor controller for frequencies below 1 Hz. The analysis showed that the reference tracking input had the most steady characteristic in terms of both magnitude and phase.

The results show that due care must be taken when a ΔQ POD is designed for a given site, since grid strength, WT voltage controller design, and WPP controller configuration and tuning all can significantly affect the requirements for phase compensation in the ΔQ POD. It is therefore necessary to consider all these elements when assessing the control parameters for a ΔQ POD.

5.2 Potential Use of Common Park Level POD

From a practical perspective, a common WPP POD may prove advantageous over individual WT PODs due to, for example *1)* only one POD needs to be tuned, *2)* single point of access if connected to a wide-area measurement system (WAMS). But it necessitates that the same con-

trol may be applied for the individual WTs in terms of controllability of the ith eigenvalue. The modular characteristic of a WPP means that the configuration within the WPP cannot be considered constant, since individual WTs or entire radials may be disconnected due to faults or maintenance while the WPP remains in operation. The distributed nature of a WPP means that the WTs are not necessarily in the same state of operation and may have different terminal conditions. Therefore, a WPP POD needs to be insensitive to the internal state of the WPP, and the interaction between the WPP and WT controllers or between the WT controllers must not counteract the modulated output that is demanded by the POD.

The results presented in sections 5.2.1 and 5.2.2 are based on Knüppel et al. [63], which is found as appendix A.5, whereas the results in section 5.2.3 are from Knüppel et al. [60], cf. appendix A.6. The studies are all based on the five area, 68 generator system described in section 2.1.1.4. A WPP is connected to bus 212, which consists of nineteen feeders that are distributed over three park transformers to form three subs within the WPP. The single-line diagram is schematically shown in Figure 5.6, while further details on the distribution of the WTs on the feeders and the parameters for the network elements are found in [63] and in appendix A.5.

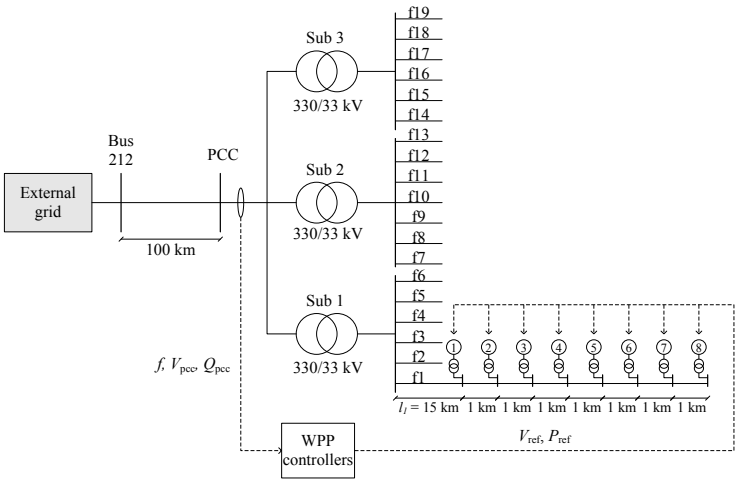

Figure 5.6: Single-line diagram showing the layout of the 150 WT WPP and the connection to the 68 generator system shown in Figure 2.4.

5.2.1 Residue Sensitivity Towards Individual WTs and Internal WPP State of Operation

The residue for the ith eigenvalue for input u and output y gives the eigenvalue sensitivity to a scalar feedback between y and u, cf. section 2.3. Residue analysis can therefore be utilized to assess how each WT should be controlled to add pure damping to the ith eigenvalue, and comparison of the residues for the individual WTs reveals information on the feasibility of a WPP POD. A limited variation in the residue angles across the WTs shows that the WTs have a similar effect on the mode shift of the ith eigenvalue when given the same control signal. Whereas a large variation indicate that only suboptimal performance is obtainable with a WPP POD.

For the residue analysis, the WTs are represented as constant PQ sources to which a controllable ΔP or ΔQ component can be added. The residues are evaluated for the transfer function from the bus frequency, here represented by the change in voltage angle, to the controllable component of active or reactive power modulation.

Four cases are considered and listed in Table 5.1 that capture some of the characteristics of a WPP. In all cases the dispatch of the synchronous generators is adjusted for nominal power output of the WPP. Case 1 is considered the base case, in the sense of the planned operating condition for the power system, while cases 2-4 are deviations from the plan caused by non-uniform wind conditions and equipment failure.

Table 5.1: List of studied scenarios with the WPP being in different internal states.

Case 1	All WTs operating at nominal active power output
Case 2	All WTs operating at 0.6 pu active power output
Case 3	WPP is operating with only sub 1 and 2 in service with all WTs producing nominal active power
Case 4	Different active power output for the subs, i.e. nominal power output in sub 1, 0.8 pu power output in sub 2, and 0.7 pu power output in sub 3

An overview of the impact of the analyzed WPP operating conditions is presented in Figure 3.1 in terms of the eigenvalues of the system. It is noted that only a limited movement of the eigenvalues is seen. The oscillations described by λ_{1-2} are global with all the areas participating, whereas λ_3 is contained mainly within area 3 and λ_4 mainly has participation from area 1 and 2.

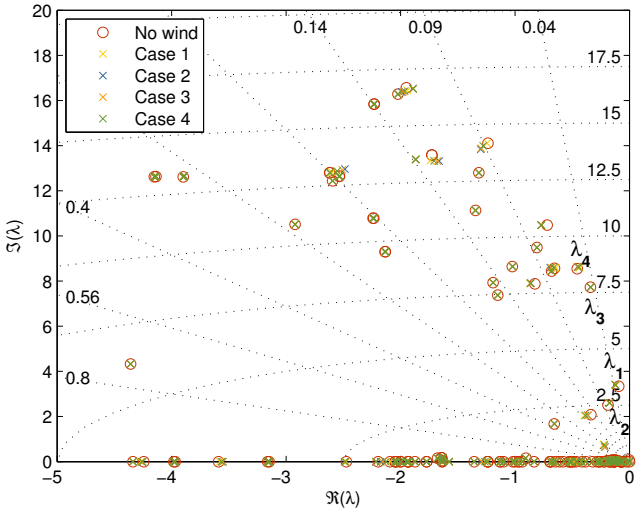

Figure 5.7: Complex plane with the system eigenvalues.

The magnitudes and angles for the λ_1 residues are for the individual WTs in the WPP presented in Figure 5.8 and 5.9 for, respectively, active and reactive power modulation. The feeders are indicated with vertical dashed lines and the feeder number, while the three subs are shown with solid vertical lines.

From the residue magnitudes in both Figure 5.8 and 5.9, it is noted that the efficiency of the damping modulation decreases as the distance to the PCC increases. The residue magnitude decreases gradually from the first to the last WT in each feeder. The differences in the offsets are given by the distance from the PCC to the first WT. The curvature formed by the residue magnitudes are similar for all investigated WPP operating scenarios, while the base line is case dependent.

The residue angles for active power modulation are seen to be much less sensitive to both the WT location within the WPP as well as to the WPP operating condition, than those for reactive power modulation. For reactive power modulation, the residue angles between the WTs span more than 6° within one case, while a span of less than 0.5° was found for active power modulation. Between the investigated cases, a maximum span of almost 14° was found with reactive power modulation, while less than 3° was found for active power modulation.

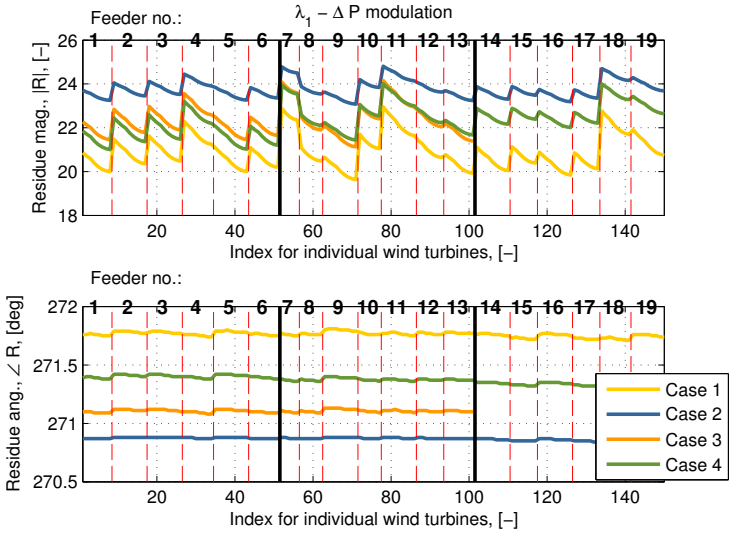

Figure 5.8: Residue magnitudes and angles for WT active power modulation for λ_1.

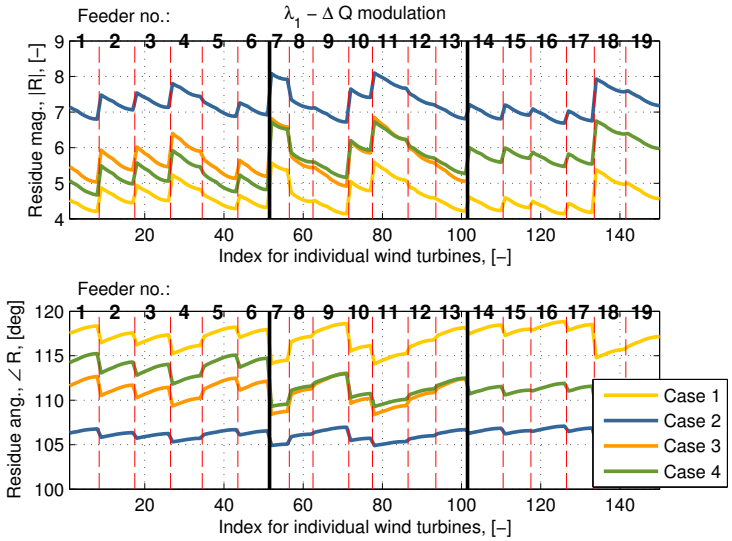

Figure 5.9: Residue magnitudes and angles for WT reactive power modulation for λ_1.

5.2.2 Time Domain Evaluation of ΔP and ΔQ POD

Although a very important tool for revealing fundamental system properties, the residue analysis presented in section 5.2.1 is based on a linearized model and only valid in the vicinity of the point of linearization. The linear representation does, furthermore, not include the inherent limitations of the system and its component. Therefore, it is always good practice to complement linear analysis with time domain studies to check the findings.

The WPP is equipped with either a ΔP or a ΔQ POD that from a local measurement computes a stabilizing reference signal that is distributed to the WTs. For the ΔP POD, the active power reference is modified directly, while the voltage reference is regulated by the ΔQ POD to create a reactive power modulation. The PCC frequency is used as input signal to the PODs, which is here synthesized by the imperfect time derivative of the PCC voltage angle. A time delay of 50 ms is considered between the WPP POD and the WTs to account for both processing time at the WPP and the WTs, as well as the actual transmission time for dispatching the stabilizing signal to the WTs. The power oscillations between the five areas of the power system are excited by a distant 50 ms three-phase short-circuit at bus 307, cf. section 2.1.1.4. All the WTs are for the time domain studies represented by the dynamic model described in section 2.1.2.

Time domain traces are shown for only eight selected WTs. The WTs are the first and the last WT in three selected feeders, which are characterized by the distance of the first WT to the PCC, l_1, and number of connected WTs, N_{WT}

1. short distance: $l_1 = 1$ km, $N_{\mathrm{WT}} = 9$, WT_{80-88}, and
2. medium distance: $l_1 = 15$ km, $N_{\mathrm{WT}} = 8$, WT_{1-8},
3. long distance: $l_1 = 20$ km, $N_{\mathrm{WT}} = 7$, $\mathrm{WT}_{127-133}$.

The change in active and reactive power output of the selected WTs as well as the total WPP output are shown in Figure 5.10 for both the ΔP and the ΔQ POD. With the ΔP POD in service, an almost identical response is seen for each WT and also for the PCC response, whereas more variation is seen in both the magnitude and the phase for the ΔQ POD. The WTs receive an oscillating voltage reference from the ΔQ POD and due to the different terminal conditions at the WTs, it is not the same amount of reactive power modulation that is needed in order to follow the reference. A closer comparison of the phase of the

reactive power modulations in Figure 8, reveals that the WTs nearer to the PCC are leading those further away and that the maximum phase difference is around 15°. The response of the WPP as measured from the PCC is seen to lie in between the maximum phase lag and phase lead, which shows the averaging effect over the individual WTs.

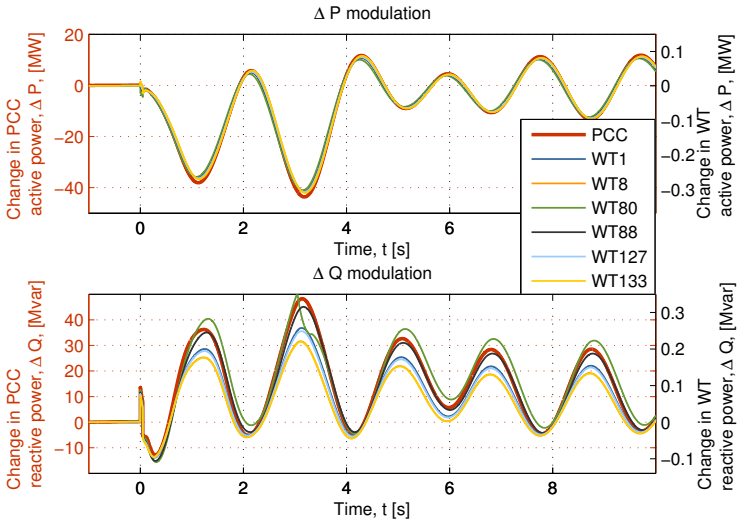

Figure 5.10: Comparison of selected WT power outputs with the corresponding WPP power output at the PCC.

The resulting oscillations in the speed of a dominant synchronous generator in each area are shown in Figure 5.11 for the three cases *1)* no WPP POD, *2)* WPP ΔP POD, and *3)* WPP ΔQ POD. It is found that both PODs increase the damping of the oscillations and that very similar improvements are achieved with similar control effort.

5.2.3 Interaction between WPP Voltage Controller and ΔQ POD

WPPs are, as previously discussed, routinely equipped with park level controllers that act to coordinate the response of the WTs to achieve a common WPP response as viewed from a specific bus. For WPP voltage control, this would be in the form of controlling the voltage at a certain bus, for instance at the PCC. As discussed in section 5.1.1, the speed requirements of todays WPP voltage controllers mean that the ΔQ POD cannot be evaluated independently from the WPP voltage

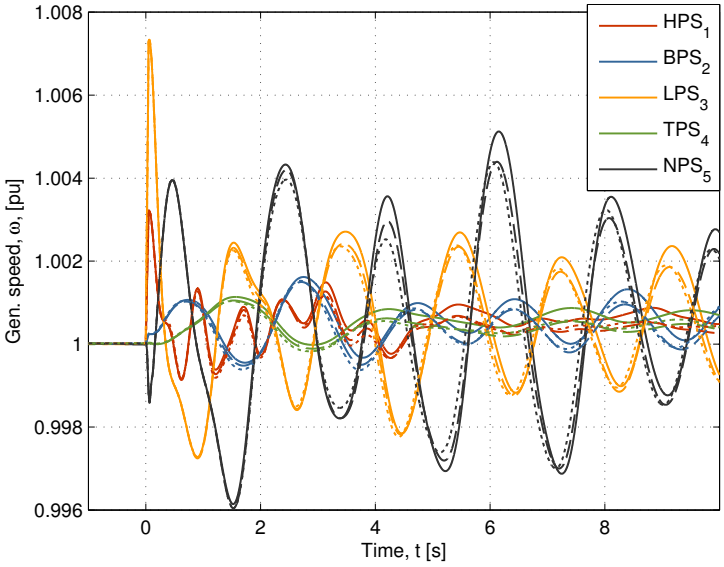

Figure 5.11: Speed of selected generators. Solid: no WPP POD, dashed: WPP ΔP POD, dotted: WPP ΔQ POD.

controller, since both controllers are active in an overlapping frequency range.

The investigated setup with the park level voltage controller is shown in Figure 5.6. The same output delay of 50 ms, which was used in section 5.2.2, is included in the "WPP controllers" block in Figure 5.6. The ΔQ POD is interfaced to the voltage controller at input V_{POD1} as shown in Figure 5.2. The simulation setup in terms of models and applied disturbance is the same as used in section 5.2.2 and the same WTs are selected for the time traces.

The common WPP response at the PCC is shown in Figure 5.12 for the WPP equipped with voltage control and with and without a ΔQ POD. With only the WPP voltage controller in operation, oscillations are noted in both the voltage and in the reactive power. The oscillations originate from the disturbance and the response of the WPP voltage controller to the induced voltage oscillations. When the ΔQ POD is in operation, it is interesting to observe that the PCC voltage oscillates in almost counter phase to the no POD case and that the amplitude of the oscillations have reduced. Increased reactive power oscillations are seen, as commanded by the ΔQ POD.

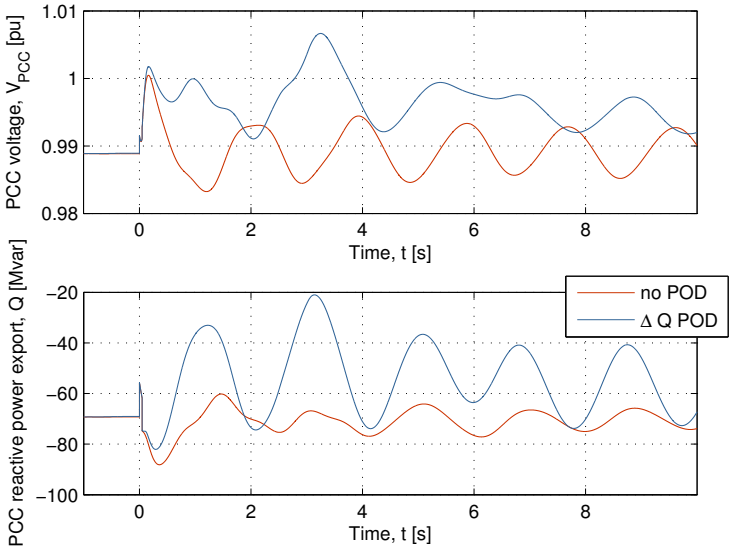

Figure 5.12: Impact of ΔQ POD operation during a distant three-phase short-circuit on the PCC voltage and reactive power transfer.

The operation of the ΔQ POD is illustrated in Figure 5.13 with the synthesized PCC frequency input, the ΔQ POD output, and the voltage reference that is transmitted to the WTs. The larger control action from the ΔQ POD compared to the voltage controller is clearly seen when comparing the resulting voltage references. The synthesized frequency measurement shows the increased damping of the oscillations from the ΔQ POD operation. A plot of the generator speed of a dominant generator in each area is shown in appendix A.6.

The reactive power output of the selected WTs is shown in Figure 5.14 during the applied disturbance. The different steady state operating conditions for the WTs are clearly noted from Figure 5.14 where WT_{80} is exporting reactive power, $WT_{8,133}$ are importing reactive power, and $WT_{1,88,127}$ are close to unity power factor. The influence of the ΔQ POD on the reactive power output is clearly seen when comparing the time traces in Figure 5.14. With the ΔQ POD in operation, the reactive power output has a notably higher amplitude and it is slightly phase shifted when compared to the pure WPP voltage controller response. The terminal voltage of the WTs is almost overlapping and despite the different operating condition in terms of reactive power output, the interaction between the WTs within the WPP does not affect the ability

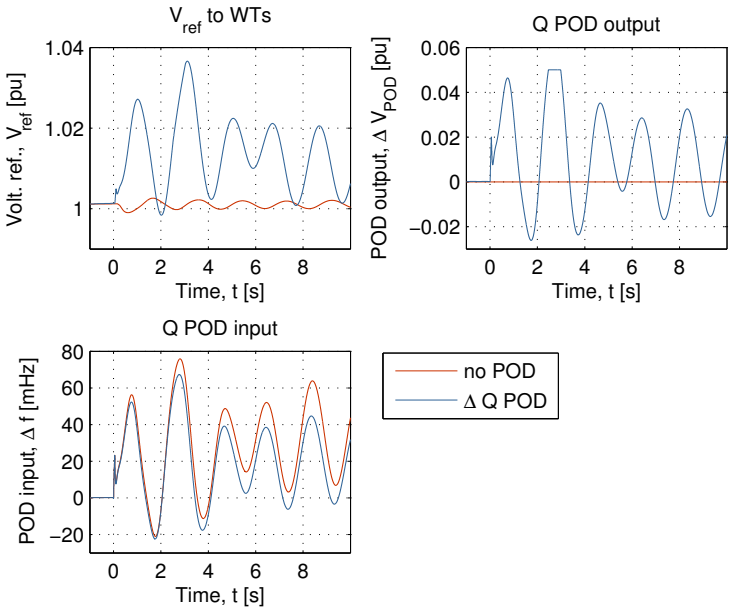

Figure 5.13: Input and output signals of the WPP control during a distant treephase short-circuit.

of the WTs to track the received voltage reference. The plot is found in the paper in appendix A.6.

5.2.4 Discussion

The results from both the residue and the time domain analysis encourage that a park level POD is feasible. In the residue analysis, residue angle differences $< 6°$ was found between the WTs, which for a 0.5 Hz oscillation correspond to a time delay of 33 ms and thus in the order of the transmission delay used for the study. In the time domain study, both the active and the reactive power modulation of the WTs had close resemblance with the resulting output at the PCC, although notably more variation was seen in the reactive power modulation than in the active power modulation. A similar performance was achieved with both PODs with a similar control effort, although it should be remembered that the mode controllability with active and reactive power modulation is highly dependent on the in-feed location as was shown in section 4.1.

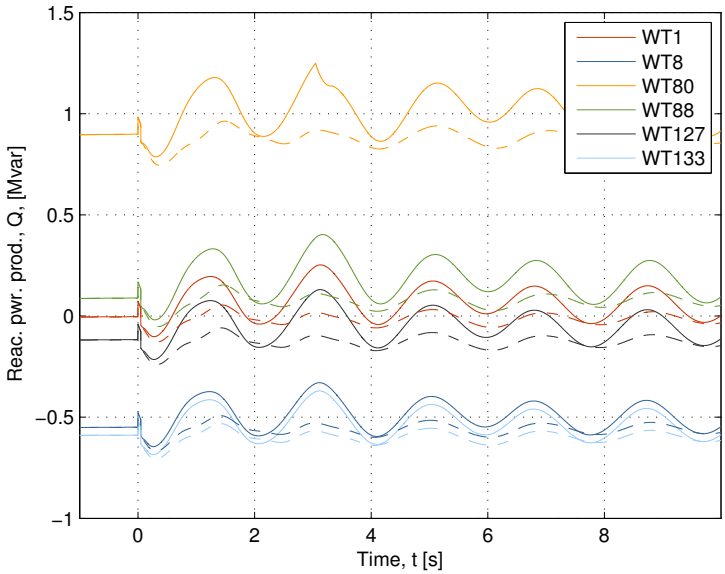

Figure 5.14: Selected WT reactive power outputs during a distant three-phase short-circuit with and without the ΔQ POD in operation. Dashed: no ΔQ POD, solid: ΔQ POD.

For the investigated WPP operating scenarios, residue angle differences below 14° was found for the ΔQ POD while residue angle differences below 3° was found for the ΔP POD. The presented study only considers changes to the internal state of the WPP and does therefore not deal with or assess the robustness of the PODs towards changing operating conditions of the power system. For practical applications this is clearly a very important topic, since it is a requirement that the POD contributes positively to the modal damping for all critical operating conditions, and at the very least that the POD does not deteriorate an already critical situation. Such analysis has not been conducted as part of this thesis but it is a topic that has received at lot of attention in the academic literature for FACTS PODs as presented in section 1.2.2.

Generally, the ΔP POD was less sensitive than the ΔQ POD to both the location of the WT within the WPP and also to the WPP state of operation. This could be seen to advance the ΔP POD over the ΔQ POD. In that regard, it should also be considered that the ΔP POD is also the controller that has the largest impact on the operation of the WTs, and on the WT components due to the commanded oscil-

lating active power reference. This element was discussed further in section 4.2.3.

It should be noted that the operation of the ΔQ POD necessitate that sufficient capacity is reserved for the reactive power modulation. Although such statement might seem trivial, the distributed and modular characteristics of a WPP and the fact that WPP substations are regularly equipped with equipment for static and dynamic voltage regulation such as capacitor banks and SVCs, this can for an actual project be a complicated task to handle. As shown in Figure 5.14, the steady state operating point varies with the location of the WT within the WPP. And where only a single operating condition was considered in the presented study, the designer would during an actual design process need to ensure sufficient capacity over a wide range of operating conditions, while including the impact of switchable reactive compensation such as reactors and capacitor banks. If the WPP substation has equipment for dynamic voltage regulation, the ΔQ POD response must, furthermore, be coordinated with this equipment to ensure that it does not attempt to cancel the response.

The modular nature of a WPP also means that it is likely that the damping performance from the ΔQ POD would gradually degrade with the number of WTs that have insufficient reactive capacity available. This might allow for a less strict evaluation of the necessary reactive capacity of the WPP including substation equipment, if studies show a *satisfactory* performance from the ΔQ POD, although an amount of WTs cannot contribute fully to the two sided response. Such study was deliberately omitted here, since it would not be possible to give an accurate picture of the impact and the retained damping performance without the details of both the range of operating conditions the design should endure and the control systems of equipment for reactive compensation. Both of which are highly project specific.

Domínguez-García et al. [24] investigate the ability of an off-shore WPP to contribute to the modal damping of the inter-area mode in a two area system. Off-shore WPPs may be located tens of kilometers from the on-shore connection point, and in [24] the dependency of the export cable length to the performance of the WPP PODs is investigated when only locally available measurements are considered candidates for the POD control. It is concluded that the performance of the POD decreases with the cable length but that a significant contribution is, nevertheless, delivered.

5.3 Impact of WPP Model Complexity on Computed Damping Contribution

The results presented in section 5.2 dealt with the feasibility of a park level POD controller and considered a detailed WPP model with 150 individual WT models for this assessment. While such representation is necessary for some studies, it is impractical for stability studies of large power systems due to model complexity and the resulting computational effort. A detailed representation of the WTs in a WPP would result in a model of disproportionate complexity when compared to a similar sized power station. Therefore, WPPs are often aggregated into simpler equivalents when used for power system stability studies [9, 16, 86, 108].

Although widely used in practice, the validity and accuracy of such aggregation should be studied when new applications are considered. Here, the impact of the level of WPP aggregation on the WPP mode controllability is studied to assess the use of aggregated equivalents for studies of power oscillation damping.

The results presented are a subset of those presented in [63], cf. appendix A.5 for the full paper.

5.3.1 Aggregation Method and Controllability Estimation

The WPP is simplified in terms of aggregation of the WTs using the method proposed by the National Renewable Energy Laboratory (NREL) in [86] and validated with simulation cases of single and multiple WT representations of a WPP in [16]. Four levels of complexity are here considered:

1. full model where all the WTs are represented individually, $N_{\mathrm{WT}} = 150$,
2. feeder aggregate model where the WPP is simplified to one aggregate WT per feeder, $N_{\mathrm{WT}} = 19$,
3. sub aggregate model where the WPP is simplified to one WT per park transformer, $N_{\mathrm{WT}} = 3$, and
4. single aggregate model where the WPP is represented by a single upscaled WT model, $N_{\mathrm{WT}} = 1$.

The nominal layout of the WPP is used with all WTs connected and with all WTs delivering rated power output.

The mode controllability is estimated by use of the "long distance transfer function" as defined by Elenius et al. [29]. The long distance transfer function, $H_{ld}(j\omega)$, is the frequency response from a controlled active or reactive power modulation to the active power variation on an inter-tie with high mode observability. Elenius et al. [29] show that the relative variations of the frequency response of $H_{ld}(j\omega)$ at system resonance frequencies, contain the same information as the relative variations of controllability factors from modal analysis. The long distance transfer function is given as

$$H_{ld}(j\omega) = \frac{\Delta P(j\omega)}{\Delta U(j\omega)} \tag{5.1}$$

where $\Delta P(j\omega)$ is the measured variation in active power and where $\Delta U(j\omega)$ is the controlled output of the unit. Here, $\Delta U(j\omega)$ represents the output of the ΔP and the ΔQ POD, which are transmitted to the individual WTs and controls the active and reactive power modulation, respectively.

The long distance transfer function in (5.1) is evaluated directly on the non-linear system where $\Delta U(j\omega)$ and $\Delta P(j\omega)$ are estimated from the time domain traces using Fast Fourier Transformations (FFT). The system is excited through the output of the ΔP and the ΔQ POD by a low amplitude Fourier series that contain linearly spaced frequencies in the interval between 0.1 Hz and 2.0 Hz.

5.3.2 Results for Aggregated WPP Representations

The long distance transfer function is shown in Figure 5.15 for the four levels of WPP modeling complexity for a ΔQ POD. It is noted that minor differences are observed for $N_{\mathrm{WT}} = 1$ but that the responses are in fact almost overlapping. Similar characteristics are found for a ΔP POD and a plot of the frequency response is available in the paper in appendix A.5.

The estimated controllability factors are for both the ΔQ and the ΔP POD shown in Figure 5.16 for the active power flow on one inter-tie at bus 309. This location was selected due to its good observability of all four dominant eigenvalues, although the observability of the local area modes, $\lambda_{3,4}$ were not as large as that of the inter-area modes, $\lambda_{1,2}$. The naming of the eigenvalues shown on Figure 5.16 is consistent to the one in Figure 5.7. The estimated controllability factors show great

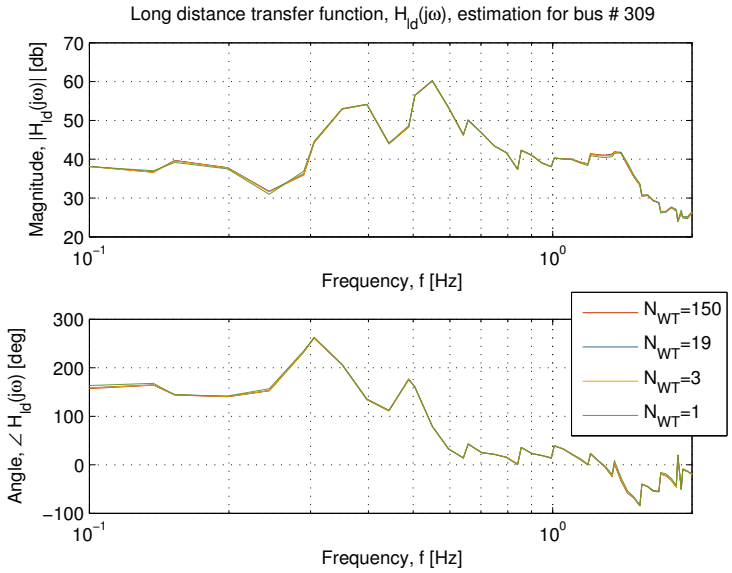

Figure 5.15: Long distance transfer function for a ΔQ POD and the active power measured at one inter-tie of bus 309.

consistency in both magnitude and phase, irrespective of the level of WPP aggregation.

The impact of the number of represented WTs is finally evaluated with time domain simulations where the distant short-circuit used in section 5.2.2 is reapplied for each of the four levels of WPP complexity. The change in active power flow between the major areas of the system is plotted in Figure 5.17 and it is seen that the inter-area dynamics are retained even with the highly simplified equivalent WPP models. A closer inspection of the change in active power flow across bus 416, reveals a minor offset for $N_{\mathrm{WT}} = 1$ whereas an almost overlapping response is found between the other three areas. Only results with the ΔQ POD in service are shown here and in appendix A.5, but similar results are found for the ΔP POD.

5.3.3 Discussion

The ability to aggregate a WPP into simpler equivalent models is, as previously discussed, very important in relation to power system stability studies. In the study conducted here, both the frequency response estimations and the time domain simulations showed very consistent

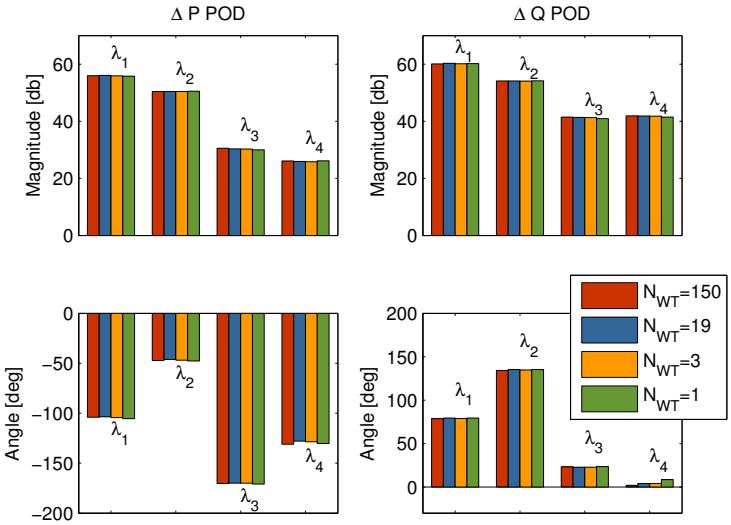

Figure 5.16: Controllability factors evaluated from the long distance transfer function to active power variation at one inter-tie of bus 309 for both a ΔP POD (left side plots) and a ΔQ POD (right side plots).

results when comparing across the different levels of analyzed WPP aggregation. These initial results encourage that a WPP can be represented with only a fraction of the actual number of WTs for power oscillation damping studies. In this study, the WPP could be aggregated into only three equivalent WTs without giving notably different results, while minor differences were found when only a single upscaled WT model was used.

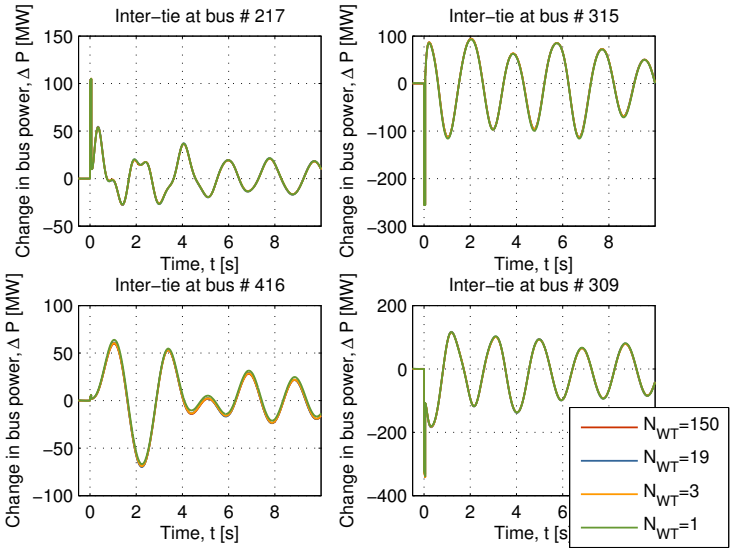

Figure 5.17: Change in active power between the system areas as measured at a single inter-tie of the respective busses. The WPP is equipped with a ΔQ POD.

Chapter 6

Field Test

An actual WPP is a complex design that includes a number different physical units, for example WTs, WPP controllers, and substation equipment, that are geographically dispersed and which interact both physically and through communications networks. On the next level, each WT consists of a number of different components that interact either physically, through communications networks, or both. From a control perspective, a WPP consists of a number of cascaded controllers that are not installed on the same hardware but are interconnected through communications networks, which inevitably add the complexity of potential latency to the analysis of the system.

The system that was studied in sections 5.2 and 5.3 included a 150 WT WPP with a representation of each WT and the corresponding collector grid. And although a complex representation, many aspects of an actual WPP have not been represented in detail in this model. A realizable representation of a WPP for power system studies will inevitably involve a number of assumptions and average value models, since it is not practically feasible to model the interaction between all the different components and controllers in detail.

To gain further insight into the actual response of a contemporary WPP when subject to a park level oscillating reactive or active power reference, a series of open-loop field tests have been conducted.

Open-loop tests were chosen due to the inherent difficulties associated with the evaluation of the closed-loop performance of a converter based POD. The small-signal stability properties of a power system is, as previously discussed, a system property, where inter-area oscillations, furthermore, are characterized by the global participation of the synchronous machines in the system. This implies that the closed-loop test involves excitation of a weakly damped system mode that the stabilizing control should aid to damp. In [67], verification tests of a SVC POD are presented where system oscillations are excited by rapid step-wise changes to an HVDC link in the system. Open-loop tests are, nevertheless, an important first step to gain understanding with the response of a WPP to POD reference signals. Successful open-loop tests that demonstrate the ability of the WPP to properly respond to a POD reference is a necessary prerequisite for a WPP POD.

6.1 Test Setup

The field tests were conducted on a small WPP with 13 2.3 MW Siemens Wind Power WTs where oscillating reactive or active power references of different frequencies were applied to the park level reactive power and frequency controller.

The conducted tests are open-loop in the sense that there are no feedback to the POD control that is simulated in the tests. Measurements of PCC reactive and active power, as used by the WPP reactive power and frequency controllers, were kept intact to include the feedback path from the WTs, through the PCC measurements, to the summing point for the oscillating input.

The tests have been conducted with a test version of the WPP park controllers where additional inputs were defined in both the reactive power and the frequency controller. Through these inputs, a low amplitude sinusoidal signal was superimposed onto the reference signal and the WPP response was measured at the PCC. The oscillating input signal will in the following for simplicity be termed as the ΔP (or ΔQ) POD signal, although the signal does not have the feedback that an actual ΔP (or ΔQ) POD signal is characterized by. The tests are similarly termed ΔP and ΔQ POD tests for, respectively, the applied oscillating active and reactive power reference.

Each frequency was treated independently, that is, a single frequency of oscillation was applied at a time and the output recorded. The amplitude was selected such that it was just large enough to have a clear and measurable oscillating response at the PCC. The frequency

of the POD signal was in each case kept constant for at least 70 seconds, which includes a 5 second transition period at each end. The settling periods were subsequently removed to see the "steady state" response of the WPP to the applied POD signal. In all time domain plots in sections 6.2 and 6.3, the POD signal with the oscillating reference is enabled at $t = 0$ seconds.

6.2 Reactive Power Modulation

The ΔQ POD signal is connected to a developed WPP reactive power controller, that has a similar structure to the voltage control shown in Figure 5.2, at the V_{POD1} summing point. The frequency of the ΔQ POD signal has been changed in discrete steps of 0.05 Hz between 0.1 and 1.0 Hz.

6.2.1 WPP Level

The recorded reactive and active power flow at the park transformer are shown in Figure 6.1 and 6.2, respectively. The responses are shown for a subset of the tested frequencies that captures the tested frequency range. The dependency of the frequency of the reactive power reference on the magnitude and phase of the resulting reactive power oscillation at the PCC is clearly noted from Figure 6.1. The active power measurements in Figure 6.2 have been detrended with the least squares best fit linear function, but a high variability is, nevertheless, seen in the response.

The FFT and the power spectral density (PSD) for the PCC reactive power measurements are shown in Figure 6.3 and 6.4, respectively. Both figures show distinct magnitude peaks only at the frequency of the ΔQ POD signal.

The frequency content in the PCC active power measurement is shown in Figure 6.5, and here it is seen that the reactive power modulation creates a distinct active power modulation with the same frequency. This is identified in Figure 6.5 with a black marking.

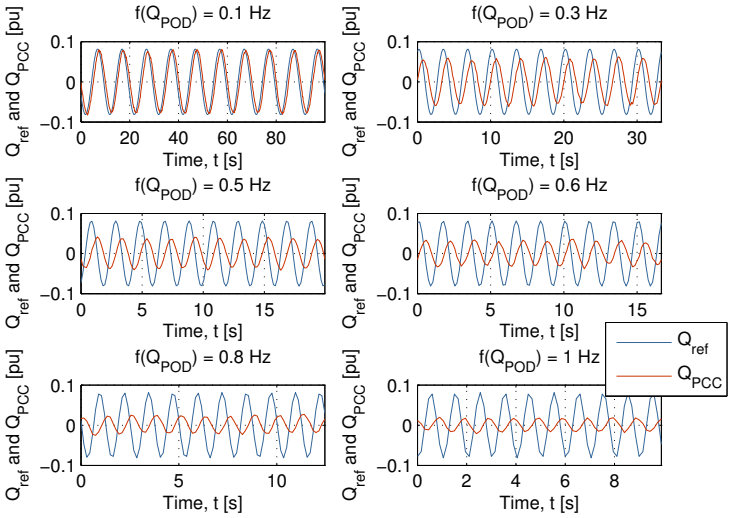

Figure 6.1: ΔQ POD signal and measurements of the PCC reactive power with reactive power modulation at a subset of the tested frequencies

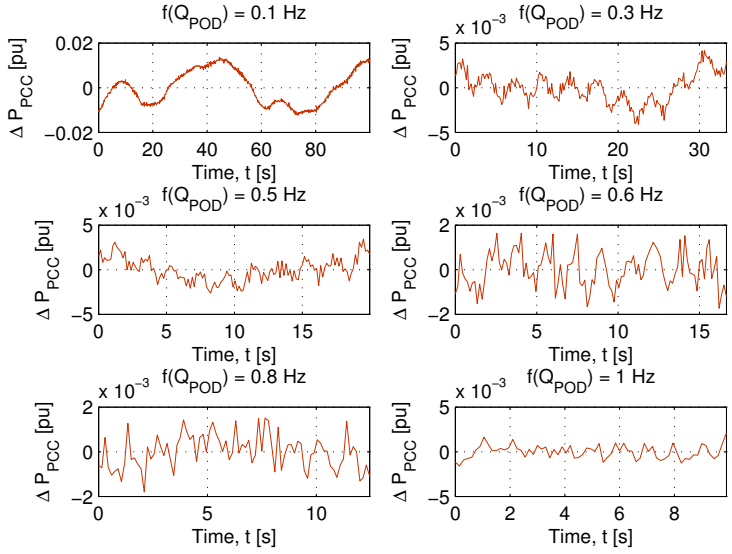

Figure 6.2: Detrended measurements of the PCC active power with reactive power modulation at a subset of the tested frequencies

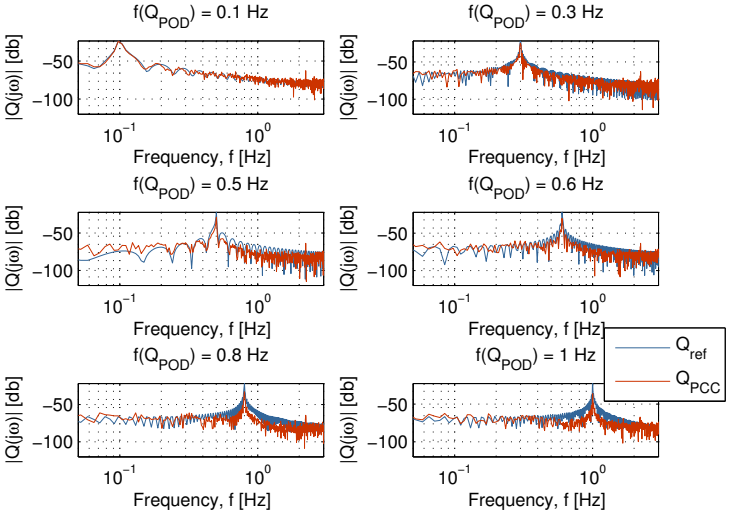

Figure 6.3: FFT of ΔQ POD signal and PCC reactive power with reactive power modulation at a subset of the tested frequencies

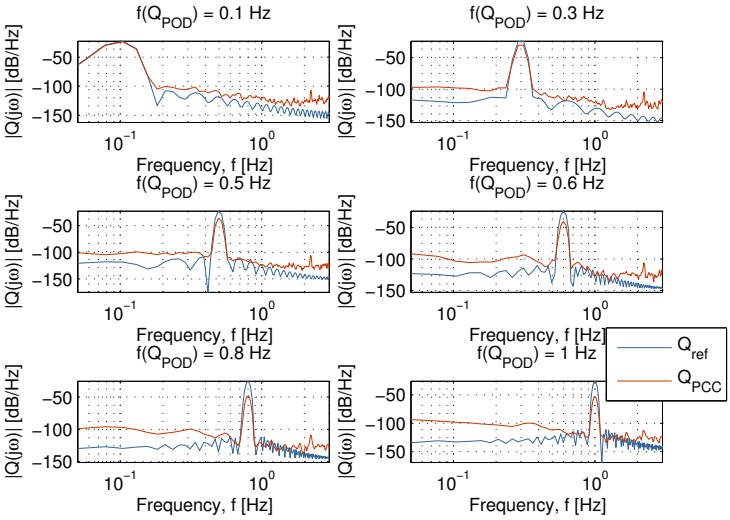

Figure 6.4: PSD of ΔQ POD signal and PCC reactive power with reactive power modulation at a subset of the tested frequencies

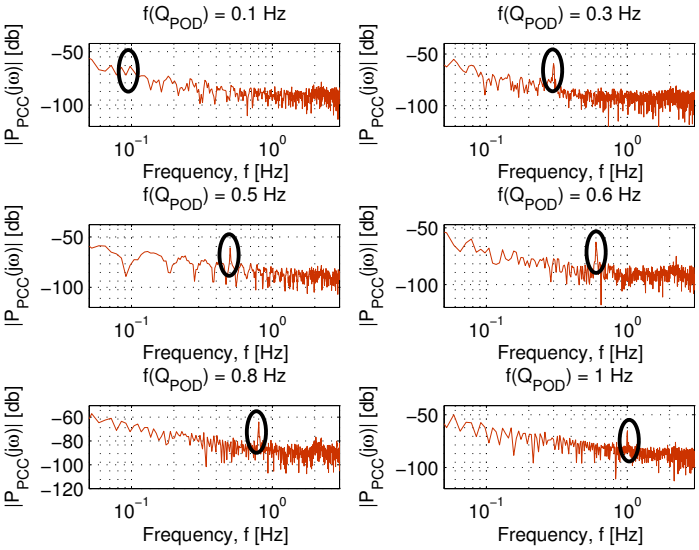

Figure 6.5: FFT of PCC active power with reactive power modulation at a subset of the tested frequencies

6.2.2 WT Level

The active and reactive power output of all the WTs are in Figure 6.6 shown for a full test period with an applied ΔQ POD frequency of 0.3 Hz. The diverse operating conditions for the WTs are apparent, since the active power output ranges from 110 to 1 480 kW and since some WTs are importing reactive power while others are exporting. The superimposed reactive power oscillation is evident from the reactive power output of the WTs.

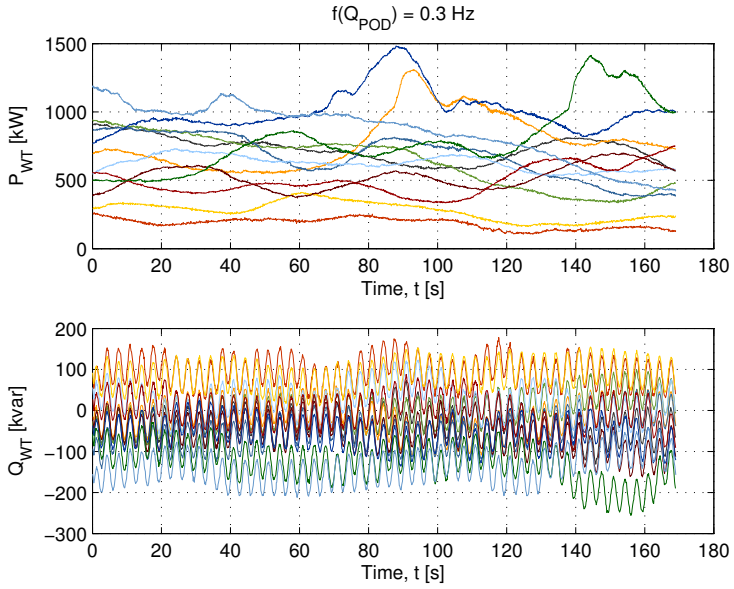

Figure 6.6: Measurements of the WT active and reactive power with reactive power modulation for a full test period with an applied frequency of oscillation of 0.3 Hz.

To enhance the visibility of the ability of the WTs to track the ΔQ POD signal, five cycles of reactive power measurements have been detrended with the least squares linear fit and are for selected ΔQ POD frequencies shown in Figure 6.7. Some variation is noted between the reactive power output of the individual WTs, but the overall picture is a quite aligned response from the WTs.

A FFT plot of the reactive power output of the WTs is shown in Figure 6.8 for six selected ΔQ POD frequencies and distinct peaks are found at the ΔQ POD frequencies for all the WTs.

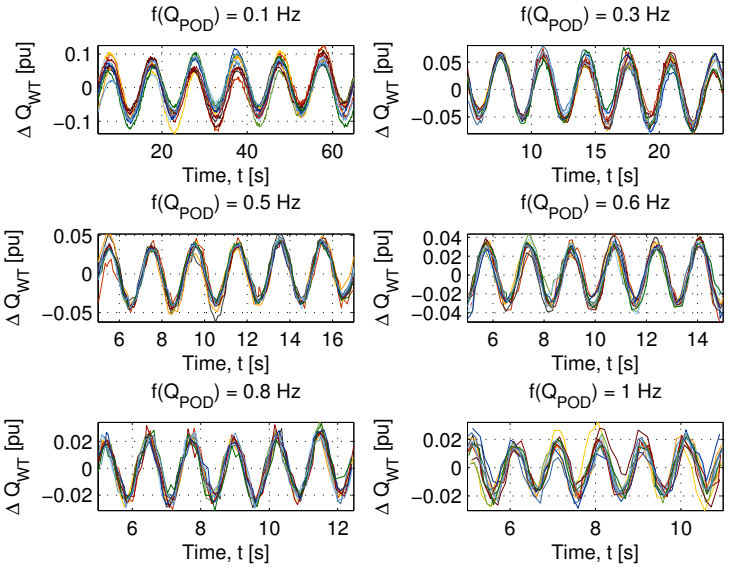

Figure 6.7: Detrended measurements of the WT reactive power with reactive power modulation at a subset of the tested frequencies

A property of the FFT shown in Figure 6.8 is that it does not contain any time information. That is, from the FFT calculation it is not possible to identify whether the frequency characteristics are evolving with time. When the ability of a WPP to track an oscillating reference is evaluated, it is, however, important to investigate the time dependency of the spectral information. That is, does the WPP produce a reactive power output with consistent phase with respect to the reference. The Wigner-Ville Distribution (WVD) is here used to decompose the measured responses into an energy distribution in time and frequency. The WVD preserves time and frequency shifts [14, p.58], which means that it has a very high resolution in both time and in frequency domain, and therefore well suited for analysis of the ability of the WPP to track the oscillating reference. A discussion on the general use and interpretation of the concept of instantaneous frequency that may vary in time is provided by Boashash [15].

The WVD of the reactive power output of a single WT is in Figure 6.9 compared with the combined response at the PCC. The contours of the energy distribution show that a uniform oscillation with the applied frequency of oscillation is achieved throughout the test period. It is

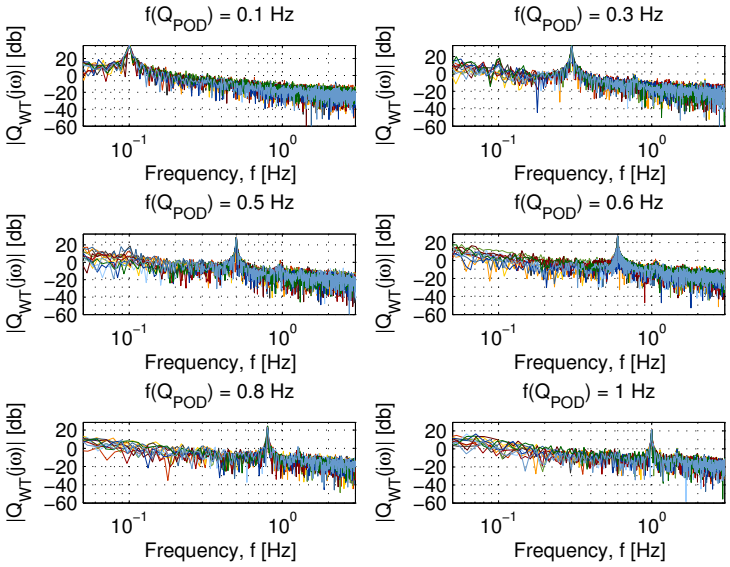

Figure 6.8: FFT of WT reactive power with reactive power modulation at a subset of the tested frequencies.

apparent that the WVD of the WT output has great similarity to the WVD of the PCC output, although some small variations are noted in the contours of the WT WVD. The most unsteady WT WVD is found for a ΔQ POD frequency of 0.1 Hz. Similar WVDs are found for all the WTs within the WPP, which shows the good tracking capabilities of the WTs for the ΔQ POD signal. The plots are not shown due to space considerations.

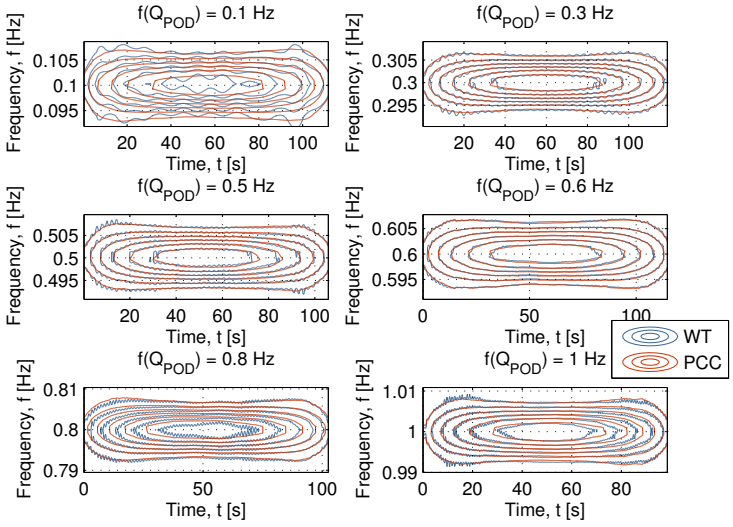

Figure 6.9: WVD of the reactive power output of a single WT and of the PCC reactive power output with reactive power modulation at a subset of the tested frequencies.

6.3 Active Power Modulation

The tests were performed during medium wind conditions, which meant that there was a rather high variability in the WT active power output. The WPP was down regulated during the tests to reduce the variability in the output. The response of the WPP to the active power modulation was tested for the ΔP POD frequencies 0.1, 0.2, 0.5, 0.8, and 1.0 Hz.

6.3.1 WPP Level

The measured active and reactive power flow at the park transformer are shown in Figure 6.10 and 6.11, respectively. For a ΔP POD frequency of 0.1 and 0.2 Hz, the PCC active power output follows the reference with only minor differences in phase and magnitude. For higher frequencies, increasing phase lag and amplification are noted in the signal. From the PCC reactive measurement in Figure 6.11, it is seen that clear oscillations are induced on the PCC reactive power, although of small amplitude.

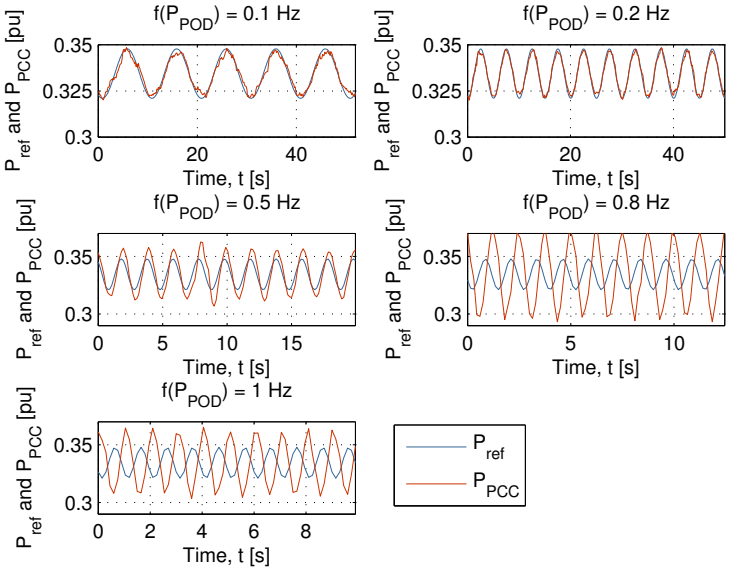

Figure 6.10: ΔP POD signal and measurements of the PCC active power with active power modulation.

The FFT of the PCC active power measurements are shown in Figure 6.12 and the PSD is shown in Figure 6.13. The applied ΔP POD

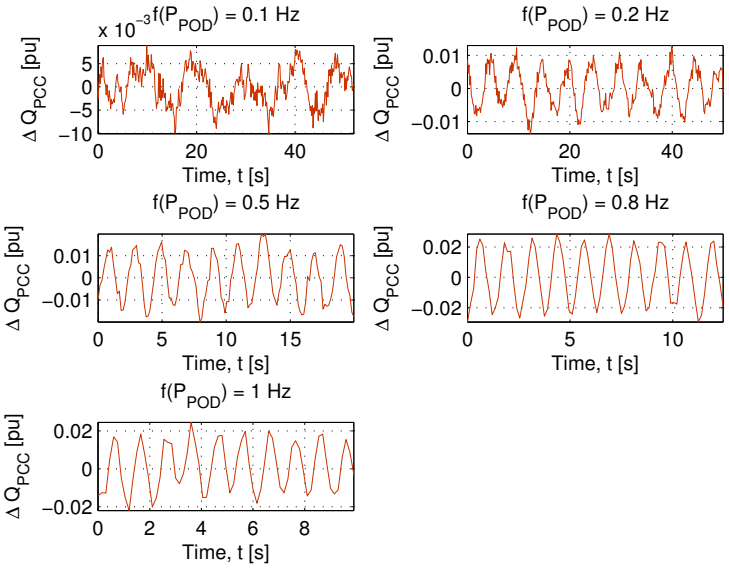

Figure 6.11: Measurements of the PCC reactive power with active power modulation.

signal creates distinct peaks in both the FFT and the PSD plots. But is it also noted that both the FFT and the PSD contain a number of smaller magnitude peaks at frequencies beside that of the applied ΔP POD signal.

The frequency content in the PCC reactive power measurement is shown in Figure 6.14 and here it is seen that the active power modulation creates a distinct reactive power modulation at the same frequency. This means that the active power modulation has a cross coupling to a reactive power modulation, which is also clear from the time traces in Figure 6.11. As discussed in section 4.1.4, this is to be understood since the modulated active power output affects the reactive power consumption in the WPP collector network, which, in turn, will impact the voltage and, hence, the control action of the WT voltage controller.

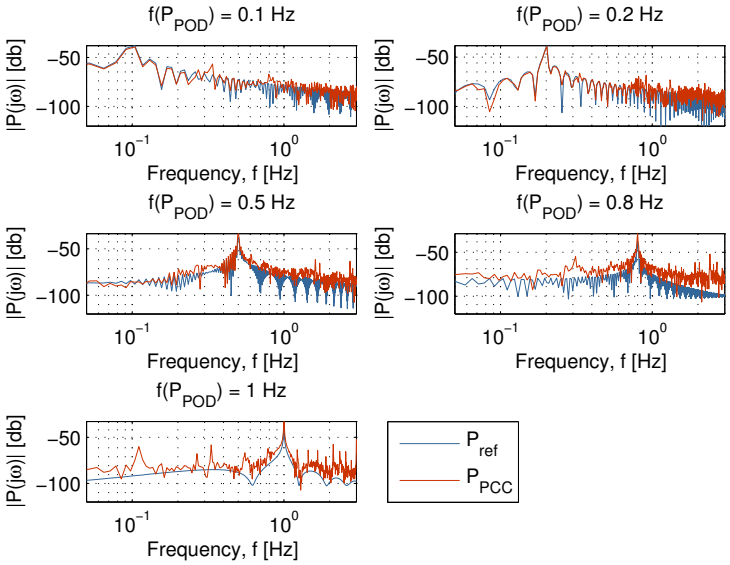

Figure 6.12: FFT of ΔP POD signal and PCC active power with active power modulation.

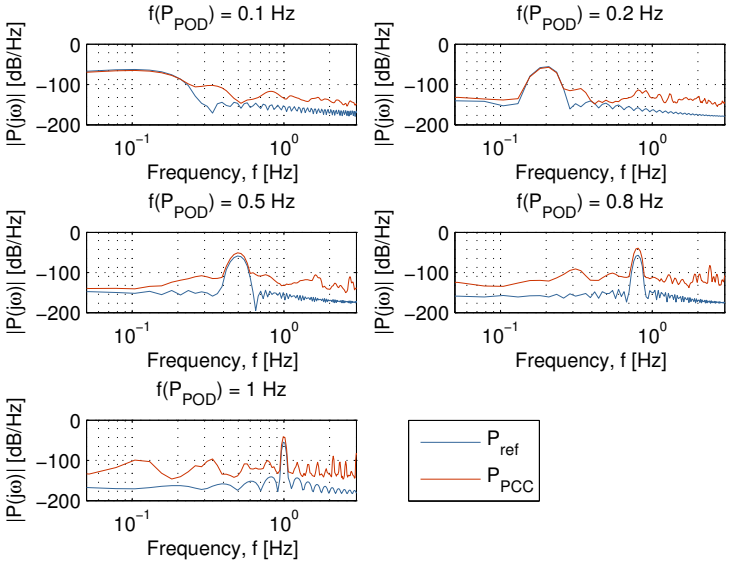

Figure 6.13: PSD of ΔP POD signal and PCC active power with active power modulation.

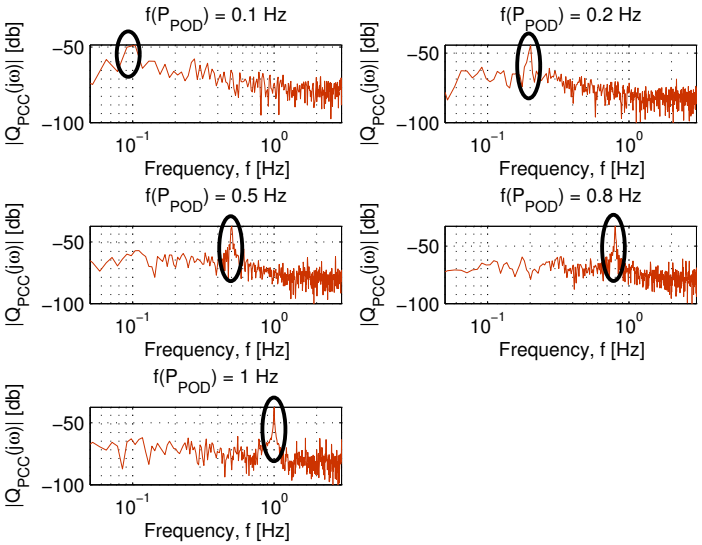

Figure 6.14: FFT of PCC reactive power with active power modulation.

6.3.2 WT Level

The active and reactive power output from all the WTs are shown in Figure 6.15 for the full time range with a ΔP POD frequency of 0.5 Hz. The applied frequency of oscillation is evident in both the active and the reactive power output.

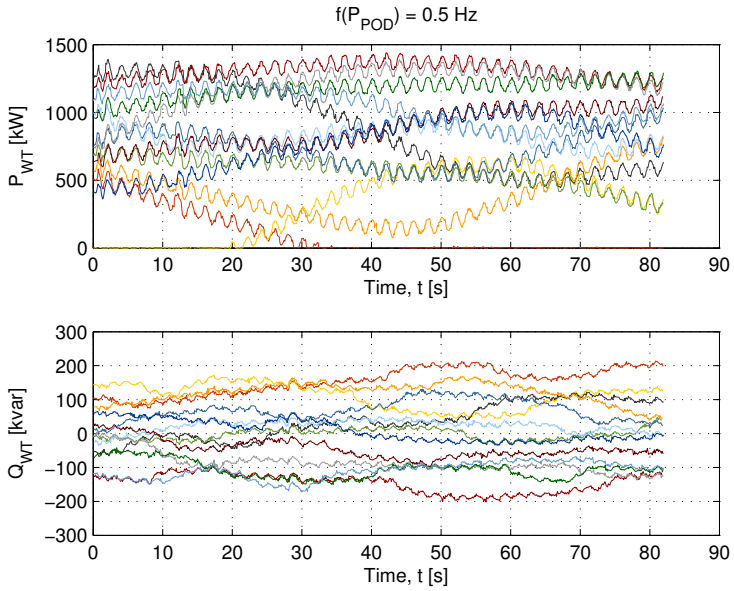

Figure 6.15: Measurements of the WT active and reactive power with reactive power modulation for a full test period with an applied frequency of oscillation of 0.5 Hz.

The active power output of each WT is shown in Figure 6.16, where the active power measurements have been detrended to more clearly illustrate the active power oscillation in the outputs. For a ΔP POD frequency of 0.1 Hz it is seen that the simple linear detrending is not able to remove the variability due to the longer time series for this frequency.

The FFT of the active power output of the WTs is shown in Figure 6.17. As also discussed for the FFT of the PCC active power measurement, peaks are identified at frequencies beside the applied oscillation. The magnitude and at which frequencies those are present vary from test to test.

The WVDs for the active power output of a single WT and the active

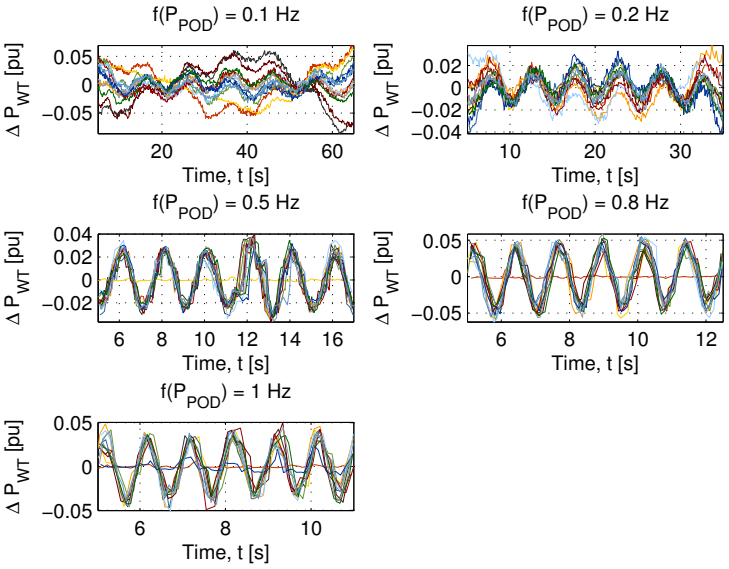

Figure 6.16: Detrended measurements of the WT active power with active power modulation.

power flow at the PCC are shown in Figure 6.18. The PCC measurements are seen to be well centered around the applied ΔP POD frequency and the contours are smooth. The WT WVDs show good resemblance to the PCC WVDs for the investigated ΔP POD frequencies of 0.5 Hz and above, although some smaller variations are noted in the contours.

A somewhat different WVD is found for the ΔP POD frequency of 0.1 and 0.2 Hz where the WT WVD has large variations in the contours that create a distinct pattern that goes across the PCC WVD contours. The details are shown in Figure 6.19 for the ΔP POD frequency of 0.2 Hz where the plot has been enlarged and where the contours have been colored according to the energy content. The variations around the contours of the PCC WVD are clearly seen from the plot. The WVDs have similar average frequency bands, which is to be understood since both signals are stemming from the same source signal, that is, the applied oscillating active power reference. But it is noted that the WT WVD has oval-shaped contours in the frequency dimension across the applied frequency of oscillation where the PCC WVD has a narrow frequency band that is constant in time. The contours that

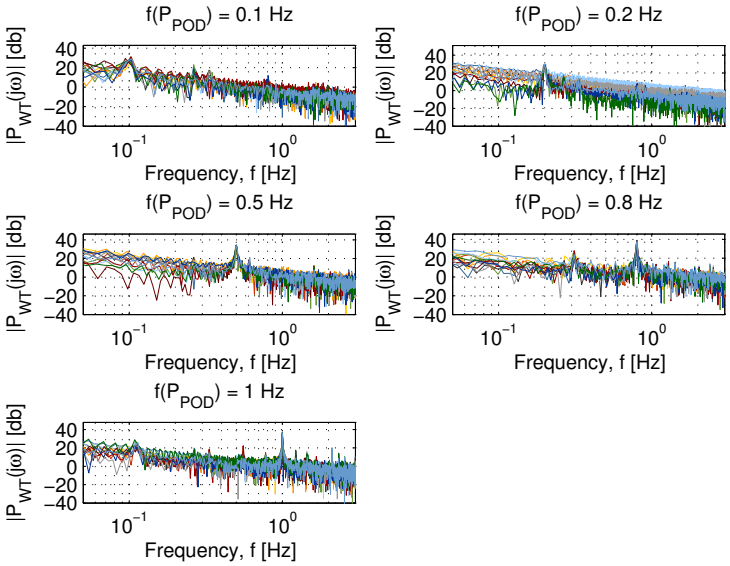

Figure 6.17: FFT of WT active power with active power modulation.

extend into the frequency dimension describe variations in the frequency of the active power output that are non-uniform in time. It is noted that the observed frequency variations are centered around the nominal frequency and that they only have a limited band of around 1.5 % of the nominal frequency. The smooth contours for the PCC measurement is likely caused by the averaging effect over the WTs.

When the WVD is computed for the different WTs, a more diverse picture is seen when compared to the reactive power modulation. For some WTs for some frequencies, the variations around the contours become prominent like shown in Figure 6.18 for a ΔP POD frequency of 0.2 Hz.

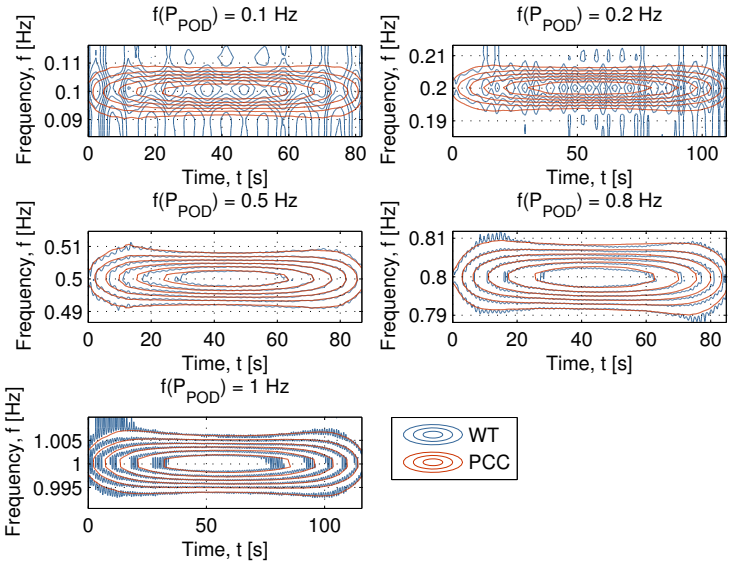

Figure 6.18: WVD of the active power output of a single WT and of the PCC active power output with active power modulation.

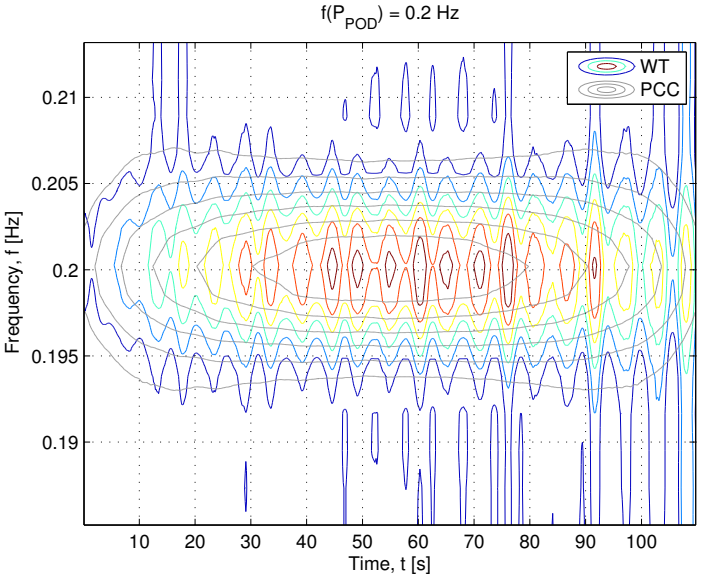

Figure 6.19: Enlarged plot of Figure 6.18 with a frequency of oscillation of 0.2 Hz.

6.4 ΔQ POD Frequency Response

Two frequency sweep tests were conducted from which the frequency response from the oscillating reactive reference to the reactive power output at the PCC has been estimated. The frequency response analysis were repeated with a single machine infinite bus system, cf. Figure 5.1, to see how well the frequency response could be represented. The theoretical evaluations are similar to those presented in section 5.1. The frequency responses have been calculated for a sweep of SCRs to illustrate the sensitivity to this parameter and due to the inherent uncertainty of its size.

In the first test, which is shown in Figure 6.20, the measurement filter in the WPP reactive controller was set to a high value of 5.0 seconds to limit the influence from the feedback path through the WPP controller. It is seen that the dominant characteristic is captured by the analytical model, although the gain is generally lower in the analytical model and the phase response deviates for low frequencies, that is, $f \leq 0.15$ Hz.

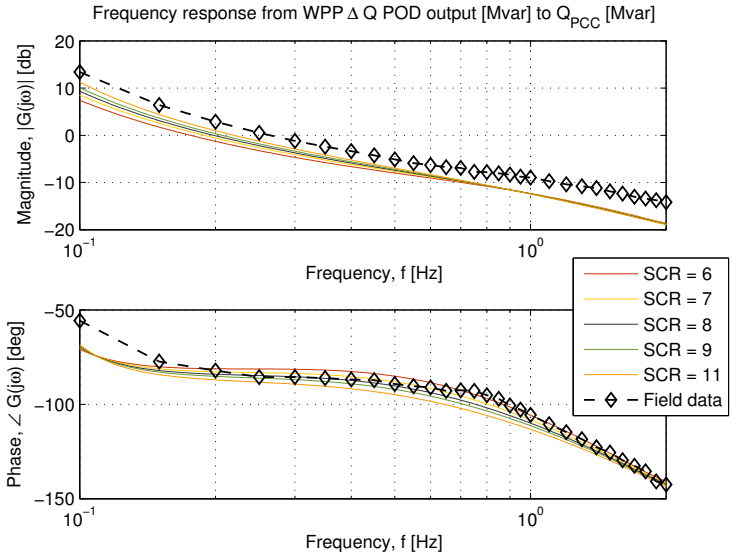

Figure 6.20: Frequency response from WPP ΔQ POD to reactive power flow measured at the PCC in test where a high filter time constant in the reactive power measurement reduces the impact from the feedback.

In the second test, the time constant in the reactive power measurement

filter was restored to its regular value to get the full impact from the feedback path through the park controller. The comparison between the estimated response and the analytical response is shown in Figure 6.21. The gain is seen to roll-off faster in the field test data than with the analytical model but there is overall a good agreement between the frequency characteristics.

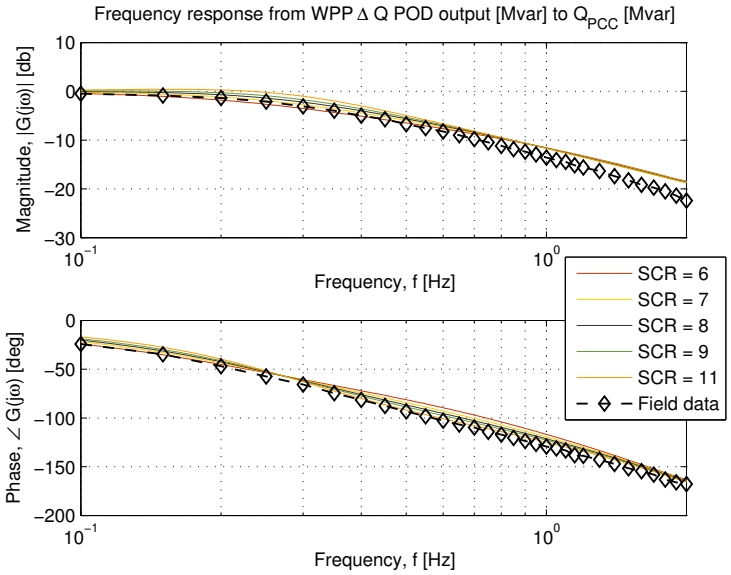

Figure 6.21: Frequency response from WPP ΔQ POD to reactive power flow measured at the PCC with nominal time constant in the reactive power measurement filter.

6.5 Discussion

The field tests showed that it was possible to deliver a park level ΔP or a ΔQ POD signal in the frequency range of 0.1 to 1.0 Hz to the WTs within a WPP, and achieve a common active or reactive power modulation at the PCC with the specified frequency and phase.

A good representation of the reactive power reference was achieved until around 1 Hz with the ΔQ POD tests where it was found that the WTs were capable of tracking the received reference signal to produce an aligned reactive power oscillation.

More variability was found in the active power output of the individual WTs for the ΔP POD tests, cf. Figure 6.17, when compared to the reactive power output for the ΔQ POD tests, cf. Figure 6.8.

A time varying frequency of oscillation around a nominal frequency of oscillation, means that a wider spectrum is found for the resulting signal, due to the variations around the nominal frequency. For the FFT and the PSD representations of the signal, this implies that wider peaks are obtained. Clearly, such implicit information is not easily quantifiable. WVD was applied to explicitly consider both the time and the frequency dimension of the measured data. The use of WVD for analysis of power system oscillations is presented by Palmer [91] where the WVD is used for assessment of the amount of non-linearity in a ring-down signal.

The instantaneous frequency in the WVD is related to the group delay, since these are dual representations and are approximately identical when the product between the duration and the bandwidth of the signal is large [14, 15]. This product is by Boashash [15] described as a measure of the richness of information that is available in the signal. The group delay is for a linear system given by $\tau_g = \frac{\mathrm{d}\phi(\omega)}{\mathrm{d}\omega}$, where $\phi(\omega)$ is the phase response of the system, and a time varying group delay therefore gives a time varying phase response. The duality between the instantaneous frequency and the group delay is comparable to the ambiguity between phase and frequency changes in electrical power systems.

The variability in the frequency of the WT active power output with the ΔP POD test signal, is especially clear when the WVDs are compared. While the WT reactive power output have very similar WVD as the common PCC measurement for the ΔQ POD tests, a time varying frequency of the WT active power output is found for the ΔP POD. This might be explained by the amount of processing that is necessary for an active power reference when compared to a voltage reference, which may be handled directly by the grid side converter. Clearly, the longer the processing path, the higher the risk of any latency in the signal. An aspect of this is discussed in Mehmedalic et al. [77] where it is prosed to add the ΔP POD output directly to the converter power reference to achieve a sufficiently fast processing of the signal. Although this proposal raises a number of practical challenges, it does highlight the importance of a fast and low latency processing path when oscillating references are considered.

Although the WVD of the WT active power output shown in Figure 6.19 showed a time varying component of the frequency of the re-

sulting active power modulation, this was only seen for a subset of the tested ΔP POD frequencies and the variation was centered around the applied frequency of the oscillation. The extension of its contour was less than 1.5 % around the nominal frequency of the oscillation. No significant time varying frequency component was found in the response at the PCC, which is probably caused by the averaging effect over the WTs in the WPP.

In the FFT of the WT active power output in Figure 6.17, a number of frequencies were identified beside the applied ΔP POD frequency. The importance of the identified frequencies in terms of the extent by which they are induced by the ΔP POD signal, as well as of the added stress on the WT mechanical system has not been assessed or attempted assessed with the field tests conducted here. The potential impact on the WT mechanical system was further discussed in section 4.2.3 but an evaluation of this has been considered out of the scope of the present work.

The cross coupling that is observed from the field tests for reactive power modulation in Figure 6.5, and for active power modulation in Figure 6.14 was also discussed in section 4.1.4. Here, residue analysis showed that the characteristics of the residues for a WPP ΔP and a ΔQ POD was a combination of those of the pure active or reactive power modulation. For the residue study, the largest cross coupling was seen from the reactive power modulation to an active power modulation due to an induced network response of a nearby impedance load, whereas the opposite cross coupling was most apparent from the field tests.

A fairly accurate representation of the frequency response for a ΔQ POD was achieved with a simple single machine infinite bus system that required only little parameter fittings. It should be mentioned that further tests on a different site would be needed to verify the findings and to gain further confidence with the accuracy of the representation in the simulation model. The importance of including any WPP voltage or reactive power controller as part of the design study for a ΔQ POD is evident when the two field tests are compared, cf. Figure 6.20 and 6.21. The frequency responses from the two investigated parameter sets for the WPP reactive controller show distinct characteristics that with advantage should be included in the ΔQ POD design. The study presented in section 5.1 arrives at a similar conclusion from an analytical study on a single machine infinite bus system where also power factor and voltage control are considered.

Chapter 7

Conclusion

The work conducted during this project and reported in this thesis can naturally be categorized in four parts. The first part treats the influence of wind power plants (WPPs) based on full converter wind turbines (WTs) on low frequency, small amplitude rotor angle oscillations, that is, rotor angle small-signal stability. The second part explores the interaction between the controlled output of a WPP and the modal damping. In the third part, the potential use of park level power oscillation damping controllers (PODs) is investigated, while the fourth part report the findings from the conducted field tests.

7.1 Summary of Results

The participation of WPPs based on full converter WTs in inter-area oscillations was analyzed for a number of different WT operating regimes for a range of WPP capacities. The study was conducted to deliberately keep the power flow unchanged in the system as the WPP capacity was increased. This was done to isolate the impact of the WT from indirect effects from a changed steady state solution. The modal characteristics of the inter-area modes were found to be largely unaffected as the power rating of the WPP was increased. The results generally showed a very low participation of the WT mechanical system in the inter-area mode. The computed WPP participations were orders of magnitude smaller than the participation of the synchronous generators. The largest par-

ticipation was found from the reactive power controllers in the WPP and in the WT, which was supported by sensitivity analysis of selected control parameters.

An analysis of the torques that are induced onto the synchronous generators due to WPP level voltage and frequency controllers, showed that the frequency support had a positive contribution to the modal damping when the WPP was interfaced close to either of the oscillating areas, while only limited impact was found for the WPP voltage controller.

A simple two mass swing system was analyzed to investigate the mechanisms by which a WPP may interact with the synchronous generators to affect the modal damping. It was shown that the impact of an active or a reactive power modulation from a non-synchronous power production unit could be decomposed into a perturbation of the voltage magnitude and angle at the terminals of the synchronous generators. The active power modulation affected primarily the voltage angle, while both the voltage magnitude and angle were affected by the reactive power modulation. The highly simplified representation allowed for an analytical investigation, but entailed that no controllers beside the active power POD (ΔP POD) or the reactive power POD (ΔQ POD) were considered and that all WPP dynamics were neglected. The study was repeated on larger power system model where synchronous generator control and the WPP dynamics were included. And here it was found that the residue characteristics from the idealized system, that have also previously been reported in the literature, in general, cannot be transferred to more complex systems where the controller dynamics are considered. Here, a cross coupling was found between the residue characteristics for active and reactive power modulation. The cross coupling entailed that the ΔP POD had an element of induced reactive power modulation, while the ΔQ POD had an element of induced active power modulation. The existence of the cross coupling was demonstrated with the conducted field tests.

It was investigated how the kinetic energy stored in the WT mechanical system could be utilized to supply positive damping power for a ΔP POD without the need to curtail the power production, and this was demonstrated with time domain simulations in both high and medium wind conditions. The conducted study only considered the energy perspective of such control scheme, but it is clear that the impact on the WT mechanical system as well as on its normal operation need to be carefully investigated due to the potential large impact on both.

The potential for WPP level ΔP or ΔQ PODs was investigated using both time and frequency domain analysis on a 150 WT WPP. The re-

sults from the residue analysis encourage that a common WPP POD is feasible, since only limited residue angle differences were found between the individual WTs. The time domain results showed that the interaction between the WTs did not adversely affect the ability of the WTs to produce a common WPP response at the point of common connection (PCC). It was found in both frequency and time domain analysis that the ΔP POD was less sensitive than the ΔQ POD to both the location of the WT within the WPP and also to the state of operation of the WPP.

For power system stability studies, the use of detailed WPP models are impractical due to modeling complexity and computational effort. The impact of the WPP modeling complexity on the eigenvalue controllability was assessed both through frequency response estimation and through closed-loop time domain simulations. The results showed that the 150 WT WPP could be simplified into a 3 WT equivalent without giving notably different results, while minor deviations were noted when only a single aggregated machine was used.

The ΔQ POD was shown to have a not insignificant interaction with a WPP voltage, reactive power, or power factor controller. This is to be understood given the response time requirements for, for example, voltage support. The implication is that the tuning of the ΔQ POD must be coordinated with the desired WPP voltage, reactive power, or power factor control in order to achieve the expected phase of the modulated reactive power at the PCC.

Open-loop field tests were conducted on a small WPP with 13 WTs to test the response of the WTs to WPP level oscillating active and reactive power references in the range from 0.1 to 1.0 Hz. The applied reference signals had similar characteristics to those from, respectively, a ΔP and a ΔQ POD. The results showed that is was possible to control the WTs to deliver an common WPP response with consistent frequency and phase. The previously discussed cross couplings between the active and the reactive power modulations were evident from the field test results. For the open-loop ΔP POD tests, distinct reactive power oscillations were measured at the PCC, while distinct active power oscillations were measured for the ΔQ POD tests, although the later case was not as pronounced in the field test results.

Two frequency sweep tests were conducted on the WPP to verify the frequency response characteristics for the ΔQ POD that were computed with linear analysis of the simulation model. The comparison showed that a quite accurate representation of the frequency characteristics was achieved with the employed single machine infinite bus system.

The field test results supported the conclusion that any WPP level controllers for voltage or reactive power should be included in the design process of a ΔQ POD.

7.2 Future Research

During the course of this research project, several topics have been identified as suitable candidates for further research. This includes a variety of topics from studies to increase the confidence with the WT and WPP models used today for small-signal stability studies, design consideration for a WPP or WT POD, and studies to increase the understanding of the impact of WPP PODs on the power system stability.

The circumstance that small-signal stability is a property of the power system as a whole has some implications for the accumulation of confidence with the WPP representations used for small-signal stability studies. To finally verify the behavior of any model of a physical unit, tests and measurements are needed where the dynamic properties of this particular unit play a dominant part in the measured response. This is needed in order to align the analytical model with the experiences that are obtained in the field. The list of topics include:

- The initial results reported in this work as well as in some referenced work, find that the direct impact of WPPs with full converter WTs on the small-signal stability is small. As previously discussed, this, of course, does not preclude indirect impacts caused from changed power flow patterns and generator dispatch. The challenge with such results is that they are extremely difficult to have verified in the field. An effort should therefore be put into the accumulation of practical experiences that can aid to provide the needed confidence to the analytical results.

- Closed-loop WPP POD field tests could be important for verification of the impact of WPPs on the power system small-signal stability, since the power system for such tests is put in state where the response of the WPP has a large impact on the dynamic properties of the power system.

Both simulation results and field test results encourage that a WPP POD is realizable. An important next step is to assess the value of the stabilizing control from WPPs in terms of the added power system stability, where the assessment should include:

- A more detailed assessment than what has previously been published on the contribution to the modal damping that can be achieved from WPP PODs under realistic operating conditions.
- Commissioning of a WPP POD will inevitably add to the complexity of the power system control, since the POD must be both maintained and monitored to ensure that it delivers a positive damping torque at all times.
- The robustness of WPP ΔQ and ΔP PODs towards changing operating conditions need to be further assessed. If the level of robustness is found to be unsatisfactory, the experiences from design of FACTS PODs might be useful.

A POD control will have an impact on the operation of the WPP and for the individual WTs, the details of which has not yet been established. The ΔP POD would have the most extensive impact on the WT operation, since an active power modulation is directly associated with loads of the mechanical system. Topics needing further clarification include:

- Impact of ΔP POD operation on the WT mechanical system, including an assessment of any reduction in the expected lifetime of the WT.
- A ΔP POD will have an immediate impact on the operation of the WTs, since the ΔP POD reference will interact directly with the power control of the WT, which is essential for satisfactory operation. This interaction should be studied further to be able to assess the impact of a ΔP POD.
- A ΔQ POD will have an interaction with WPP components for dynamic or static voltage support, which needs to be managed and fully understood to ensure that the response of the different components is coordinated.
- Operation of a ΔQ POD necessitate that sufficient reactive capacity is available for the reactive modulation commanded by the ΔQ POD. This can potentially affect the requirements for reactive compensation at the substation, in order to ensure that sufficient reactive capacity is available at the WTs.

Bibliography

[1] A. S. Achilles, P. Vyas, and R. W. Delmerico. Wide area transmission control of windfarms. United States Patent. No.: US 8,058,753 B2, Nov. 2011. Filed: 2008-10-31. General Electric Company, Schenectady, NY, USA. 9

[2] T. Ackermann, editor. *Wind power in power systems*. John Wiley & Sons, Ltd, John Wiley & Sons, Ltd, The Atrium, Southern Gatem Chichester, West Sussex PO19 8SQ, England, online edition, October 2005. ISBN: 9780470012680. 22

[3] A. Adamczyk, R. Teodorescu, and P. Rodriguez. Control of full-scale converter based wind power plants for damping of low frequency system oscillations. In *PowerTech, 2011 IEEE Trondheim*, pages 1–7, June 2011. doi: 10.1109/PTC.2011.6019421. 7, 8, 55

[4] V. Ajjarapu and B. Lee. Bifurcation theory and its application to nonlinear dynamical phenomena in an electrical power system. *Power System, IEEE Transactions on*, 7(1):424–431, 1992. ISSN 08858950. 39

[5] V. Akhmatov. Variable-speed wind turbines with doubly-fed induction generators, part I: Modelling in dynamic simulation tools. *Wind Engineering*, 26(2):85, 2002. ISSN 0309524x. 22

[6] V. Akhmatov. Variable-speed wind turbines with doubly-fed induction generators part III: Model with the back-to-back converters. *Wind Engineering*, 27(2):79–91, 2003. ISSN 0309524x. 22

[7] V. Akhmatov. Full-load converter connected asynchronous generators for MW class wind turbines. *Wind Engineering*, 29(4): 341–351, 2005. ISSN 0309524x. 22

[8] V. Akhmatov. *Induction Generators for Wind Power*. Multi-Science Publishing Co., Essex, U.K., June 2007. ISBN 0 906522 40 4. 22

[9] V. Akhmatov and H. Knudsen. An aggregate model of a grid-connected, large-scale, offshore wind farm for power stability investigations–importance of windmill mechanical system. *International Journal of Electrical Power & Energy Systems*, 24(9):709 – 717, 2002. ISSN 0142-0615. doi: DOI:10.1016/S0142-0615(01)00089-8. URL http://www.sciencedirect.com/science/article/B6V2T-44NKYWJ-1/2/3bbb77404df13a1c5dec092c947f1675. 22, 95

[10] F. B. Alhasawi and J. V. Milanovic. Ranking the importance of synchronous generators for renewable energy integration. *IEEE Transactions on Power Systems*, 27(1):416–423, 2012. ISSN 08858950, 15580679. doi: 10.1109/TPWRS.2011.2159250. 46, 47

[11] O. Anaya-Lara, F. Hughes, N. Jenkins, and G. Strbac. Power system stabiliser for a generic dfig-based wind turbine controller. *AC and DC Power Transmission, 2006. ACDC 2006. The 8th IEE International Conference on*, pages 145–149, 2006. 20

[12] O. Anaya-Lara, F. Hughes, N. Jenkins, and G. Strbac. Influence of windfarms on power system dynamic and transient stability. *Wind Engineering*, 30(2):107–127, 2006. ISSN 0309524x. doi: 10.1260/030952406778055018. 5

[13] D. K. Arrowsmith and C. M. Place. *An Introduction to Dynamical Systems*. Cambridge University Press, The Pitt Building, Trumpington Street, Cambridge CB2 1RP, England, 1990. ISBN: 0-521-31650-2. 39

[14] F. Auger, P. Flandrin, P. Gonçalvès, and O. Lemoine. *Time-Frequency Toolbox – For Use with* MatLab. CNRS, France and Rice University, USA, 1996. Tutorial. 108, 121

[15] Boashash. Estimating and interpreting the instantaneous frequency of a signal. i. fundamentals. *Proceedings of the IEEE*,

80(4):520–538, 1992. ISSN 00189219, 15582256. doi: 10.1109/5.135376. 108, 121

[16] J. Brochu, C. Larose, and R. Gagnon. Validation of single- and multiple-machine equivalents for modeling wind power plants. *IEEE Transactions on Energy Conversion*, 26(2):532–541, 2011. ISSN 08858969, 15580059. doi: 10.1109/TEC.2010.2087337. 22, 95

[17] P. Bueno de Araujo and J. Zanetta, L.C. Pole placement method using the system matrix transfer function and sparsity. *International Journal of Electrical Power and Energy Systems*, 23(3): 173–178, 2001. ISSN 01420615, 18793517. 9

[18] N. R. Chaudhuri and B. Chaudhuri. Impact of wind penetration and HVDC upgrades on dynamic performance of future grids. *IEEE Power & Energy Society General Meeting*, pages 1–8, 2011. ISSN 19449925, 19449925. doi: 10.1109/PES.2011.6039366. 5, 7, 55

[19] N. R. Chaudhuri, A. Domahidi, B. Chaudhuri, R. Majumder, P. Korba, S. Ray, and K. Uhlen. Power oscillation damping control using wide-area signals: A case study on nordic equivalent system. In *Transmission and Distribution Conference and Exposition, 2010 IEEE PES*, pages 1–8, April 2010. doi: 10.1109/TDC.2010.5484295. 8, 9

[20] K. Clark, N. W. Miller, and J. J. Sanchez-Gasca. Modeling of GE wind turbine-generators for grid studies. Technical Report Version 4.4, General Electric International, Inc., One River Road, Schenectady, NY 12345, USA, September 2009. 22

[21] Cresap and Mittelstadt. Small-signal modulation of the Pacific HVDC intertie. *IEEE Transactions on Power Apparatus and Systems*, 95(2):536–541, 1976. ISSN 00189510. 6

[22] R. L. Cresap, W. A. Mittelstadt, D. N. Scott, and C. W. Taylor. Operating experience with modulation of the pacific hvdc intertie. *Power Apparatus and Systems, IEEE Transactions on*, PAS-97 (4):1053 –1059, July 1978. ISSN 0018-9510. doi: 10.1109/TPAS.1978.354584. 55, 56

[23] P. Denholm, M. Hand, M. Jackson, and S. Ong. Land-use requirements of modern wind power plants in the united states. Technical

Report NREL/TP-6A2-45834, National Renewable Energy Laboratory, U.S. Department of Commerce, 5285 Port Royal Road Springfield, VA 22161, August 2009. 77

[24] J. L. Domínguez-García, O. Gomis-Bellmunt, F. Bianchi, A. Sumper, and A. Sudrià-Andreu. Power system stabiliser capability of offshore wind power plants. In *Proceedings of EWEA 2012*, Science & research track, Copenhagen, April 2012. European Wind Energy Association. 7, 55, 94

[25] Z. Y. Dong. *Advanced Methods for Small Signal Stability Analysis and Control in Modern Power Systems*. PhD thesis, Department of Electrical and Information Engineering, The University of Sidney, Australia, August 1998. URL http://espace.uq.edu.au/view/UQ:9646. 39

[26] J. Ekanayake and N. Jenkins. Comparison of the response of doubly fed and fixed-speed induction generator wind turbines to changes in network frequency. *Energy Conversion, IEEE Transactions on*, 19(4):800–802, 2004. ISSN 08858969. doi: 10.1109/TEC.2004.827712. 67

[27] J. Ekanayake, L. Holdsworth, and N. Jenkins. Comparison of 5th order and 3rd order machine models for doubly fed induction generator (DFIG) wind turbines. *Electric Power Systems Research*, 67(3):207 – 215, 2003. ISSN 03787796. 22

[28] J. Ekanayake, L. Holdsworth, X. Wu, and N. Jenkins. Dynamic modeling of doubly fed induction generator wind turbines. *Power System, IEEE Transactions on*, 18(2):803–809, 2003. ISSN 08858950. 22

[29] S. Elenius, K. Uhlen, and E. Lakervi. Effects of controlled shunt and series compensation on damping in the nordel system. *Power Systems, IEEE Transactions on*, 20(4):1946 – 1957, Nov. 2005. ISSN 0885-8950. doi: 10.1109/TPWRS.2005.857278. 49, 96

[30] K. Elkington. *Modelling and control of doubly fed induction generators in power systems: Towards understanding the impact of large wind parks on power system stability*. Phd thesis, KTH, Electric Power Systems, SE-100 44, Stockholm, Sweden, April 2009. URL http://urn.kb.se/resolve?urn=urn:nbn:se:kth:diva-10206. ISBN: 978-91-7415-264-7. 7, 55

[31] L. Fan. Review of robust feedback control applications in power systems. In *Power Systems Conference and Exposition, 2009.*

PSCE '09. IEEE/PES, pages 1–7, March 2009. doi: 10.1109/PSCE.2009.4840041. 7

[32] L. Fan, H. Yin, and Z. Miao. On active/reactive power modulation of DFIG-based wind generation for interarea oscillation damping. *Energy Conversion, IEEE Transactions on*, 26(2):513 –521, June 2011. ISSN 0885-8969. doi: 10.1109/TEC.2010.2089985. 7, 55, 74

[33] R. Fernández, R. Mantz, and P. Battaiotto. Contribution of wind farms to the network stability. In *Power Engineering Society General Meeting, 2006. IEEE*, pages 1–6, 2006. doi: 10.1109/PES.2006.1709274. 7, 8, 55

[34] R. Fernández, P. Battaiotto, and R. Mantz. Wind farm non-linear control for damping electromechanical oscillations of power systems. *Renewable Energy*, 33(10):2258 – 2265, 2008. ISSN 0960-1481. doi: DOI:10.1016/j.renene.2008.01.004. URL http://www.sciencedirect.com/science/article/B6V4S-4S094X3-1/2/388a241524a7241643d93d4c18a21170. 8

[35] R. Fernández, R. Mantz, and P. Battaiotto. Potential contribution of wind farms to damp oscillations in weak grids with high wind penetration. *Renewable and Sustainable Energy Reviews*, 12 (6):1692–1711, 2008. ISSN 13640321. 7, 55

[36] M. Furini, A. Pereira, and P. Araujo. Pole placement by coordinated tuning of power system stabilizers and FACTS-POD stabilizers. *International Journal of Electrical Power and Energy Systems*, 33(3):615–622, 2011. ISSN 01420615, 18793517. doi: 10.1016/j.ijepes.2010.12.019. 9

[37] D. Gautam, L. Goel, R. Ayyanar, V. Vittal, and T. Harbour. Control strategy to mitigate the impact of reduced inertia due to doubly fed induction generators on large power systems. *Power Systems, IEEE Transactions on*, 26(1):214 –224, Feb. 2011. ISSN 0885-8950. doi: 10.1109/TPWRS.2010.2051690. 7, 52

[38] D. Gautam, V. Vittal, R. Ayyanar, and T. Harbour. Supplementary control for damping power oscillations due to increased penetration of doubly fed induction generators in large power systems. In *2011 IEEE/PES Power Systems Conference and Exposition (PSCE 2011)*, pages 1 – 6. Department of Electrical Engineering Arizona State University Tempe, AZ 85287, 2011. doi: 10.1109/PSCE.2011.5772501. ISBN: 9781612847870. 7, 55

[39] M. Gibbard. Co-ordinated design of multimachine power system stabilisers based on damping torque concepts. *Generation, Transmission and Distribution, IEE Proceedings C*, 135(4):276–284, Jul. 1988. ISSN 0143-7046. 37

[40] M. Gibbard and D. Vowles. Reconciliation of methods of compensation for psss in multimachine systems. *Power Systems, IEEE Transactions on*, 19(1):463–472, Feb. 2004. ISSN 0885-8950. doi: 10.1109/TPWRS.2003.820689. 37

[41] M. Gibbard and D. Vowles. Simplified 14-generator model of the SE Australian power system. Technical Report 2, School of Electrical & Electronic Engineering, The University of Adelaide, South Australia, May 2008. URL http://www.eleceng.adelaide.edu.au/Groups/PCON/PowerSystems/IEEE/BenchmarkData/index.html. V, 20, 21

[42] M. Gibbard, D. Vowles, and P. Pourbeik. Interactions between, and effectiveness of, power system stabilizers and FACTS device stabilizers in multimachine systems. *Power Systems, IEEE Transactions on*, 15(2):748–755, May 2000. ISSN 0885-8950. doi: 10.1109/59.867169. 9, 37

[43] E. Hagstrom, I. Norheim, and K. Uhlen. Large-scale wind power integration in norway and impact on damping in the nordic grid. *WIND ENERGY*, 8(3):375–384, JUL-SEP 2005. ISSN 1095-4244. doi: 10.1002/we.168. 5

[44] E. Hendricks, O. Jannerup, and P. H. Sørensen. *Linear Systems Control – Deterministic and stochastic methods*. The Technical University of Denmark, Ørsted•DTU, section of Automation, 2005. 8, 25

[45] J. Hongjie, Y. Xiaodan, and C. Xiaodong. Impact of the exciter voltage limit to small signal stability region of a three-bus power system. *International Journal of Electrical Power and Energy Systems*, 33(10):1598–1607, 2011. ISSN 01420615, 18793517. doi: 10.1016/j.ijepes.2011.01.013. 39

[46] D. Huang and R. Billinton. Effects of wind power on bulk system adequacy evaluation using the well- being analysis framework. *Power Systems, IEEE Transactions on*, 24(3):1232–1240, Aug. 2009. ISSN 0885-8950. doi: 10.1109/TPWRS.2009.2021232. 42

[47] H. Huang, C. Mao, J. Lu, and D. Wang. Small-signal modelling and analysis of wind turbine with direct drive permanent magnet synchronous generator connected to power grid. *IET Renewable Power Generation*, 6(1):48–58, 2012. ISSN 17521416, 17521424. doi: 10.1049/iet-rpg.2010.0217. 6, 22

[48] F. Hughes, O. Anaya-Lara, N. Jenkins, and G. Strbac. A power system stabilizer for dfig-based wind generation. *Power System, IEEE Transactions on*, 21(2):763–772, 2006. ISSN 08858950. 7, 55

[49] P.-K. Keung, P. Li, H. Banakar, and B. T. Ooi. Kinetic energy of wind-turbine generators for system frequency support. *Power Systems, IEEE Transactions on*, 24(1):279–287, Feb. 2009. ISSN 0885-8950. doi: 10.1109/TPWRS.2008.2004827. 67

[50] M. Klein, G. Rogers, and P. Kundur. A fundamental study of inter-area oscillations in power systems. *Power System, IEEE Transactions on*, 6(3):914–921, 1991. ISSN 08858950. 2, 19

[51] T. Knüppel, V. Akhmatov, J. N. Nielsen, K. H. Jensen, A. Dixon, and J. Østergaard. Small-signal stability analysis of full-load converter interfaced wind turbines. In *8th International Workshop on Large-Scale Integration of Wind Power into Power Systems as well as on Transmission Networks for Offshore Wind Farms*, 2009. 14

[52] T. Knüppel, V. Akhmatov, J. N. Nielsen, K. H. Jensen, A. Dixon, and J. Østergaard. On small-signal stability of wind power system with full-load converter interfaced wind turbines. In *WINDPOWER 2010 Conference & Exhibition, Dallas, TX, USA*. American Wind Energy Association, 2010. 14

[53] T. Knüppel, J. Thisted, B. Andresen, M. N. Frydensbjerg, V. Akhmatov, and J. N. Nielsen. Grid support capabilities of full-load converter interfaced wind turbines. In *POWER-GEN India & Central Asia*. PennWell Corporation, April 2010. 14

[54] T. Knüppel, J. N. Nielsen, K. H. Jensen, A. Dixon, and J. Østergaard. Power oscillation damping controller for wind power plant utilizing wind turbine inertia as energy storage. In *2011 IEEE PES General Meeting*, pages 1–8, Detroit, MI, USA, July 2011. IEEE Power & Energy Society. doi: 10.1109/PES.2011.6038908. ISBN: 978-1-4577-1001-8. 13, 56, 69

[55] T. Knüppel, J. N. Nielsen, K. H. Jensen, A. Dixon, and J. Østergaard. Induced torques on synchronous generators from operation of wind power plant based on full-load converter interfaced wind turbines. In F. A. Aranda, editor, *Scientific Proceedings of the European Wind Energy Conference & Exhibition*, pages 68–71. The European Wind Energy Association, March 2011. 13, 43, 49

[56] T. Knüppel, J. N. Nielsen, K. H. Jensen, A. Dixon, and J. Østergaard. Power oscillation damping capabilities of wind power plant with full converter wind turbines considering its distributed and modular characteristics. In *Proceedings of IET Renewable Power Generation Conference 2011*, Radisson Blu, Edinburgh, UK, September 2011. The Institution of Engineering and Technology, IET RPG. doi: 10.1049/cp.2011.0130. 14

[57] T. Knüppel, P. Thuring, S. Kumar, M. N. Kragelund, R. Nielsen, and K. André. Frequency activated fast power reserve for wind power plant delivered from stored kinetic energy in the wind turbine inertia. In U. Betancourt and T. Ackermann, editors, *10th International Workshop on Large-Scale Integration of Wind Power into Power Systems as well as on Transmission Networks for Offshore Wind Farms*, pages 464–469, Scandinavian Congress Centre, Aarhus, Denmark, October 2011. Energynautics GmbH. ISBN: 978-3-98 13870-3-2. 67

[58] T. Knüppel, B. Andresen, and M. N. Frydensbjerg. Power oscillation damping by a converter-based power generation device. World Intellectual Property Organization, International Publication No.: WO 2012/041527 A1, April 2012. International Filing Date: 2011-01-19. Siemens AG. 14

[59] T. Knüppel, S. Kumar, and P. Thuring. Power oscillation damping controller. World Intellectual Property Organization, International Publication No.: WO 2012/041543 A1, April 2012. International Filing Date: 2011-06-10. Siemens AG. 14

[60] T. Knüppel, S. Kumar, P. Thuring, M. Støttrup, and J. Friman. Towards a reactive power oscillation damping controller for wind power plant based on full converter wind turbines. In *2012 IEEE PES General Meeting*, pages 1 – 8, San Diego, CA, USA, July 2012. IEEE Power & Energy Society. 13, 78, 80, 84

[61] T. Knüppel, J. N. Nielsen, K. H. Jensen, A. Dixon, and J. Østergaard. Small-signal stability of wind power system with full-load

converter interfaced wind turbines. *IET Renewable Power Generation*, 6(2):79–91, 2012. doi: 10.1049/iet-rpg.2010.0186. ISSN 1752-1416. 13, 20, 22, 42, 43

[62] T. Knüppel, J. N. Nielsen, K. H. Jensen, A. Dixon, and J. Østergaard. Power oscillation damping control of inter-area oscillation through active and reactive power modulation from wind power plants with full converter wind turbines. *Unsubmitted manuscript*, 2012. 13, 51, 56, 57

[63] T. Knüppel, J. N. Nielsen, K. H. Jensen, A. Dixon, and J. Østergaard. Power oscillation damping capabilities of wind power plant with full converter wind turbines considering its distributed and modular characteristics. *Accepted for publication in IET Renewable Power Generation Special Issue*, 2012. 13, 78, 84, 95

[64] Korba, Larsson, and Rehtanz. Detection of oscillations in power systems using kalman filtering techniques. In *The proceedings of the IEEE Conference on Control Applications*, volume 1, pages 183–188 vol.1, 2003. doi: 10.1109/CCA.2003.1223290. 8

[65] N. Kshatriya, U. D. Annakkage, F. M. Hughes, and A. M. Gole. Optimized partial eigenstructure assignment-based design of a combined PSS and active damping controller for a DFIG. *Power Systems, IEEE Transactions on*, 25(2):866 –876, may 2010. ISSN 0885-8950. doi: 10.1109/TPWRS.2009.2032190. 7, 55

[66] P. S. Kundur. *Power System Stability and Control*. The EPRI Power System Engineering Series. McGraw-Hill, Inc., 1994. ISBN: 0-07-035958-X. 2, 3, 17, 24, 32, 33, 37

[67] M. Lahtinen, T. Rauhala, H. Kuisti, J. Peltola, and P. Halonen. Static var compensator enhancing the operational reliability of finnish transmission network. In *Proceedings of CIGRE Session 2010*, Paris, France, August 2010. Paper B4-206. 55, 56, 102

[68] E. Larsen, J. Sanchez-Gasca, and J. Chow. Concepts for design of FACTS controllers to damp power swings. *Power Systems, IEEE Transactions on*, 10(2):948–956, May 1995. ISSN 0885-8950. doi: 10.1109/59.387938. 8

[69] E. Lerch, D. Povh, and L. Xu. Advanced svc control for damping power system oscillations. *Power Systems, IEEE Transactions on*, 6(2):524 –535, May 1991. ISSN 0885-8950. doi: 10.1109/59.76694. 9

[70] H. Li and Z. Chen. Overview of different wind generator systems and their comparisons. *IET Renewable Power Generation*, 2(2): 123–138, 2008. ISSN 17521416. 22

[71] M. Liserre, R. Cárdenas, M. Molinas, and J. Rodriguez. Overview of multi-mw wind turbines and wind parks. *Industrial Electronics, IEEE Transactions on*, 58(4):1081 –1095, April 2011. ISSN 0278-0046. doi: 10.1109/TIE.2010.2103910. 22

[72] N. Magaji and M. Mustafa. Optimal location and signal selection of upfc device for damping oscillation. *International Journal of Electrical Power and Energy Systems*, 33(4):1031–1042, 2011. ISSN 01420615, 18793517. doi: 10.1016/j.ijepes.2011.01.020. 8

[73] Y. V. Makarov, V. A. Maslennikov, and D. J. Hill. Calculation of oscillatory stability margins in the space of power system controlled parameters. In *Proc. of the International Symposium on Electric Power Engineering Stockholm Power Tech: Power Systems*, pages 18–22, 1995. 39

[74] C. Martinez, G. Joos, and B. Ooi. Power system stabilizers in variable speed wind farms. In *Power Energy Society General Meeting, 2009. PES '09. IEEE*, pages 1 –7, July 2009. doi: 10.1109/PES.2009.5275595. 7, 8, 55

[75] I. Martinez, A. R. Messina, and E. Barocio. Higher-order normal form analysis of stressed power systems: A fundamental study. *Electric Power Components and Systems*, 32(Issue 12):1301–1317, December 2004. doi: 10.1080/15325000490446818. URL http://dx.doi.org/10.1080/15325000490446818. 39

[76] J. M. Mauricio, A. Marano, A. Gomez-Exposito, and J. L. Martinez Ramos. Frequency regulation contribution through variable-speed wind energy conversion systems. *Power Systems, IEEE Transactions on*, 24(1):173–180, Feb. 2009. ISSN 0885-8950. doi: 10.1109/TPWRS.2008.2009398. 67

[77] J. Mehmedalic, T. Knüppel, and J. Østergaard. Using H_∞ to design robust POD controllers for wind power plants. In *47th International Universities' Power Engineering Conference*, Brunel University, London, UK, September 2012. 14, 121

[78] A. Mendonca and J. Lopes. Robust tuning of power system stabilisers to install in wind energy conversion systems. *Renewable Power Generation, IET*, 3(4):465–475, December 2009. ISSN 1752-1416. doi: 10.1049/iet-rpg.2008.0066. 8

[79] A. R. Messina, O. Begovich, J. H. López, and E. N. Reyes. Design of multiple facts controllers for damping inter-area oscillations: a decentralised control approach. *International Journal of Electrical Power & Energy Systems*, 26(1):19 – 29, 2004. ISSN 0142-0615. doi: DOI:10.1016/S0142-0615(03)00067-X. URL http://www.sciencedirect.com/science/article/B6V2T-49DN6VC-1/2/ab5a3d7c05115434bad4c6a5453df94c. 9

[80] Z. Miao, L. Fan, D. Osborn, and S. Yuvarajan. Control of dfig based wind generation to improve inter-area oscillation damping. *Power and Energy Society General Meeting - Conversion and Delivery of Electrical Energy in the 21st Century, 2008 IEEE*, pages 1–7, July 2008. ISSN 1932-5517. doi: 10.1109/PES.2008.4596741. 7, 55

[81] A. Miller, E. Muljadi, and D. Zinger. A variable speed wind turbine power control. *Energy Conversion, IEEE Transactions on*, 12(2):181–186, 1997. ISSN 08858969. 22

[82] N. Miller, J. Sanchez-Gasca, W. Price, and R. Delmerico. Dynamic modeling of ge 1.5 and 3.6 MW wind turbine-generators for stability simulations. *2003 IEEE Power Engineering Society General Meeting (IEEE Cat. No.03CH37491)*, 3:1977–1983 Vol. 3, 2003. 22

[83] N. Mithulananthan, C. Canizares, J. Reeve, and G. Rogers. Comparison of pss, svc, and statcom controllers for damping power system oscillations. *Power Systems, IEEE Transactions on*, 18 (2):786 – 792, May 2003. ISSN 0885-8950. doi: 10.1109/TPWRS.2003.811181. 8, 39

[84] N. Modi, T. K. Saha, and N. Mithulananthan. Effect of wind farms with doubly fed induction generators on small-signal stability - a case study on australian equivalent system. In *2011 IEEE PES Innovative Smart Grid Technologies (ISGT Australia)*, pages 1–7, 2011. doi: 10.1109/ISGT-Asia.2011.6167076. 5, 6, 47

[85] J. Morren, J. Pierik, and S. W. de Haan. Inertial response of variable speed wind turbines. *Electric Power Systems Research*, 76(11):980–987, 2006. ISSN 03787796. 67

[86] E. Muljadi, S. Pasupulati, A. Ellis, and D. Kosterov. Method of equivalencing for a large wind power plant with multiple turbine representation. *IEEE Power Engineering Society General Meeting*, pages 1–9, 2008. ISSN 19325517. doi: 10.1109/PES.2008.4596055. 22, 95

[87] A. H. Nayfeh. *Method of Normal Forms*. Wiley Series in Nonlinear Science. John Wiley & Sons, Inc., 605 Third Avenue, New York, NY, 1993. ISBN: 0-471-59354-0. 39

[88] N. Negra, O. Holmstrom, B. Bak-Jensen, and P. Sørensen. Aspects of relevance in offshore wind farm reliability assessment. *Energy Conversion, IEEE Transactions on*, 22(1):159–166, 2007. ISSN 08858969. 42

[89] H. Nguyen-Duc, L.-A. Dessaint, A. F. Okou, and I. Kamwa. A power oscillation damping control scheme based on bang-bang modulation of FACTS signals. *Power Systems, IEEE Transactions on*, 25(4):1918–1927, Nov. 2010. ISSN 0885-8950. doi: 10.1109/TPWRS.2010.2046504. 9

[90] J. N. Nielsen, V. Akhmatov, J. Thisted, E. Grøndahl, P. Egedal, M. N. Frydensbjerg, and K. H. Jensen. Modelling and fault-ride-trough tests of Siemens Wind Power 3.6 MW variable-speed wind turbines. *Wind Engineering*, 31:441–452(12), December 2007. doi: 10.1260/030952407784079753. 22

[91] E. Palmer. Non-linear effects on modal estimates obtained from power system ringdowns. *IEEE Power & Energy Society General Meeting*, pages 1–6, 2011. ISSN 19449925, 19449925. doi: 10.1109/PES.2011.6039705. 121

[92] National Grid plc. The grid code. Technical Report Issue 4 Revision 2, National Grid Electricity Transmission plc, National Grid House, Warwick Technology Park, Gallows Hill, Warwick, CV34 6DA, UK, March 2010. 80

[93] Pourbeik, Kundur, and Taylor. The anatomy of a power grid blackout. *IEEE Power and Energy Magazine*, 4(5):22–29, 2006. ISSN 15407977, 15584216. doi: 10.1109/MPAE.2006.1687814. 1

[94] P. Pourbeik and M. Gibbard. Damping and synchronizing torques induced on generators by FACTS stabilizers in multimachine power systems. *Power Systems, IEEE Transactions on*, 11(4):1920–1925, Nov. 1996. ISSN 0885-8950. doi: 10.1109/59.544664. 37, 38

[95] P. Pourbeik and M. Gibbard. Simultaneous coordination of power system stabilizers and FACTS device stabilizers in a multimachine power system for enhancing dynamic performance. *Power Systems, IEEE Transactions on*, 13(2):473 –479, May 1998. ISSN 0885-8950. doi: 10.1109/59.667371. 9

[96] P. Pourbeik, M. Gibbard, and D. Vowles. Proof of the equivalence of residues and induced torque coefficients for use in the calculation of eigenvalue shifts. *Power Engineering Review, IEEE*, 22 (1):58–60, Jan. 2002. ISSN 0272-1724. doi: 10.1109/MPER.2002.4311662. 38, 56

[97] R. Ramos, L. Alberto, and N. Bretas. A new methodology for the coordinated design of robust decentralized power system damping controllers. *Power Systems, IEEE Transactions on*, 19(1):444 – 454, Feb. 2004. ISSN 0885-8950. doi: 10.1109/TPWRS.2003.820690. 9

[98] S. Ray, B. Chaudhuri, and R. Majumder. Appropriate signal selection for damping multi-modal oscillations using low order controllers. In *Power and Energy Society General Meeting - Conversion and Delivery of Electrical Energy in the 21st Century, 2008 IEEE*, pages 1 –7, July 2008. doi: 10.1109/PES.2008.4596564. 8

[99] G. Rogers. *Power System Oscillations*. Power Electronics and Power Systems. Kluwer Academic Publishers, 1st edition, 2000. ISBN-10: 0792377125. 1, 5, 7, 17, 24, 25, 32, 33, 35, 55, 56

[100] S. Y. Ruan, G. J. Li, B. T. Ooi, and Y. Z. Sun. Power system damping from real and reactive power modulations of voltage-source-converter station. *IET Generation Transmission & Distribution*, 2(3):311–320, May 2008. ISSN 1751-8687. doi: 10.1049/iet-gtd:20070021. 19, 36, 51, 56, 57, 58

[101] S.-Y. Ruan, G.-J. Li, B.-T. Ooi, and Y.-Z. Sun. Power system damping from energy function analysis implemented by voltage-source-converter stations. *Electric Power Systems Research*, 78 (8):1353–1360, 2008. ISSN 03787796. doi: 10.1016/j.epsr.2007.12.003. 8, 52

[102] J. L. Rueda, D. G. Colome, and I. Erlich. Assessment and enhancement of small signal stability considering uncertainties. *Power Systems, IEEE Transactions on*, 24(1):198–207, Feb. 2009. ISSN 0885-8950. doi: 10.1109/TPWRS.2008.2009428. 42

[103] R. Sadikovic, P. Korba, and G. Andersson. Self-tuning controller for damping of power system oscillations with facts devices. In *Power Engineering Society General Meeting, 2006. IEEE*, page 6 pp., 2006. doi: 10.1109/PES.2006.1709473. 8

[104] C. Samarasinghe and D. Vowles. Wind generation investigation project - effect of wind generation on small signal stability. Technical Report Investigation 8, TRANSPOWER New Zealand, The National Grid, March 2008. 5

[105] O. Samuelsson. *Power System Damping – Structural Aspects of Controlling Active Power*. Phd thesis, University of Lund, Sweden, Department of Industrial Electrical Engineering and Automation (IEA), Lund Institute of Technology (LTH), P.O. Box 118, S-221 00 LUND, SWEDEN, 1997. ISBN 91-88934-05-5. 3, 4, 18, 52

[106] J. Sanchez-Gasca, V. Vittal, M. Gibbard, A. Messina, D. Vowles, S. Liu, and U. Annakkage. Inclusion of higher order terms for small-signal (modal) analysis: committee report-task force on assessing the need to include higher order terms for small-signal (modal) analysis. *Power Systems, IEEE Transactions on*, 20(4): 1886–1904, Nov. 2005. ISSN 0885-8950. doi: 10.1109/TPWRS.2005.858029. 39

[107] R. Seydel. *Practical Bifurcation and Stability Analysis*, volume 5 of *Interdisciplinary Applied Mathematics*. Springer, Universität zu Köln, Mathematisches Institut, Weyertal 86-90, 50931 Köln, 3rd. edition, 2010. doi: 10.1007/978-1-4419-1740-9. ISBN: 978-1-4419-1740-9. 39

[108] A. Shafiu, O. Anaya-Lara, G. Bathurst, and N. Jenkins. Aggregated wind turbine models for power system dynamic studies. *Wind Engineering*, 30(3):171–85, 2006. ISSN 0309524x. doi: 10.1260/030952406778606205. 22, 95

[109] L. B. Shi, C. Wang, L. Z. Yao, L. M. Wang, and Y. X. Ni. Analysis of impact of grid-connected wind power on small signal stability. *Wind Energy*, 14(4):517–537, 2011. ISSN 10954244, 10991824. doi: 10.1002/we.440. 42

[110] L. Sigrist and L. Rouco. Design of damping controllers for doubly fed induction generators using eigenvalue sensitivities. In *Power Systems Conference and Exposition, 2009. PSCE '09. IEEE/PES*, pages 1–7, March 2009. doi: 10.1109/PSCE.2009.4840184. 7, 8, 55

[111] J. Slootweg and W. Kling. The impact of large scale wind power generation on power system oscillations. *Electric Power Systems Research*, 67(1):9 – 20, 2003. ISSN 03787796. 5

[112] T. Smed and G. Andersson. Utilizing HVDC to damp power oscillations. *Power Delivery, IEEE Transactions on*, 8(2):620 – 627, Apr. 1993. ISSN 0885-8977. doi: 10.1109/61.216868. 4, 6, 19, 36, 51, 55, 56, 57, 58, 66

[113] J. Starke. Nonlinear dynamics in engineering and science, Spring 2009. Lecture Notes for the Course 01625 at the Technical University of Denmark. 39

[114] N. Strachan and D. Jovcic. Stability of a variable-speed permanent magnet wind generator with weak ac grids. *Power Delivery, IEEE Transactions on*, 25(4):2779 –2788, Oct. 2010. ISSN 0885-8977. doi: 10.1109/TPWRD.2010.2053723. 22, 47

[115] G. Sybille and et al. *SimPowerSystems^{TM} 5 - User's Guide*. Hydro-Québec and MathWorks, Inc, March 2010. URL http://www.mathworks.com/access/helpdesk/help/pdf_doc/physmod/powersys/powersys.pdf. 19

[116] A. Tabesh and R. Iravani. Small-signal dynamic model and analysis of a fixed-speed wind farm-a frequency response approach. *Power Delivery, IEEE Transactions on*, 21(2):778–787, 2006. ISSN: 0885-8977. 6

[117] A. Tabesh and R. Iravani. Small-signal model and dynamic analysis of variable speed induction machine wind farms. *Renewable Power Generation, IET*, 2(4):215–227, December 2008. ISSN 1752-1416. doi: 10.1049/iet-rpg:20070107. 6

[118] M. Tazil, V. Kumar, R. Bansal, S. Kong, Z. Dong, and W. Freitas. Three-phase doubly fed induction generators: an overview. *Electric Power Applications, IET*, 4(2):75 –89, February 2010. ISSN 1751-8660. doi: 10.1049/iet-epa.2009.0071. 22

[119] D. Trudnowski. Estimating electromechanical mode shape from synchrophasor measurements. *Power Systems, IEEE Transactions on*, 23(3):1188–1195, Aug. 2008. ISSN 0885-8950. doi: 10.1109/TPWRS.2008.922226. 17

[120] D. Trudnowski, J. Hauer, J. Pierre, W. Litzenberger, and D. Maratukulam. Using the coherency function to detect large-scale dynamic system modal observability. In *American Control Conference, 1999. Proceedings of the 1999*, volume 4, pages 2886–2890 vol.4, 1999. doi: 10.1109/ACC.1999.786601. 17

[121] G. Tsourakis and C. Vournas. A controller for wind generators to increase damping of power oscillations. In *Circuits and Systems (ISCAS), Proceedings of 2010 IEEE International Symposium on*, pages 2195 –2198, 302010-june2 2010. doi: 10.1109/ISCAS.2010.5537200. 7, 55

[122] G. Tsourakis, B. Nomikos, and C. Vournas. Effect of wind parks with doubly fed asynchronous generators on small-signal stability. *Electric Power Systems Research*, 79(1):190 – 200, 2009. ISSN 0378-7796. doi: 10.1016/j.epsr.2008.05.018. URL http://www.sciencedirect.com/science/article/B6V30-4T0FHRM-1/2/3b6ac71f22cac8ff81670dcc6944a0f9. 6, 49

[123] G. Tsourakis, B. Nomikos, and C. Vournas. Contribution of doubly fed wind generators to oscillation damping. *Energy Conversion, IEEE Transactions on*, 24(3):783 –791, Sep. 2009. ISSN 0885-8969. doi: 10.1109/TEC.2009.2025330. 7, 55

[124] S. Ustinov, J. Milanovic, and V. Maslennikov. Inherent dynamic properties of interconnected power systems. *International Journal of Electrical Power and Energy Systems*, 24(5):371–378, 2002. ISSN 01420615. 3

[125] E. Vittal, M. O'Malley, and A. Keane. Rotor angle stability with high penetrations of wind generation. *IEEE Transactions on Power Systems*, 27(1):353–362, 2012. ISSN 08858950, 15580679. doi: 10.1109/TPWRS.2011.2161097. 6, 49

[126] V. Vittal, N. Bhatia, and A. Fouad. Analysis of the inter-area mode phenomenon in power systems following large disturbances. *Power Systems, IEEE Transactions on*, 6(4):1515 –1521, Nov. 1991. ISSN 0885-8950. doi: 10.1109/59.116998. 38

[127] S. Wang and J. Chow. Coprime factors, strictly positive real functions, lmi and low-order controller design for siso systems. In *Decision and Control, 1998. Proceedings of the 37th IEEE Conference on*, volume 3, pages 2738 –2744 vol.3, 1998. doi: 10.1109/CDC.1998.757869. 8

[128] D. Wilson, J. Bialek, and Z. Lubosny. Banishing blackouts [power system oscillations stability]. *Power Engineer*, 20(2):38 –41, April-May 2006. ISSN 1479-8344. 1, 5, 41

[129] F. Wu, X.-P. Zhang, and P. Ju. Small signal stability analysis and control of the wind turbine with the

direct-drive permanent magnet generator integrated to the grid. *Electric Power Systems Research*, 79(12):1661 – 1667, 2009. ISSN 0378-7796. doi: DOI:10.1016/j.epsr.2009.07.003. URL http://www.sciencedirect.com/science/article/B6V30-4X0W4NT-1/2/149a798cfc8682687a41ed25cdbccb26. 22

[130] L. Yang, Z. Xu, J. Østergaard, Z. Y. Dong, K. P. Wong, and X. Ma. Oscillatory stability and eigenvalue sensitivity analysis of a dfig wind turbine system. *IEEE Transactions on Energy Conversion*, 26(1):328–339, 2011. ISSN 08858969, 15580059. doi: 10.1109/TEC.2010.2091130. 39

[131] R. Zarate-Minano, F. Milano, and A. J. Conejo. An opf methodology to ensure small-signal stability. *IEEE Transactions on Power Systems*, 26(3):1050–1061, 2011. ISSN 08858950, 15580679. doi: 10.1109/TPWRS.2010.2076838. 42

[132] X.-P. Zhang, C. Rehtanz, and B. Pal. Linear control design and simulation of power system stability with FACTS. In *Flexible AC Transmission Systems: Modelling and Control*, Power Systems, pages 347–380. Springer Berlin Heidelberg, 2006. ISBN 978-3-540-30607-8. doi: 10.1007/3-540-30607-2_13. URL http://dx.doi.org/10.1007/3-540-30607-2_13. 7

[133] C. Zheng and M. Kezunovic. Impact of wind generation uncertainty on power system small disturbance voltage stability: A PCM-based approach. *Electric Power Systems Research*, 84(1):10–19, 2012. ISSN 03787796. doi: 10.1016/j.epsr.2011.10.001. 42

Appendices

Appendix A

Selected Publications

A.1 Paper I

T. Knüppel, J. N. Nielsen, K. H. Jensen, A. Dixon, and J. Østergaard. Small-signal stability of wind power system with full-load converter interfaced wind turbines. *IET Renewable Power Generation*, 6(2):79–91, 2012. doi: 10.1049/iet-rpg.2010.0186. ISSN 1752-1416.

Small-signal stability of wind power system with full-load converter interfaced wind turbines

Thyge Knüppel*, Jørgen N. Nielsen†, Kim H. Jensen‡
Andrew Dixon§, Jacob Østergaard¶

March 29, 2012

Abstract

Small-signal stability analysis of power system oscillations is a well established field within power system analysis, but not much attention has yet been paid to systems with a high penetration of wind turbines (WTs) and with large wind power plants (WPPs). A comprehensive analysis is presented, which assesses the impact of full-load converter interfaced wind turbines on power system small-signal stability. The study is based on a seven-generator network with lightly damped inter-area modes. A detailed WT model with all grid relevant control functions is used in the study. The WT is, furthermore, equipped with a park-level WPP voltage controller and comparisons are presented. The WT model for this work is a validated dynamic model of the 3.6 MW Siemens Wind Power WT. The study is based on modal analysis which is complemented with time domain simulations on the non-linear system.

Keywords: wind turbines, wind power plant, wind power plant controller, power systems, small-signal stability, modal analysis

1 Introduction

With the rapid development in installed capacity of wind power and with the increasing size of each installation, the role and impact of wind power on power system operation is changing. In grid codes from some transmission system operators this development is already noted, given that large wind power plants (WPPs) are termed power park modules and must comply with similar requirements to those for other generation units. In continuation of this, large WPPs

*T. Knüppel is with Siemens Wind Power A/S, DK-7330 Brande, Denmark and Centre for Electric Technology, Department of Electrical Engineering, Technical University of Denmark, DK-2800 Lyngby, Denmark (thyge.knuppel@siemens.com)

†J. N. Nielsen is with Siemens Wind Power A/S, DK-7330 Brande, Denmark (joergen_nygaard.nielsen@siemens.com)

‡K. H. Jensen is with Siemens Wind Power A/S, DK-7330 Brande, Denmark (kim_hoej.jensen@siemens.com)

§A. Dixon is with National Grid Electricity Transmission plc (National Grid), Warwick CV34 6DA, UK (andrew.dixon@uk.ngrid.com)

¶J. Østergaard is with Centre for Electric Technology, Department of Electrical Engineering, Technical University of Denmark, DK-2800 Lyngby, Denmark (joe@elektro.dtu.dk)

are often equipped with a supervisory voltage and frequency controller, that is, a controller on park level designed to coordinate the response of the individual units in the park. The effect and intention of such supervisory controllers on park level is that the combined response of the wind turbines (WTs), evaluated at the interface between the WPP and the power system, are comparable with other power plants. The ability of WPPs to deliver active power reserves is treated in number of publications [1–4], as well as voltage and reactive power control [5, 6]. In some countries, for instance Denmark and UK, WPPs are already applied for ancillary services, for example, advanced voltage control and frequency reserve.

Regarding power system stability investigations, considerable attention has been paid to low-voltage fault- ride-through (FRT) capabilities of the WTs; that is, the ability of WTs to stay connected during external disturbances in the grid and provide necessary voltage support [6–8]. With increasing penetration of wind power and increasing size of each installed WPP, new stability considerations arise. A topic of increasing importance is the effect of WPPs on power system small-signal stability, including influence on power system oscillations.

The damping of critical inter-area oscillations is affected by number of factors, such as network topography, generator excitation control, HVDC control, transmission line power flows, and so on [9, 10]. Also, the presence of non-synchronous generation units can have an impact on the damping of inter-area oscillations. In [11, 12] comparisons are presented on the influence of power system oscillations of WPPs based on fixed-speed induction generators (FSIG) and doubly-fed induction generators (DFIG). Slootweg *et al.* [12] found that particularly FSIG WPPs tend to improve the damping of inter-area oscillations, while no significant effect is observed for intra-area oscillation. It is, however, noticed that the results become ambiguous when a large part of the synchronous generation in an oscillatory node is replaced with wind power. In [11] it is found that both FSIG and DFIG WPPs improve the damping of inter- area oscillations, although to a lesser extent for the DFIG WPP. In [13,14] also full-load converter interfaced WPPs are included in the comparison. Hagstrom *et al.* [13] noted that the DFIG does not have any significant effect on the damping while the full-load converter-type WPP, here modelled as a negative load, decreases the damping. In [14] it is concluded that the characteristics of the variable speed WPPs, DFIG and full-load converter WPP are practically identical, while the FSIG WPPs result in slightly better system damping. A WT based on a direct-drive permanent magnet generator is analysed in [15].

In [16] the influence is analysed of the voltage/VAR control mode of DFIG-based WPPs on inter-area oscillations. The study found that by increasing the penetration of wind power generally had a favourable effect, with increased frequency and damping of the inter-area mode between a weak and a stronger system. With the WPP in voltage control mode the authors of [16] found that, for some parameter-set, an adverse interaction is noticed; it is, however, noted that these interactions can be avoided with appropriate tuning of the voltage controller.

In [17, 18] a generic small-signal stability model is developed for fixed- and variable-speed WTs with corresponding collector and utility grid to which the units are connected. The approach is based on sensitivity analysis and singular value decomposition.

A few publications have investigated the possibility of using variable-speed

WPPs actively to damp power system oscillations [19–21]. In a recent PhD thesis by Elkington, it is concluded that DFIG-based WPPs can provide a positive contribution to damping of power system oscillations by adding an auxiliary controller [22]. In [23, 24] optimisation approaches are proposed for the tuning of the WPP damping controller.

The configuration in the full-load converter WT has the effect of decoupling the generator dynamics from the grid dynamics, and following this argumentation the WT generators cannot contribute to system oscillations. However, as the WTs and the WPPs are controlled to provide various system services, it is possible that the control capability of the WTs and WPPs can interact with system dynamics. Here, different implementations of the control will give different results in terms of impact on system dynamics. This phenomenon is known from control interactions of HVDC stations or FACTS devices in subsynchronous torsional interactions (SSTI), for example [25, 26], and exemplified in [16] for a WPP voltage control system. Thus, the validity of damping results depends on an accurate representation of the control systems. So far most publications on small-signal stability of variable-speed WTs have dealt with generic models with a varying degree of details, whereas this study is conducted on a verified WT model with a detailed representation of all grid relevant components and controls [27].

In this paper the impact of full-load converter-interfaced WTs on small-signal stability, that is, participation in power system oscillations, is investigated. The system is analysed for the WPP with and without a park-level voltage controller. The analysis is based on a seven-generator network, which illustrates some aspects of the dynamic behaviour of the UK power system, namely inter-area oscillations between major areas of the system.

The paper is organised as follows. In section 2 the basis for the analysis is established with a brief description of modal analysis and power system oscillations. Section 3 presents the case network and the analysed WT concept, while section 4 presents the case studies performed and the results from the analysis. Finally, the discussion and conclusion are found in sections 5 and 6, respectively.

2 Method

Power system oscillations are inherent in interconnected power systems based on synchronous generators [28]. Power system oscillations and the application of eigenvalue analysis as means of analysis are well described in the literature, for example [9, 29]. Another approach is to use signal processing of measured data [30, 31]. When analysing very large systems this measurement-based approach has the advantage that it is not dependent on the accuracy of a large dynamic model.

2.1 Eigenvalue analysis

The eigenvalues provide important information on the dynamics of the system, that is, the frequency and damping of any oscillations. If the ith eigenvalue is given as $\lambda_i = a \pm jb$, the natural frequency, ω_n, the damped frequency, ω_d, and

the damping ratio, ζ, are defined as

$$\omega_n = \sqrt{a^2 + b^2} \quad \left[\frac{\text{rad}}{\text{sec}}\right], \quad \omega_d = b \quad \left[\frac{\text{rad}}{\text{sec}}\right], \quad \zeta = \frac{-a}{\omega_n} \quad [-]$$

From classical control theory of continuous time systems, it is given that mode λ_i is asymptotically stable only if $a < 0$.

Power system oscillations are often divided into inter-, intra- and local-area modes depending on the global or local scope of the oscillation. Besides the frequency of oscillation, the concepts of mode-shape, ϕ, and participation factor, p_{ji} are used to correctly identify the source, nature and significance of a mode.

3 Study case

The analysis is performed in MatLab/Simulink where the case network is modelled in SimPowerSystems [32] and where the linearization is performed with the Simulink Control Design toolbox [33]. The linearisation is done directly on the power system model defined and initialised in SimPowerSystems. Exact linearisation is used for every function in the model that has an analytical first derivative, whereas numerical perturbation is used for those elements, such as look-up tables, that cannot be linearised analytically. The analytical first derivative is preprogrammed for the individual Simulink functions and the Jacobian is hence computed by evaluating these derivatives at the found steady-state operating condition.

3.1 Case network

The study is based on the 18-node, seven-generator system depicted in Figure 1, which furthermore consists of six loads and an aggregated WPP with the corresponding collector grid. The network model has been developed in collaboration with National Grid as an extension of the three-generator system presented in [11] to achieve a higher level of flexibility and numerical stability. The system represents a large network that has been reduced to a small number of nodes.

The synchronous generators are modelled as round rotor machines, since this is the dominant generator type of the UK power system, using the standard RMS model of SimPowerSystems. The generators are aggregated machines, each representing several smaller and larger generation units; the total capacity for each unit is given in Table 7, where transformer reactances and load distributions are also given. The network model is tuned for a light-load situation and the distribution of load and generation imply a southbound power flow of approximately 1 900 MW. The parameters for the dynamic generator models and the network parameters are given in Table 8 and 9, respectively. Parameters for the synchronous machines with corresponding exciter and PSS models are selected to represent the dominant unit type in each area and have been provided by National Grid for this study. Furthermore each generator is equipped with a standard IEEEG0 governor.

Note that the model does not accurately represent particular aspects of the UK network, and hence should not be used to draw conclusions regarding the performance of this network. The developed model does, however, assist

in understanding of power oscillations between major areas of the UK power system.

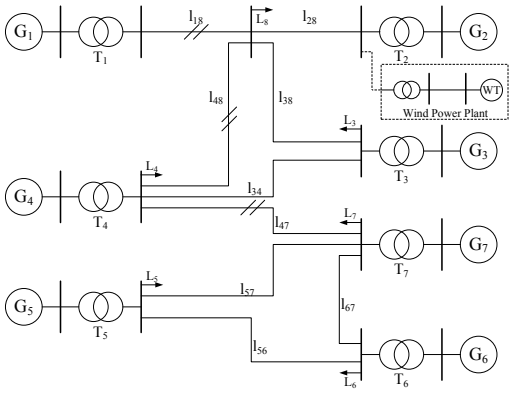

Figure 1: Single-line diagram of the analysed case network

3.2 Wind turbine technology

The WT concept for this study has an induction generator and is interfaced through a full-load converter system as illustrated in Figure 2. The WT is pitch controlled and has variable-speed operation to maximise the active power output. The dynamic model represents a 3.6 MW Siemens Wind Power WT and the dynamic FRT response of the model has been validated from field tests [27]. The WT is represented with a reduced order, positive sequence, RMS model suitable for dynamic power system studies. In this study, an aggregated WT model is used and the analysis thus only considers the main interaction between the power system and the WPP.

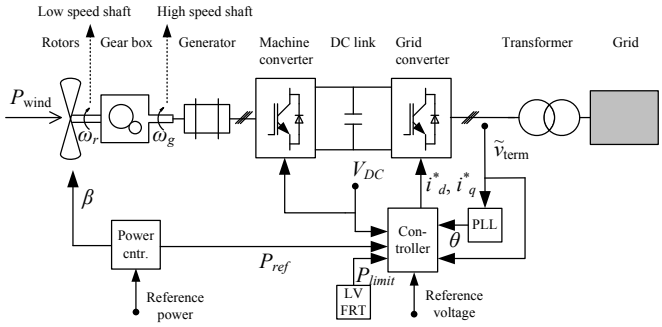

Figure 2: Wind turbine concept used in the analysis, that is, full-load converter interfaced WT

A block diagram showing the overall connections is shown in Figure 3 and below is a brief description given of the subsystems.

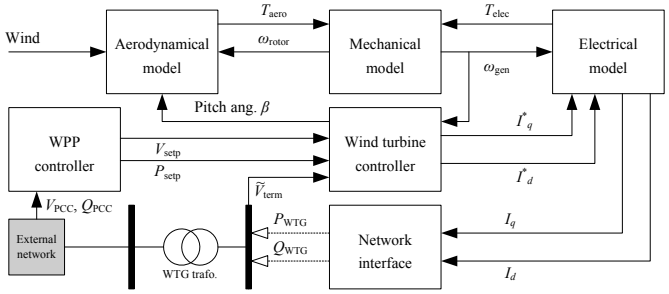

Figure 3: Overall block diagram of the WT model

Aerodynamic model A variable wind speed aerodynamic model is used, which includes power coefficient with pitch angle and tip-speed ratio. The pitch system is represented by a first-order system.

Mechanical model The mechanical system is modelled as a third order, two-mass model, which includes shaft stiffness and damping [34].

$$\dot{\omega}_g = \tfrac{1}{J_g}(K_s\theta_s + D_s(\omega_r - \omega_g) - T_e) \tag{1a}$$

$$\dot{\omega}_r = \tfrac{1}{J_r}(T_a - K_s\theta_s - D_s(\omega_r - \omega_g)) \tag{1b}$$

$$\dot{\theta} = \omega_r - \omega_g \tag{1c}$$

In (1), ω_r and ω_g are rotor and generator speed, θ_s shaft twist angle, J_r and J_g are rotor and generator inertia, T_a and T_e are aerodynamic and electromagnetic torque, K_s is shaft stiffness and D_s is the shaft damping coefficient.

Electrical model The WT converter system comprises machine and grid-side converter, DC-link and a generic reduced-order control scheme. The converters are represented as ideal converters and the generator as a zeroth-order system. Hence, all generator flux dynamics have been eliminated to reflect the rapid response of the converter system [35], which acts to decouple the fast generator dynamics from the grid side.

Wind turbine controller The active and reactive power injection is controlled by two first-order systems and is subject to various machine and converter limits. A phase- locked loop (PLL) computes the angle of the terminal voltage phasor, which is used to align the internal dq-reference frame. A FRT function is, furthermore, included which monitors for system faults and shapes the current injection into the grid upon detection, although this mode is not activated in the operating points analysed here.

Network interface The WT is interfaced to the network through a controlled current source.

3.3 WPP collector grid

The collector grid is modelled as a T-equivalent with the entire capacitance lumped as a shunt and with half the inductance and half the resistance as a series impedance on each side. For $P_{\mathrm{WPP}} = 180$ MW the network parameters are given in Table 10. The collector grid parameters are scaled according to the size of the WPP such that the same voltage profile is achieved, that is

$$z_{\mathrm{scale}} = \frac{S^B_{\mathrm{base}}}{S_{\mathrm{base,WPP}}} \quad R = z_{\mathrm{scale}} R^B$$

$$X_L = z_{\mathrm{scale}} X^B_L \quad B_C = \frac{B^B_C}{z_{\mathrm{scale}}}$$

where the superscript $.^B$ refers to the values in Table 10 with $P_{\mathrm{WPP}} = 180$ MW.

3.4 WPP voltage controller

The WPP voltage controller is an outer, corrective controller that controls the voltage at the point of common connection (PCC) at the interface to the power system. The WPP voltage controller distributes voltage set-points to the individual WTs based on the conditions at the PCC, where the WT voltage controller controls the voltage at the WT terminals according to its set-point.

The block diagram of the WPP voltage controller is shown in Figure 4 and the relation to the WT system is shown in the block diagram in Figure 3. The droop controller prevents chasing of adjacent units both controlling the voltage by dividing the responsibility between the units. Furthermore, the droop controller ensures that a predictable amount of reactive power is delivered for a given deviation from the PCC reference voltage. The applied model of the WPP voltage controller has been provided by Siemens wind power for this analysis, although Siemens Wind Power does not necessarily apply exactly the same control.

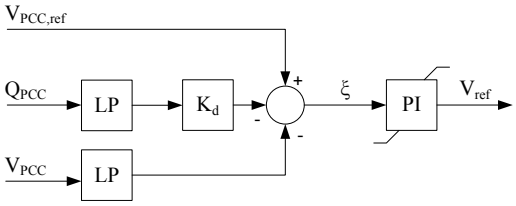

Figure 4: Block diagram of the WPP voltage droop controller. LP: low-pass filter, PI: PI-controller

The operation of the WPP voltage controller is dependent on the strength of the grid, and the controller must be carefully tuned for the conditions at the PCC. For this analysis, a 4% droop, that is, $K_d = 0.04$, is used and the WPP

voltage controller is tuned to deliver 90 % of its response within one second in a well-damped manner [36]. The tuning of the WPP voltage controller is performed for this study as presented in [37].

3.5 Characteristics of case network

A list of dominant eigenvalues is given in Table 1. Three lightly damped inter-area modes are present in the system, λ_{1-3}, for which the modal characteristics are given in Table 2.

Table 1: Qualitative description of dominant eigenvalues

λ_1	Inter-area mode between G_{1-2} and G_{3-7}
λ_2	Inter-area mode between $G_{4,7}$ and G_{5-6}
λ_3	Inter-area mode between G_4 and G_7

Table 2: Characteristics for the three inter-area modes in the base case without wind power

#	λ [-]	ω_d [Hz]	ζ [-]
λ_1	$-0.275 \pm j3.10$	0.493	0.088
λ_2	$-0.658 \pm j6.26$	0.997	0.105
λ_3	$-0.643 \pm j8.83$	1.41	0.073

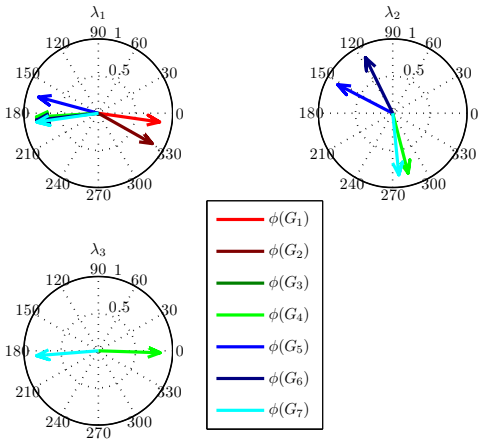

Figure 5: Mode shapes for the generator speed states for the three inter-area modes in the base case without wind power

The participation factors are shown in Table 3 for the inter-area modes for the generator rotor angle states. The mode shapes for the three inter-area modes, λ_{1-3}, are given in Figure 5, where the characteristic 180° displacement between oscillating groups of generators is seen.

Table 3: Normalised rotor angle participation factors for the inter-area modes λ_{1-3} for the system with no wind power connected

State variable	$\lvert p_{j1}\rvert$	$\lvert p_{j2}\rvert$	$\lvert p_{j3}\rvert$
$\delta\ (G_1)$	1.0	$< 10^{-2}$	$< 10^{-4}$
$\delta\ (G_2)$	0.50	$< 10^{-2}$	$< 10^{-4}$
$\delta\ (G_3)$	0.014	0.031	0.024
$\delta\ (G_4)$	0.14	1.0	0.17
$\delta\ (G_5)$	0.18	0.065	$< 10^{-2}$
$\delta\ (G_6)$	0.36	0.67	$< 10^{-2}$
$\delta\ (G_7)$	0.039	0.085	1.0

The modal analysis is a linear method and it should thus be complemented with dynamic simulations on the non-linear system. In Figure 6 and 7 the dynamic response is shown after a three-phase short-circuit at line l_{48}. For now, there is no wind power in the system. The fault is applied midway between the busses, on a single circuit, and it is cleared after 140 ms. Figure 6 shows the active and reactive power flow on the double circuit l_{48} during and after the short-circuit. The short-circuit excites inter-area oscillation λ_1 between G_{1-2} and G_{3-7}, which is noted by the grouping of the generators in Figure 7 where the generator rotor speeds are plotted.

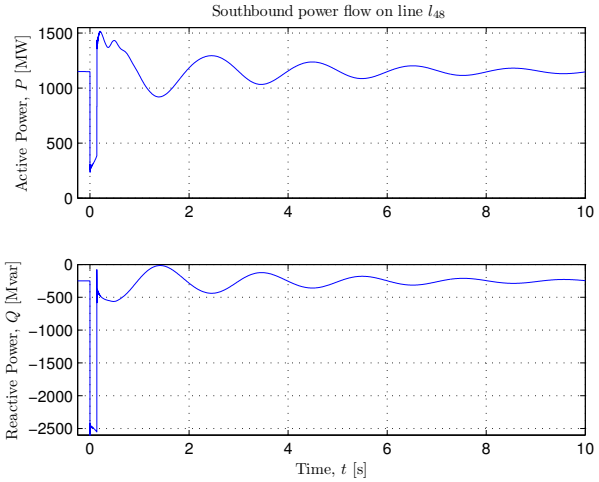

Figure 6: Active and reactive power flow on line l_{48} after a short-circuit on one of the l_{48} lines

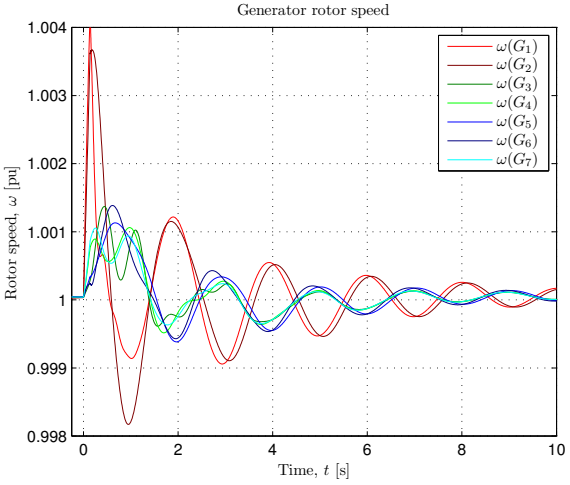

Figure 7: Generator rotor speeds after a short-circuit on one of the l_{48} lines

4 Selected cases

The aim of the study is to analyse the influence of increased wind power penetration on power oscillations in the system, with emphasis on the previously mentioned inter-area modes.

Two cases with a varying penetration of wind power are investigated and compared to the base case with only synchronous generation.

1. P_{setp} of G_2 is reduced as the penetration of wind power is increased while the MVA rating is maintained

2. MVA rating of G_2 is reduced as the penetration of wind power is increased while the loading of G_2 is maintained

In all cases and for all wind power penetration levels, active power production is shifted between only G_2 and the WPP and the power flow in the system is thus unchanged.

In case 1 the introduction of wind power does not displace any conventional units and only the active power set-point is reduced to accommodate the power produced by the WPP. In case 2 the wind power displaces conventional units and the MVA rating of G_2 is reduced accordingly. In each case the size of the WPP is varied linearly from 36 to 1 000 MW in 10 steps. Cases 1 and 2 are treated in sections 4.1 and 4.2, respectively.

Variable-speed WTs have several modes of operation and all do not apply the same control. Different dynamics are hence in play for different modes of operation. First of all, the operation and active power output of any WT is subject to local wind conditions. The optimisation of captured wind energy is subject to the tip-speed ratio and is, for variable speed WTs, done by varying

the rotational speed of the mechanical system according to the wind conditions. Three wind speeds are investigated here:

- *High wind.* The WT operates at rated power output and rated rotor speed. The pitch control limits the captured energy to the rated power of the machine, i.e. $P_{eo} = 1$ pu.
- *Medium wind.* The WT is operated at partial power output, $P_{eo} \simeq 0.69$ pu, with the mechanical system rotating at rated speed.
- *Low wind.* The WT operates at partial power output, $P_{eo} \simeq 0.14$ pu, and the rotor speed is controlled to maximise the wind energy extraction.

Second, the WT can be commanded to only deliver partial power output. This is useful for frequency reserve or if local grid conditions require curtailed power production. Two cases are here selected where the power reference is set to match the power output in medium and low wind.

Modern WPPs are often equipped with an outer voltage controller, for example, as described in section 3.4, which coordinates the response from the individual WTs. To investigate the influence that such controller may have, the studies are repeated with WPP voltage controller for the high, medium and low wind scenarios.

The operating conditions of G_2 and the WPP for the investigated scenarios are summarised in Table 4. The active power output of G_2 is in each step adjusted to compensate for the active power production from the WPP according to the two strategies given above as cases 1 and 2. The power flow in the system is hereby kept unchanged. For case 2, the MVA rating of G_2 is updated by

$$S_{\text{base,new}} = S_{\text{base,orig}} - \frac{P_{\text{WPP}}}{P_{\text{setp}}}, \tag{2}$$

where P_{setp} is the pu active power set-point of G_2 and is kept constant.

Table 4: Limits of MVA rating of G_2 and active power output of the WPP for the investigated WPP operating scenarios

	G_2 MVA rating		WPP active power	
	min.	max.	min.	max.
WPP operation	[MVA]	[MVA]	[MW]	[MW]
high wind	1 222	2 400	36.0	1 000
medium wind	1 588	2 400	24.8	690.1
low wind	2 235	2 400	5.0	140.1
medium P_{eo}	1 588	2 400	24.8	690.1
low P_{eo}	2 235	2 400	5.0	140.1
high wind, WPP VC	1 222	2 400	36.0	1 000
medium wind, WPP VC	1 588	2 400	24.8	690.1
low wind, WPP VC	2 235	2 400	5.0	140.1

An overview is given in Figure 8 of the system eigenvalues, which includes a qualitative description of the eigenvalues. The overview is given for both cases 1 and 2 for a high wind scenario where the WPP penetration level is 1 000 MW. The WPP is equipped with a park level voltage controller.

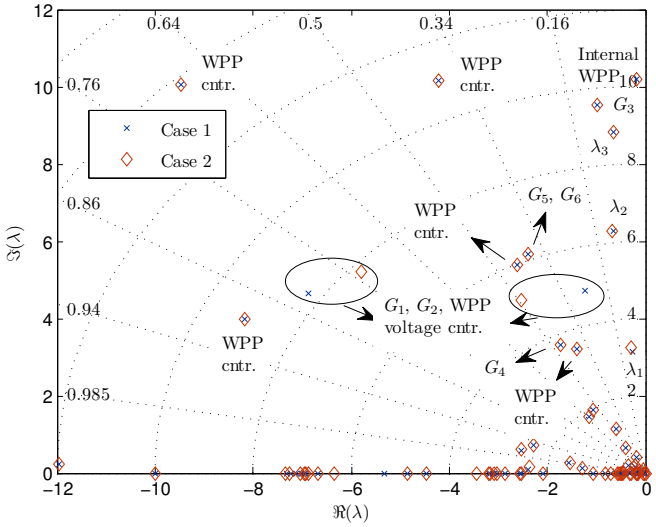

Figure 8: Overview of the complex plane with the system eigenvalues for both cases 1 and 2 with 1 000 MW of wind power

4.1 Case 1

The eigenvalue trajectories for λ_{1-3} are plotted in Figure 9, 10, and 11, respectively, as the WPP capacity is increased to 1 000 MW. A grid showing constant damping ratios, ζ, and constant natural frequencies of oscillation, ω_n, is superimposed onto the eigenvalue trajectories. From Figure 10 and 11 it is seen that λ_{2-3} only experience limited movement as the WPP capacity increases. The maximum relative deviation from the base case is below 10^{-2} % for ω_d and 0.9 % for ζ.

A summary of the modal characteristics of λ_1 with a WPP capacity of 1 000 MW is given in Table 5. When compared to the base case, the frequency of oscillation increases slightly, ~ 1 %, for all WPP operating scenarios. When the WPP is operated at rated power output, Table 5 gives that the damping ratio is reduced with < 0.9 % when compared to the base case. When the active power output of the WPP is reduced, the damping increases slightly. It should be noted that the maximum 5.5 % increase in damping ratio corresponds to an increase from $\zeta_0 = 0.0885$ to $\zeta = 0.0933$.

A comparison of selected, normalised participation factors for λ_1 are plotted in Figure 12 for all investigated operating scenarios for the iteration with 1 000 MW installed WPP capacity. The WPP mechanical participation in λ_1 is, irrespective of operating condition, found to be very small, $\lesssim 10^{-5}$. The largest WPP participation is found in either the WT voltage controller or the WPP voltage controller. It is noted that the power output from the WPP does not significantly affect the participation of generator G_{1-7} in the oscillation, since uniform ratios of the participation factors appear for all operating scenarios.

Table 5: Eigenvalues for inter-area mode λ_1 for case 1 with 1 000 MW of wind power and the relative modal difference compared to the no wind case

	λ [-]	$\frac{\omega_d - \omega_{d0}}{\omega_{d0}}$ [%]	$\frac{\zeta - \zeta_0}{\zeta_0}$ [%]
high wind	$-0.277 \pm j3.12$	1.0	-0.16
medium wind	$-0.285 \pm j3.13$	1.1	2.6
low wind	$-0.293 \pm j3.13$	0.98	5.5
medium P_{eo}	$-0.284 \pm j3.13$	0.97	2.4
low P_{eo}	$-0.293 \pm j3.13$	0.94	5.4
high wind, WPP VC	$-0.276 \pm j3.13$	1.1	-0.80
medium wind, WPP VC	$-0.284 \pm j3.13$	1.2	1.9
low wind, WPP VC	$-0.291 \pm j3.13$	1.1	4.7

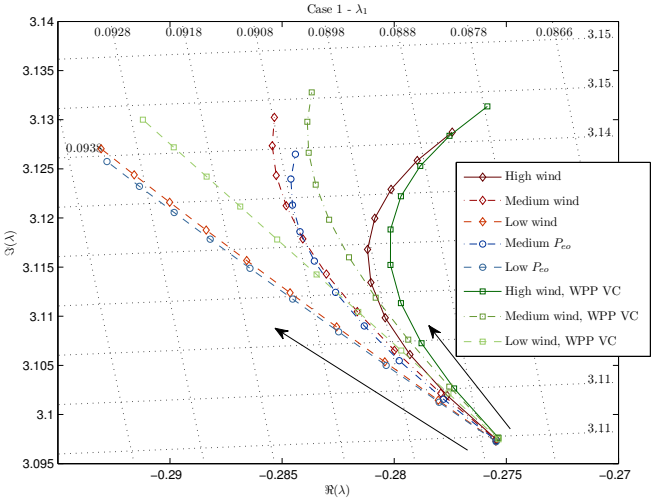

Figure 9: Comparison of eigenvalue trajectories for inter-area mode, λ_1, for integration strategy case 1

4.2 Case 2

The trajectories for inter-area modes λ_{1-3} are given in Figure 13, 14, and 15, respectively, as the WPP penetration is increased from 36 to 1 000 MW. It is noted that the eigenvalues are moving leftwards in the complex plane as the WPP penetration increases. The plot of the eigenvalue trajectories for λ_1 in Figure 13 reveals that three distinct paths exist and that the grouping of the operating scenarios is based on the active power output level.

The modal characteristics for λ_1 are summarised in Table 6 for the system with a WPP capacity of 1 000 MW. Compared to the base case, cf. Table 2, the damped frequency of oscillation, ω_d, have increased between 1.5 and 4.7 %, while the damping ratio, ζ, have changed between -1.0 and 5.1 %. From Table 6

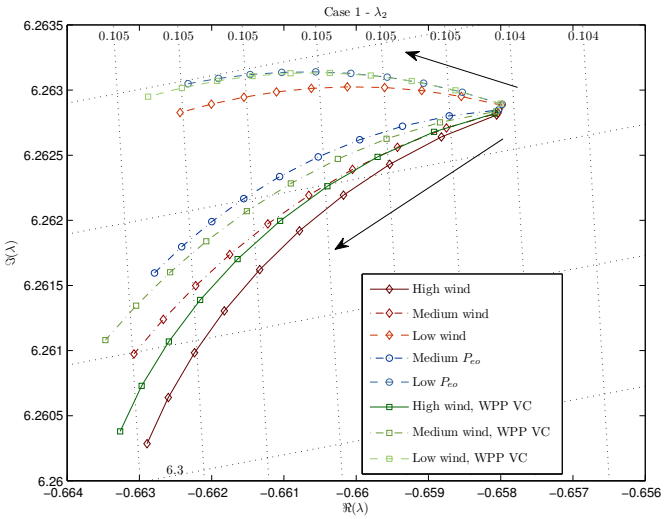

Figure 10: Comparison of eigenvalue trajectories for inter-area mode, λ_2, for integration strategy case 1

it is seen that although the eigenvalues have a leftwards movement in Figure 13, ζ decreases slightly in the two scenarios where the WPP is operating at rated active power output.

Table 6: Eigenvalues for inter-area mode λ_1 for case 2 with 1 000 MW of wind power and the relative modal difference compared to the no wind case

	λ [-]	$\frac{\omega_d - \omega_{d0}}{\omega_{d0}}$ [%]	$\frac{\zeta - \zeta_0}{\zeta_0}$ [%]
high wind	$-0.286 \pm j3.24$	4.7	−0.88
medium wind	$-0.290 \pm j3.21$	3.7	1.7
low wind	$-0.294 \pm j3.14$	1.5	5.1
medium P_{eo}	$-0.289 \pm j3.21$	3.6	1.4
low P_{eo}	$-0.293 \pm j3.14$	1.5	5.0
high wind, WPP VC	$-0.285 \pm j3.25$	4.8	−1.0
medium wind, WPP VC	$-0.289 \pm j3.21$	3.8	1.3
low wind, WPP VC	$-0.292 \pm j3.14$	1.6	4.4

In Figure 16, a comparison of selected, normalised participation factors for λ_1 are presented for the iteration with a 1 000 MW WPP capacity. Comparing Figure 16 with Figure 12 it is clear that for case 2 the operating scenario has an effect on the ratios of the participations factors of G_{1-7}. A closer inspection reveals that the magnitude of the participation factors reflect the size of G_2, which in this case is adjusted according to the WPP active power production.

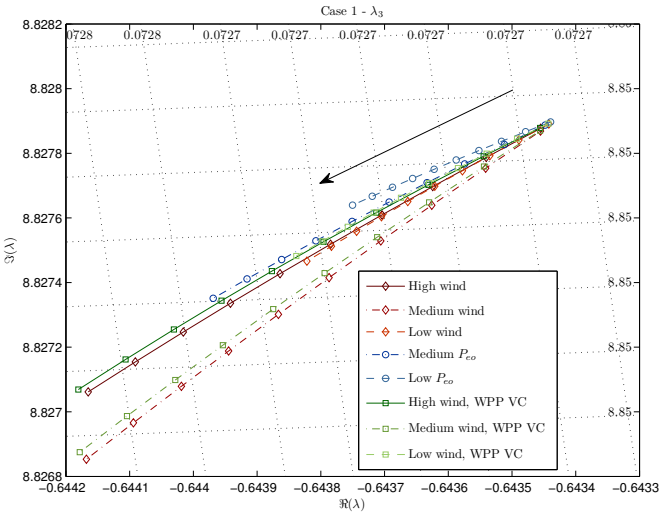

Figure 11: Comparison of eigenvalue trajectories for inter-area mode, λ_3, for integration strategy case 1

4.3 Impact of WT and WPP controls

To evaluate the impact of WT and WPP controls on the modal characteristics of the inter-area mode, a sensitivity analysis is carried out where control parameters in turn are varied from their nominal value with ±40 %. Analysed controllers are WT voltage control, WT active power control, park-level WPP voltage control and WT pitch control. For all controllers the parameters affecting both the speed and the gain are analysed within the given range. The trajectories for inter-area mode λ_1 are given in Figure 17, for a case 1 high wind scenario with the WPP producing 1 000 MW. The arrows in Figure 17, indicate increasing parameter values, that is, from −40 % to +40 % of the nominal value, and the intersection of the trajectories corresponds to nominal parameter values.

From Figure 17 it is seen that the speed of the local WT voltage controller has the largest impact on the inter-area mode, λ_1, followed by speed and gain of the park-level voltage controller. The active power control and the pitch control have only a limited impact on λ_1. The maximum change in damping ratio, ζ, when compared to the nominal system is −1.7 % and is found for the speed of the WT voltage controller.

5 Discussion

To accommodate the production from additional generation units, assuming that load and power transfer to neighbouring systems do not increase, the pro-

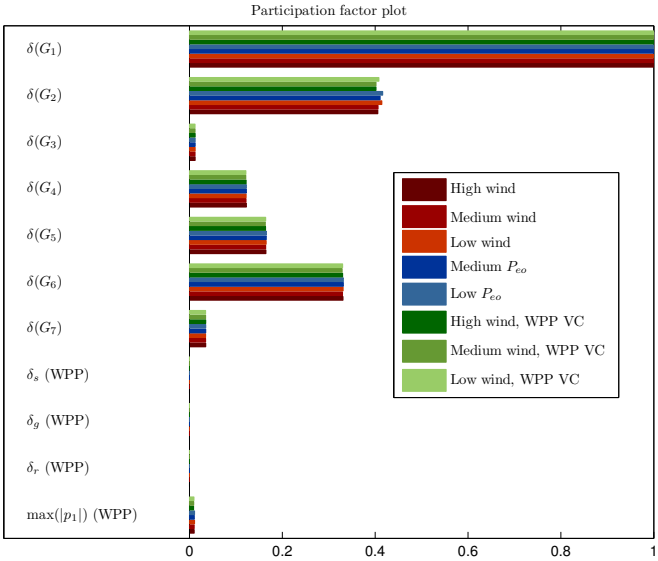

Figure 12: Comparison of selected, normalised participation factors for inter-area mode λ_1 for case 1. For the WPP, participation factors are shown for mechanical shaft-, generator-, and rotor-angle states, as well as the maximum participation over all WPP states

duction from the existing units should decrease accordingly to keep the power balanced. This can happen in two ways: (i) all units stay connected but with reduced active power output, or (ii) a proportion of the existing units are taken out of service to ensure good utilisation of the units in service. Three lightly damped inter-area modes are monitored as the penetration of wind power increases, and both with and without WPP voltage controller, in high, medium and low power output, the inter-area modes seem largely unaffected by the increased capacity of the WPP and by the applied accommodation strategy. Comparing the inter-area characteristics in Table 2, 5, and 6, it is noted that the modal characteristics of the three inter-area modes are almost constant.

The degree of interaction of the WPP in the power system oscillations is evaluated with the aid of participation factors. The participation in the system oscillations of the WPP mechanical system are orders of magnitude smaller than those computed for the synchronous machines. For this study where the WPP, as designed for and intended, is operated within its operational limits it can be concluded that a high level of decoupling exists. A number of different operating scenarios, that is, high, medium and low wind conditions, as well as power curtailment mode and with a WPP voltage controller in operation, was investigated with the same result of decoupling.

A sensitivity study on selected WT and WPP control parameters was conducted and the results show that the WT and WPP voltage controllers have the

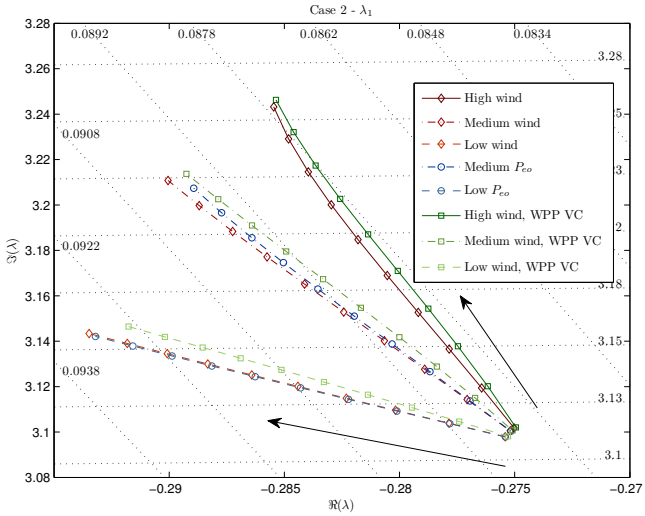

Figure 13: Comparison of eigenvalue trajectories for inter-area mode, λ_1, for integration strategy case 2

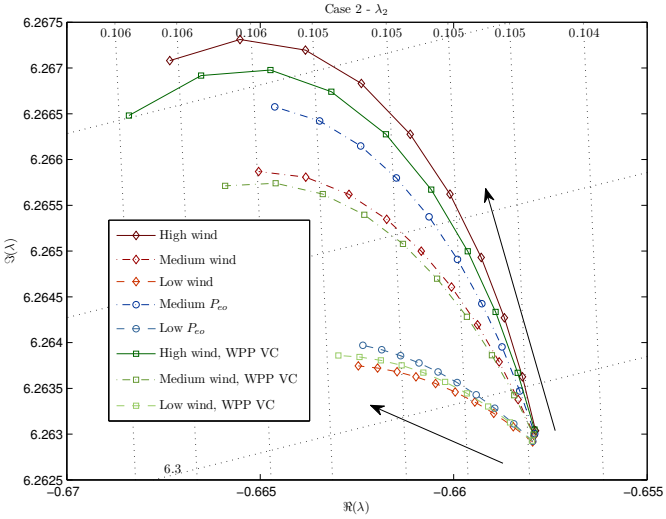

Figure 14: Comparison of eigenvalue trajectories for inter-area mode, λ_2, for integration strategy case 2

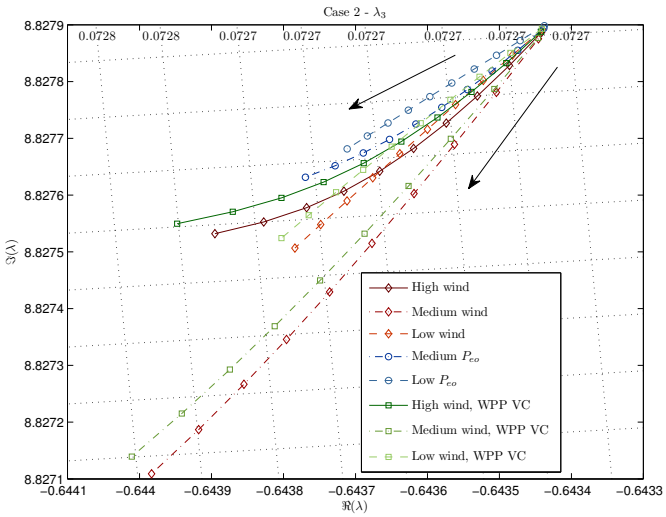

Figure 15: Comparison of eigenvalue trajectories for inter-area mode, λ_3, for integration strategy case 2

largest impact on the dominant inter-area mode, whereas only limited impact was found from the active power and pitch controllers.

These findings support that there is a general decoupling between the grid dynamics and the WPP mechanical system by the full-load converter when the WPP is operated within its limits. In the case where one or more components or controllers are forced to their limits, the degree of coupling or decoupling is not easily assessed. Modal analysis is based on Taylor expansion, which describes the system in terms of deviations from the steady state, and when a limit is encountered this description is not valid, since deviations are only feasible in one direction. Time-domain simulations, for example, with Fourier series perturbation, may reveal some of these characteristics, but finding the right initial conditions to activate the limits of interest may prove challenging.

In this study the active power production from the WPP is balanced by a reduction in production of an adjacent generator, thereby keeping the power flow unchanged in the remaining system. This was chosen to be able to isolate the impact of the WPP while not considering derived consequences of expanding with wind power. In practise the net effect is, beside the generator technology and control which was investigated here, also affected by the location of the WPP as well as the generation being displaced, distance to load centres, variability of power, voltage compensation strategy and requirements, and so on [10].

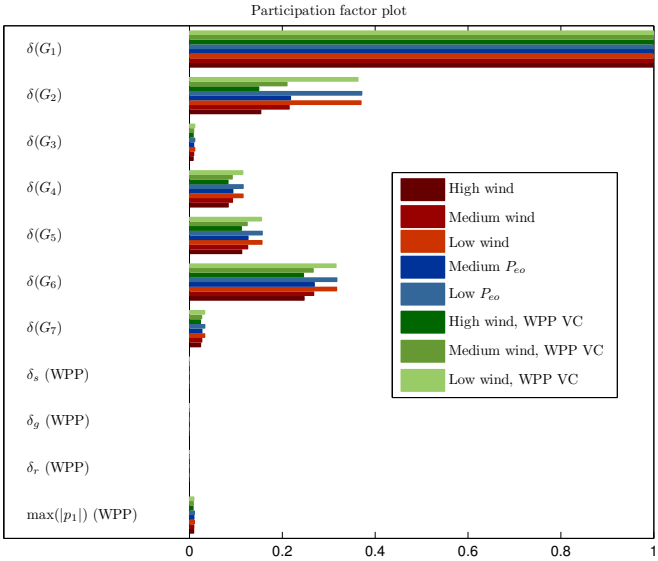

Figure 16: Comparison of selected, normalised participation factors for inter-area mode λ_1 for case 2. For the WPP, participation factors are shown for mechanical shaft-, generator-, and rotor–angle states, as well as the maximum participation over all WPP states

6 Conclusion

In this paper a modal analysis is presented, where the impact of full-load converter interfaced WTs on power system oscillations is evaluated. The analysis is repeated for various wind power penetration levels, different wind conditions, and with the WPP in power curtailment mode. Furthermore, two different strategies for accommodating the wind energy are investigated and the WPP is represented with and without a park-level voltage controller. The impact of selected WT and WPP control parameters was investigated through parameter sensitivity analysis.

The study found that the inter-area modes were largely unaffected by the increased capacity of the WPP, with the modal characteristics being almost unchanged. From the sensitivity analysis, it was found that the local and the park- level voltage controllers had the largest impact on the dominant inter-area mode, while only a limited impact was found for the active power and the pitch controllers.

The participation in the system oscillatory modes of the WPP's mechanical system was found to be orders of magnitudes smaller than those of the synchronous generators' mechanical system. The very low participation factors imply that the WPP does not interact with these system modes.

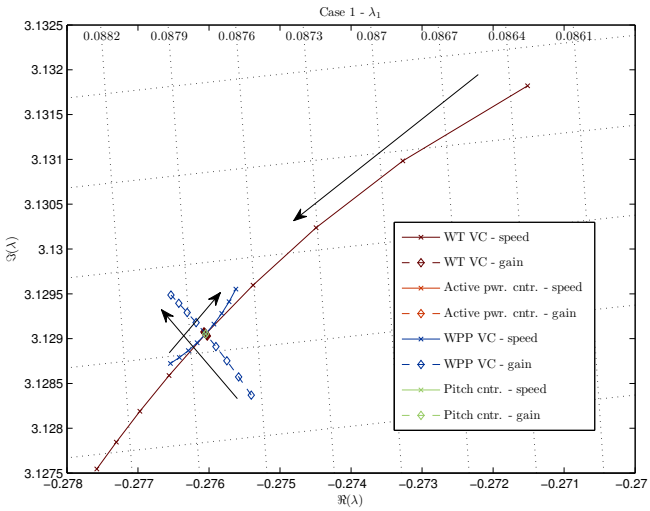

Figure 17: Sensitivity of inter-area mode λ_1 to perturbations of ± 40 % on selected WT and WPP control parameters. Sensitivities are evaluated for case 1 with a 1 000 MW of wind power

A System parameters

Table 7: Generator ratings, transformer reactances, and load characteristics. Transformer rating is same as generator rating and the reactance is given on this base

Generators [MVA]		Transformers [%]		Loads [MVA]	
G_1	3 000	T_1	$X_L = 16$	L_3	$755 + j220$
G_2	2 400	T_2	$X_L = 16$	L_4	$4\,320 + j1\,580$
G_3	1 000	T_3	$X_L = 16$	L_5	$3\,200 + j954$
G_4	7 300	T_4	$X_L = 16$	L_6	$6\,310 + j2\,030$
G_5	2 900	T_5	$X_L = 16$	L_7	$2\,910 + j960$
G_6	5 500	T_6	$X_L = 16$	L_8	$2\,500 + j775$
G_7	2 800	T_7	$X_L = 16$		

Table 8: Machine parameters for all synchronous generators on machine base.

	G_1	G_2	G_3	G_4	G_5	G_6	G_7
H [s]	4.237	4.464	4.358	5.562	5.474	4.879	4.066
D [s]	0	0	0	0	0	0	0
R_s [pu]	0.002	0.001	0.010	0.001	0.002	0.001	0.002
X_l [pu]	0.167	0.187	0.167	0.169	0.167	0.180	0.183
X_d [pu]	2.360	2.116	2.001	2.470	2.235	2.158	2.510
X_q [pu]	2.261	2.043	1.937	2.301	2.113	2.069	2.447
X'_d [pu]	0.297	0.312	0.293	0.278	0.269	0.300	0.313
X'_q [pu]	0.297	0.312	0.293	0.278	0.609	0.300	0.313
X''_d [pu]	0.209	0.250	0.219	0.203	0.198	0.227	0.226
X''_q [pu]	0.209	0.248	0.227	0.248	0.209	0.237	0.226
T'_{do} [s]	0.692	1.008	0.933	0.721	1.002	1.004	0.691
T'_{qo} [s]	0.692	1.008	0.933	0.721	1.002	1.004	0.691
T''_{do} [s]	0.031	0.023	0.036	0.019	0.032	0.065	0.026
T''_{qo} [s]	0.031	0.064	0.040	0.020	0.047	0.071	0.026

Table 9: Network parameters

	R [Ω]	X_L [Ω]	B_C [μS]
l_{18}	0	4.00	0
l_{28}	0	32.00	0
l_{38}	11.93	114.64	0
l_{48}	6.47	64.37	1189.91
l_{34}	0.40	4.91	1007.73
l_{47}	0.09	1.28	902.17
l_{57}	2.35	30.20	1512.05
l_{67}	0.38	4.88	1502.76
l_{56}	1.70	26.17	1475.95

Table 10: WPP collector network parameters for $P_{\mathrm{WPP}} = 180$ MW

Network			Park trafo.
R [Ω]	X_L [Ω]	B_C [μS]	X_T [%]
0.086	0.070	3219.7	12.2

References

[1] Mauricio J.M., Marano A., Gomez-Exposito A., Martinez Ramos J.L.: 'Frequency regulation contribution through variable-speed wind energy conversion systems', IEEE Trans. Power Syst., 2009, 24, (1), pp. 173–180

[2] de Almeida R.G., Lopes J.A.P.: 'Participation of doubly fed induction wind generators in system frequency regulation', IEEE Trans. Power Syst., 2007, 22, (3), pp. 944–950

[3] Morren J., Pierik J., de Haan S.W.H.: 'Inertial response of variable speed wind turbines', Electric Power Syst. Res., 2006, 76, (11), pp. 980–987

[4] Keung P.K., Li P., Banakar H., Ooi B.T.: 'Kinetic energy of wind-turbine generators for system frequency support', IEEE Trans. Power Syst., 2009, 24, (1), pp. 279–287

[5] Akhmatov V.: 'Variable-speed wind turbines with doubly-fed induction generators part III: Model with the back-to-back converters', Wind Engineering, 2003, 27, (2), pp. 79–91

[6] Akhmatov V.: 'Full-load converter connected asynchronous generators for MW class wind turbinesÂ´, Wind Engineering, 2005, 29, (4), pp. 341–351

[7] Akhmatov V.: 'Variable-speed wind turbines with doubly-fed induction generators. Part IV: uninterrupted operation features at grid faults with converter control coordination', Wind Engineering, 2003, 27, (6), pp. 519–529

[8] Morren J., de Haan S.W.H.: 'Ridethrough of wind turbines with doubly-fed induction generator during a voltage dip', IEEE Trans. Energy Convers., 2005, 20, (2), pp. 435–441

[9] Rogers G.: 'Power System Oscillations' (Kluwer Academic Publishers, Power Electronics and Power Systems, 1st ed. 2000), ISBN-10: 0792377125

[10] Wilson D., Bialek J., Lubosny Z.: 'Banishing blackouts [power system oscillations stability]', Power Engineer, 2006, 20, (2), pp. 38–41

[11] Anaya-Lara O., Hughes F.M., Jenkins N., Strbac G.: 'Influence of windfarms on power system dynamic and transient stability', Wind Engineering, 2006, 30, (2), pp. 107–127

[12] Slootweg J.G., Kling W.L.: 'The impact of large scale wind power generation on power system oscillations', Electric Power Syst. Res., 2003, 67, (1), pp. 9–20

[13] Hagstrom E., Norheim I., Uhlen K.: 'Large-scale wind power integration in Norway and impact on damping in the Nordic grid', Wind Energy, 2005, 8, (3), pp. 375–384

[14] Samarasinghe C., Vowles D.: 'Wind generation investigation project - effect of wind generation on small signal stability' (TRANSPOWER New Zealand, The National Grid, 2008, Investigation 8)

[15] Wu F., Zhang X.P., Ju P.: 'Small signal stability analysis and control of the wind turbine with the direct-drive permanent magnet generator integrated to the grid', Electric Power Systems Research, 2009, 79, (12), pp. 1661–1667

[16] Tsourakis G., Nomikos B.M., Vournas C.D.: 'Effect of wind parks with doubly fed asynchronous generators on small-signal stability', Electric Power Syst. Res., 2009, 79, (1), pp. 190–200

[17] Tabesh A., Iravani R.: 'Small-signal dynamic model and analysis of a fixed-speed wind farm-a frequency response approach', IEEE Trans. Power Deliver., 2006, 21, (2), pp. 778–787

[18] Tabesh A., Iravani R.: 'Small-signal model and dynamic analysis of variable speed induction machine wind farms', IET Renew. Power Gener., 2008, 2, (4), pp. 215–227

[19] Hughes F.M., Anaya-Lara O., Jenkins N., Strbac G.: 'A power system stabilizer for DFIG-based wind generation', IEEE Trans. Power Syst., 2006, 21, (2), pp. 763–772

[20] Miao Z., Fan L., Osborn D., Yuvarajan S.: 'Control of DFIG based wind generation to improve inter-area oscillation damping', Power and Energy Society General Meeting, Pittsburgh, Pennsylvania, USA, July 2008, pp. 1–7

[21] Ledesma P., Gallardo C.: 'Contribution of variable-speed wind farms to damping of power system oscillations', Power Tech, Lausanne, Switzerland, July 2007, pp. 190–194

[22] Elkington K.: 'Modelling and control of doubly fed induction generators in power systems: Towards understanding the impact of large wind parks on power system stability'. PhD Thesis, KTH, Electric Power Systems, Stockholm, Sweden, 2009, ISBN: 978-91-7415-264-7.

[23] Mendonca A., Lopes J.A.P.: 'Robust tuning of power system stabilisers to install in wind energy conversion systems', IET Renew. Power Gener., 2009, 3, (4), pp. 465–475

[24] Kshatriya N., Annakkage U.D., Hughes F.M., Gole A.M.: 'Optimized partial eigenstructure assignment-based design of a combined PSS and active damping controller for a DFIG', IEEE Trans. Power Syst., 2010, 25, (2), pp. 866 –876

[25] Tang J.: 'Reader's guide to subsynchronous resonance', IEEE Trans. Power Syst., 1992, 7, (1), pp. 150–157

[26] Rostamkolai N., Piwko R.J., Larsen E.V., Fisher D.A., Mobarak M.A., Poitras A.E.: 'Subsynchronous interactions with static VAR compensators-concepts and practical implications', IEEE Trans. Power Syst., 1990, 5, (4), pp. 1324 –1332

[27] Nielsen J.N., Akhmatov V., Thisted J., Grøndahl E., Egedal P., Frydensbjerg M.N., Jensen, K.H.: 'Modelling and fault-ride-trough tests of Siemens Wind Power 3.6 MW variable-speed wind turbines', Wind Engineering, 2007, 31, (12), pp. 441–452

[28] Klein M., Rogers G.J., Kundur P.: 'A fundamental study of inter-area oscillations in power systems', Power System, IEEE Transactions on. 1991, 6, (3), pp. 914–921

[29] Kundur P.S.: 'Power System Stability and Control' (McGraw-Hill Inc., The EPRI Power System Engineering Series, 1994), ISBN: 0-07-035958-X

[30] Trudnowski D.J.: 'Estimating electromechanical mode shape from synchrophasor measurements', IEEE Trans. Power Syst., 2008, 23, (3), pp. 1188–1195

[31] Trudnowski D., Hauer J., Pierre J., Litzenberger W., Maratukulam D.: 'Using the coherency function to detect large-scale dynamic system modal observability', Proc. American Control Conference, 1999, vol. 4, pp. 2886–2890

[32] The MathWorks, Inc.: 'SimPowerSystems™ 5 - User's Guide', 2010

[33] The MathWorks, Inc.: 'Simulink®Control Design™ 3 – User's Guide', 2010

[34] Mei F., Pal B.: 'Modelling and small-signal analysis of a grid connected doubly-fed induction generator', Power Engineering Society General Meeting, June 2005, San Francisco, Californian, USA, pp. 1503–1510

[35] Ellis A., Kazachkov Y., Muljadi E., Pourbeik P., Sanchez-Gasca J.J.: 'Description and technical specifications for generic WTG models – A status report', 2011 IEEE/PES Power Systems Conference and Exposition (PSCE 2011), 2011, pp. 1-8

[36] National Grid plc: 'The grid code' (National Grid Electricity Transmission plc, UK, 2010, Issue 4, Revision 2)

[37] Knüppel T., Akhmatov V., Nielsen J.N., Jensen K.H., Dixon A., Østergaard J.: 'On small-signal stability of wind power system with full-load converter interfaced wind turbines', WINDPOWER 2010 Conference & Exhibition, Dallas, TX, USA, May 2010

A.2 Paper II

Thyge Knüppel, Jørgen N. Nielsen, Kim H. Jensen, Andrew Dixon, and Jacob Østergaard. Induced torques on synchronous generators from operation of wind power plant based on full-load converter interfaced wind turbines. In Félix Avia Aranda, editor, *Scientific Proceedings of the European Wind Energy Conference & Exhibition*, pages 68–71. The European Wind Energy Association, March 2011.

Induced Torques on Synchronous Generators from Operation of Wind Power Plant based on Full-Load Converter Interfaced Wind Turbines

Thyge Knüppel[1,2], Jørgen N. Nielsen[1], Kim H. Jensen[1], Andrew Dixon[3], Jacob Østergaard[2]
[1] Siemens Wind Power A/S, Denmark
[2] Technical University of Denmark
[3] National Grid Electricity Transmission plc (National Grid), UK

***Abstract*—It is expected that large wind power plants (WPP) contribute to stable and reliable operation of the electric power system. This includes participation with delivery of system services such as voltage and frequency support. With variable-speed WPPs this can be achieved by adding auxiliary controllers that control the active and reactive power output accordingly. While being designed for a given system service, any feedback control affects the closed-loop behavior of the overall system and thereby its small-signal stability properties. Eigenvalue analysis conveniently determines the stability properties from the closed-loop system. A method based on induced torque coefficients (ITC) is here presented for assessing the closed-loop behavior from the open-loop system. Results are presented using both modal analysis and ITC prediction, which demonstrate that the dominant closed-loop behavior can be predicted with the presented method. The work is based on a nonlinear, dynamic model of the 3.6 MW Siemens Wind Power wind turbine.**

***Index Terms*—wind turbines, wind power plant, wind farm controller, frequency control, voltage control, power systems, small-signal stability, induced torque coefficient (ITC)**

I. Introduction

In an interconnected power system the rotational speed of the synchronous generators is constantly adjusting to imbalances between generation and demand. With variable speed wind turbines (WT) this direct relationship between its rotational speed and the overall power balance does not exist. Most modern WTs connected today are asynchronously connected to the grid, either partially or fully through electronic power converters, and will, as discussed in [1], not themselves cause system oscillations. This point is elaborated in [2] where it is presented that the participation of the full-load converter type WT in power system oscillations is very low. A large scale integration of wind power can, however, indirectly change the modal characteristics of the system by *1)* significantly change the dispatch of the existing power units, *2)* significantly alter the power flows in the system, and *3)* interacting with the synchronous machines through the transmission network to change the synchronizing and damping torques induced on their shafts. Here, *1)* and *2)* are the consequence of a changed power in-feed pattern and as such not related to any specific power production technology. A more elaborate discussion is carried out in [3]. Case *3)*, on the other hand, does depend on the power conversion technology and the utilized control, with the latter point emphasizing the importance of accurate representation of the control when such studies are conducted.

Regarding wind power conversion units, several studies have investigated the impact on power system oscillations of wind power plants (WPP) based on primarily the fixed-speed induction generator (FSIG) and the doubly-fed induction generator (DFIG) [4]–[7]. In [8]–[11] it has been proposed to actively damp selected system modes using variable speed WPPs.

In recent years the role and impact of wind power on power system operation is changing due to the number of WTs erected and the number of WTs in each installation, and large WPPs must comply with similar requirements to those for other generation units. In continuation of this, WPPs are often equipped with auxiliary controllers for e.g. voltage or frequency control, i.e. controllers on park level designed to coordinate the response of the individual units in the park. While being designed for a specific task, e.g. voltage or frequency control, it is clear that any feedback control will affect the closed-loop performance of the power system and thereby its modal characteristics. In [7] the impact on power system oscillations of the reactive power control mode of DFIG WPPs is studied, and in [2] an overall WPP voltage controller is included in the analysis. In this paper a general framework is presented to analyze the impact that WPP auxiliary controllers have on the small-signal stability. The framework is based on a calculation of the torques that are induced on the synchronous generators due to the inclusion of the auxiliary controller [12], [13]. The advantage of this approach is that the sensitivity of a planned control, in terms of small-signal stability, is evaluated on the open-loop system and that important design parameters, i.e. acceptable gain or phase compensation, is achieved prior to the actual design of the controller. Here, two commonly used WPP auxiliary controllers, i.e. frequency and voltage droop controllers, are considered, which are implemented into a WPP model that has the

dynamic performance of a commercially available WT [14].

Energy conversion from renewable energy sources necessitate availability of the energy source at the production site. From a power oscillation perspective this means that the WPP is interacting with the synchronous machines from different locations within the oscillation. To include this characteristic in the study, different in-feed locations, traversing the length between two groups of oscillating machines, are investigated.

The paper is organized as follows. In section II the basis for the analysis is established with an introduction of power system oscillations, the concept of induced torque coefficients (ITC) and its use in wind power applications. Section III presents the study case, the analyzed WT concept, the case studies performed, and the results from the analysis. Finally, the discussion and conclusion are found in sections IV and V, respectively.

II. Background

Power system oscillations are inherent in interconnected power systems based on synchronous generators [15]. Power system oscillations and the application of eigenvalue analysis as means of analysis are well described in the literature, e.g. [16], [17].

A. Model Setup

The analysis is based on the non-linear set of system equations, dynamic relations as well as network equations, which are linearized in an operating point to obtain a linear system of differential and algebraic equations (DAE). When the algebraic relations are eliminated and the system described purely by ordinary differential equations (ODE), the system is in the classical state space form

$$\begin{aligned} \Delta\dot{x} &= A\Delta x + B\Delta u \\ \Delta y &= C\Delta x + D\Delta u \end{aligned} \tag{1}$$

where $A^{n\times n}$ is the system state matrix, $B^{n\times r}$ the input matrix, $C^{m\times n}$ the output matrix, $D^{m\times r}$ the feed forward matrix, $\Delta x^{n\times 1}$ the state vector, $\Delta u^{r\times 1}$ the input vector, and $\Delta y^{m\times 1}$ the output vector.

B. Synchronizing and Damping Torques

The synchronizing and damping torques for a synchronous machine are defined from the swing equation of this machine, i.e. the relation between the rate of change of speed and the torque imbalance on the shaft

$$\Delta\dot{\delta} = \omega_0\Delta\omega \tag{2a}$$

$$\begin{aligned} \Delta\dot{\omega} &= \tfrac{1}{2H}\left(\Delta T_m - \Delta T_e\right) \\ &= \tfrac{1}{2H}\left(\Delta T_m - K_s\Delta\delta - K_d\Delta\omega\right) \end{aligned} \tag{2b}$$

where H is the inertia constant, ω_0 the base rotational speed, ΔT_m and ΔT_e the mechanical and electromagnetic torque, and K_s and K_d are known as the synchronizing and the damping torque coefficient, respectively [16]. The synchronizing and damping torques are hence the component of electromagnetic torque, ΔT_e, in phase with rotor angle, $\Delta\delta$, and rotor speed, $\Delta\omega$, respectively.

Fig. 1 provides an overview of the machine interactions in a multimachine system with N synchronous machines and a full-load converter interfaced machine j. Although greatly simplified, Fig. 1 shows how the rotational system of the synchronous machines is directly coupled to the network, since the injected currents are a function of rotor angle and field flux, $\Delta\delta$ and $\Delta\psi_{fd}$. For the WPP, however, the only connection between the network and the rotational system is through the controller with the generator side converter controlling the rotational speed of the generator, ω_g. As a result the terms synchronizing and damping torques of the WPP rotational system has little meaning in the conventional sense of (2b).

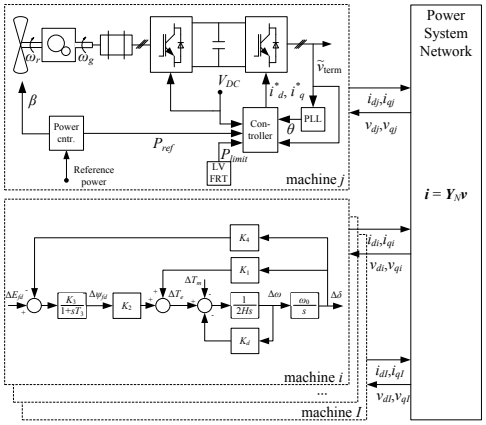

Fig. 1. Machine interactions in a multimachine power system.

C. Induced Torque Coefficient

Eigenvalue analysis is commonly used to analyze systems for small-signal stability and provide valuable information about the inherent stability properties of the system. A challenge with the method is to identify the root cause of a an observed shift in the stability properties. In [12], [18] induced torque coefficients (ITC) are introduced as a means to analyze the damping impact from FACTS stabilizers in multimachine systems. ITCs are introduced based on the PVr transfer function, which is the transfer function from reference voltage to active power output computed with all shaft dynamics disabled [13], [19]. The rationale behind ITC is that although a FACTS stabilizer, or in this case a WPP, does not have a mass, which is synchronously connected to the network, there is still a path from the currents, i_{dj}, i_{qj}, of machine j through the network to the electromagnetic torque of machine i. From machine j it is thus possible to induce an electromagnetic torque on machine i and that torque may be decomposed into torques in phase with $\Delta\delta_i$ and $\Delta\omega_i$.

For the ith machine the damping torque induced by the jth stabilizing unit, D_{ij}, is thus the component of torque in phase with $\Delta\omega_i$, where it is utilized that the per unit air-gap power, ΔP_e, equals the per unit air-gap torque, ΔT_e, [16]. The transfer function is then given as

$$D_{ij} = \frac{\Delta T_{e,ij}}{\Delta\omega_i} = \frac{\Delta P_{e,ij}}{\Delta\omega_i} \tag{3a}$$

$$= \underbrace{\frac{\Delta P_{e,ij}}{\Delta u_j}}_{H_{\text{PVr}}} \underbrace{\frac{\Delta u_j}{\Delta y_j}}_{j\text{th PSS}} \frac{\Delta y_j}{\Delta\omega_i} \tag{3b}$$

where Δu_j is the input signal to the machine from the stabilizer and Δy_j is the signal from which the oscillation is observed. In (3b) the last expression relates the speed deviation on machine i to the stabilizing input signal of the jth stabilizing unit, i.e. PSS, FACTS device, etc. If only the hth mode, λ_h, is excited, then the state vector is described as $\Delta x = \phi_h e^{\lambda_h t}$ [16]. Any output Δy_j is then given by $C_j\phi_h$, where C_j is the row of the output matrix in (1) that corresponds to Δy_j. Equation (3b) is then given as

$$D_{ij}^h = \frac{\Delta P_{e,ij}}{\Delta u_j}(\lambda_h)\frac{\Delta u_j}{\Delta y_j}(\lambda_h)\frac{C_j\phi_h}{C_i\phi_h} \tag{4a}$$

$$= \chi_{ij}^h \frac{\Delta u_j}{\Delta y_j}(\lambda_h). \tag{4b}$$

where each transfer function is evaluated at $s = \lambda_h$, where C_i is the row in the output matrix that corresponds to $\Delta\omega_i$, and where χ_{ij}^h is a complex number, which is independent of the applied control and which represents the impact of stabilizer j on the ITC of the ith synchronous generator for the $h$ht mode. From the ITC for the hth mode, D^h, a first order approximation of the mode shift of the hth mode is given as [12]

$$\Delta\lambda_{h,ij} = -\frac{p_{ih}}{2H_i}D_{ij}^h \tag{5a}$$

$$= -\frac{p_{ih}}{2H_i}\chi_{ij}^h \frac{\Delta u_j}{\Delta y_j}(\lambda_h) \tag{5b}$$

where H_i is the inertia constant of the ith synchronous generator and p_{ih} is the participation factor of the speed state of the ith synchronous generator. Let

$$\xi_{ij}^h = -\frac{p_{ih}}{2H_i}\chi_{ij}^h \tag{6}$$

and denote $\xi_j^h = \sum_{\forall i}\xi_{ij}^h$. It can then be proved [20] that ξ_j^h is equivalent to the residue between output Δy_j and input Δu_j, and examining the elements of ξ_{ij}^h thus reveals the contribution of each synchronous generator to the residue of the hth system mode.

Summing over all i in (5) then gives the predicted mode shift when the controller $\frac{\Delta u_j}{\Delta y_j}$ is inserted into the loop

$$\Delta\lambda_{h,j} = \frac{\Delta u_j}{\Delta y_j}(\lambda_h)\sum_{\forall i}\xi_{ij}^h. \tag{7}$$

Using (7) it is possible to predict the mode shift of the hth eigenvalue due to the presence of the jth controller, $\frac{\Delta u_j}{\Delta y_j}$. Similarly, summing over all j gives the total mode shift due to the stabilizing action of the j stabilizing units. The prediction of the hth closed-loop eigenvalue, $\hat{\lambda}_{h,cl}$, is then given from the open-loop eigenvalue, $\lambda_{h,ol} = \lambda_h$, and the predicted mode shift calculated in (7)

$$\hat{\lambda}_{h,cl} = \lambda_{h,ol} + \Delta\lambda_{h,j} \tag{8}$$

D. A Wind Power Perspective

A trend in wind power is that more functionalities and system services are expected delivered from the WPPs. To achieve the expected functionalities the WPPs are fitted with auxiliary controllers optimized for the service in question, and as with any feedback control these auxiliary controllers will affect the closed-loop performance of the power system.

The framework outlined in section II-C offers the possibility of directly assessing the impact of a WPP control on the small-signal stability of the power system. In a WPP context the transfer function $\frac{\Delta u_j}{\Delta y_j}$ could be frequency control, voltage control, or any other auxiliary controller. This is schematically illustrated in Fig. 2a where $G(s)$ is the open-loop system, i.e. the power system model without the additional control, $H(s)$ the proposed control, and k the control gain. The concept of residue angle and required phase compensation of $H(s)$ to achieve pure damping is illustrated in Fig. 2b.

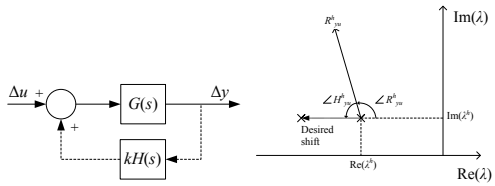

(a) Feedback control. (b) Eigenvalue sensitivity.

Fig. 2. Effect of controller tuning on modal damping.

III. Four Generator System

To present the methodology in section II-C a benchmark system is considered which includes the dynamics of the generators, exciters, PSSs, governors, WPP, as well as voltage dependency of the loads. The network shown in Fig. 3 is based on the four machine system in [21], which is a modified version of the two area system originally defined in [15].

At bus 11 a WPP is connected through a park transformer, collector grid, and a WT transformer. The connection point at bus 11 is hereafter termed "point of common connection" (PCC).

There is an active power flow of approximately 450 MW flowing from area 1 to area 2. There is no voltage control at the load busses, and the power flow across the interconnector thus depends on the load flow solution.

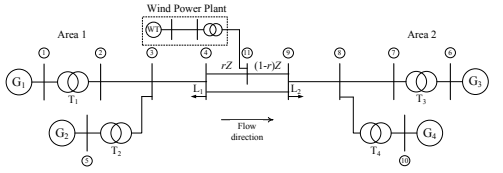

Fig. 3. Single-line diagram of the four generator, two area case network.

A. Wind Turbine Technology

The WT concept for this study is a variable-speed, pitch controlled, full-load converter interfaced WT as illustrated in Fig. 1. The WT is represented with a reduced order model suitable for transient and dynamic power system studies. The model represents a 3.6 MW Siemens Wind Power WT [14] and includes:

- *Aerodynamic model*. A variable wind speed aerodynamic model which includes power coefficient with pitch angle and tip-speed ratio.
- *Shaft model*. Implements a two-mass model of rotor, gearbox, and generator.
- *Converter system*. The WT converter system comprises machine and grid side converter, DC-link, and a generic reduced order control scheme.
- *DC link*. Implements the link, including the DC capacitance, between the machine and the network side converter.
- *Fault ride through*. Monitors for system faults and shapes the current injection into the grid upon detection.

In the study an aggregated WT model is used and the WT is operated in voltage control mode, regulating for 1.04 p.u. at the WT terminal to support the voltage at PCC.

B. WPP Auxiliary Controllers

The WPP is equipped with generic droop controllers for PCC voltage and frequency control. The block diagrams for the droop controllers are depicted in Fig. 4 where, d is the droop characteristic, LP a low-pass filter, and PI a proportional, integral controller. The dead band in Fig. 4b is used for time domain simulation and can be omitted for small-signal analysis.

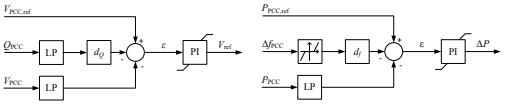

(a) Park level voltage controller. (b) Park level frequency controller.

Fig. 4. Block diagrams of generic voltage and frequency controllers.

For the voltage control a droop factor of 4 % is used whereas a droop factor of 0.6 $\frac{\text{pu}}{\text{Hz}}$ is used for the frequency control.

C. Results

To evaluate the impact of WPP in-feed location, the analysis is repeated where r is varied from 0.1 to 0.99, cf. Fig. 3. Two different WPP penetration levels are investigated with the WPP consisting of *1)* 30 WTs and *2)* 90 WTs, which, respectively, correspond to $P_{\text{WPP}} = 108$ and $P_{\text{WPP}} = 324$ MW. The active power production from the WPP is balanced equally with the synchronous generators in area 1 to keep the active power flow unchanged.

1) Open-Loop System: For the open-loop analysis the WPP is considered without the auxiliary controllers described in section III-B. By evaluating the residue properties of an output/input configuration it is possible to assess the impact of a feedback controller between the output and the input, cf. section II-D. In this part only the feedback signal that represents the control objective is considered, i.e. frequency and voltage for the frequency and the voltage controller, respectively.

The impact on the inter-area mode, λ_1, of a feedback controller between PCC bus frequency and active power output is shown in Fig. 5 for two WPP penetration levels. The presented ξ^h parameter is calculated using (6). From Fig. 5 it is seen that the impact of the feedback control is dominated by the synchronous generators closest to the WPP and that the impact approaches zero in a neighborhood around $r = 0.5$. Whereas from the phase characteristic it is seen that G_{1-2} and G_{3-4} are separated by approximately $180°$, which means that G_{1-2} and G_{3-4} will have an opposite impact on λ_1.

A frequency controller is designed to track the set point frequency, i.e. typically 50 or 60 Hz, hence, if an increasing frequency is registered a reduced active power output is ordered, and the control therefore adds 180° to the residue phase. Referring to $\angle\xi_j^1$ in Fig. 5 this means that the frequency control has a positive impact on the stability of the inter-area mode except in a the transition region around $r = 0.5$. However, in this region the impact on λ_1 of the control is approaching zero.

The impact of a feedback controller between PCC voltage magnitude and WPP set point voltage is given in Fig. 6 for the two investigated WPP penetration levels. It is noted that the magnitude of ξ_{ij}^h is not grouped with the two areas of the power system, as was the case for the frequency control. The size of the WPP is, furthermore, seen to have larger effect on the characteristic than what was noted in Fig. 5.

For a voltage controller, designed to achieve a set point PCC voltage, a high input yields a reduced output, i.e. similar to the discussion on the frequency control, and the controller adds 180° to the phase characteristic. However, the phase characteristic for the voltage controller is somewhat more complicated than that of the frequency controller and the net impact is not readily assessed without the phase characteristic for the voltage controller.

2) Closed-Loop System: For the closed-loop analysis, the auxiliary controllers in Fig. 4 are implemented into the WPP model and the eigenvalues are calculated.

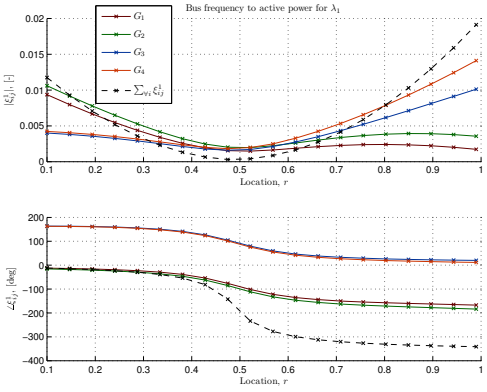

(a) $P_{\text{WPP}} = 108$ MW

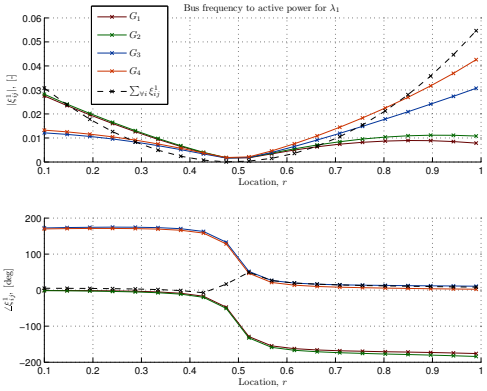

(b) $P_{\text{WPP}} = 324$ MW

Fig. 5. Effect of feedback controller between bus frequency and active power set point.

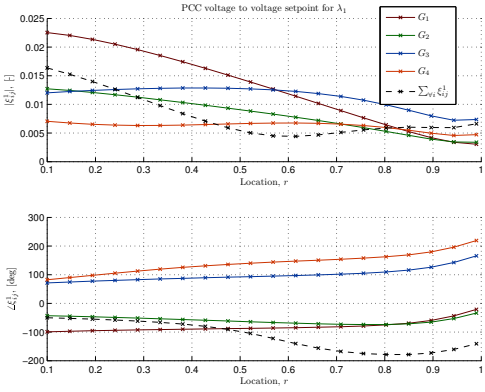

(a) $P_{\text{WPP}} = 108$ MW

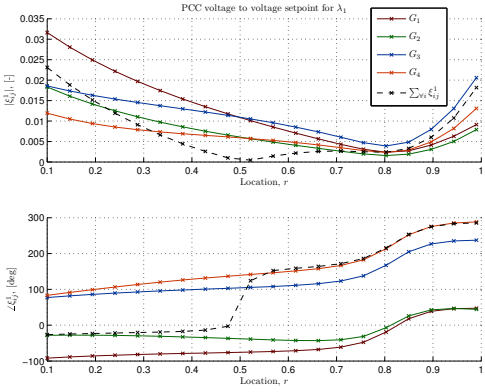

(b) $P_{\text{WPP}} = 324$ MW

Fig. 6. Effect of feedback controller between PCC voltage magnitude and voltage set point.

The predicted mode shift in the closed-loop system is calculated from (7) where $\frac{\Delta u_j}{\Delta y_j}$ is replaced with the transfer functions of the auxiliary controls as given from Fig. 4.

In Fig. 7 the predicted shift of the inter-area mode, $\hat{\lambda}_{cl}$, due to the frequency or the voltage controller is compared to the actual mode shift evaluated on the closed-loop system. The predicted eigenvalues are calculated based on the open-loop eigenvalues, λ_{ol}, which are also plotted in Fig. 7. The linear prediction, $\hat{\lambda}_{cl}$, is seen to capture the closed-loop dynamics with the auxiliary controllers in service.

IV. Discussion

The investigated controllers are not designed with small-signal stability in mind but instead to support the power system with other important services, i.e. voltage and frequency support. It is, however, clear that there will be a derived impact from these controllers on the small-signal stability, which depending on the controller, WPP location and size, etc. can be positive or negative, small or large. In this paper a framework is presented to assess the impact on critical system modes of an auxiliary controller. The advantage of the presented method is that the sensitivity of critical modes to a proposed control is determined directly from the open-loop system before the control is implemented and tuned. Remedial actions or in-depth clarifying studies can then be commenced earlier in the process, should certain critical system modes show signs of being deteriorated by a planned WPP control functionality.

From the discussion in section III-C1 it is seen that the impact on the closed-loop system can be qualitatively determined from the ξ^h parameter without knowledge of the exact structure of the controller and its parameters.

It is found that both in-feed location, WPP size, and its auxiliary control affect the modal characteristics of the inter-area mode. An increased frequency of oscillation is found for all cases as the WPP is moved toward area 2. The damping characteristics are more dependent on the applied auxiliary control. The frequency control has the largest impact on the inter-area mode, with added

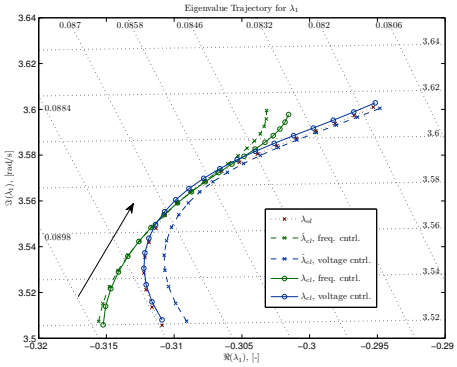

(a) $P_{\text{WPP}} = 108$ MW

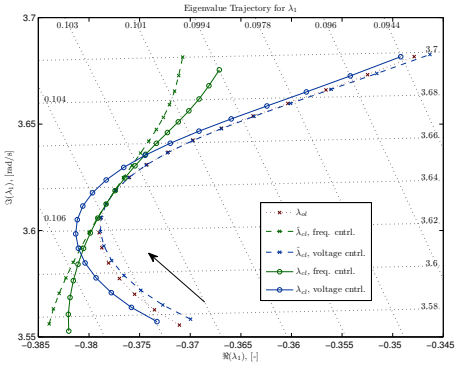

(b) $P_{\text{WPP}} = 324$ MW

Fig. 7. Eigenvalue trajectories predicted from open-loop system, $\hat{\lambda}_{cl}$, and evaluated on closed-loop system, λ_{cl}, with r going from 0 to 1.

damping that is especially notable when the WPP is located toward either end of the transmission line, cf. Fig. 7. Around the center of the oscillation only a very limited impact is observed from the control, which is also predicted from the induced torque calculations. Comparing the two investigated WPP penetration levels in Fig. 7a and 7b it is noted that better damping is obtained with the larger WPP penetration of $P_{\text{WPP}} = 324$ MW with a maximum improvement of around 5 % compared to the open-loop system. The impact of the voltage control is less pronounced than that of the frequency control, and the modal characteristic of the inter-area mode resembles that of the open-loop system. These findings are consistent with those in [2] where a similar voltage control is analyzed.

V. Conclusion

Variable-speed wind power plants (WPP) are routinely equipped with auxiliary controllers on park level that coordinate the response of the individual wind turbines to provide power system services such as voltage and frequency support. To assess the impact of the auxiliary controllers on the small-signal stability properties of the system, a method is here presented to predict the closed-loop behavior directly from the open-loop system. This is achieved through induced torque coefficients (ITC), which are the torques induced on the synchronous generators due to the operation of the auxiliary controllers.

Two commonly applied auxiliary controllers, i.e. voltage and frequency droop controllers, have been tested to illustrate the use of ITC for small-signal stability assessment. The frequency controller is shown to have a positive effect on the damping of the inter-area mode when the WPP is located toward either of the oscillating areas. When the WPP is located around the center of the oscillation the frequency controller has only a very limited influence on the inter-area mode whose damping approaches that of the open-loop system. The voltage controller is not found to affect the damping to any great extent. The closed-loop behavior predicted from the ITCs is compared to the actual closed-loop eigenvalues, and the results show that the prediction captures the dominant properties of the analyzed inter-area mode.

References

[1] C. Samarasinghe and D. Vowles, "Wind generation investigation project - effect of wind generation on small signal stability," TRANSPOWER New Zealand, The National Grid, Tech. Rep. Investigation 8, March 2008.

[2] T. Knüppel, J. N. Nielsen, K. H. Jensen, A. Dixon, and J. Østergaard, "Small-signal stability of wind power system with full-load converter interfaced wind turbines," *Submitted for publication to IET Renewable Power Generation*.

[3] D. Wilson, J. Bialek, and Z. Lubosny, "Banishing blackouts [power system oscillations stability]," *Power Engineer*, vol. 20, no. 2, pp. 38 –41, april-may 2006.

[4] O. Anaya-Lara, F. Hughes, N. Jenkins, and G. Strbac, "Influence of windfarms on power system dynamic and transient stability," *Wind Engineering*, vol. 30, no. 2, pp. 107–27, 2006.

[5] J. Slootweg and W. Kling, "The impact of large scale wind power generation on power system oscillations," *Electric Power Systems Research*, vol. 67, no. 1, pp. 9 – 20, 2003.

[6] E. Hagstrom, I. Norheim, and K. Uhlen, "Large-scale wind power integration in norway and impact on damping in the nordic grid," *WIND ENERGY*, vol. 8, no. 3, pp. 375–384, JUL-SEP 2005.

[7] G. Tsourakis, B. Nomikos, and C. Vournas, "Effect of wind parks with doubly fed asynchronous generators on small-signal stability," *Electric Power Systems Research*, vol. 79, no. 1, pp. 190 – 200, 2009. [Online]. Available: http://www.sciencedirect.com/science/article/B6V30-4T0FHRM-1/2/3b6ac71f22cac8ff81670dcc6944a0f9

[8] F. Hughes, O. Anaya-Lara, N. Jenkins, and G. Strbac, "A power system stabilizer for dfig-based wind generation," *Power System, IEEE Transactions on*, vol. 21, no. 2, pp. 763–772, 2006.

[9] K. Elkington, "Modelling and control of doubly fed induction generators in power systems: Towards understanding the impact of large wind parks on power system stability," PhD Thesis, KTH, Electric Power Systems, SE-100 44, Stockholm, Sweden, April 2009, ISBN: 978-91-7415-264-7. [Online]. Available: http://urn.kb.se/resolve?urn=urn:nbn:se:kth:diva-10206

[10] Z. Miao, L. Fan, D. Osborn, and S. Yuvarajan, "Control of dfig based wind generation to improve inter-area oscillation damping," *Power and Energy Society General Meeting - Conversion and Delivery of Electrical Energy in the 21st Century, 2008 IEEE*, pp. 1–7, July 2008.

[11] P. Ledesma and C. Gallardo, "Contribution of variable-speed wind farms to damping of power system oscillations," *2007 IEEE Lausanne Power Tech*, pp. 190–194, 2007.

[12] P. Pourbeik and M. Gibbard, "Damping and synchronizing torques induced on generators by facts stabilizers in multimachine power systems," *Power Systems, IEEE Transactions on*, vol. 11, no. 4, pp. 1920–1925, Nov 1996.
[13] M. Gibbard, "Co-ordinated design of multimachine power system stabilisers based on damping torque concepts," *Generation, Transmission and Distribution, IEE Proceedings C*, vol. 135, no. 4, pp. 276–284, Jul 1988.
[14] J. N. Nielsen, V. Akhmatov, J. Thisted, E. Grøndahl, P. Egedal, M. N. Frydensbjerg, and K. H. Jensen, "Modelling and fault-ride-trough tests of Siemens Wind Power 3.6 mw variable-speed wind turbines," *Wind Engineering*, vol. 31, pp. 441–452(12), December 2007. [Online]. Available: http://www.ingentaconnect.com/content/mscp/wind/2007/00000031/00000006/art00006
[15] M. Klein, G. Rogers, and P. Kundur, "A fundamental study of inter-area oscillations in power systems," *Power System, IEEE Transactions on*, vol. 6, no. 3, pp. 914–921, 1991.
[16] P. S. Kundur, *Power System Stability and Control*, ser. The EPRI Power System Engineering Series. McGraw-Hill, Inc., 1994, ISBN: 0-07-035958-X.
[17] G. Rogers, *Power System Oscillations*, 1st ed., ser. Power Electronics and Power Systems. Kluwer Academic Publishers, 2000, ISBN-10: 0792377125.
[18] M. Gibbard, D. Vowles, and P. Pourbeik, "Interactions between, and effectiveness of, power system stabilizers and facts device stabilizers in multimachine systems," *Power Systems, IEEE Transactions on*, vol. 15, no. 2, pp. 748–755, May 2000.
[19] M. Gibbard and D. Vowles, "Reconciliation of methods of compensation for psss in multimachine systems," *Power Systems, IEEE Transactions on*, vol. 19, no. 1, pp. 463–472, Feb. 2004.
[20] P. Pourbeik, M. Gibbard, and D. Vowles, "Proof of the equivalence of residues and induced torque coefficients for use in the calculation of eigenvalue shifts," *Power Engineering Review, IEEE*, vol. 22, no. 1, pp. 58 –60, jan. 2002.
[21] G. Sybille and et al., *SimPowerSystems™ 5 - User's Guide*, Hydro-Québec and MathWorks, Inc, March 2010. [Online]. Available: http://www.mathworks.com/access/helpdesk/help/pdf_doc/physmod/powersys/powersys.pdf

Thyge Knüppel received his M.Sc.E.E. degree from the Technical University of Denmark (DTU) in the spring of 2008 where he specialized in power systems and control theory. Currently, he is employed as research engineer at Siemens Wind Power A/S and is pursuing a PhD degree from DTU.

Jørgen N. Nielsen holds M.Sc. (1996) and Ph.D. (2000) degrees from the Technical University of Denmark, Kgs. Lyngby, Denmark. He has a broad and comprehensive knowledge and experience on power system planning, network investigations and power system simulations. Jørgen N. Nielsen has performed and been responsible for a number of network investigations and studies issued the integration of wind power in the power system and been deeply involved into the development of numerical PSS/E simulation models of the fixed- and variable-speed wind turbines.

Kim H. Jensen holds M.Sc. (1999) and Ph.D. (2003) degrees from the Technical University of Denmark, Kgs. Lyngby, Denmark. He has been working in a transmission company (NESA), consultant company (Elsam Engineering) and now a wind turbine company (Siemens Wind power). In these companies he has worked with transmission system planning, network designs, wind turbine modelling, grid codes studies and harmonic analysis and stability studies. He has also worked as technical specialist on an number wind farm integration projects.

Andrew Dixon holds B.Sc. and Ph.D. degrees in Applied Mathematics (1984. 1988) from the University of St Andrews, Scotland and an M.Sc. in Electric Power Systems (2005) from the University of Bath, England. Dr. Dixon has worked for 19 years for the National Grid Company, UK, consisting of: Research & Development (security-constrained optimization of reactive compensation) - 2 years; System Development & Grid Code - 6 years; Operational Planning - 4 years; Asset Management - 2 years; System Technical Performance (dynamics, including transient stability, small-signal stability & sub-synchronous resonance) - 5 years.

Jacob Østergaard is professor in Electric Technology, Head of Centre for Electric Technology (CET) and Head of Section for Electric Power Engineering at the Department of Electrical Engineering, DTU. From 1995 to 2005 he worked as research engineer and area responsible at Research Institute for Danish Electric Utilities (DEFU). Current activities include research within electricity production, transmission, distribution and demand. Prof. Østergaard is presently involved in activities related to an intelligent power system with focus of new electricity and information architectures, system integration of distributed generation and increased flexibility in the power system by use of demand side participation. Prof. Østergaard is project leader of more than 10 research projects. and serves in several professional organizations including the EU SmartGrids advisory council.

A.3 Paper III

T. Knüppel, J. N. Nielsen, K. H. Jensen, A. Dixon, and J. Østergaard. Power oscillation damping control of inter-area oscillation through active and reactive power modulation from wind power plants with full converter wind turbines. *Unsubmitted manuscript.*

Power Oscillation Damping Control of Inter-Area Oscillation Through Active and Reactive Power Modulation from Wind Power Plants With Full Converter Wind Turbines

Thyge Knüppel*, Jørgen N. Nielsen†, Kim H. Jensen‡
Andrew Dixon§, Jacob Østergaard¶

December 18, 2012

Abstract

This work analyzes aspects of the potential use of wind power plants (WPPs) with full converter wind turbines (WTs) to contribute with damping torque to synchronous generators. The impact of the active and reactive power modulation on the modal damping of an inter-area mode is analyzed with residues to give the modal sensitivity to the power oscillation damping control (POD). The residues are calculated for the WPP in-feed traversing the length of the transmission line between the oscillating areas, to analyze its impact on the interaction between the WPP and the oscillating areas. The generator speed difference across the inter-tie is used as POD input to have a clear reference from which the impact of active and reactive power modulation can be assessed. The study is conducted with both a simple, constant *PQ* WT model and a non-linear, dynamic model of the 3.6 MW Siemens Wind Power wind turbine. The results show that the idealistic residue characteristics from the constant *PQ* WT model are not applicable when an actual converter control is considered. Here, a cross coupling is found, the extent of which depends on both WPP size, type of power modulation, and WPP location.

Keywords: wind turbines, wind farms, wind power plants, wind power plant controller, power systems, small-signal stability, damping torque, power oscillation damping control

*T. Knüppel is with Siemens Wind Power A/S, DK-7330 Brande, Denmark and Centre for Electric Technology, Department of Electrical Engineering, Technical University of Denmark, DK-2800 Lyngby, Denmark (thyge.knuppel@siemens.com)

†J. N. Nielsen is with Siemens Wind Power A/S, DK-7330 Brande, Denmark (joergen_nygaard.nielsen@siemens.com)

‡K. H. Jensen is with Siemens Wind Power A/S, DK-7330 Brande, Denmark (kim_hoej.jensen@siemens.com)

§A. Dixon is with National Grid Electricity Transmission plc (National Grid), Warwick CV34 6DA, UK (andrew.dixon@uk.ngrid.com)

¶J. Østergaard is with Centre for Electric Technology, Department of Electrical Engineering, Technical University of Denmark, DK-2800 Lyngby, Denmark (joe@elektro.dtu.dk)

1 Introduction

With the rapid development in installed capacity of wind power and with the increasing size of each installation, the role and impact of wind power on power system operation is changing. In grid codes from some transmission system operators this is already noted, given that large wind power plants (WPPs) are termed power park modules and must comply with similar requirements to those for other generation units.

Most modern WPPs connected today consist of wind turbines (WTs) that are asynchronously connected to the grid, either partially or fully through electronic power converters, and will, as discussed in [1], not themselves cause system oscillations. This point is elaborated in [2] where it is presented that the participation of the full converter type WPP in power system oscillations is very low. A large scale integration of wind power can, however, indirectly change the modal characteristics of the system by *1)* significantly change the dispatch of the existing power units, *2)* significantly alter the power flows in the system, and *3)* interacting with the synchronous machines through the transmission network to change the synchronizing and damping torques induced on their shafts. Here, *1)* and *2)* are the consequence of a changed power in-feed pattern and as such not related to any specific power production technology. A more elaborate discussion is carried out in [3]. Case *3)*, on the other hand, does depend on the power conversion technology and the utilized control, with the latter point emphasizing the importance of accurate representation of the control when such studies are conducted.

Regarding wind power conversion units, several studies have investigated the impact on power system oscillations of WPPs based on primarily the fixed-speed induction generator (FSIG) and the doubly-fed induction generator (DFIG) [3–6]. In [7], the impact on power system oscillations of the reactive power control mode of DFIG WPPs is studied, whereas the effect of inertial response of DFIG WPPs is presented in [8].

If, furthermore, the WPPs are to participate with power system damping, as proposed by [9–14], analysis of mode controllability and choice of power modulation become important tasks. As demonstrated in [15, 16] the effectiveness of a voltage-source-converter interfaced power station, in terms of damping performance, is highly dependent on the type of power modulation, that is either active or reactive power, as well as the location of the station.

Parallels may be drawn to the siting problem of FACTS devices for stability purposes, which has received considerable attention, for example [17–19]. For a WPP damping controller also active power modulation can be used in the control, which adds another dimension to the siting problem. On the other hand, siting may already be decided by, for instance, considerations on wind resources and transmission system access, and the problem to solve is how to achieve maximum damping contribution by combined control of active and reactive power.

In this paper two case studies are presented where the impact of in-feed location and power modulation is assessed. Firstly, in section 3 a simple two machine case network is analyzed analytically where also the procedure for setting up the system equations is presented. Secondly, in section 4 the study is repeated on

a four machine benchmark system with auxiliary controllers included to which a detailed WPP model is connected. Finally, the discussion and conclusion are found in section 5 and 6, respectively.

2 Background

Power system oscillations are inherent in interconnected power systems based on synchronous generators [20]. Power system oscillations and the application of eigenvalue analysis as means of analysis are well described in the literature, for example [21].

2.1 Synchronizing and Damping Torques

The rotational mechanical system of a synchronous machine is directly coupled to the network, since the injected currents are a function of the rotor angle, $\Delta\delta$, and the field flux, $\Delta\psi_{fd}$. For the WT, however, the only connection between the network and the rotational system is through the controller with the generator side converter controlling the rotational speed of the generator, ω_g. As a result the terms synchronizing and damping torques of the WT rotational system have little meaning in the conventional sense. To analyze the indirect impact of FACTS units, induced torque coefficients (ITC) are introduced in [22,23], which are based on the PVr transfer function [24, 25]. The concept of ITC has been shown to be equivalent to residues [26] and can be considered a linear decomposition of the residue for an input/output pair on the synchronous machines. The rationale behind ITC is that although a FACTS stabilizer, or in this case a WT, does not a mass, which is synchronously connected to the network, there is still a path from the current output, i_{dj} and i_{qj}, of machine j through the network to the electromagnetic torque of machine i. From machine j it is thus possible to induce an electromagnetic torque on machine i in phase with $\Delta\delta_i$ or $\Delta\omega_i$, that is, a synchronizing or a damping torque component.

3 Two Generator System

The two machine network shown in Figure 1 was introduced in [15] to study the impact of HVDC on system damping and later used in [16] to study power system damping by power modulation of a voltage-source-converter power station. The network represents a two area power system, which has been reduced into a two machine equivalent. The system has here been extended with a constant load at both ends of the inter-connector between the two areas.

The generators in Figure 1 are modeled with the classical model, that is, a voltage source behind the transient reactance of the generator, while the transmission lines are purely inductive. The parameters are shown in appendix B and have been computed to resemble the four generator system studied in section 4. At bus 3 a WPP is connected, which is modeled as a constant power input, P_3 and Q_3, superimposed with a stabilizing power injection, ΔP_3 and ΔQ_3. The constant power model for the WPP implies that all dynamics except the stabilizing input are neglected. The electrical location of bus 3 is determined by the

parameter r. The equations that govern the system in Figure 1 are derived in appendix A.

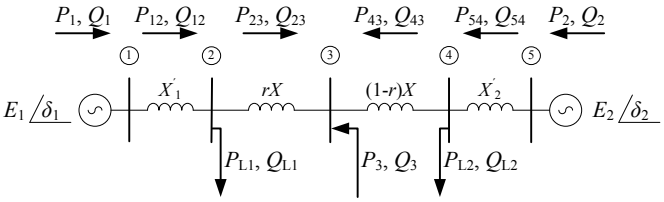

Figure 1: Single-line diagram of the two generator network.

To increase the damping of a critical mode, good observability and good controllability are required in order to *1)* detect the oscillation, and *2)* affect the mode damping. Generally, the stabilizing signal for a full converter WT needs to be available in the network, as for example frequency, voltage, current, or power, due to the previously mentioned asynchronous connection of a full converter WT. For this study, however, the speed signals, $\Delta\omega_1$ and $\Delta\omega_2$, are used in order to have a consistent POD input signal as the WPP is traversing between the two areas. This is done to be able to assess the modal sensitivity without the influence of the observability changing with the in-feed location. Simple proportional power oscillation damping controllers (POD) are then constructed as proposed in [16]

$$\Delta P_3 = k_p(\Delta\omega_1 - \Delta\omega_2) \tag{1a}$$
$$\Delta Q_3 = k_q(\Delta\omega_1 - \Delta\omega_2) \tag{1b}$$

The damping controllers in (1) are inserted into the system with the feedback law, $u = Ky$, where K is either k_p or k_q according to (1). The closed-loop system matrix is given by substitution into (11)

$$A_{cl} = A - BKC. \tag{2}$$

The feedback (2) with (1) modifies the $A_{\omega\omega}$ subsystem of (11) and as presented in section 2.1 $A_{\omega\omega}$ describes the damping of the generators. For the system in Figure 1, $\Delta\omega_1$ is in phase with $-\Delta\omega_2$ for the swing mode and a positive contribution to the damping torque is hence given when the diagonal elements of $A_{\omega\omega}$ are negative and the off-diagonal positive.

From (2) it is seen that changes in damping torque derive from B as both K and C are constant matrices that do not depend on the location r. Expanding (10b) of the open-loop system with $\hat{B} = A_{22}^{-1}B_2$ yields

$$\Delta\dot{\omega}_1 : \quad \eta_{V_1}\hat{B}_{V_1} + \eta_{\theta_1}\hat{B}_{\theta_1} \tag{3a}$$
$$\Delta\dot{\omega}_2 : \quad \eta_{V_2}\hat{B}_{V_2} + \eta_{\theta_2}\hat{B}_{\theta_2} \tag{3b}$$

where η's are the non-zero elements of A_{12}, where $\Delta\dot{\omega}_i$ is the differential equation that is affected by the control, and where the subscript of $\hat{B}$ corresponds to the algebraic variable mapped through this element. In other terms, $\hat{B}_{V_1}$ is

a mapping from ΔP_3 and ΔQ_3 to ΔV_1. From (3) the effect of the damping controller (1) can be decomposed into a perturbation of the generator terminal voltage magnitude, ΔV_i, and angle, $\Delta\theta_i$. The terminal conditions of G_1 and G_2 are mapped through A_{12} to a perturbation of $A_{\omega\omega}$, which describes the damping torques of G_1 and G_2. In other words, $\eta_{V_i}\hat{B}_{V_i}$ is the component of induced damping torque on machine i that derive from a changes in terminal voltage magnitude, while $\eta_{\theta_i}\hat{B}_{\theta_i}$ is the component that derive from changes in terminal voltage angle.

3.1 Results

As presented in section 2.1, damping torque is the torque component in phase with generator speed. Examining the DAE for the system (5), (7), (8), and (1) it is clear that the only source of damping present in the system is the damping controller at the WPP. Hence, for $\Delta P_3 = \Delta Q_3 = 0$ the system is undamped with a sustained oscillation and changing r will only affect the frequency of the oscillation.

Three cases are investigated with the steady state active power output of the WPP, P_{30}, equal to 108, 216, and 324 MW, and in each case the production of G_1 is adjusted such that there is an active power of 433 MW flowing into the area represented by G_2, cf. Table 1. The load-flow has been solved with a Newton-Raphson method where it is assumed that $E_1 = E_2 = V_{30} = 1$ pu, $\delta_{20} = 0$ degrees.

Table 1: Generator output in generator convention for the investigated power outputs a bus 3. The column "No loads" corresponds to section 3.1.1 and the column "Shunt loads" to section 3.1.2

		No loads		Shunt loads	
	P_{30}	P_{10}	P_{20}	P_{10}	P_{20}
Case #	[MW]	[MW]	[MW]	[MW]	[MW]
C1	108	325	−433	1 292	1 334
C2	216	217	−433	1 184	1 334
C3	324	109	−433	1 076	1 334

3.1.1 No Shunt Loads

Initially the loads are neglected, that is $P_{L1} = P_{L2} = Q_{L1} = Q_{L2} = 0$, and the system simplifies to the one studied in [15, 16].

Figure 2 shows the residues as a function of the location, r, for the WPP equipped with either ΔP_3 or ΔQ_3 POD. The residues are calculated for the open-loop system. The generator speed difference, $\Delta\omega_1 - \Delta\omega_2$, is used as input to the PODs while the outputs are ΔP_3 and ΔQ_3 for, respectively, active and reactive power modulation. If the eigenvalues are calculated for the closed-loop system with the damping controllers in (1) inserted, the resulting damping ratios, ζ, have the same characteristic curve as those of the residue magnitudes.

The residue for an eigenvalue for the transfer function between a certain output and a certain input is the sensitivity of this eigenvalue to a scalar feed-back control. The magnitude of the residue is thus a measure of the impact of

the control gain on the eigenvalue, while the angle indicates the direction of the eigenvalue movement. For the same input/output pair, a decreasing magnitude of the residue means that the leverage on the eigenvalue damping is also decreasing. Thus, to retain a certain left shift of the eigenvalue a higher controller gain is needed and, hence, a larger modulated damping power. The residue magnitude is therefore an important parameter when assessing the efficiency of a proposed damping control.

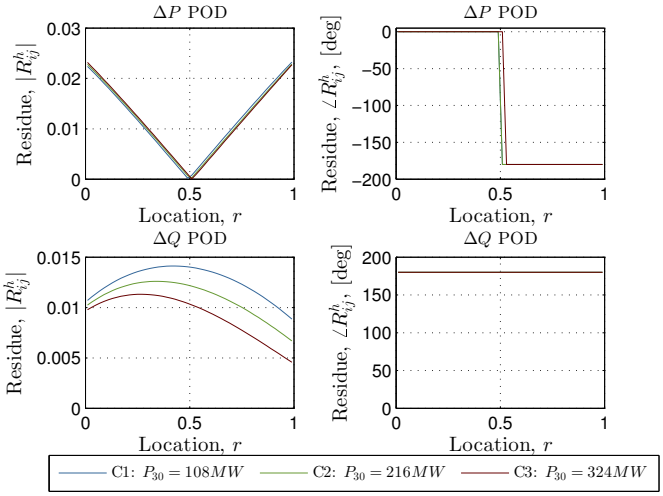

Figure 2: Open-loop residues as a function of the location r for a damping controller based on ΔP_3 (upper) or ΔQ_3 (lower) modulation. Arrow shows increasing r. Results are for the two generator system without shunt loads.

The results for the ΔP_3 POD are presented in Figure 2. The effectiveness of this control will be better when the WPP is located close to the oscillating machines, while the residue approaches zero at $r = 0.50$. The discontinuity in the residue angles at $r = 0.50$ is caused by a polarity change of the oscillation at the inertia scaled center point and shows that ΔP_3 should be in phase with the speed deviation of the "nearest" generator [15, 16]. For the damping controller based on reactive power injection, the best performance is achieved when the in-feed is located close to the electrical center point and when P_{30} is small. Comparing with the ΔP_3 POD it is noted that this controller is less effective.

The results presented in Figure 2 match well with those presented in [15, 16] for a similar system.

3.1.2 With Shunt Loads

Next, the system is extended with shunt loads adjacent to the inter-connector to get a closer resemblance with the network considered in section 4. The active power flow across the inter-connector is still 433 MW.

The residues for the WPP equipped with either a ΔP_3 or a ΔQ_3 POD are presented in Figure 3. For both controllers it is noted that the residue magnitudes, and hence the level of damping, are affected by the active power production at bus 3. The closed-loop damping ratios, ζ, show the same curvature as the residue magnitude and equal zero when the residue is zero. For the ΔP_3 POD it is, furthermore, found that the location of the center point where the oscillation changes polarity, moves toward G_2 with increasing P_{30}. When the loads are considered, a more complicated characteristic is obtained for the ΔQ_3 POD. From Figure 3 it is clear that the feedback changes sign, that is, $\angle R_{ij}^h$ jumps 180°, at a location r which depends on the active power production at bus 3.

The choice of a constant PQ representation of the loads, clearly means that any load induced response has been neglected. This element is further discussed in section 4.2.1.

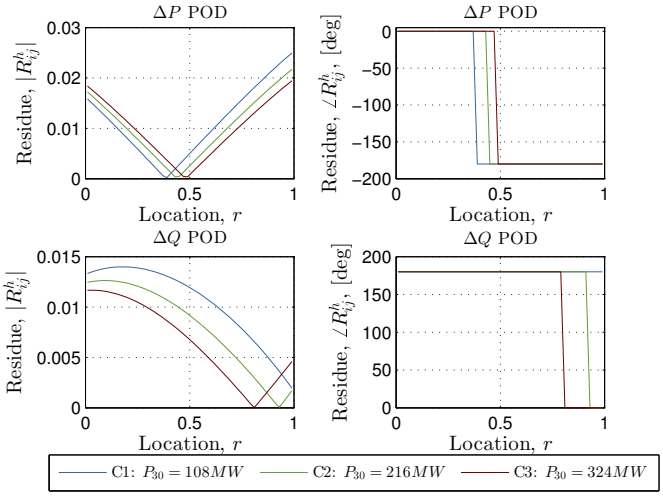

Figure 3: Open-loop residues as a function of the location r for a damping controller based on ΔP_3 (upper) or ΔQ_3 (lower) modulation. Arrow shows increasing r. Results are for the two generator system with shunt loads.

As shown in (3), the WPP PODs can only affect system damping by altering the terminal voltage, ΔV_i and $\Delta\theta_i$, of the synchronous generators and thereby induce damping torques on these machines. A ΔP_3 modulation would predominantly affect $\Delta\theta_i$, whereas a ΔQ_3 modulation has a large impact on both ΔV_i and $\Delta\theta_i$. This result is noted in Figure 4 where the decomposition in (3) of the contributions to the damping torques are shown for the ΔP_3 and the ΔQ_3 PODs. The ΔP_3 POD effectively damps the system by adding positive damping torque to only one generator, while an amount of negative damping torque is added to the other. As bus 3 moves from G_1 toward G_2, the positive damping torque added to G_1 decreases while the negative damping torque added to

G_2 increases. At the center of the oscillation these contributions counter each other and the oscillation is undamped. When the sign of k_p in Figure 2 and 3 is changed at the center point, the role of G_1 and G_2 as discussed above is effectively reversed. For the ΔQ_3 POD it is noted that the contribution from modifying ΔV_i at some location, r, is completely countered by an opposing contribution from $\Delta\theta_i$, thereby effectively changing the sign of the feedback. This location is marked in Figure 4 with dash-dotted vertical lines.

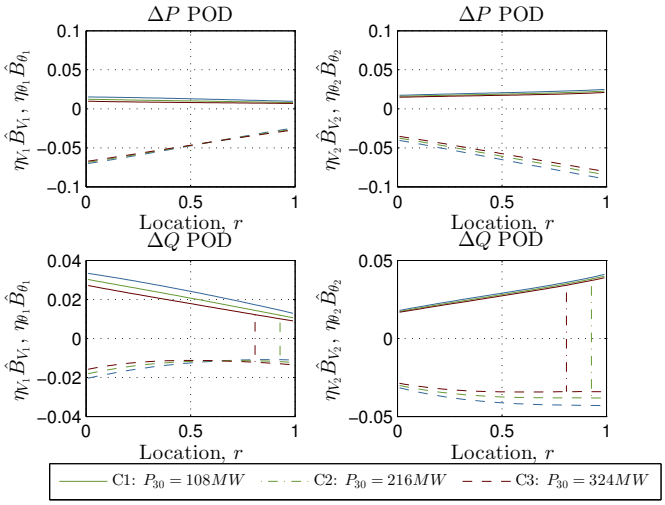

Figure 4: Contribution of ΔV and $\Delta\theta$ to damping as a function of the location r for a damping controller based on ΔP_3 (upper) or ΔQ_3 (lower) modulation. The left hand side graphs show the induced damping torques on G_1 and the right hand side graphs the induced torques on G_2. $\eta_V \hat{B}_V$: solid, $\eta_\theta \hat{B}_\theta$: dashed.

4 Four Generator System

To extend the findings from section 3, a more complex system is considered next where the dynamics of the generators, exciters, PSSs, governors, WPP, as well as voltage dependency of the loads are included. The network shown in Figure 5 is based on the four machine system in [27], which is a modified version of the two area system originally presented in [20]. At bus M a WPP is connected through a park transformer, collector grid, and a scaled WT transformer.

The basic PODs in (1) are for the four generator system equipped with low-pass and wash-out filters, phase compensation, and output limitations. The designed PODs have the general structure

$$\frac{\Delta y_{\text{stab}}}{\Delta u} = \underbrace{K}_{Gain} \underbrace{\frac{1}{sT_{lp}+1}}_{\text{Low pass}} \underbrace{\frac{sT_w}{sT_w+1}}_{\text{Wash out}} \underbrace{\left(\frac{1+\tau_1 s}{1+\tau_2 s}\right)^2}_{\text{Phase compensation}} \tag{4}$$

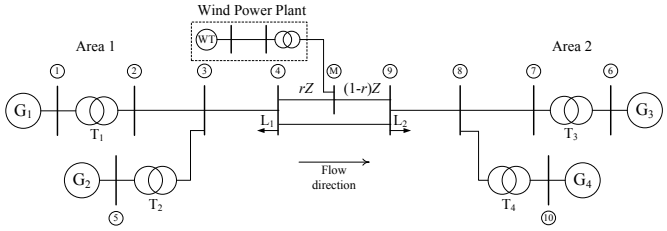

Figure 5: Single-line diagram of the four generator, two area case network.

where $\Delta u = \Delta\omega_1 - \Delta\omega_3$, Δy_{stab} is the input to the WT controls, which is added to either the active power or the voltage reference to achieve the desired active and/or reactive power modulations. For all calculations $T_{lp} = 0.03$ and $T_w = 2$.

For practical applications, the obvious stabilizing signal for a non-synchronous generator based POD may not be the speed of any generator, since the aim of the POD is to damp certain modes while being insensitive to others [19]. Another practical challenge with remote signals is the potential latency in the transmission from the measurement location to the location of the unit. In [28] a method with adaptive phase compensation of the POD is proposed to account for latency in the feedback signal. The speed difference is here used to be able to isolate the modal sensitivities of the ΔP and the ΔQ power modulations as the WPP traverses the length of the inter-tie, since the observability of this input signal is independent of the WPP in-feed location. This will, furthermore, allow for comparison with the idealistic residue characteristics computed in section 3 that did not consider the converter control. To have a reference to a locally available signal, the residues for case 3 with $P_{30} = 324$ MW are also computed with the frequency at the point of common connection (PCC) as input to the PODs. The PCC frequency are here synthesized by the imperfect time derivative of the voltage angle and is computed with $\frac{s}{s\,0.02+1}$.

The base power balance is adjusted according to the power balance given in appendix B and Table 1, which results in an active power flow of 433 MW across bus 10 into the area with G_{3-4}. There are, however, a few notable differences to the system analyzed in section 3. In this system there is no voltage control at bus M, the loads are represented as constant impedances, and the power flow across the inter-connector thus depends on the load flow solution as the WPP is moved from area 1 towards area 2.

4.1 Wind Turbine Model

The WPP connected at bus M in Figure 5 is represented by a single upscaled WT model that is operated in voltage control mode. The WT concept for this study is a variable-speed, pitch controlled, full converter interfaced WT.The WT is represented with a reduced order model suitable for transient and dynamic power system studies. The model represents a 3.6 MW Siemens Wind Power WT [29]. The model includes a variable wind speed aerodynamic model, a two-

mass model of rotor, gearbox, and generator, machine and grid side converter, DC-link, and a generic reduced order control scheme.

4.2 Results

First, a modal analysis is performed to compare with the findings in section 3 after which time domain simulations are performed with the non-linear model.

4.2.1 Modal Analysis

The residues are calculated for the open-loop system, while the eigenvalues correspond to the closed-loop system where the phase compensation in each step is computed from the complement of the residue angle. The gain, K, is selected such that the loop gain of (4) at the modal frequency of the inter-area oscillation equals 25. The loop-gain has been selected from root locus analysis and results in active and reactive power modulations of reasonable magnitudes.

The residue and the trajectory for the inter-area mode are in Figure 6 shown for the ΔP POD as a function of the location r. The residues have a clear resemblance to those in Figure 3 for the simpler system with the characteristic V-shape in the magnitude and a 180° shift in residue angle at the oscillatory center point. It is noticed that the characteristic for the residue magnitude for the frequency input is similar to the speed difference input, although its curvature is softer. The residue phase characteristic for the frequency input is similar to the speed difference input in that it has a phase shift at the center point of the oscillation. Where the phase characteristic for the speed difference input has a 180° shift to have a signal that is in phase with the "nearest" generator, this property is given with the frequency and after the phase jump the residue angle returns to a value that is shifted only 8° with respect to the initial residue angle.

For the ΔQ POD the dependence on the location, r, of the residue and the inter-area mode are given in Figure 7. When compared to the system in section 3.1.2, it is noticed that the damping characteristics are turned upside down, with increased damping ratios as the size of the WPP increases. Furthermore, as r approaches 1 a steep increase is observed in the damping of the inter-area mode, with case 3 experiencing the steepest increase. Also for the ΔQ modulation, the dominant characteristics of the residues based on generator speed difference are reflected in those based on PCC frequency.

The residues in Figure 7 have a more complicated behavior than those previously shown. With increasing size of the WPP, the magnitude of the residue approaches the V-shape of the ΔP POD. For case 1 and 2, however, the curvature is softer and there is a region around $r \simeq 0.5$ with larger residues than in the case 3 system. A low WPP penetration at bus M entails a larger production at G_1 and hence that more active power is transferred across the entire length of the inter-connector, which according to Figure 2 and previous studies [15, 16] yield better performance for a ΔQ POD. Also, depending on the size of the WPP, the phase characteristic of the residues has a soft or a steep transition. The same is, although to a lesser extent, found for the ΔP POD in Figure 6. The residues for ΔP POD are not quite as pointy and, especially for case 1 where

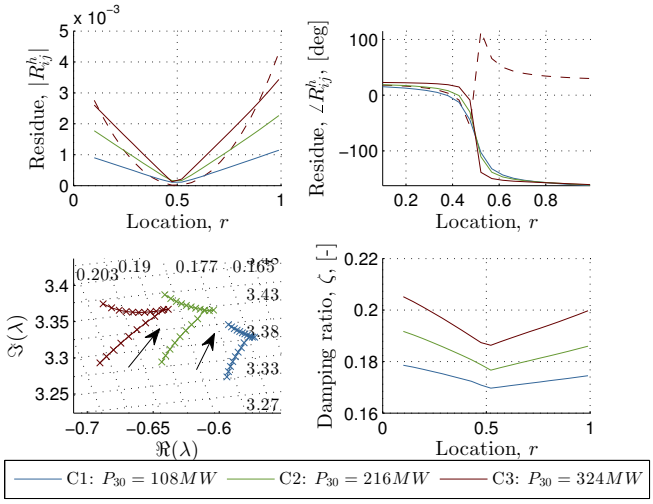

Figure 6: Open-loop residues and closed-loop eigenvalues and damping as a function of the location r for a damping controller based on ΔP modulation. Results are for the inter-area mode in the four generator system. Dashed curves in residue plots are with PCC frequency as POD input and the magnitude is scaled with 10^{-1}.

ΔQ modulation in Figure 2 showed to have the largest impact, a curvature is noticed around the tip of the residue magnitude in Figure 6.

The shape of the residue plot appears by superposition of the ΔQ and ΔP residues and is caused by a combination of converter control and induced network response. The induced network response means that, for example, the applied reactive power modulation will induce an active power modulation of the nearby impedance load of $P(t) = P_0 \left(\frac{V(t)}{V_0}\right)^2$. An active power modulation will, on the other hand, change the reactive power consumption of the WPP collector grid, which will impact the WT terminal voltage and result in control action from the WT voltage controller.

4.2.2 Time Domain Simulations

The linear models and modal analysis provide valuable information on the dynamics of the system. However, due to the linear nature of the analysis, limiters and other highly non-linear phenomena are not accurately represented in the analysis, which should be complemented by time domain simulations on the non-linear model.

The simulations presented here are with the case 3 WPP penetration level of 324 MW and the WPP is located at $r = 0.1$. The oscillations are excited by a 0.2 second 5% step to the exciter reference voltage of G_1 in area 1.

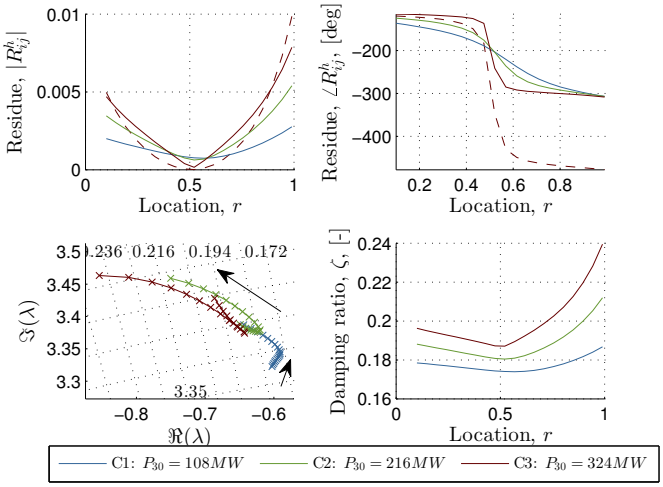

Figure 7: Open-loop residues and closed-loop eigenvalues and damping as a function of the location r for a damping controller based on ΔQ modulation. Results are for the inter-area mode in for four generator system. Dashed curves in residue plots are with PCC frequency as input and the magnitude is scaled with 10^{-1}.

For the system analyzed in section 4.2.1 the dynamic response of the inter-area mode and the control action from the WPP PODs are shown in Figure 8. The difference in the generator speed between area 1 and 2, that is between G_1 and G_3, is plotted to show the impact of the applied POD control on the inter-area oscillation. Investigated WPP POD configurations are

- $P, Q \in \{0, 0\}$: no WPP POD
- $P, Q \in \{1, 0\}$: ΔP WPP POD
- $P, Q \in \{0, 1\}$: ΔQ WPP POD
- $P, Q \in \{1, 1\}$: both ΔP and ΔQ WPP POD.

As seen from Figure 8, the PODs increase the damping. A comparison between the analytical modal characteristics of the inter-area mode and those extracted from the time domain responses is presented in Table 2. First it is noted that there is a very good agreement between the linear and the non-linear model for all investigated WPP POD configurations. Secondly, it is seen that a slightly higher damping ratio is achieved with the ΔP POD when compared to the ΔQ POD and that the highest damping ratio is found with the combined use of both ΔP and ΔQ PODs.

The damping contribution is more clearly noted if the PSSs at the synchronous machines are disabled; here the system is small-signal unstable as

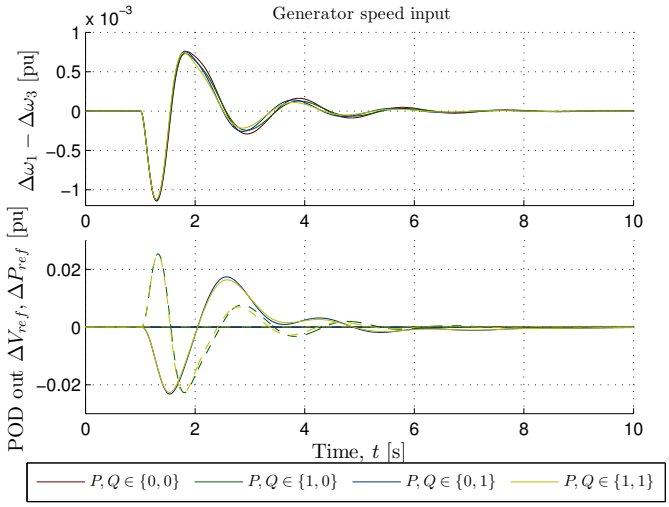

Figure 8: Top: Generator speed difference between area 1 and 2, that is $\Delta\omega_1 - \Delta\omega_3$. Bottom: Output reference of the WPP POD where solid is the active power reference and dashed is the voltage reference. Synchronous machine PSSs are in service and the WPP PODs are driven by the generator speed difference between G_1 and G_3.

Table 2: Modal characteristics for the inter-area mode as computed from both eigenvalue analysis and as extracted from time domain simulations.

	Modal analysis		Time domain	
	ζ	ω_d	ζ	ω_d
Configuration	[-]	[Hz]	[-]	[Hz]
$P, Q \in \{0, 0\}$	0.186	0.529	0.186	0.527
$P, Q \in \{1, 0\}$	0.205	0.524	0.210	0.537
$P, Q \in \{0, 1\}$	0.196	0.546	0.200	0.543
$P, Q \in \{1, 1\}$	-	-	0.223	0.539

illustrated in Figure 9 with increasing amplitude of the oscillation between the areas. When either the WPP PODs are enabled, the system is stabilized with oscillations of decreasing amplitude. The combined use of ΔP and ΔQ PODs in the control is shown to have a positive impact on the damping, in terms of improved performance when compared to the pure ΔP or ΔQ POD. The simulation in Figure 9 is conducted with the local measurement of the PCC frequency as input to the WPP PODs. For the frequency input, the time constant for the low-pass filter in the PODs has been increased to $T_{lp} = 0.07$ to reduce interaction with a higher frequency eigenvalue, and the POD gain is scaled with the ratio of the residue magnitudes for the speed difference input and the frequency input. The simulation was also done with the speed difference as input and it was seen that similar improvements were achieved in the damping of the

inter-area mode with a similar control effort.

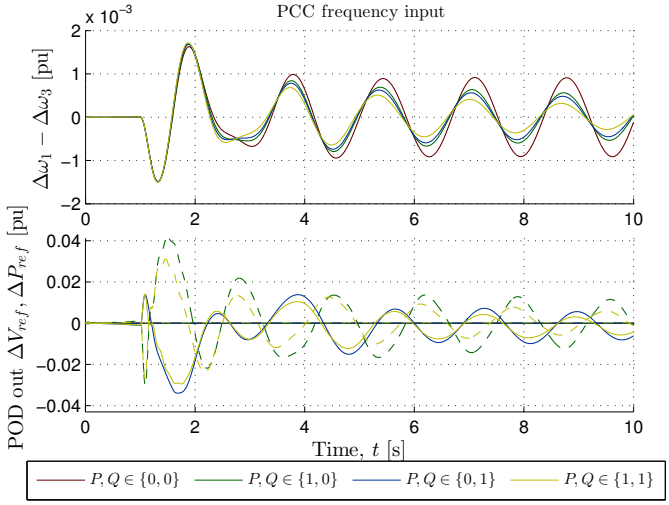

Figure 9: Top: Generator speed difference between area 1 and 2, that is $\Delta\omega_1 - \Delta\omega_3$. Bottom: Output reference of the WPP POD where solid is the active power reference and dashed is the voltage reference. Synchronous machine PSSs disabled and WPP POD is driven by a synthesized PCC frequency.

5 Discussion

This study investigates the possibility of utilizing WPPs for delivery of damping torque to the synchronous generators in the power system, and the dependency of the location of the WPP in the ability to affect the modal damping. The rotational masses of a full converter WT are electrically decoupled from those of the synchronous machines. Through the converter it is therefore only possible to exercise indirect control of the damping through alteration of the terminal voltage of the synchronous generators. The study found that for a POD based on ΔP modulation, primarily the terminal voltage angles were affected, while both the terminal voltage magnitudes and angles were affected by a ΔQ POD. First a simple two generator system was analyzed after which the findings were extended to a more detailed system, with a detailed representation of the generator control, and with a dynamic WPP model that represents the dynamic behavior of a commercially available WT.

From the results it is clear that the WPP indeed does have damping capabilities, but also that the findings on the simplified and idealistic two generator system cannot not be directly transferred to more realistic systems. In [15,16] a two area equivalent network is analyzed with similar results as those presented

in section 3.1.1. When shunt loads were connected to each end of the interconnector, while keeping the power transfer constant, it was found that these results were not generally valid. For a ΔQ POD it was here found that at some location, r, the positive damping torque induced from perturbation of the terminal voltage magnitude was completely countered by a negative damping torque, which was induced by changes in the terminal voltage angle. Depending on the active power output of the WPP, this change of phase occurred at different locations. Such characteristic will pose some practical challenges with the ΔQ POD if the WPP is located within that band where the change of residue phase occurs.

For the four generator system, the results with the ΔP POD were similar to those with the simple two generator system, although a small cross coupling to the response of the ΔQ POD was observed. This was mostly noted for the lower active power outputs of the WPP and resulted in a less steep change of phase of the residue angle when compared to the idealistic responses shown for the two generator system. With a POD based on ΔQ modulation, a much larger cross coupling to active power was revealed, where a larger coupling was observed for larger sizes of the WPP, cf. Figure 7. A consequence of the cross coupling was that the necessary phase compensation showed a large dependency to both the size of the WPP and the location, since the effective residues were a mixture between those obtained with the pure ΔP or ΔQ PODs. The modular nature of a WPP means that the power rating of the WPP as a unit is not fixed, since one or more WTs can be disconnected while the remaining stay in operation. In [30], the sensitivity of the residues to the internal state of a WPP is investigated for a ΔP and a ΔQ POD. The study finds that the ΔQ POD has a higher sensitivity to the internal state of the WPP than the ΔP POD, which matches well with the results presented here. A high sensitivity of the residues to the operating condition or the internal state of the WPP complicates the controller design and may necessitate that adaptive [31] or robust control is used [32], or simply require that the controller is disabled under certain operating conditions.

The residue calculations were repeated using the synthesized frequency at the PCC to have a locally obtained input signal to compare against. The results showed that the dominant characteristics of both the residue magnitude and phase were very similar for the two input signals, although a somewhat softer curvature was found in the characteristic for the residue magnitude for the frequency input. The large similarity indicates that the conclusions are not limited to a POD using the generator speed difference as input.

Different configurations of ΔP and ΔQ PODs were designed for the frequency input and tested with time domain simulations. Both in terms of contribution to the damping of the inter-area oscillation and in terms of the WPP control action, the performance of the frequency driven PODs were very similar to the performance of the PODs that used the generator speed difference.

The efficiency of both ΔP and ΔQ PODs were found to be highly dependent on the location of the WPP within the oscillation, cf. Figure 6 or 7 And since wind power projects among other things are sited based on the wind resources and transmission system access rather than on damping capabilities, the damping contribution from some sites may be diminishing.

The significance of the shown damping contribution depends on the state of the power system, which was clearly shown in Figure 9 where the damping

contribution from the WPP stabilized the power system from an otherwise unstable state, whereas only a minor improvement was noted in the stable case in Figure 8. While equipping WPPs with a POD can have a positive damping contribution, it is clear that also the complexity of the power system control increases, which is discussed in [33] regarding inertial response from WPPs. For a particular case it would thus be relevant to evaluate whether the WPP can give a significant contribution to the damping or whether the required damping power is more easily provided for elsewhere.

6 Conclusion

In this paper, the ability to contribute with damping torque of wind power plants (WPPs) based on full converter wind turbines (WTs) was investigated. It has been demonstrated via modal and time domain analysis that full converter based WPPs are capable of contributing with damping torque to increase the small-signal stability of a power system. The damping contribution was achieved using either active or reactive power modulation, or a combination of both.

It has been shown that the idealistic results found with a two generator equivalent model, in general cannot be transferred to more complex systems where the actual machine control and induced network responses are considered. For a power oscillation damping controller (POD) based on reactive power, a large cross coupling was found to the response of an active power POD. Where the larger the active power output of the WPP, the larger the cross coupling. For the investigated system, the damping capabilities of a reactive power POD was dominated by the induced active power modulations with residue magnitudes that approached zero around the center of the oscillation.

The effectiveness of the damping control has been shown to be very dependent on the system conditions, location of the WPP, selection of active or reactive power for the damping control, and the size of the WPP.

A Model Setup for Two Machine System

The dynamics of the system in Figure 1 are governed by the swing equations of G_1 and G_2.

$$\Delta\dot{\delta}_j = \omega_0 \Delta\omega_j \tag{5a}$$

$$\Delta\dot{\omega}_j = \frac{1}{2H_j}(P_{m,j} - P_{e,j} - K_{dj}\Delta\omega_j) \tag{5b}$$

for $j = 1, 2$, where $\Delta P_j = P_{jm} - P_{je}$, where H_j is the inertia constant for the jth machine, and where K_{dj} is the equivalent damping.

The active and reactive power received at bus R from sending bus S are given as

$$P = \gamma V_S V_R \sin(\theta_S - \theta_R) \tag{6a}$$

$$Q = \gamma V_S V_R \cos(\theta_S - \theta_R) - \gamma V_R^2 \tag{6b}$$

where the voltage at bus S is defined as $V_S \angle \theta_S$, and where γ is the admittance between bus R and S. Let (6) be linearized around the steady state operating point given by $\{V_{R0}, V_{S0}, \theta_{R0}, \theta_{S0}\}$ to obtain

$$\begin{aligned}\Delta P = \gamma\Big(&V_{R0}\sin(\theta_{S0}-\theta_{R0})\Delta V_S \\ &+ V_{S0}\sin(\theta_{S0}-\theta_{S0})\Delta V_R \\ &+ V_{S0}V_{R0}\cos(\theta_{S0}-\theta_{R0})\Delta\theta_S - \\ &- V_{S0}V_{R0}\cos(\theta_{S0}-\theta_{R0})\Delta\theta_R\Big) \end{aligned} \tag{7a}$$

$$\begin{aligned}\Delta Q = \gamma\Big(&V_{R0}\cos(\theta_{S0}-\theta_{R0})\Delta V_{S0} \\ &+ \Big(V_{S0}\cos(\theta_{S0}-\theta_{R0}) - 2V_{R0}\Big)\Delta V_R \\ &- V_{S0}V_{R0}\sin(\theta_{S0}-\theta_{R0})\Delta\theta_S \\ &+ V_{S0}V_{R0}\sin(\theta_{S0}-\theta_{R0})\Delta\theta_R\Big) \end{aligned} \tag{7b}$$

The power injection from machine j is given from (7) by replacing θ_S with δ_j, V_S with E_j, and by neglecting terms with ΔV_S since E_j is constant by definition.

The power balance at bus 2, 3, and 4 dictates

$$\Delta P_1 = \quad \Delta P_{L1} - \Delta P_{23} \quad \Delta Q_1 = \quad \Delta Q_{L1} - \Delta Q_{23} \tag{8a}$$

$$\Delta P_2 = \quad \Delta P_{L2} + \Delta P_{43} \quad \Delta Q_2 = \quad \Delta Q_{L2} + \Delta Q_{43} \tag{8b}$$

$$\Delta P_3 = -\Delta P_{23} - \Delta P_{43} \quad \Delta Q_3 = -\Delta Q_{23} - \Delta Q_{43} \tag{8c}$$

where $\Delta P_{L1} = \Delta P_{L2} = \Delta Q_{L1} = \Delta Q_{L2} = 0$ since the load is assumed constant, and where ΔP_3, ΔQ_3 are modulated powers from the WPP that can be controlled to increase system damping.

The system equations (5) and (7) are set up in the system of differential and algebraic equations (DAE) in (9) with $\Delta x = [\Delta\delta_1\ \Delta\delta_2\ \Delta\omega_1\ \Delta\omega_2]^T$, $\Delta v = [\Delta V_1\ \Delta V_2\ \Delta V_3\ \Delta\theta_1\ \Delta\theta_2\ \Delta\theta_3]^T$, $u = [\Delta P_3\ \Delta Q_3]^T$, and $y = \Delta\omega_1 - \Delta\omega_2$. The algebraic subsystem is prepared by substitution of (7) into (8) and collecting terms for Δx and Δv.

The advantage of the DAE description is that the inherent structures in the algebraic subsystem are preserved, hence residues and participations can be computed also for the algebraic variables [34]. Let the DAE system be defined as

$$\begin{aligned}\begin{bmatrix} \Delta\dot{x} \\ 0 \end{bmatrix} &= \begin{bmatrix} A_{11} & A_{12} \\ A_{21} & A_{22} \end{bmatrix}\begin{bmatrix} \Delta x \\ \Delta v \end{bmatrix} + \begin{bmatrix} B_1 \\ B_2 \end{bmatrix}\Delta u \\ \Delta y &= \begin{bmatrix} C_1 & C_2 \end{bmatrix}\begin{bmatrix} \Delta x \\ \Delta v \end{bmatrix} + D_1\Delta u \end{aligned} \tag{9}$$

where $x^{n\times 1}$ is the state vector, $v^{o\times 1}$ the algebraic vector, $u^{r\times 1}$ the input vector,

$y^{m\times 1}$ the output vector. The algebraic variables, v, are eliminated with

$$A = A_{11} - A_{12}A_{22}^{-1}A_{21} \tag{10a}$$
$$B = B_1 - A_{12}A_{22}^{-1}B_2 \tag{10b}$$
$$C = C_1 - C_2A_{22}^{-1}A_{21} \tag{10c}$$
$$D = D_1 - C_2A_{22}^{-1}B_2. \tag{10d}$$

With (9) described purely by ordinary differential equations (ODE), the system is in the classical state space form

$$\begin{aligned} \Delta\dot{x} &= A\Delta x + B\Delta u \\ \Delta y &= C\Delta x + D\Delta u \end{aligned} \tag{11}$$

where $A^{n\times n}$ is the system state matrix, $B^{n\times r}$ the input matrix, $C^{m\times n}$ the output matrix, and $D^{m\times r}$ the feed forward matrix.

B Parameters for Two Machine System

$S_{\text{base}} = 1800$ MVA $\quad U_{\text{base,LL}} = 230$ kV $\quad \omega_0 = 2\pi f$

$S_1 = S_{\text{base}}$	$X_1' = 0.72$ pu	$H_1 = 6.5$ s
$K_{D1} = 0$	$P_{L1} = 967$ MW	$Q_{L1} = -287$ Mvar
$S_2 = S_{\text{base}}$	$X_2' = 0.72$ pu	$H_2 = 6.175$ s
$K_{D2} = 0$	$P_{L2} = 1767$ MW	$Q_{L2} = -437$ Mvar
$X = 1.97$ pu	$k_q = 25$	$k_p = 25$

References

[1] Vowles, D., Samarasinghe, C., Gibbard, M., and Ancell, G.: 'Effect of wind generation on small-signal stability - a new zealand example', in Power and Energy Society General Meeting - Conversion and Delivery of Electrical Energy in the 21st Century, 2008 IEEE (2008), ISSN 1932-5517, pp. 1–8, doi:10.1109/PES.2008.4596444

[2] Knüppel, T., Nielsen, J.N., Jensen, K.H., Dixon, A., and Østergaard, J.: 'Small-signal stability of wind power system with full-load converter interfaced wind turbines', IET Renewable Power Generation, 2012, 6, (2), pp. 79–91, doi:10.1049/iet-rpg.2010.0186, ISSN 1752-1416

[3] Wilson, D., Bialek, J., and Lubosny, Z.: 'Banishing blackouts [power system oscillations stability]', Power Engineer, April-May 2006, 20, (2), pp. 38 –41, ISSN 1479-8344

[4] Anaya-Lara, O., Hughes, F., Jenkins, N., and Strbac, G.: 'Influence of windfarms on power system dynamic and transient stability', Wind Engineering, 2006, 30, (2), pp. 107–127, ISSN 0309524x, doi:10.1260/030952406778055018

[5] Hagstrom, E., Norheim, I., and Uhlen, K.: 'Large-scale wind power integration in norway and impact on damping in the nordic grid', WIND ENERGY, JUL-SEP 2005, 8, (3), pp. 375–384, ISSN 1095-4244, doi: 10.1002/we.168

[6] Slootweg, J., and Kling, W.: 'The impact of large scale wind power generation on power system oscillations', Electric Power Systems Research, 2003, 67, (1), pp. 9 – 20, ISSN 03787796

[7] Tsourakis, G., Nomikos, B., and Vournas, C.: 'Effect of wind parks with doubly fed asynchronous generators on small-signal stability', Electric Power Systems Research, 2009, 79, (1), pp. 190 – 200, ISSN 0378-7796, doi:10.1016/j.epsr.2008.05.018
URL http://www.sciencedirect.com/science/article/B6V30-4T0FHRM-1/2/3b6ac71f22cac8ff81670dcc6944a0f9

[8] Gautam, D., Goel, L., Ayyanar, R., Vittal, V., and Harbour, T.: 'Control strategy to mitigate the impact of reduced inertia due to doubly fed induction generators on large power systems', IEEE Transactions on Power Systems, Feb. 2011, 26, (1), pp. 214 –224, ISSN 0885-8950, doi: 10.1109/TPWRS.2010.2051690

[9] Hughes, F., Anaya-Lara, O., Jenkins, N., and Strbac, G.: 'A power system stabilizer for dfig-based wind generation', IEEE Transactions on Power System, 2006, 21, (2), pp. 763–772, ISSN 08858950

[10] Elkington, K.: 'Modelling and control of doubly fed induction generators in power systems: Towards understanding the impact of large wind parks on power system stability', Phd thesis, KTH, Electric Power Systems, SE-100 44, Stockholm, Sweden, April 2009, ISBN: 978-91-7415-264-7
URL http://urn.kb.se/resolve?urn=urn:nbn:se:kth:diva-10206

[11] Miao, Z., Fan, L., Osborn, D., and Yuvarajan, S.: 'Control of dfig based wind generation to improve inter-area oscillation damping', Power and Energy Society General Meeting - Conversion and Delivery of Electrical Energy in the 21st Century, 2008 IEEE, July 2008, pp. 1–7, ISSN 1932-5517, doi:10.1109/PES.2008.4596741

[12] Ledesma, P., and Gallardo, C.: 'Contribution of variable-speed wind farms to damping of power system oscillations', 2007 IEEE Lausanne Power Tech, 2007, pp. 190–194

[13] Tsourakis, G., Nomikos, B., and Vournas, C.: 'Contribution of doubly fed wind generators to oscillation damping',IEEE Transactions on Energy Conversion, Sep. 2009, 24, (3), pp. 783 –791, ISSN 0885-8969, doi:10.1109/TEC.2009.2025330

[14] Fernandez, R., Mantz, R., and Battaiotto, P.: 'Contribution of wind farms to the network stability', in Power Engineering Society General Meeting, 2006. IEEE (2006), pp. 1–6, doi:10.1109/PES.2006.1709274

[15] Smed, T., and Andersson, G.: 'Utilizing HVDC to damp power oscillations', IEEE Transactions on Power Delivery, Apr. 1993, 8, (2), pp. 620 –627, ISSN 0885-8977, doi:10.1109/61.216868

[16] Ruan, S.Y., Li, G.J., Ooi, B.T., and Sun, Y.Z.: 'Power system damping from real and reactive power modulations of voltage-source-converter station', IET GENERATION TRANSMISSION & DISTRIBUTION, MAY 2008, 2, (3), pp. 311–320, ISSN 1751-8687, doi:10.1049/iet-gtd:20070021

[17] Haque, M.: 'Damping improvement by facts devices: A comparison between statcom and sssc', Electric Power Systems Research, 2006, 76, (9-10), pp. 865 – 872, ISSN 0378-7796, doi:DOI:10.1016/j.epsr.2005.11.001 URL http://www.sciencedirect.com/science/article/B6V30-4J2M6X8-2/2/658c1cc87c3de4d379805e807baff170

[18] Mithulananthan, N., Canizares, C., Reeve, J., and Rogers, G.: 'Comparison of pss, svc, and statcom controllers for damping power system oscillations', IEEE Transactions on Power Systems, May 2003, 18, (2), pp. 786 – 792, ISSN 0885-8950, doi:10.1109/TPWRS.2003.811181

[19] Larsen, E., Sanchez-Gasca, J., and Chow, J.: 'Concepts for design of facts controllers to damp power swings', IEEE Transactions on Power Systems, May 1995, 10, (2), pp. 948–956, ISSN 0885-8950, doi:10.1109/59.387938

[20] Klein, M., Rogers, G., and Kundur, P.: 'A fundamental study of inter-area oscillations in power systems', IEEE Transactions on Power System, 1991, 6, (3), pp. 914–921, ISSN 08858950

[21] Rogers, G.: Power System Oscillations, Power Electronics and Power Systems, (Kluwer Academic Publishers, 1st edition, 2000), ISBN-10: 0792377125

[22] Pourbeik, P., and Gibbard, M.: 'Damping and synchronizing torques induced on generators by facts stabilizers in multimachine power systems', IEEE Transactions on Power Systems, Nov. 1996, 11, (4), pp. 1920–1925, ISSN 0885-8950, doi:10.1109/59.544664

[23] Gibbard, M., Vowles, D., and Pourbeik, P.: 'Interactions between, and effectiveness of, power system stabilizers and facts device stabilizers in multimachine systems', IEEE Transactions on Power Systems, May 2000, 15, (2), pp. 748–755, ISSN 0885-8950, doi:10.1109/59.867169

[24] Gibbard, M.: 'Co-ordinated design of multimachine power system stabilisers based on damping torque concepts', Generation, Transmission and Distribution, IEE Proceedings C, Jul 1988, 135, (4), pp. 276–284, ISSN 0143-7046

[25] Gibbard, M., and Vowles, D.: 'Reconciliation of methods of compensation for psss in multimachine systems', IEEE Transactions on Power Systems, Feb. 2004, 19, (1), pp. 463–472, ISSN 0885-8950, doi:10.1109/TPWRS.2003.820689

[26] Pourbeik, P. and Gibbard, M. and Vowles, D.; 'Proof of the Equivalence of Residues and Induced Torque Coefficients for Use in the Calculation of Eigenvalue Shifts', IEEE Power Engineering Review, 2002, 22, (1), pp. 58–60, doi:10.1109/MPER.2002.4311662

[27] Sybille, G., and et al.: SimPowerSystems^{TM} 5 - User's Guide, Hydro-Québec and MathWorks, Inc, March 2010
URL `http://www.mathworks.com/access/helpdesk/help/pdf_doc/physmod/powersys/powersys.pdf`

[28] Chaudhuri, N.R., Ray, S., Majumder, R., and Chaudhuri, B.: 'A new approach to continuous latency compensation with adaptive phasor power oscillation damping controller (POD)', IEEE Transactions on Power Systems, May 2010, 25, (2), pp. 939 –946, ISSN 0885-8950, doi:10.1109/TPWRS.2009.2031908

[29] Nielsen, J.N., Akhmatov, V., Thisted, J., Grøndahl, E., Egedal, P., Frydensbjerg, M.N., and Jensen, K.H.: 'Modelling and fault-ride-trough tests of Siemens Wind Power 3.6 MW variable-speed wind turbines', Wind Engineering, December 2007, 31, pp. 441–452(12), doi:doi:10.1260/030952407784079753

[30] Knüppel, T., Nielsen, J.N., Jensen, K.H., Dixon, A., and Østergaard, J.: 'Power Oscillation Damping Capabilities of Wind Power Plant with Full Converter Wind Turbines Considering its Distributed and Modular Characteristics', in Proceedings of IET Renewable Power Generation Conference 2011 (IET-RPG 2011), pp. 1–6, doi:10.1049/cp.2011.0130

[31] Korba, P., Larsson, M., Chaudhuri, B., Pal, B., Majumder, R., Sadikovic, R., and Andersson, G.: 'Towards real-time implementation of adaptive damping controllers for FACTS devices', in Power Engineering Society General Meeting, 2007. IEEE (2007), ISSN 1932-5517, pp. 1 –6, doi:10.1109/PES.2007.385953

[32] Ramos, R., Alberto, L., and Bretas, N.: 'A new methodology for the coordinated design of robust decentralized power system damping controllers', IEEE Transactions onPower Systems, Feb. 2004, 19, (1), pp. 444 – 454, ISSN 0885-8950, doi:10.1109/TPWRS.2003.820690

[33] Burges, K., and Boemer, J.: 'System inertia and wind power – impacts and options for maintaining system robustness', in 9th International Workshop on Large-Scale Integration of Wind Power into Power Systems as well as on Transmission Networks for Offshore Wind Farms (2010), pp. 1–7, Québec City, Québec, Canada

[34] Samuelsson, O.: 'Power system damping – structural aspects of controlling active power', Phd thesis, University of Lund, Sweden, Department of Industrial Electrical Engineering and Automation (IEA), Lund Institute of Technology (LTH), P.O. Box 118, S-221 00 LUND, SWEDEN, 1997, ISBN 91-88934-05-5

A.4 Paper IV

Thyge Knüppel, Jørgen N. Nielsen, Kim H. Jensen, Andrew Dixon, and Jacob Østergaard. Power oscillation damping controller for wind power plant utilizing wind turbine inertia as energy storage. In *2011 IEEE PES General Meeting*, pages 1–8, Detroit, MI, USA, July 2011. IEEE Power & Energy Society. doi: 10.1109/PES.2011.6038908. ISBN: 978-1-4577-1001-8.

Power Oscillation Damping Controller for Wind Power Plant Utilizing Wind Turbine Inertia as Energy Storage

Thyge Knüppel, Jørgen N. Nielsen, Kim H. Jensen, Andrew Dixon, Jacob Østergaard *Senior Member, IEEE*

***Abstract*—For a wind power plant (WPP) the upper limit for active power output is bounded by the instantaneous wind conditions and therefore a WPP must curtail its power output when system services with active power are delivered. Here, a power oscillation damping controller (POD) for WPPs is presented that utilizes the stored kinetic energy in the wind turbine (WT) mechanical system as energy storage from which damping power can be exchanged. This eliminates the need for curtailed active power production. Results are presented using modal analysis and induced torque coefficients (ITC) to depict the torques induced on the synchronous generators from the POD. These are supplemented with nonlinear time domain simulations with and without an auxiliary POD for the WPP. The work is based on a nonlinear, dynamic model of the 3.6 MW Siemens Wind Power wind turbine.**

***Index Terms*—wind turbines, wind power plant, wind power plant controller, power oscillation damping controller (POD), power systems, small-signal stability, induced torques**

I. Introduction

MOST modern wind turbines (WT) connected today are asynchronously connected to the grid, either partially or fully through electronic power converters, and will, as discussed in [1], not themselves cause system oscillations. This point is elaborated in [2] where it is presented that the participation of the full-load converter type WT in power system oscillations is very low. A large scale integration of wind power can, however, indirectly change the modal characteristics of the system by *1)* significantly altering the power flow, cf. [3], and *2)* interacting with the synchronous machines through the transmission network to change the synchronizing and damping torques induced on their shafts. The latter point depends on the power conversion technology and the utilized control; thereby emphasizing the importance of accurate representation of the control for such studies.

Regarding wind power conversion units, several studies have investigated the impact on power system oscillations of wind power plants (WPP) based on primarily the fixed-speed induction generator (FSIG) and the doubly-fed induction generator (DFIG) [4]–[7].

With expanding penetration of wind power it must be expected that power plants based on synchronous generators at some point start being displaced. This is to be expected due to multiple reasons; it is first of all important to keep the power balance in the system, and secondly, it may be economically and energy inefficient to keep a large number of partially loaded synchronous generators on-line. Synchronous machines equipped with power system stabilizers (PSS) are today the most cost-effective method of improving the small-signal stability [8]. Besides synchronous generators equipped with PSSs, also FACTS devices, e.g. SVCs or STATCOMs [9]–[11], and HVDC stations [12], [13] are used to deliver the required damping torque.

Variable-speed WTs interfaced to the grid with voltage source converters offer decoupled control of active and reactive power [14], and these control capabilities are used for active, e.g. [15], [16], and reactive power control, e.g. [16], [17]. In [18]–[21] it has been proposed to actively damp selected system modes using variable speed WTs, and in [22], [23] robust controller tuning is presented for a WPP power oscillation damping controller (POD).

When damping is based on active power modulation the WPP normally has to curtail its active power output, since the amount of active power that can be delivered from a WPP at any given time is subject to the wind conditions. Here, an extension to the work on WPP power oscillation damping capabilities is presented that eliminates this need for curtailed production. To achieve this, a POD is proposed that utilizes the kinetic energy in the WT mechanical system as a storage from which damping power can be exchanged. The advantage of this control is that the WPP can be set to deliver maximum power output, while still being capable of contributing with damping power. Control of the stored rotational energy of the WT mechanical system has recently been proposed for inertial response of converter interfaced WTs [24]–[27].

The POD is implemented into a WPP model that has the dynamic performance of a commercially available WT [28], and the performance of the WPP POD is illustrated with a benchmark power system prone to power system oscillations. The study is conducted under the assumption of constant wind and the impact of the fluctuating wind is hence not considered.

The paper is organized as follows. In section II the concept of utilizing the rotational mechanical system as energy storage

T. Knüppel is with Siemens Wind Power A/S, DK-7330 Brande, Denmark and Centre for Electric Technology, Department of Electrical Engineering, Technical University of Denmark, DK-2800 Lyngby, Denmark (thyge.knuppel@siemens.com)

J. N. Nielsen is with Siemens Wind Power A/S, DK-7330 Brande, Denmark (joergen_nygaard.nielsen@siemens.com)

K. H. Jensen is with Siemens Wind Power A/S, DK-7330 Brande, Denmark (kim_hoej.jensen@siemens.com)

A. Dixon is with National Grid Electricity Transmission plc (National Grid), Warwick CV34 6DA, UK (andrew.dixon@uk.ngrid.com)

J. Østergaard is with Centre for Electric Technology, Department of Electrical Engineering, Technical University of Denmark, DK-2800 Lyngby, Denmark (joe@elektro.dtu.dk)

for active damping power is presented with a lumped mass swing system and the incorporation into a POD is explained. Section III presents the study case, the analyzed WT concept, the case studies performed, and the results from the analysis. Finally, the discussion and conclusion are found in sections IV and V, respectively.

II. Background

A. Wind Turbine Inertia

For rotating machinery there is a coupling between the energy stored in the rotational masses and the speed by which they rotate. This kinetic energy is given from

$$E = \tfrac{1}{2} J \omega_m^2 \tag{1}$$

where J is the moment of inertia and ω_m the rotational speed. In the event that the rotational speed of a synchronous machine drops, a corresponding amount of kinetic energy is released and injected into the network. For a variable-speed WT ω_m is not determined by the system frequency but rather by the control of the WT. To calculate the power, P, delivered due to a change in speed consider the time derivative of (1)

$$\frac{\mathrm{d}E}{\mathrm{d}t} = P = J\omega_m \frac{\mathrm{d}\omega_m}{\mathrm{d}t}. \tag{2}$$

Often the inertia of the rotating system is expressed in terms of the inertia time constant, H, which indicates the time in seconds that the rotating mass can supply rated power

$$H = \frac{J\omega_m^2}{2S}. \tag{3}$$

In (3), S is the rated apparent power of the generator. When calculating the moment of inertia for a WT blade it can be assumed that it has its mass middle point at about $\frac{1}{3}$ of the blade length, and the total moment of inertia for a three bladed rotor is hence [24]

$$J = 3m_b \left(\frac{r}{3}\right)^2 = \tfrac{1}{9} m_r r^2 \tag{4}$$

where m_b is the mass of one blade, m_r the mass of the whole rotor, and r the radius of the rotor. From [24] the approximate relation between rotor mass and diameter, d_r, is given by

$$m_r = 0.486 d_r^{2.6} \tag{5}$$

From (3), (4), and (5) an estimate of the WT inertia constant can be determined from publicly available information.

B. Power Oscillation Damping Controller for Wind Power Plant

Delivery of damping torque from active power modulation is only associated with delivery of active power when the power system is perturbed from its steady state; in steady state no additional active power is delivered due to the damping controller. Clearly, a simple way to achieve this is to operate the WPP at curtailed power production and thereby have a predetermined amount of active power available for the controller. Compared to fossil power stations a specialty with wind power is that the fuel is free and, naturally, the WPP owner wants to deliver the maximum available power in order to maximize his profit. The goal is hence to minimize any lost production caused by the delivery of damping torque.

The oscillatory nature of the response furthermore means that the net energy in the modulated active power will be low, or even negative. In the proposed controller this is utilized by making use of the rotational energy in the mechanical system as storage, from where the damping power can be exchanged. When positive active power is required energy is drawn from the rotational system hence decreasing its rotational speed, while the rotational speed of the mechanical system is increased in the half cycle where negative damping power is delivered.

To illustrate the impact on the rotational speed from the POD, consider the lumped mass, per unit, swing equation

$$\Delta\dot{\delta} = \omega_0 \Delta\omega_m \tag{6a}$$

$$\Delta\dot{\omega}_m = \tfrac{1}{2H}(T_m - T_e - \widehat{K}_d \Delta\omega_m) \tag{6b}$$

$$= \tfrac{1}{2H}(T_m - K_s\Delta\delta - K_d\Delta\omega_m) \tag{6c}$$

where T_m is the mechanical torque, T_e the electrical torque, δ the generator rotor angle, ω the generator speed, and $\widehat{K}_d$ the inherent mechanical damping of the generator. For simplicity assume that (6b) is initially in steady state, $\Delta\dot{\omega}_m = 0$, that mechanical damping is neglected, and that the only perturbation to the energy balance is the additional active power, P_d, requested by the POD. In Fig. 1 the time domain solution of (6b) is shown for four different inertia sizes for a 0.10 p.u. active power damping contribution. In Fig. 1 a damping ratio of $\zeta = 0.10$ has been assumed for the oscillation.

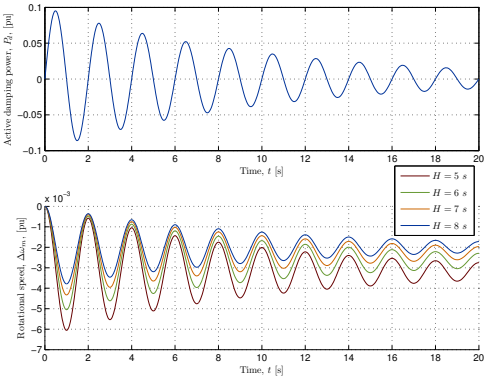

Fig. 1. Induced mechanical oscillations when P_d active power is exchanged with the rotational system.

For a full-load converter interfaced WPP the behavior in Fig. 1 may be achieved by controlling the active power reference of the grid side converter. The overall power balance and control may be explained from Fig. 2. When the grid side converter increases its active power output, the machine side converter likewise increases the power injected into the DC link to maintain the DC voltage. The additional power injected to the DC link is drawn from the generator thereby increasing the electrical torque, which creates a negative torque on the mechanical system that according to (6b) decelerates the rotor.

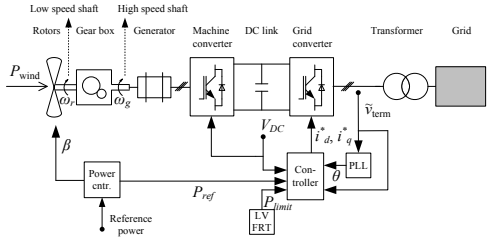

Fig. 2. Schematic layout of a full-load converter interfaced WT.

The purpose of the POD loop is to shape the modulated active power such that the control creates additional damping to one or more system modes. The designed POD has the general structure

$$\frac{\Delta P_{\text{stab}}}{\Delta u} = \underbrace{K}_{Gain} \underbrace{\frac{1}{sT_{lp}+1}}_{\text{Low pass}} \underbrace{\frac{sT_w}{sT_w+1}}_{\text{Wash out}} \underbrace{\frac{1+c_1 s+c_2 s^2\ldots}{1+d_1 s+d_2 s^2\ldots}}_{\text{Phase compensation}} \tag{7}$$

where ΔP_{stab} is the change in active power set point demanded by the POD, Δu is the POD input signal, and the phase compensation block is designed to add damping to selected modes as e.g. shown in section III-B.

Although the net energy in the damping power is low, the damping controller imposes an oscillating power output on the WT where the permissible magnitude of the associated power gradients is subject to the capabilities of the WT mechanical system. The maximum rate of change for the active power is a function of both the frequency of oscillation and the amplitude of the modulated active power. In Fig. 3 the maximum rate of change is plotted as a function of the damping contribution for a range of frequencies for a sinusoidal stabilizing signal.

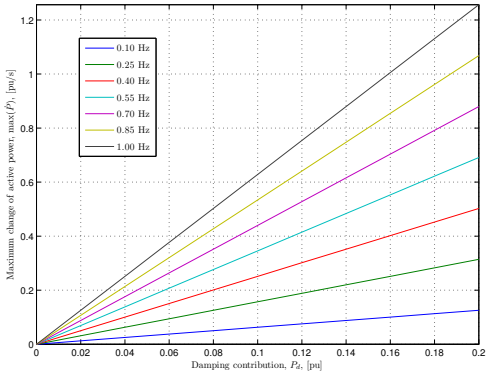

Fig. 3. Maximum rate of change for the active damping power, P_d, as a function of damping contribution, P_d, and frequency of oscillation, ω.

C. Power System Oscillations for Non-Synchronous Generation

Power system oscillations are inherent in interconnected power systems based on synchronous generators [29]. The rotational system of synchronous generators are directly coupled to the network and in a multimachine system this coupling does that all generators spin at synchronous speed when in steady state. For a stable system, i.e. with positive synchronizing and damping torques, whenever the generators are perturbed from their equilibrium, forces act to restore the steady state operating point with all generators running at synchronous speed.

For the full-load converter interfaced WPP depicted in Fig. 2, however, the only connection between the network and the rotational system is through the controller with the machine side converter controlling the rotational speed of the generator, ω_g. As a result the terms synchronizing and damping torques of the WPP rotational system has little meaning in the conventional sense of (6c). Instead, the concept of induced torque coefficients can be used as explained in section II-E.

D. Model Setup

The analysis is based on the non-linear set of system equations, dynamic relations as well as network equations, which are linearized in an operating point to obtain a linear system of differential and algebraic equations (DAE) . When the algebraic relations are eliminated and the system described purely by ordinary differential equations (ODE), the system is in the classical state space form

$$\begin{aligned} \Delta\dot{x} &= A\Delta x + B\Delta u \\ \Delta y &= C\Delta x + D\Delta u \end{aligned} \tag{8}$$

where $A^{n\times n}$ is the system state matrix, $B^{n\times r}$ the input matrix, $C^{m\times n}$ the output matrix, $D^{m\times r}$ the feed forward matrix, $\Delta x^{n\times 1}$ the state vector, $\Delta u^{r\times 1}$ the input vector, and $\Delta y^{m\times 1}$ the output vector.

E. Induced Torque Coefficient

Eigenvalue analysis is commonly used to analyze systems for small-signal stability and provides valuable information about the inherent stability properties of the system [8], [30]. A challenge with the method is to identify the root cause of a an observed shift in the stability properties. In [31], [32] induced torque coefficients (ITC) are introduced as a mean to analyze the damping impact from FACTS stabilizers in multimachine systems. The ITC coefficients are introduced based on the PVr transfer function, which is the transfer function from reference voltage to active power output computed with all shaft dynamics disabled [33], [34]. The rationale behind ITC is that although a FACTS stabilizer, or in this case a WPP, does not have a mass, which is synchronously connected to the network, there is still a path from i_{dj}, i_{qj} of machine j through the network to the electromagnetic torque of machine i. From machine j it is thus possible to induce an electromagnetic torque on machine i and that torque may be decomposed into torques in phase with $\Delta\delta_i$ and $\Delta\omega_i$.

For the ith machine the damping torque induced by the jth stabilizing unit, D_{ij}, is thus the component of torque in phase with ω_i, where it is utilized that the per unit air-gap power

equals the per unit air-gap torque [30]. The transfer function is then given as

$$D_{ij} = \frac{\Delta T_{e_{ij}}}{\Delta \omega_i} = \frac{\Delta P_{e_{ij}}}{\Delta \omega_i} \tag{9a}$$

$$= \underbrace{\frac{\Delta P_{e_{ij}}}{\Delta U_j}}_{H_{\text{PVr}}} \underbrace{\frac{\Delta U_j}{\Delta y_j}}_{j\text{th PSS}} \frac{\Delta y_j}{\Delta \omega_i} \tag{9b}$$

where ΔU is the input signal to the machine from the POD and Δy is the signal from which the oscillation is observed. In (9b) the last expression relates the speed deviation on machine i to the stabilizing input signal of the jth stabilizing unit, i.e. PSS, FACTS device, etc. If only the hth mode is excited, then the state vector is described as $\Delta x = \phi_h e^{\lambda_h t}$ [30]. Any output Δy_j is then given by $C_{y_j}\phi_h$, where C_{y_j} is the row of the output matrix in (8) that corresponds to y_j. Equation (9b) is then given as

$$D_{ij}^h = \frac{\Delta P_{e_{ij}}}{\Delta U_j}(\lambda_h)\frac{\Delta U_j}{\Delta y_j}(\lambda_h)\frac{C_{y_j}\phi_h}{C_{\omega_i}\phi_h} \tag{10a}$$

$$= \chi_{ij}^h \frac{\Delta U_j}{\Delta y_j}(\lambda_h). \tag{10b}$$

where χ_{ij}^h is a complex number, which is independent of the applied control and which represents the impact of stabilizer j on the ITC of the ith synchronous generator. From the ITC for the hth mode, D^h, a first order approximation of the mode shift of the h mode is given as [31]

$$\Delta\lambda_{ij}^h = -\frac{p_{ih}}{2H_i} D_{ij}^h \tag{11a}$$

$$= -\frac{p_{ih}}{2H_i}\chi_{ij}^h \frac{\Delta U_j}{\Delta y_j}(\lambda_h) \tag{11b}$$

where H_i is the inertia constant of the ith synchronous generator and p_{ih} is the participation factor of the speed state of the ith synchronous generator. Let

$$\xi_{ij}^h = -\frac{p_{ih}}{2H_i}\chi_{ij}^h \tag{12}$$

and denote $\xi_j^h = \sum_{\forall i} \xi_{ij}^h$. It can then be proved [35] that ξ_j^h is equivalent to the residue between output Δy_j and input ΔU_j, and examining the elements of ξ_{ij}^h thus reveals the contribution of each synchronous generator to the residue of the hth system mode.

Summing over all i in (11) then gives the predicted mode shift when the controller $\frac{\Delta U_j}{\Delta y_j}$ is inserted into the loop

$$\Delta\lambda_j^h = \frac{\Delta U_j}{\Delta y_j}(\lambda_h)\sum_{\forall i}\xi_{ij}^h. \tag{13}$$

Using (13) it is possible to predict the mode shift of the hth eigenvalue due to the presence of the jth controller, $\frac{\Delta U_j}{\Delta y_j}$. Similarly, summing over all j gives the total mode shift due to the stabilizing action of the j stabilizing units. The prediction of the hth closed-loop eigenvalue, $\hat{\lambda}_{cl}^h$, is then given from the open-loop eigenvalue, λ_{ol}^h, and the predicted mode shift calculated in (13)

$$\hat{\lambda}_{cl}^h = \lambda_{ol}^h + \Delta\lambda_j^h \tag{14}$$

III. Four Generator System

To present the methodology in section II-B a benchmark system is considered which includes the dynamics of the generators, exciters, PSSs, governors, WPP, as well as voltage dependency of the loads. The network shown in Fig. 4 is based on the four machine system in [36], which is a modified version of the two area system originally defined in [29]. Although very simplified compared to the complexity of actual power systems, the system in Fig. 4 possesses fundamental oscillatory properties, which makes it suitable for analysis of the WPP POD control functionality.

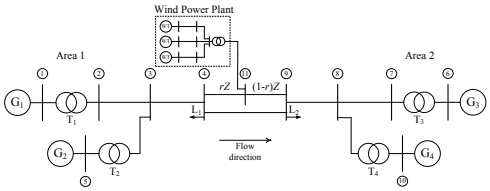

Fig. 4. Single-line diagram of the four generator, two area case network.

At bus 11 a WPP is connected, which consists of three radial feeders connected through a common park transformer. The connection point at bus 11 is hereafter termed "point of common connection" (PCC). Each feeder consists of a collector grid, a WT transformer, and an aggregated WT. Collector grid parameters and the distribution of the WTs within the park are given in TABLE III.

There is an active power flow of approximately 450 MW flowing from area 1 to area 2. A summary of load and generation is given in TABLE II.

A. Wind Turbine Technology

The WT concept for this study is a variable-speed, pitch controlled, full-load converter interfaced WT as illustrated in Fig. 2. The WT is represented with a reduced order model suitable for transient and dynamic power system studies. The model represents a 3.6 MW Siemens Wind Power WT [28] and includes:

- *Aerodynamic model*. A variable wind speed aerodynamic model which includes power coefficient with pitch angle and tip-speed ratio.
- *Shaft model*. Implements a two-mass model of rotor, gearbox, and generator.
- *Converter system*. The WT converter system comprises machine and grid side converter, DC-link, and a generic reduced order control scheme.
- *DC link*. Implements the link, including the DC capacitance, between the machine and the network side converter.
- *Fault ride through*. Monitors for system faults and shapes the current injection into the grid upon detection.

In the study, three aggregated WT models are used and the WTs are operated in voltage control mode, regulating for 1.02 p.u. at the WT terminal to support the voltage at bus 11.

B. Phase Compensation for Damping Controller

As shown in [37] the impact of a damping controller and the required phase compensation is highly dependent on the in-feed location. While the individual WTs in a WPP for stability studies are often represented with a single, aggregated WT, the effectiveness of a WPP damping controller depends on the ability of each WT to deliver a positive contribution to the damping. For the layout in Fig. 4 this corresponds to having individual PODs versus having one POD on park level. The magnitude and angle of the residues for the inter-area mode are shown in Fig. 5 for the speed difference of synchronous generator G_1 and G_3, $\Delta u_{d\omega}$, and PCC bus frequency, Δu_f. To evaluate the impact of WPP in-feed location, the residues are computed for values of r between 0 to 1, cf. Fig. 4.

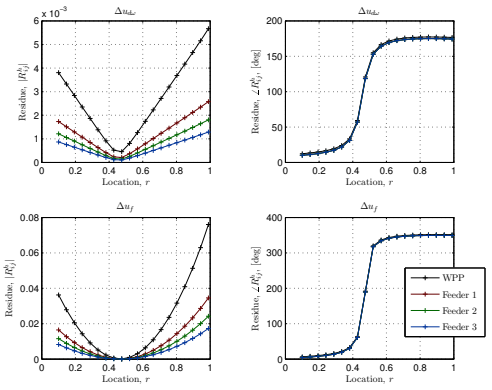

Fig. 5. Residues from generator speed difference, $\Delta u_{d\omega}$, and PCC bus frequency, Δu_f, to WPP active power set-point.

The speed difference between synchronous generators in each area is the reference signal for observing the inter-area mode. In practice it is normally desirable to have a locally available measurement with good observability of the mode. The bus frequency is an example of such local signal [8]. From Fig. 5 it is noted that both signals are most effective when the WPP is located close to either area, and both phase characteristics experience a phase jump around the center point of the oscillation.

A procedure for tuning FACTS stabilizers based on residues is proposed in [31] where the phase compensation in the POD loop is determined from the complement to the residue angle. From Fig. 5 it is seen that similar phase characteristics are obtained when one central POD is considered compared to when each feeder has its own POD.

C. Modal Analysis

The induced torques on G_{1-4} from the POD as evaluated from (10a) are shown in TABLE I for the WPP connected at $r = 0.1$. A POD with either control input adds damping to the inter-area mode and has limited effect on the local-area mode in area 2. The POD with PCC frequency as input also adds damping to the local-area mode in area 1 while the damping is decreased with the $\Delta u_{d\omega}$ input.

The shift in the inter-area and the local-area modes due to the POD is shown in Fig. 6 for increasing POD gains. The linear prediction of the eigenvalue shift in (14) is compared to the actual eigenvalues obtained with the closed loop system. For the POD with PCC frequency input $K \in [0.5;\ 3]$ while for input $\Delta u_{d\omega}$ $K \in [5;\ 30]$.

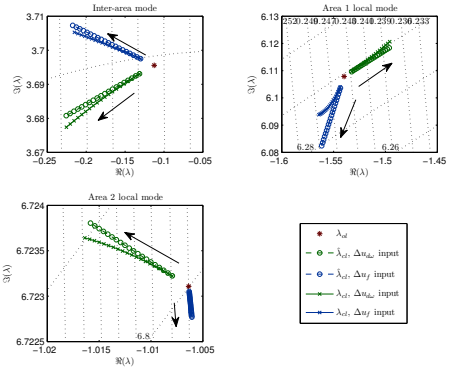

Fig. 6. Comparison of predicted and actual shift in inter-area and local-area modes as a function of POD gain.

D. Simulation Results

The time domain responses for a 1 second, 5 % step to the exciter voltage reference of G_3 are presented in section III-D1 and III-D2 for high and medium wind conditions, respectively. Here, high wind conditions are defined as 12 $\frac{\text{m}}{\text{s}}$ with the WPP supplying rated power output, while medium wind conditions are defined as 10 $\frac{\text{m}}{\text{s}}$ with the WPP delivering around 0.69 p.u. In medium wind conditions the reduction in WPP active power is balanced by the generators in area 1 to keep the same level of power flow between the areas.

Results are presented for the WPP having *1)* no POD, *2)* a POD driven by the speed difference of generator G_1 and G_3, $\Delta u_{d\omega}$, and *3)* a POD using the PCC bus frequency, Δu_f, as input. For these simulations the WPP is connected at $r = 0.1$, cf. Fig. 4, and the POD gain for the $\Delta u_{d\omega}$ input is $K = 20$, while the gain for the Δu_f input is $K = 1.5$.

1) High Wind Conditions: The impact of the voltage reference perturbation is identified from the generator rotor speeds in Fig. 7. Initially the area 2 local-area mode is excited while after around 3 seconds the inter-area mode starts to dominate. After around 1 second there is a common dip in generator speed. When no POD is installed at the WPP it is seen from Fig. 8 that the WPP delivers a constant active power output where each feeders delivers rated power.

Based on the findings in section III-B a central POD is employed for both of the shown configurations. Both controllers deliver additional damping to the rotor speed oscillations plotted in Fig. 7. The POD using frequency as input causes a faster stabilization to nominal speed since it detects the common dip in speed and injects active power as countermeasure. After 2-3 seconds the response of the two PODs have similar waveforms.

TABLE I

INDUCED TORQUES ON G_{1-4} FROM WPP POD AT THE MODAL FREQUENCIES OF THE INTER-AREA MODE, D^1, LOCAL-AREA MODE FOR AREA 1, D^2, AND AREA 2, D^3. RESULTS ARE SHOWN FOR POD USING BOTH SPEED DIFFERENCE, $\Delta u_{d\omega}$, AND PCC FREQUENCY AS INPUT, Δu_f.

	$\Delta u_{d\omega}$ input			Δu_f input		
	D^1	D^2	D^3	D^1	D^2	D^3
G_1	$0.07\angle\ 177°$	$0.08\angle\ 165°$	$0.004\angle -65°$	$0.05\angle\ 163°$	$0.04\angle\ \ 21°$	$10^{-4}\angle\ \ 75°$
G_2	$0.07\angle\ 179°$	$0.10\angle -10°$	$0.008\angle\ \ 35°$	$0.05\angle\ 165°$	$0.06\angle -154°$	$3\cdot 10^{-4}\angle\ 171°$
G_3	$0.03\angle -12°$	$0.003\angle\ 147°$	$0.03\angle -27°$	$0.02\angle -26°$	$0.002\angle\ \ 4°$	$0.001\angle\ 110°$
G_4	$0.04\angle -13°$	$0.004\angle\ \ 73°$	$0.04\angle\ 162°$	$0.03\angle -26°$	$0.002\angle\ -71°$	$0.002\angle -61°$

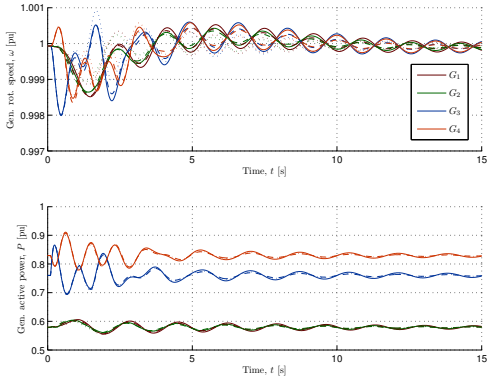

Fig. 7. Generator speed and active power output following a 1 second, 5 % step on the voltage reference of G_3 in high wind conditions. Solid: no WPP POD, dashed: $\Delta u_{d\omega}$ input, dotted: Δu_f input.

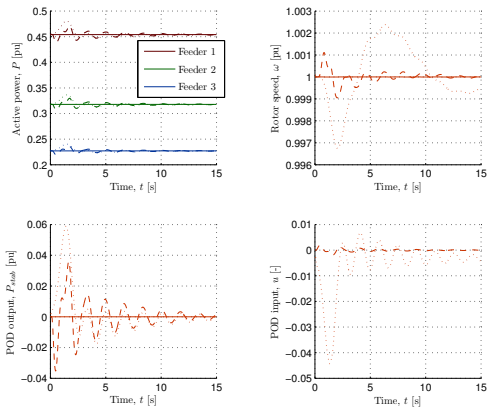

Fig. 8. WPP active power output, rotor speed, and POD input and output following a 1 second, 5 % step on the voltage reference of G_3 in high wind conditions. Solid: no WPP POD, dashed: $\Delta u_{d\omega}$ input, dotted: Δu_f input.

2) Medium Wind Conditions: The time domain simulations for medium wind conditions are given in Fig. 9 for generator speed and active power responses and Fig. 10 for WPP quantities. The results are similar to those for high wind conditions.

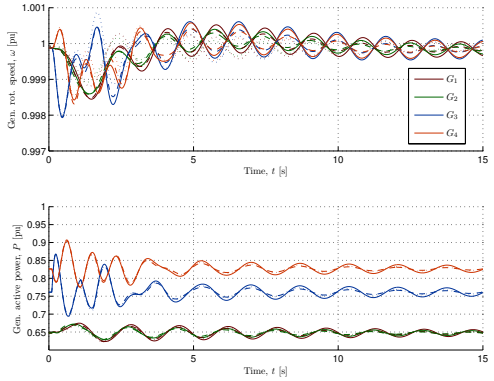

Fig. 9. Generator speed and active power output following a 1 second, 5 % step on the voltage reference of G_3 in medium wind conditions. Solid: no WPP POD, dashed: $\Delta u_{d\omega}$ input, dotted: Δu_f input.

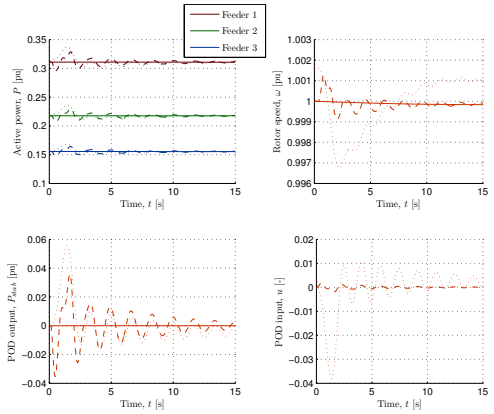

Fig. 10. WPP active power output, rotor speed, and POD input and output following a 1 second, 5 % step on the voltage reference of G_3 in medium wind conditions. Solid: no WPP POD, dashed: $\Delta u_{d\omega}$ input, dotted: Δu_f input.

IV. DISCUSSION

A trend in wind power is that more functionalities and system services are expected delivered from the WPPs. For system services with active power this posses the challenge that the power output of a WPP is subject to the instantaneous wind conditions, i.e. the active power cannot readily

be increased unless the WPP is curtailing its output. As with other power production units based on non-storable energy sources, the incentive of a WPP owner is to produce maximum active power. The ability of converter interfaced power units to provide small-signal damping has been shown by e.g. [13], [37] and for WPP application by e.g. [18]. Here this work is extended upon such that active damping power can be delivered even though the WPP is operated for maximum production. This is achieved by utilizing the energy in the WT mechanical system as storage from which damping power is exchanged.

When no POD is installed on the WPP, a constant active power is delivered during the oscillation and the rotational speed of the WT rotors remain constant, cf. Fig. 8 and 10. Simulation results are presented for the POD in two different wind scenarios, namely high and medium wind conditions. In high wind conditions the WT is pitched to reduce the captured energy, and when oscillations are induced on the rotor the control of the pitch helps smooth the rotor oscillations. However, when the WPP is operated in medium wind conditions the pitch angle is locked for maximum power extraction and the smoothing capability of the pitch control is not available. The consequence of this is noticed when the rotor speeds of Fig. 8 and 10 are compared. In medium wind conditions for the PCC frequency driven POD, the main rotor oscillation is slower and has a superimposed oscillation with the inter-area mode frequency.

As shown in Fig. 5 the effect of the POD is highly dependent on the location of the WPP. For plant locations where an active power POD proves ineffective it is in [37] proposed to use a combination of active and reactive power to increase the damping performance. The controller described in section II-B could be extended with a parallel POD for reactive power control.

Wind fluctuations are, as previously mentioned, not considered in the study and further analysis must reveal the impact of fluctuating wind conditions on the damping performance. Means of impact include *1)* control interactions between the POD and other WT controls, and *2)* wind induced changes to the operating condition.

V. Conclusion

A power oscillation damping control (POD) is proposed that utilizes the kinetic energy in the wind turbine (WT) mechanical system as a storage from which active damping power is exchanged. The wind power plant (WPP) can thus deliver active damping power while delivering maximum available active power.

In full-load converter interfaced WTs the rotational speed of the rotor is controlled by the machine side converter to optimize the power extraction. Having control of the rotational speed means that the release of kinetic energy can be controlled, which is here used to provide active damping power.

Damping capabilities and the effect of the POD on the remaining synchronous generators are analyzed with modal analysis and induced torque coefficients (ITC). The POD is implemented on a WT model, which has the dynamic performance of a commercially available WT. The ability to exchange damping power with the WT rotational system is demonstrated with time domain simulations of both high and medium wind speed conditions.

Appendix

TABLE II
Summary of load and generation for the case network in Fig. 4.

Generation			Load (constant Z)			
	S_{base} [MVA]	P [MW]		P [MW]	Q_L [Mvar]	Q_C [Mvar]
G_1	900	581	L_1	967	100	-387
G_2	900	581	L_2	1767	100	-537
G_3	900	683				
G_4	900	700				

TABLE III
Characteristics for WPP collector network.

Feeder	# WTs	P_{base} [MW]	R [Ω]	L [mH]	C [μF]
1	50	180	0.09	0.22	10.2
2	35	126	0.11	0.29	13.3
3	25	90	0.07	0.18	8.2

References

[1] C. Samarasinghe and D. Vowles, "Wind generation investigation project - effect of wind generation on small signal stability," TRANSPOWER New Zealand, The National Grid, Tech. Rep. Investigation 8, March 2008.

[2] T. Knüppel, J. N. Nielsen, K. H. Jensen, A. Dixon, and J. Østergaard, "Small-signal stability of wind power system with full-load converter interfaced wind turbines," *Submitted for publication to IET Renewable Power Generation*.

[3] D. Wilson, J. Bialek, and Z. Lubosny, "Banishing blackouts [power system oscillations stability]," *Power Engineer*, vol. 20, no. 2, pp. 38 –41, april-may 2006.

[4] O. Anaya-Lara, F. Hughes, N. Jenkins, and G. Strbac, "Influence of windfarms on power system dynamic and transient stability," *Wind Engineering*, vol. 30, no. 2, pp. 107–27, 2006.

[5] J. Slootweg and W. Kling, "The impact of large scale wind power generation on power system oscillations," *Electric Power Systems Research*, vol. 67, no. 1, pp. 9 – 20, 2003.

[6] E. Hagstrom, I. Norheim, and K. Uhlen, "Large-scale wind power integration in norway and impact on damping in the nordic grid," *WIND ENERGY*, vol. 8, no. 3, pp. 375–384, JUL-SEP 2005.

[7] G. Tsourakis, B. Nomikos, and C. Vournas, "Effect of wind parks with doubly fed asynchronous generators on small-signal stability," *Electric Power Systems Research*, vol. 79, no. 1, pp. 190 – 200, 2009.

[8] G. Rogers, *Power System Oscillations*, 1st ed., ser. Power Electronics and Power Systems. Kluwer Academic Publishers, 2000, ISBN-10: 0792377125.

[9] E. Lerch, D. Povh, and L. Xu, "Advanced svc control for damping power system oscillations," *Power Systems, IEEE Transactions on*, vol. 6, no. 2, pp. 524 –535, may 1991.

[10] N. Mithulananthan, C. Canizares, J. Reeve, and G. Rogers, "Comparison of pss, svc, and statcom controllers for damping power system oscillations," *Power Systems, IEEE Transactions on*, vol. 18, no. 2, pp. 786 – 792, may 2003.

[11] E.-Z. Zhou, "Application of static var compensators to increase power system damping," *Power Systems, IEEE Transactions on*, vol. 8, no. 2, pp. 655 –661, may 1993.

[12] G. Liu, Z. Xu, Y. Huang, and W. Pan, "Analysis of inter-area oscillations in the south china interconnected power system," *Electric Power Systems Research*, vol. 70, no. 1, pp. 38 – 45, 2004.

[13] T. Smed and G. Andersson, "Utilizing hvdc to damp power oscillations," *Power Delivery, IEEE Transactions on*, vol. 8, no. 2, pp. 620 –627, apr 1993.

[14] V. Akhmatov, "Variable-speed wind turbines with doubly-fed induction generators, part I: Modelling in dynamic simulation tools," *Wind Engineering*, vol. 26, no. 2, p. 85, 2002.

[15] R. de Almeida and J. Lopes, "Participation of doubly fed induction wind generators in system frequency regulation," *Power Systems, IEEE Transactions on*, vol. 22, no. 3, pp. 944–950, Aug. 2007.

[16] T. Knüppel, J. Thisted, B. Andresen, M. N. Frydensbjerg, V. Akhmatov, and J. N. Nielsen, "Grid support capabilities of full-load converter interfaced wind turbines," in *POWER-GEN India & Central Asia*. PennWell Corporation, April 2010.

[17] V. Akhmatov, "Variable-speed wind turbines with doubly-fed induction generators part II: Power system stability," *Wind Engineering*, vol. 26, no. 3, p. 171, 2002.

[18] F. Hughes, O. Anaya-Lara, N. Jenkins, and G. Strbac, "A power system stabilizer for dfig-based wind generation," *Power System, IEEE Transactions on*, vol. 21, no. 2, pp. 763–772, 2006.

[19] K. Elkington, "Modelling and control of doubly fed induction generators in power systems: Towards understanding the impact of large wind parks on power system stability," PhD Thesis, KTH, Electric Power Systems, SE-100 44, Stockholm, Sweden, April 2009, ISBN: 978-91-7415-264-7.

[20] Z. Miao, L. Fan, D. Osborn, and S. Yuvarajan, "Control of dfig based wind generation to improve inter-area oscillation damping," *Power and Energy Society General Meeting - Conversion and Delivery of Electrical Energy in the 21st Century, 2008 IEEE*, pp. 1–7, July 2008.

[21] C. Martinez, G. Joos, and B. Ooi, "Power system stabilizers in variable speed wind farms," in *Power Energy Society General Meeting, 2009. PES '09. IEEE*, July 2009, pp. 1 –7.

[22] N. Kshatriya, U. D. Annakkage, F. M. Hughes, and A. M. Gole, "Optimized partial eigenstructure assignment-based design of a combined pss and active damping controller for a dfig," *Power Systems, IEEE Transactions on*, vol. 25, no. 2, pp. 866 –876, may 2010.

[23] P. Ledesma and C. Gallardo, "Contribution of variable-speed wind farms to damping of power system oscillations," *2007 IEEE Lausanne Power Tech*, pp. 190–194, 2007.

[24] J. Morren, J. Pierik, and S. W. de Haan, "Inertial response of variable speed wind turbines," *Electric Power Systems Research*, vol. 76, no. 11, pp. 980–987, 2006.

[25] P.-K. Keung, P. Li, H. Banakar, and B. T. Ooi, "Kinetic energy of wind-turbine generators for system frequency support," *Power Systems, IEEE Transactions on*, vol. 24, no. 1, pp. 279–287, Feb. 2009.

[26] J. M. Mauricio, A. Marano, A. Gomez-Exposito, and J. L. Martinez Ramos, "Frequency regulation contribution through variable-speed wind energy conversion systems," *Power Systems, IEEE Transactions on*, vol. 24, no. 1, pp. 173–180, Feb. 2009.

[27] J. Ekanayake and N. Jenkins, "Comparison of the response of doubly fed and fixed-speed induction generator wind turbines to changes in network frequency," *Energy Conversion, IEEE Transactions on*, vol. 19, no. 4, pp. 800–802, 2004.

[28] J. N. Nielsen, V. Akhmatov, J. Thisted, E. Grøndahl, P. Egedal, M. N. Frydensbjerg, and K. H. Jensen, "Modelling and fault-ride-trough tests of siemens wind power 3.6 mw variable-speed wind turbines," *Wind Engineering*, vol. 31, pp. 441–452(12), December 2007.

[29] M. Klein, G. Rogers, and P. Kundur, "A fundamental study of inter-area oscillations in power systems," *Power System, IEEE Transactions on*, vol. 6, no. 3, pp. 914–921, 1991.

[30] P. S. Kundur, *Power System Stability and Control*, ser. The EPRI Power System Engineering Series. McGraw-Hill, Inc., 1994, ISBN: 0-07-035958-X.

[31] P. Pourbeik and M. Gibbard, "Damping and synchronizing torques induced on generators by facts stabilizers in multimachine power systems," *Power Systems, IEEE Transactions on*, vol. 11, no. 4, pp. 1920–1925, Nov 1996.

[32] M. Gibbard, D. Vowles, and P. Pourbeik, "Interactions between, and effectiveness of, power system stabilizers and facts device stabilizers in multimachine systems," *Power Systems, IEEE Transactions on*, vol. 15, no. 2, pp. 748–755, May 2000.

[33] M. Gibbard, "Co-ordinated design of multimachine power system stabilisers based on damping torque concepts," *Generation, Transmission and Distribution, IEE Proceedings C*, vol. 135, no. 4, pp. 276–284, Jul 1988.

[34] M. Gibbard and D. Vowles, "Reconciliation of methods of compensation for psss in multimachine systems," *Power Systems, IEEE Transactions on*, vol. 19, no. 1, pp. 463–472, Feb. 2004.

[35] P. Pourbeik, M. Gibbard, and D. Vowles, "Proof of the equivalence of residues and induced torque coefficients for use in the calculation of eigenvalue shifts," *Power Engineering Review, IEEE*, vol. 22, no. 1, pp. 58 –60, jan. 2002.

[36] G. Sybille and et al., *SimPowerSystems™ 5 - User's Guide*, Hydro-Québec and MathWorks, Inc, March 2010.

[37] S. Y. Ruan, G. J. Li, B. T. Ooi, and Y. Z. Sun, "Power system damping from real and reactive power modulations of voltage-source-converter station," *IET GENERATION TRANSMISSION & DISTRIBUTION*, vol. 2, no. 3, pp. 311–320, MAY 2008.

Thyge Knüppel received his M.Sc.E.E. degree from the Technical University of Denmark (DTU) in the spring of 2008 where he specialized in power systems and control theory. Currently, he is employed as research engineer at Siemens Wind Power A/S and is pursuing a PhD degree from DTU.

Jørgen N. Nielsen holds M.Sc. (1996) and Ph.D. (2000) degrees from the Technical University of Denmark, Kgs. Lyngby, Denmark. He has a broad and comprehensive knowledge and experience on power system planning, network investigations and power system simulations. Jørgen N. Nielsen has performed and been responsible for a number of network investigations and studies issued the integration of wind power in the power system and been deeply involved into the development of numerical PSS/E simulation models of the fixed- and variable-speed wind turbines.

Kim H. Jensen holds M.Sc. (1999) and Ph.D. (2003) degrees from the Technical University of Denmark, Kgs. Lyngby, Denmark. He has been working in a transmission company (NESA), consultant company (Elsam Engineering) and now a wind turbine company (Siemens Wind power). In these companies he has worked with transmission system planning, network designs, wind turbine modelling, grid codes studies and harmonic analysis and stability studies. He has also worked as technical specialist on an number wind farm integration projects.

Andrew Dixon holds B.Sc. and Ph.D. degrees in Applied Mathematics (1984. 1988) from the University of St Andrews, Scotland and an M.Sc. in Electric Power Systems (2005) from the University of Bath, England. Dr. Dixon has worked for 19 years for the National Grid Company, UK, consisting of: Research & Development (security-constrained optimization of reactive compensation) - 2 years; System Development & Grid Code - 6 years; Operational Planning - 4 years; Asset Management - 2 years; System Technical Performance (dynamics, including transient stability, small-signal stability & sub-synchronous resonance) - 5 years.

Jacob Østergaard is professor in Electric Technology, Head of Centre for Electric Technology (CET) and Head of Section for Electric Power Engineering at the Department of Electrical Engineering, DTU. From 1995 to 2005 he worked as research engineer and area responsible at Research Institute for Danish Electric Utilities (DEFU). Current activities include research within electricity production, transmission, distribution and demand. Prof. Østergaard is presently involved in activities related to an intelligent power system with focus of new electricity and information architectures, system integration of distributed generation and increased flexibility in the power system by use of demand side participation. Prof. Østergaard is project leader of more than 10 research projects. and serves in several professional organizations including the EU SmartGrids advisory council.

A.5 Paper V

Thyge Knüppel, Jørgen N. Nielsen, Kim H. Jensen, Andrew Dixon, and Jacob Østergaard. Power oscillation damping capabilities of wind power plant with full converter wind turbines considering its distributed and modular characteristics. *Accepted for publication in IET Renewable Power Generation Special Issue*, 2012.

Power Oscillation Damping Capabilities of Wind Power Plant with Full Converter Wind Turbines Considering its Distributed and Modular Characteristics

Thyge Knüppel*, Jørgen N. Nielsen†, Kim H. Jensen‡
Andrew Dixon§, Jacob Østergaard¶

December 18, 2012

Abstract

Wind power plants (WPP) are for power system stability studies often represented with aggregated models where several wind turbines (WT) are aggregated into a single up-scaled model. The advantage is a reduction in the model complexity and the computational time, and for a number of study types the accuracy of the results has been found acceptable. A large WPP is, however, both modular and distributed over a large geographical area, and feasibility of aggregating the WTs, thus, have to be reassessed when new applications are introduced for WPPs. Here, the power oscillation damping capabilities are investigated for a WPP, which includes the full layout of the collector grid and where the WTs are represented individually. With this approach, the influence of the WT control in terms of impact on oscillatory modes is assessed for the WTs individually. The initial results encourage that park level control is possible. Time domain simulations support that each WT contribute to a common WPP response. Park level active and reactive power based power oscillation damping controllers (POD) are designed and the positive damping contribution is demonstrated. Keeping the POD designs unchanged, the impact of WPP aggregation is investigated and it is shown that the level of WPP aggregation only has limited impact on the resulting modal damping. The study is based on a nonlinear, dynamic model of the 3.6 MW Siemens Wind Power WT.

*T. Knüppel is with Siemens Wind Power A/S, DK-7330 Brande, Denmark and Center for Electric Power and Energy, Department of Electrical Engineering, Technical University of Denmark, DK-2800 Lyngby, Denmark (thyge.knuppel@siemens.com)

†J. N. Nielsen is with Siemens Wind Power A/S, DK-7330 Brande, Denmark (joergen_nygaard.nielsen@siemens.com)

‡K. H. Jensen is with Siemens Wind Power A/S, DK-7330 Brande, Denmark (kim_hoej.jensen@siemens.com)

§A. Dixon is with National Grid Electricity Transmission plc (National Grid), Warwick CV34 6DA, UK (andrew.dixon@uk.ngrid.com)

¶J. Østergaard is with Center for Electric Power and Energy, Department of Electrical Engineering, Technical University of Denmark, DK-2800 Lyngby, Denmark (joe@elektro.dtu.dk)

Keywords: Wind power plant, wind turbine, power oscillation damping controller, eigenvalue analysis, equivalencing

1 Introduction

It has recently been proposed to equip wind power plants (WPP) based on variable speed wind turbines (WT) with a power oscillation damping controller (POD) to actively damp power oscillations [1–7]. The controllability of the WPPs does that PODs can be designed based on modulation of both active power (ΔP POD) and reactive power (ΔQ POD) to achieve a positive damping contribution [2,6]. Active power modulation is only feasible in practice provided that the frequency of the modulation does not excite oscillations at mechanical resonance frequencies of the WT, which for the drive train mode is studied by Fan *et al.* [2]. This constraint is WT dependent and may limit the range of frequencies where a particular WT can participate with oscillation damping.

For HVDC stations and FACTS devices the ability to contribute to the damping of power oscillations has been demonstrated for, respectively, active and reactive power modulation [8]. While the controllability of a WPP may be compared to that of other converter interfaced units, there are some distinct differences that must be considered when the power oscillation damping capabilities of a WPP are assessed. A WPP consists of a number of individual WTs that can be controlled to appear as a single unit when viewed from the point of common connection (PCC), hence, a WPP is modular with units that can be distributed over a large geographical area. In [9] the minimum geographical footprint is estimated to $5-8$ MW/km^2 for modern WTs. While the previously published studies have shown the conceptual capability of a WPP to actively damp selected oscillatory modes, these studies consider a single aggregated WPP model [1–6] or a simplified WPP layout with only few WTs represented [7], and have, thus, not considered the distributed and modular nature of the WPP.

The performance of a WPP POD is dependent on that each WT modulates its output such that it contributes to a common WPP response. Clearly, if independent PODs are employed for each WT this consideration can be ignored, however, at the cost of having to tune each WT POD individually under due consideration of potential control interactions between the WT PODs. If instead a park level POD is considered, the modularity of a WPP means that the configuration within the unit cannot be considered constant, since individual WTs or even radials can be switched out of service while the rest remain in operation. To ensure that a WPP POD indeed contributes with positive damping, the POD should be insensitive to the internal state of the WPP.

In the presented study, the capabilities of full converter WTs to actively damp power oscillations are assessed through a case study where a large generic WPP is connected to a benchmark model [10] prone to power system oscillations. The WPP is represented with all its WTs as well as with the full layout of the collector grid to include the distributed and modular characteristics of the WPP. The residues for both active and reactive power modulation are computed for the individual WTs and used for assessing the feasibility of a park level POD using either active or reactive power modulation. The modal analyses are complemented with time domain simulations on the nonlinear system.

After designing and showing the impact on the modal damping of a ΔP and a ΔQ POD on the full WPP representation, the WPP is aggregated into simpler equivalents and the modal damping is reevaluated. These findings will, furthermore, give indications of whether a WPP can be represented by an aggregate WT model when used for studies on its damping capabilities and the performance of a proposed POD.

The paper is organized as follows. A brief background on residues and their interpretation are given in section 2. The study case is presented in section 3, the residue analysis in section 4.1, and the time domain analysis in section 4.2. In section 5, the impact of the WPP modelling complexity on the resulting modal damping is evaluated. Finally, the discussion and the conclusion are given in section 6 and 7, respectively.

2 Background

Power system oscillations are inherent to large power systems based on synchronous generators [11]. The nature of power system oscillations and analysis by means of eigenvalue analysis are well described in the literature, e.g. [8,12,13].

2.1 Induced Damping

With full converter WTs, the rotational mechanical system is, at least partially, decoupled from the grid dynamics by the full load converter. The asynchronous grid connection of variable speed WTs does that these units do not themselves cause power system oscillations [14]. In [15] it is for a range of operating conditions presented that the participation of a full converter WT in power oscillations is very low. However, although a full converter WT does not have a mass which is synchronously connected to the grid, there is still a path through the network for the WT to affect the operation of the synchronous generators. Thus, the WT can affect the characteristics of oscillatory modes by inducing an electromagnetic torque onto the synchronous machines in the system, and this torque can be decomposed into a damping and a synchronizing torque component.

A framework for assessing the damping torques induced on synchronous machines from non-synchronous units is proposed in [16, 17] and demonstrated in [7, 18] for wind power applications.

The indirect interaction with the power oscillations means that the location of the POD, the selection of input and output signals, and the operating condition for the power system have a large impact on the efficiency of the damping control. This has been treated by Ruan *et al.* for a converter interfaced power station [19] and by Wang for a FACTS stabilizer [20].

2.2 Transfer Function Residue for Controller Tuning

The concept of modal residue is often used for studies on POD siting and signal selection, since it allows for evaluation of the effectiveness of the control [13]. The residue, R, for the hth eigenvalue for the transfer function between a given input,

u, and a given output, y, is the sensitivity of this eigenvalue to a scalar feedback control [8], and is computed as the product between the modal observability and modal controllability. Hence, to give a positive contribution to the damping of a critical mode, the phase shift between POD input and POD output should be the complement to the residue angle for that input output pair. This is schematically illustrated in Figure 1, where H_{yu} is the POD transfer function.

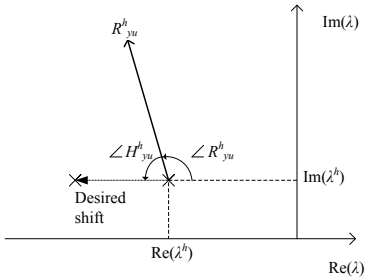

Figure 1: Schematic illustration of residue as measure for eigenvalue sensitivity.

If a park level POD is considered, this means that the difference in residue angle between the individual WTs should be small enough to be neglected. For the POD to be robust against the internal state of the WPP, a low sensitivity is required for the residue angle towards the internal configuration and operating condition of the WPP.

3 Case Study

The study is based on a power system model that was originally developed by Gibbard and Vowles [10] to provide a benchmark system for analyzing power system oscillations. A single-line diagram of the network is depicted in Figure 2 from which the 5 system areas appear. In area 2 a 540 MW WPP is connected to bus 212 as indicated in Figure 2, where the WPP is represented by 150 3.6 MW WTs.

The study is conducted with PSS®NETOMAC and its module for frequency domain analysis, NEVA [21].

For this study all the generators are equipped with standard IEEE STAB1 PSSs, which have been tuned to obtain weakly damped oscillations between the areas. The synchronous generators within the 14 power stations indicated in Figure 2 are for this study represented as individual machines, totalling 62 synchronous generators.

The generator dispatch and the distribution of the load are adopted from the "heavy load" scenario in [10], where the additional power in-feed to area 2 from the WPP is compensated by the synchronous generators in the same area to maintain the inter-area power flow as described in this scenario. The total demand in the system accounts to 22 300 MW while the total generation is 23 030 MW.

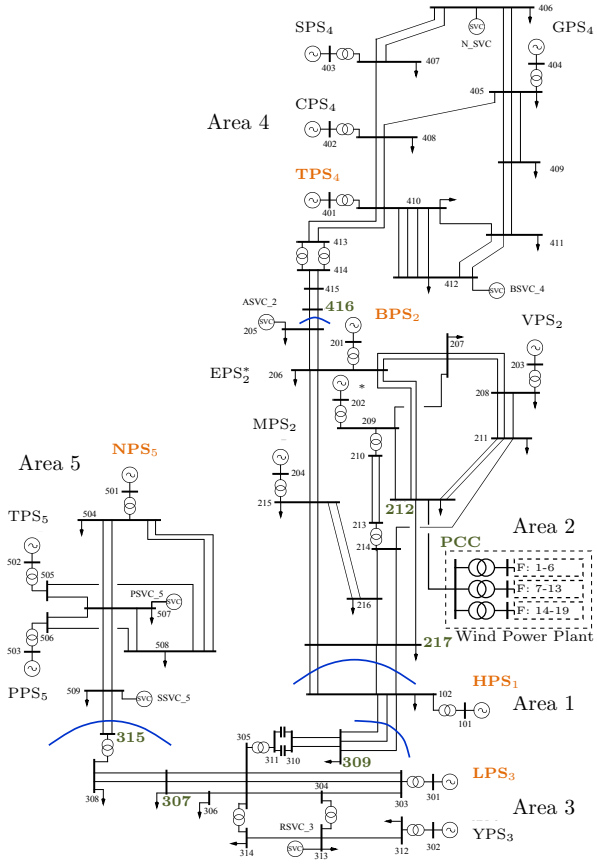

Figure 2: Single-line diagram of the studied power system [10]. The referenced busses are given with green font, the power stations shown in time domain plots with orange font, and the separations between the areas are shown with blue lines.

3.1 Layout of Wind Power Plant

The WPP is connected to the 330 kV system in area 2 through an export line defined as a 100 km long overhead line. The WPP consists of three substations (in the following abbreviated by "sub"), each connected through identical park transformers and with a number of feeders connected to the low voltage side of the transformer. The parameters for the transmission line and the park transformers are given in Table 1 and Table 2, respectively.

The WPP consists of 19 feeders with a varying number of connected WTs

Table 1: Parameters for line between PCC and area 2.

Type: overhead line, 330 kV		
r	x	c
[Ω/km]	[Ω/km]	[μF/km]
0.037	0.367	0.014

Table 2: Parameters for the park transformers.

U_r	U_k	S
[%]	[%]	[MVA]
0.30	12.5	200

and a varying distance from the first WT to the main PCC substation. For all the feeders, the distance between the WTs is defined to 1 km. The distribution of the WTs on the feeders and the distance to the first WT are presented in Table 3, while the single-line diagram of the WPP is shown in Figure 3.

Table 3: Configuration of the WTs within the WPP in terms of number of WTs per feeder, # WTs, and the distance from the PCC to the first WT, l_1.

Feeder	# WTs	l_l	Feeder	# WTs	l_l
	[-]	[km]		[-]	[km]
1	8	15	11	9	1
2	9	10	12	7	11
3	9	9	13	8	15
4	8	5	14	9	15
5	9	13	15	7	17
6	8	13	16	9	17
7	5	2	17	7	20
8	6	16	18	8	4
9	9	16	19	9	9
10	6	10			

The collector grid is modelled as a 33 kV cable network to which the individual WTs are connected through a step-up WT transformer. The requirements for current carrying capability at a particular point of a feeder depend on the number of WTs connected downstream to this point. To reflect this characteristic, three cable sizes are considered for all the feeders, the 120 mm^2 cable is used for the five last WTs on a feeder, 300 mm^2 cables are used the next three WTs, and 400 mm^2 cables are used for the remaining part of the 33 kV grid. The cable parameters are given in Table 4.

3.2 WPP Operating Scenarios

The WPP for the presented study consists of 150 WTs, which are spread over a large geographical area. Four cases are considered and listed in Table 5 that capture some of the characteristics of a WPP.

In all cases the dispatch of the synchronous generators is adjusted for nominal power output of the WPP as described in section 3. Case 1 is considered the

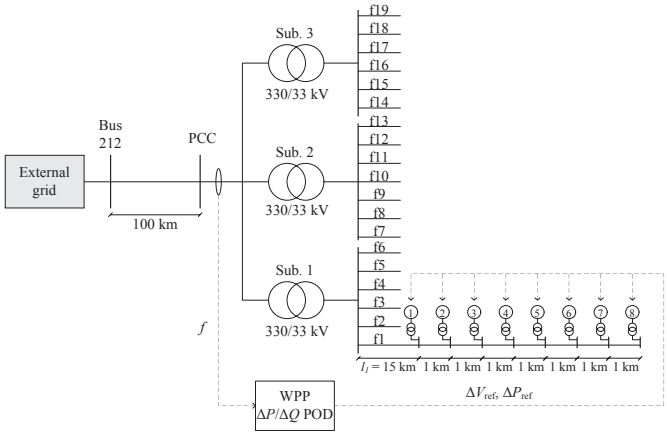

Figure 3: Single-line diagram of the WPP where also the WPP level ΔP and ΔQ PODs are shown.

Table 4: Parameters for collector grid cables.
Type: N2YSY cable, 33 kV

A [mm^2]	r [Ω/km]	x [Ω/km]	c [μF/km]	$I_{\max}$ [A]
120	0.153	0.129	0.190	380
300	0.060	0.133	0.250	590
400	0.047	0.110	0.280	1000

Table 5: List of studied scenarios with the WPP being in different internal states.

Case 1	All WTs operating at nominal active power output
Case 2	All WTs operating at 0.6 pu active power output
Case 3	WPP is operating with only sub 1 and 2 in service with all WTs producing nominal active power
Case 4	Different active power output for the subs, i.e. nominal power output in sub 1, 0.8 pu power output in sub 2, and 0.7 pu power output in sub 3

base case, i.e. the planned operating condition for the power system, while case 2-4 are deviations from the plan caused by non-uniform wind conditions and equipment failure.

3.3 Wind Turbine Model

The WT concept for this study is a variable-speed, pitch controlled, full converter interfaced WT. The WT is represented with a reduced order model suitable for transient and dynamic power system studies. The model represents a

3.6 MW Siemens Wind Power WT and the dynamic fault-ride-through (FRT) response of the model has been validated from field tests [22]. The model includes a variable wind speed aerodynamic model, a two-mass model of rotor, gearbox, and generator, machine and grid side converter, DC-link, and a generic reduced order control scheme. The model is described further in [15].

3.4 Modal Characteristics

An overview of the modal characteristics in terms of the system eigenvalues is provided in Figure 4. The section of the complex plane that is shown in Figure 4 focuses on eigenvalues that describe rotor angle oscillations between the synchronous generators in the system. The modal analysis shows that there is a number of weakly damped inter- and intra-area oscillations in the system, and that there exists a number of inter-machine oscillations between the synchronous generators within each power station. The two inter-area and the two intra-area eigenvalues with the lowest damping ratios are highlighted Figure 4 and these are described further in Table 6.

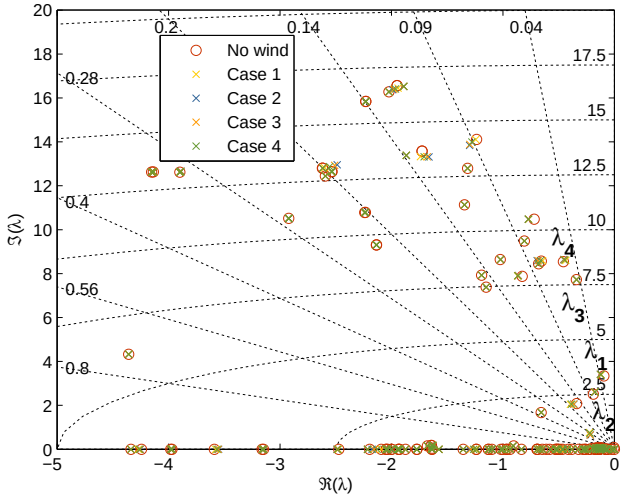

Figure 4: Complex plane with the system eigenvalues. The grid shows lines of constant damping ratio and natural frequency.

Table 6: Dominant system eigenvalues.

#	f [Hz]	ζ [-]	Dominant areas
λ_1	0.54	0.037	All areas
λ_2	0.41	0.067	All areas
λ_3	1.23	0.044	Mainly area 3
λ_4	1.38	0.052	Mainly area 1, 2

4 WPP Damping Contribution

4.1 Frequency Domain Analysis

The possibility of utilizing a common WPP POD to enhance the damping of the system is analyzed with aid of residues at the individual WT terminals. As discussed in section 2.2, the difference in residue angle between the individual WTs is an important indicator to whether a WPP level POD is possible, while the sensitivity to the internal WPP state of operation is assessed by comparing the residues across the WPP operating scenarios that are defined in section 3.2.

For this part of the study, the WTs are represented as constant PQ sources to which a controllable ΔP or ΔQ component can be added. The residues are evaluated for the transfer function from the bus frequency, here represented by the change in voltage angle, to the controllable component of active or reactive power modulation. For the residue analysis only λ_1 and λ_4 are considered due to the severeness of λ_1 and the large participation of area 2 in λ_4.

4.1.1 Active Power Modulation

The magnitude and angle for the active power modulation residues are for the individual WTs in the WPP presented for λ_1 and λ_4 in Figure 5 and 6, respectively. The feeders are indicated with vertical dashed lines and the feeder number, while the three subs are shown with solid vertical lines.

From the residue magnitudes it is noted that the efficiency of the damping modulation decreases as the distance to the PCC increases. The residue magnitude reduces gradually from the first to the last WT in a feeder and the distance from the first WT to the PCC determines the offset for the first WT. The shape of the curve is similar for the investigated cases, while the offset is case dependent.

The residue angles in Figure 5 and 6 show the same dependency to the location of the WT within the WPP as did the residue magnitude, although the shape of the residue angle curves appear more even on the plots. The residue angle varies for each case less than 0.5 degrees between the WTs. Between the cases the maximum difference is less than 3 degrees.

4.1.2 Reactive Power Modulation

For reactive power modulation, the residue magnitudes and angles are given in Figure 7 and 8 for λ_1 and λ_4, respectively.

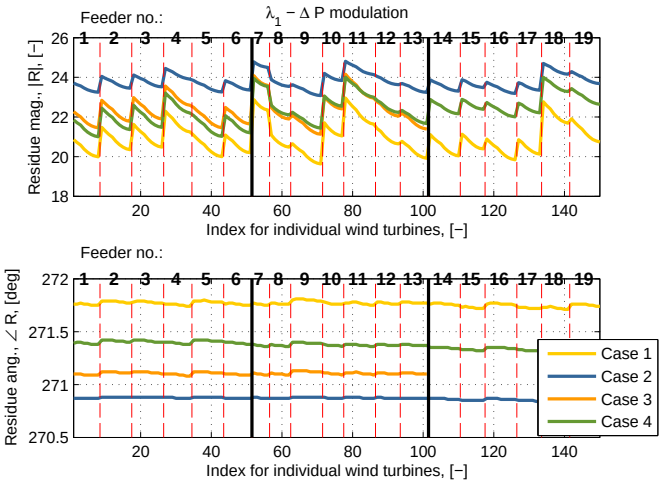

Figure 5: Residue magnitudes and angles for WT active power modulation for λ_1.

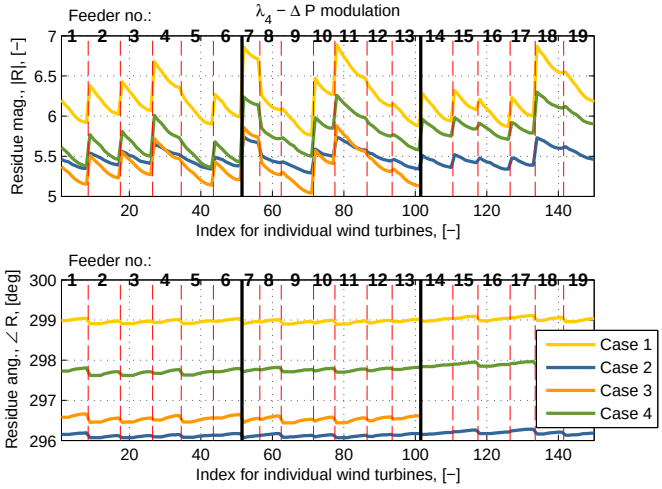

Figure 6: Residue magnitudes and angles for WT active power modulation for λ_4.

The overall characteristics of the residues in Figure 7 and 8 are similar to those described for active power modulation in section 4.1.1. However, a larger

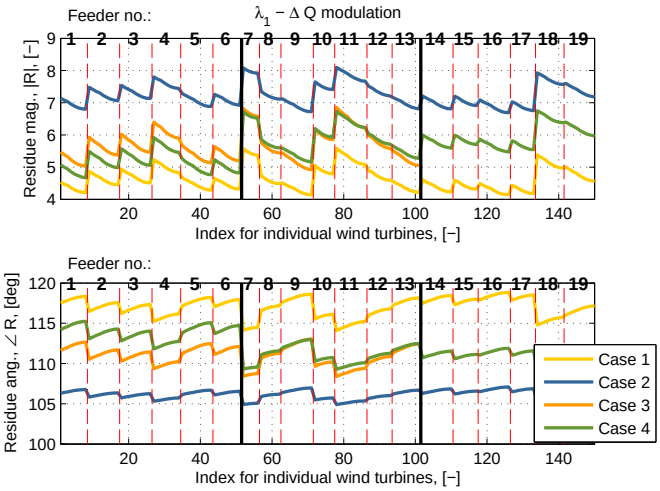

Figure 7: Residue magnitudes and angles for WT reactive power modulation for λ_1.

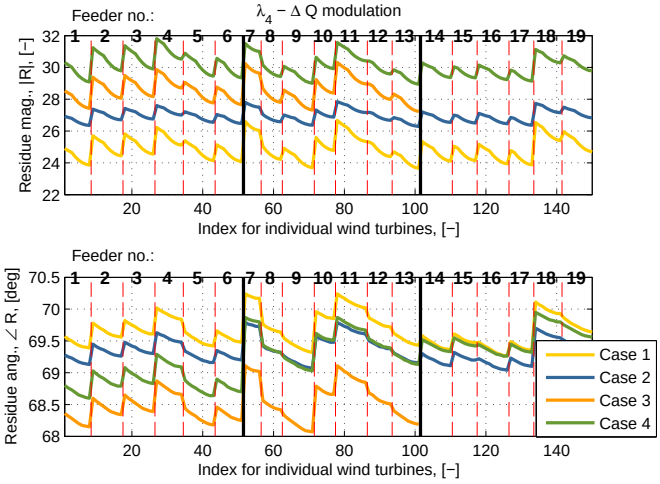

Figure 8: Residue magnitudes and angles for WT reactive power modulation for λ_4.

sensitivity is here found to both the location of the WT within the WPP as well as the operating condition of the WPP. This is especially notable in the inter-

area mode, λ_1, in Figure 7 where differences in the residue angles between the WTs of more than 6 degrees are found. For the investigated cases, a maximum span of almost 14 degrees is observed.

4.2 Time Domain Analysis

The WTs are for the time domain simulations represented with the dynamic model described in section 3.3. The case 1 scenario is used and the oscillations are excited by a 50 ms three phase short circuit at bus 307 in area 3. The short circuit is distant from the WPP and the disturbance does not activate a fault-ride-through response of the WTs.

The WPP is equipped with either a ΔP or a ΔQ POD that from a local measurement computes a stabilizing signal that is dispatched to the WTs. The ΔP POD operates directly on the active power reference to the WTs, while the ΔQ POD regulates the WT voltage reference to create a reactive power modulation. A transmission delay of 50 ms is considered between the WPP controller and the WTs to account for processing time at both WPP and WT level as well as the actual transmission time from the WPP to the WTs. The PODs are driven by the PCC frequency, which is here synthesized by the time derivative of the PCC voltage angle using $\frac{s}{s\,0.03+1}$. For both the ΔP and the ΔQ POD loops, the transfer function is defined as

$$G_{\mathrm{POD}}(s) = K\,\frac{s\,T_{wo}}{s\,T_{wo}+1}\,\frac{1}{s\,T_{lp}+1}\,G_{pc}(s) \tag{1}$$

where K is the gain, T_{wo} is the wash-out filter time constant, T_{lp} the low-pass filter time constant, and where $G_{pc}(s)$ is the transfer function for the phase compensation. For the ΔP and the ΔQ POD, the phase compensation is computed from, respectively, Figure 5 and 7 as a compromise between the requirements for phase compensation for the individual WTs. As seen from Figure 3, both PODs use the local frequency measurement at the PCC as input and the ΔP POD outputs a perturbation to the active power reference, ΔP_{ref}, while the ΔQ POD outputs a perturbation to the voltage reference, ΔV_{ref}.

Time domain simulations are presented in Figure 9 for eight selected WTs. The WTs are the first and the last WT in feeder 1, 11, and 17, which are characterized by the distance of the first WT to the PCC, l_1, and the number of connected WTs, N_{WT}.

1. short distance: $l_1 = 1$ km, $N_{\mathrm{WT}} = 9$, WT_{80-88},
2. medium distance: $l_1 = 15$ km, $N_{\mathrm{WT}} = 8$, WT_{1-8}, and
3. long distance: $l_1 = 20$ km, $N_{\mathrm{WT}} = 7$, $\mathrm{WT}_{127-133}$.

With the ΔP POD in operation, an almost identical response is given by the individual WTs and also the shape of the active power oscillation measured at the PCC is very close to the output of the WTs. For the reactive power modulation the output from the WTs has more variation in terms of both magnitude and phase. The magnitude differences are caused by the different terminal conditions of the WTs, which means that an unequal amount of reactive power

is necessary to follow the received voltage reference. A closer comparison of the phase of the reactive power modulations in Figure 9, reveals that the WTs nearer to the PCC are leading those further away and that the maximum phase difference is around 15 degrees. The combined WPP response at the PCC is seen to lie in between the extremes, which shows the averaging effect over all the WTs. It is noted that the measurement at the PCC still has a good resemblance with the responses of the WTs.

The response in the second swing of WT_{80} to the ΔQ POD command in Figure 9 is seen to be different from the other WTs. The explanation is that WT_{80} here goes into PQ saturation and therefore cannot track the received voltage reference. This element of a ΔQ POD is discussed in more detail in [23].

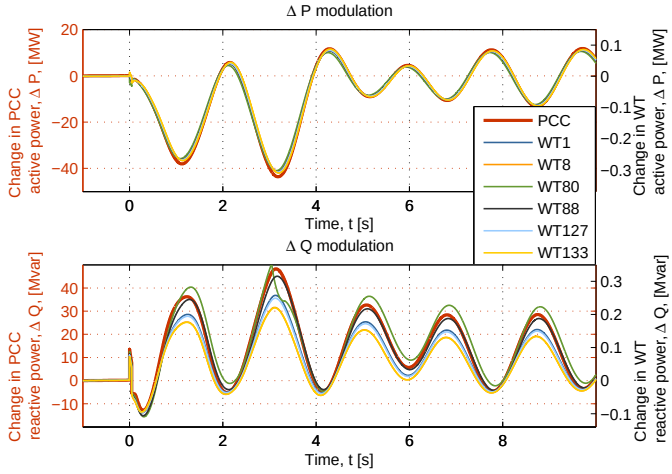

Figure 9: Comparison of selected WT power outputs with the corresponding WPP power output at the PCC.

The impact of the analyzed PODs in terms of additional damping is shown in Figure 10, where the speed of a dominant generator in each area is shown for *1)* no WPP POD, *2)* WPP ΔP POD, and *3)* WPP ΔQ POD. It is noted that both PODs increase the damping of the oscillations and that very similar improvements are achieved in the damping performance with a similar control effort.

5 Impact of WPP Model Complexity on Damping Contribution

For power system stability studies it is clearly relevant to evaluate the impact of model simplifications to assess the necessary model complexity for a given study. In section 4 the optimal POD phase shifts were evaluated for the WTs

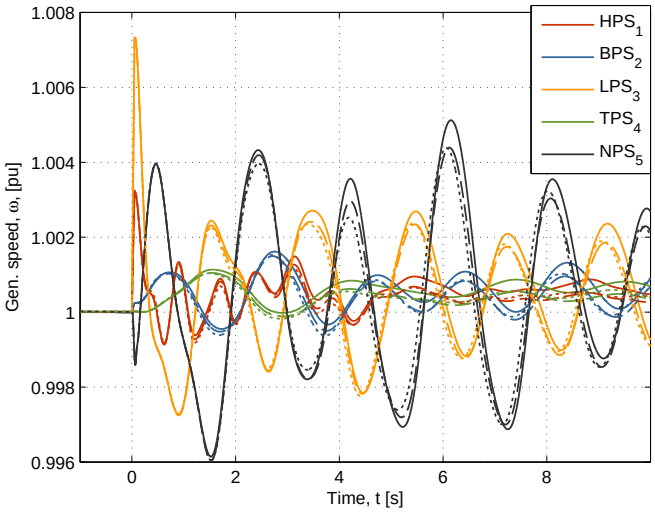

Figure 10: Speed of selected generators. Solid: no WPP POD, dashed: WPP ΔP POD, dotted: WPP ΔQ POD.

individually within the WPP. That study was based on a detailed representation of the WPP that included all the WTs. Such model complexity is justified for design studies and for very detailed analysis on the WPP itself, but for system studies a degree of model simplification would be desirable.

5.1 Aggregation Method

The WPP is simplified in terms of aggregation of the WTs using the method proposed by the National Renewable Energy Laboratory (NREL) in [24] and validated with simulation cases of single and multiple WT representations of a WPP in [25]. Four levels of complexity are here considered:

1. full model as described in section 3.1 where all WTs are represented individually, i.e. $N_{\mathrm{WT}} = 150$,
2. feeder aggregate model where the WPP is simplified to one aggregate WT per feeder, i.e. $N_{\mathrm{WT}} = 19$,
3. sub aggregate model where the WPP is simplified to one WT per park transformer, i.e. $N_{\mathrm{WT}} = 3$, and
4. single aggregate model where the WPP is represented by a single upscaled WT model, i.e. $N_{\mathrm{WT}} = 1$.

5.2 Estimation of Controllability Factor

The ability of a WPP POD to affect a power system oscillation may be evaluated using the controllability factor computed for the POD output for the eigenvalue that describe this particular oscillation. In [26] a "long distance transfer function", $H_{ld}(j\omega)$, is introduced and it is shown that relative variations of the frequency response of $H_{ld}(j\omega)$ evaluated at the resonance frequencies contain the same information as the relative variations of the controllability factors computed from modal analysis. The long distance transfer function is defined as

$$H_{ld}(j\omega) = \frac{\Delta P(j\omega)}{\Delta U(j\omega)} \tag{2}$$

where $\Delta P(j\omega)$ is the active power variations for a line with high mode observability and where $\Delta U(j\omega)$ is the controlled output of the unit where the modulated bus shunt susceptance, $\Delta B(j\omega)$, was used in [26]. Here, $\Delta U(j\omega)$ represents the output of the ΔP and the ΔQ POD, which are the control signals to the WTs for, respectively, active and reactive power modulation. For the presented study, the long distance transfer function in (2) is evaluated directly on the nonlinear time domain model by measuring the frequency response to an applied Fourier series perturbation on the POD output and it is used to compare the WPP modelling approaches in terms of impact on the grid. The Fourier perturbation is designed with

$$u_{\text{in}}(t) = A \sum_{n=2}^{40} \sin(n \cdot \Delta f \cdot 2\pi \cdot t) \tag{3}$$

where $A = 0.001$ is the signal amplitude and where $\Delta f = 0.05$ Hz is the frequency step.

The calculations are here based on the case 1 scenario from Table 5 where all the WTs are connected and deliver rated power output, cf. Table 5.

5.3 Results for Aggregated WPP Representations

The long distance transfer function for a ΔQ POD and the active power transfer at one inter-tie of bus 309 between area 1 and 3 is shown in Figure 11 while the same transfer function for a ΔP POD is shown in Figure 12. The frequency response is evaluated for all analyzed levels of aggregation and it is noted that very similar responses are obtained for both reactive and for active power modulation. Minor deviations are seen for $N_{\text{WT}} = 1$ when compared to the other levels of aggregation.

The controllability factors for the dominant modes in Table 6 have been estimated from the long distance transfer function between POD output and the active power flow on one inter-tie of bus 309. The controllability factors are compared in Figure 13 for the different levels of WPP aggregation and it is noted that the estimates are very similar in both magnitude and phase. The active power at bus 309 was used since all four dominant modes can be observed at this location, although the observability of the intra-area modes, $\lambda_{3,4}$, is

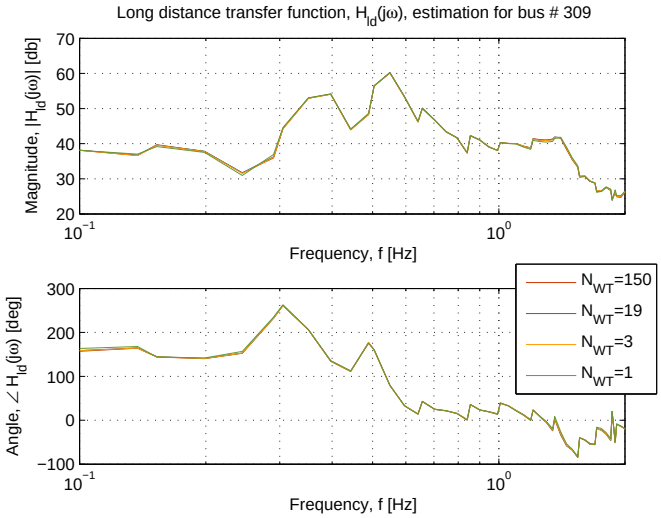

Figure 11: Long distance transfer function for a ΔQ POD and the active power measured at one inter-tie of bus 309.

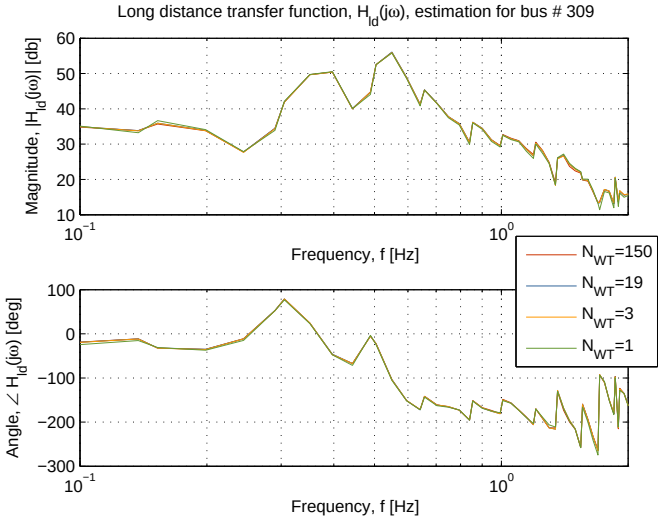

Figure 12: Long distance transfer function for a ΔP POD and the active power measured at one inter-tie of bus 309.

not as prominent as that of the inter-area modes, $\lambda_{1,2}$. The controllability factors were also estimated from the active power flow at an inter-tie at bus 217, 315, and 416. Different absolute magnitudes of $H_{ld}(j\omega_{1-4})$ were found for the investigated busses, however, the same agreement between the different WPP complexity levels was found for each bus. The differences in the absolute magnitude when $H_{ld}(j\omega)$ are based on active power measurements at different busses in the system, are to be understood since the gain of $H_{ld}(j\omega)$ describes the magnitude of the relative change of active power at the frequency $j\omega$ when subject to a perturbation of the active or reactive power output of the WPP, which would be different at different locations in the network.

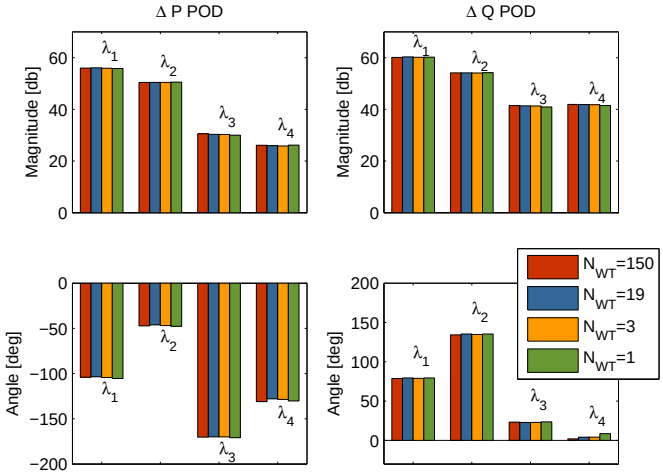

Figure 13: Controllability factors evaluated from the long distance transfer function to active power variation at one inter-tie of bus 309 for both a ΔP POD (left side plots) and a ΔQ POD (right side plots).

The resulting contribution to the power oscillation damping is evaluated with the same disturbance that was applied in section 4.2, i.e. a distant 50 ms three phase short circuit at bus 307. The generator speed of a dominant generator in each area is plotted in Figure 14 for each level of WPP aggregation for the ΔQ POD. It is seen that very comparable damping characteristics are found independently of the modelling complexity of the WPP. The change in active power flow between the five areas is shown in Figure 15 where it is seen that the inter-area dynamics are retained when the WPP is simplified into larger aggregated equivalents. A minor offset is noted in Figure 15 for $N_{\mathrm{WT}} = 1$ for the power flow across bus 416, whereas the responses for bus 217, 309, and 315 are almost overlapping. Similar responses for both the generator speed and active power flow are obtained with the ΔP POD, although these are not shown here.

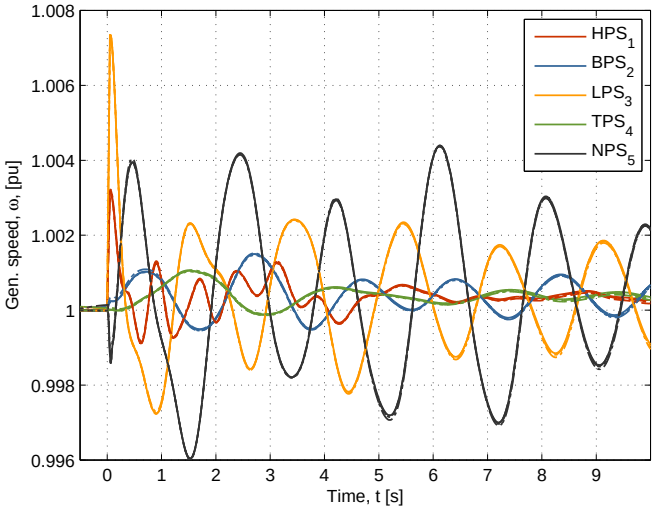

Figure 14: Speed of selected generators. Solid: $N_{\mathrm{WT}} = 150$, dashed: $N_{\mathrm{WT}} = 19$, dotted: $N_{\mathrm{WT}} = 3$, and dash-dotted: $N_{\mathrm{WT}} = 1$. The WPP is equipped with a ΔQ POD. Note that the curves for $N_{\mathrm{WT}} = 150$, $N_{\mathrm{WT}} = 19$, $N_{\mathrm{WT}} = 3$, and $N_{\mathrm{WT}} = 1$ are almost overlapping.

6 Discussion

For the calculated residues for the wind turbines (WT), only minor angle differences were noted, i.e. < 6 degrees, and the results thus indicate that a park level power oscillation damping controller (POD) would be feasible. An active power POD (ΔP POD) was less sensitive to the location of the WT than a reactive power POD (ΔQ POD). This could be regarded to make the ΔP POD the favorable option when compared to the ΔQ POD. It should, however, be considered that the ΔP POD would also have the most extensive impact on the WTs, since the active power modulation would impact the forces that act on the mechanical structures to a much higher degree than the ΔQ POD with its reactive power modulation. If the observed angular differences are converted into a time uncertainty it would for a 0.50 Hz oscillation correspond to less than 33 ms, which should be compared to the time delay of 50 ms that was used in the study to represent processing and transmission time.

For the investigated wind power plant (WPP) operating scenarios, only smaller changes in residue angle were observed for a ΔP POD. For reactive power modulation, changes in residue angles of up to 14 degrees were observed. In the presented study only changing operating conditions within the WPP were considered, while the same operating scenario was used for load and for the dispatch of the synchronous generators. This study does therefore not as such deal with the robustness of a WPP POD towards different power system operating

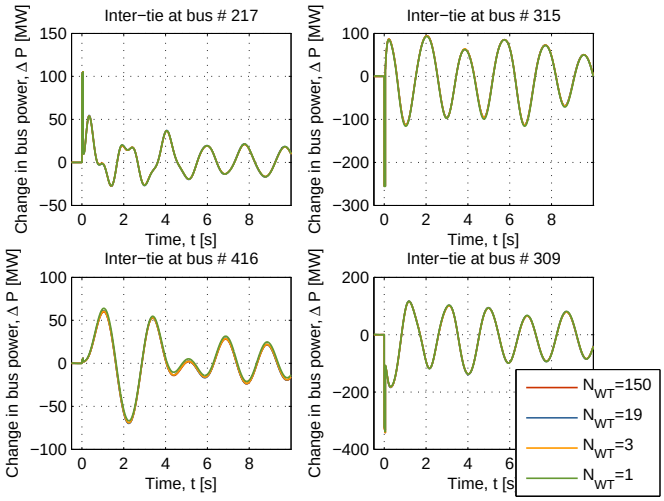

Figure 15: Change in active power between areas measured at a single inter-tie of the respective busses. The WPP is equipped with a ΔQ POD.

conditions. This is, however, a topic with some very important practical implications, since it is a requirement that a POD contributes with positive damping torque over the entire range of critical operating conditions. Robust control and optimization methods have in the literature been proposed to enhance robustness towards changing operating conditions, control interactions, and time delay uncertainties, e.g. [27–29].

The time domain simulations support the findings from the residue analysis that a park level POD seems feasible. For both active and reactive power modulation, the resulting power modulation at the PCC has close resemblance with the output of the WTs. Although more variation was found for reactive power modulation than for active power modulation, cf. Figure 9. For the presented scenario, the ΔP and the ΔQ POD had similar impact on the damping with a similar control effort. In this study the significance of the contribution to the power oscillation damping has not been treated in detail, since such conclusions are highly dependent on the state of the power system. The modal controllability is, furthermore, as shown and discussed in [19], very dependent on the in-feed location and whether active or reactive power is used for the damping control. Different levels of contribution are therefore expected for different in-feed locations and different choices of input signal; and other configurations than the one used would show a different contribution to the modal damping. A number of studies have dealt with this optimization task for damping studies with FACTS devices as e.g. [30–32]. However, such optimization is considered out of the scope of this study.

The ability to aggregate WPPs into simpler equivalents is very important with respect to practical power system studies. To evaluate the controllabil-

ity of the WPP on dominant power system oscillations and the impact of the WPP modelling complexity on this, the long distance transfer function [26] was computed for four different levels of modelling complexity. The WPP was aggregated to simpler equivalents with $N_{\mathrm{WT}} = 19$, $N_{\mathrm{WT}} = 3$, and $N_{\mathrm{WT}} = 1$, which were compared to the detailed WPP model with $N_{\mathrm{WT}} = 150$. The estimated controllability factors showed no dependency to the level of aggregation of the WTs and were very similar in both magnitude and phase as shown in Figure 13. These results were, furthermore, verified with time domain simulations in Figure 14 and 15 where the same contribution to the modal damping was observed for all analyzed levels of WPP aggregation. The results show that a WPP can be represented in power oscillation damping studies using only a fraction of the actual number of WTs in the WPP. The WPP could be aggregated to $N_{\mathrm{WT}} = 3$ without giving notably different results, while minor deviations were noted in the response when only a single upscaled WT model was used.

7 Conclusion

The capabilities of large wind power plants (WPP) to contribute to the modal damping was investigated with a 150 wind turbine (WT) WPP. A park level power oscillation damping controller (POD) was considered, where the optimal phase of an active power POD (ΔP POD) and a reactive power POD (ΔQ POD) was computed for each WT within the WPP using residue analysis. Different internal WPP configurations were considered to reflect that a WPP consists of a large number of independent units that are not necessarily in the same operating condition. The ΔP POD showed less phase variation between the individual WTs and also between the investigated internal WPP configurations than did the ΔQ POD. Both for active and reactive power modulation, the differences in the residue angles were small enough to encourage the potential use of a WPP level POD. Next, both a ΔP and a ΔQ POD were implemented and the ability of the WPP to contribute to the modal damping was demonstrated.

To investigate the impact of WPP model simplifications on the previously found contribution to the modal damping, the detailed WPP was aggregated into equivalents containing 19, 3, and 1 WT model(s). The controllability factors were computed for the dominant eigenvalues for the different levels of aggregation and very similar results were found. The similarity in the responses were verified with time domain simulations. The results show that the contribution to the modal damping of a WPP POD can be studied with good accuracy while only representing a fraction of the WTs in the WPP model.

Future work includes field tests on an actual WPP to verify the results, large signal studies to assess the interaction between the WT FRT response and the WPP ΔQ and ΔP PODs, to assess the impact from short term overload capability of the converter, and the development of methods to coordinate the WPP ΔQ POD response with static and dynamic equipment for reactive power compensation in the WPP substation.

References

[1] Elkington K.: 'Modelling and control of doubly fed induction generators in power systems: Towards understanding the impact of large wind parks on power system stability'. PhD Thesis, KTH, Electric Power Systems, SE-100 44, Stockholm, Sweden, 2009, ISBN: 978-91-7415-264-7, Available from: `http://urn.kb.se/resolve?urn=urn:nbn:se:kth:diva-10206`

[2] Fan L., Yin H., Miao Z.: 'On Active/Reactive Power Modulation of DFIG-Based Wind Generation for Interarea Oscillation Damping', IEEE Trans. Energy Conversion, 2011, 26, (2), pp. 513 – 521

[3] Gautam D., Vittal V., Ayyanar R., Harbour T.: 'Supplementary control for damping power oscillations due to increased penetration of doubly fed induction generators in large power systems'. In: 2011 IEEE/PES Power Systems Conference and Exposition (PSCE 2011). Department of Electrical Engineering Arizona State University Tempe, AZ 85287, 2011, p. 1 – 6, ISBN: 9781612847870

[4] Hughes F.M., Anaya-Lara O., Jenkins N., Strbac G.: 'A power system stabilizer for DFIG-based wind generation', IEEE Trans. Power Syst., 2006, 21, (2), pp. 763–772

[5] Tsourakis G., Nomikos B.M., Vournas C.D.: 'Contribution of Doubly Fed Wind Generators to Oscillation Damping', IEEE Trans. Energy Conversion, 2009, 24, (3), pp. 783 –791

[6] Fernandez R.D., Mantz R.J., Battaiotto P.E.: 'Contribution of wind farms to the network stability'. In: Power Engineering Society General Meeting, 2006, IEEE, 2006

[7] Knüppel T., Nielsen J.N., Jensen K.H., Dixon A., Østergaard J.: 'Power Oscillation Damping Controller for Wind Power Plant Utilizing Wind Turbine Inertia as Energy Storage'. In: 2011 IEEE PES General Meeting, Detroit, MI, USA, IEEE Power & Energy Society, 2011, pp. 1–8, ISBN: 978-1-4577-1001-8

[8] Rogers G.: 'Power System Oscillations' (Power Electronics and Power Systems, Kluwer Academic Publishers, 1st ed., 2000), ISBN-10: 0792377125

[9] Denholm P., Hand M., Jackson M., Ong S.: 'Land-Use Requirements of Modern Wind Power Plants in the United States', U.S. Department of Commerce, 5285 Port Royal Road Springfield, VA 22161, National Renewable Energy Laboratory, 2009, NREL/TP-6A2-45834

[10] Gibbard M., Vowles D.: 'Simplified 14-generator model of the SE Australian power system', School of Electrical & Electronic Engineering, The University of Adelaide, South Australia, 2008, 2, Available from: `http://www.eleceng.adelaide.edu.au/Groups/PCON/PowerSystems/IEEE/BenchmarkData/index.html`

[11] Klein M., Rogers G.J., Kundur P., 'A fundamental study of inter-area oscillations in power systems', IEEE Trans. Power Syst., 1991, 6, (3), pp. 914–921

[12] Kundur P.S.: 'Power System Stability and Control' (The EPRI Power System Engineering Series, McGraw-Hill, Inc., 1994), ISBN: 0-07-035958-X

[13] Zhang X.P., Rehtanz C., Pal B.: 'Modeling of Power Systems for Small Signal Stability Analysis with FACTS', in 'Flexible AC Transmission Systems: Modelling and Control' (Power Systems, Springer Publishing Company, Incorporated; 2006), pp. 319–346, Available from: `http://dx.doi.org/10.1007/3-540-30607-2_12`

[14] Vowles D.J., Samarasinghe C., Gibbard M.J., Ancell G.: 'Effect of wind generation on small-signal stability - A New Zealand Example'. In: Power and Energy Society General Meeting - Conversion and Delivery of Electrical Energy in the 21st Century, IEEE, 2008, pp. 1–8

[15] Knüppel T., Nielsen J.N., Jensen K.H., Dixon A., Østergaard J.: 'Small-Signal Stability of Wind Power System With Full-Load Converter Interfaced Wind Turbines', IET Renewable Power Generation, 2012, 6, (2), pp. 79–91

[16] Gibbard M.J., Vowles D.J., Pourbeik P.: 'Interactions between, and effectiveness of, power system stabilizers and FACTS device stabilizers in multimachine systems', IEEE Trans. Power Syst., 2000, 15, (2), pp. 748–755

[17] Pourbeik P., Gibbard M.J.: 'Damping and synchronizing torques induced on generators by FACTS stabilizers in multimachine power systems', IEEE Trans. Power Systems, 1996, 11, (4), pp. 1920–1925

[18] Knüppel T., Nielsen J.N., Jensen K.H., Dixon A., Østergaard J.: 'Induced Torques on Synchronous Generators from Operation of Wind Power Plant based on Full-Load Converter Interfaced Wind Turbines'. In: Aranda FA, editor. Scientific Proceedings of the European Wind Energy Conference & Exhibition. The European Wind Energy Association, 2011, pp. 68–71

[19] Ruan S.Y., Li G.J., Ooi B.T., Sun Y.Z.: 'Power system damping from real and reactive power modulations of voltage-source-converter station', IET Generation Transmission & Distribution, 2008, 2, (3), pp. 311–320

[20] Wang H.F.: 'Selection of robust installing locations and feedback signals of FACTS-based stabilizers in multi-machine power systems', IEEE Trans. Power Syst., 1999, 14, (2), pp. 569 –574

[21] Lei X., Lerch E., Povh, D., Ruhle, O.: 'A large integrated power system software package – NETOMAC'. In: Proc. Int. Conf. of Power System Technology, Aug. 1998, vol.1, pp. 17 – 22

[22] Nielsen J.N., Akhmatov V., Thisted J., Grøndahl E., Egedal P., Frydensbjerg M.N., Jensen, K.H.: 'Modelling and fault-ride-trough tests of Siemens Wind Power 3.6 MW variable-speed wind turbines', Wind Engineering, 2007, 31, (12), pp. 441–452

[23] Knüppel T., Kumar S., Thuring P., Støttrup M., Friman J.: 'Towards a Reactive Power Oscillation Damping Controller for Wind Power Plant Based on Full Converter Wind Turbines'. In: 2012 IEEE PES General Meeting, San Diego, CA, USA, IEEE Power & Energy Society, 2012, pp. 1–8

[24] Muljadi E., Pasupulati S., Ellis A., Kosterov D.: 'Method of equivalencing for a large wind power plant with multiple turbine representation'. In: IEEE Power Engineering Society General Meeting, 2008, pp. 1–9

[25] Brochu J., Larose C., Gagnon R.: 'Validation of Single- and Multiple-Machine Equivalents for Modeling Wind Power Plants', IEEE Trans. Energy Conversion, 2011, 26, (2), pp. 532–541

[26] Elenius S., Uhlen K., Lakervi E.: 'Effects of controlled shunt and series compensation on damping in the Nordel system', IEEE Trans. Power Syst., 2005, 20, (4), pp. 1946 – 1957

[27] Ramos R.A., Alberto L.F.C., Bretas N.G.: 'A new methodology for the coordinated design of robust decentralized power system damping controllers', IEEE Trans. Power Syst., 2004, 19, (1), pp. 444 – 454

[28] Messina A.R., Begovich O., López J.H., Reyes E.N.: 'Design of multiple FACTS controllers for damping inter-area oscillations: a decentralised control approach', International Journal of Electrical Power & Energy Systems, 2004, 26, (1), pp. 19 – 29

[29] Chaudhuri N.R., Ray S., Majumder R., Chaudhuri B.: 'A New Approach to Continuous Latency Compensation With Adaptive Phasor Power Oscillation Damping Controller (POD)', IEEE Trans. Power Syst., 2010, 25, (2), pp. 939 –946

[30] Ray S., Chaudhuri B., Majumder R.: 'Appropriate signal selection for damping multi-modal oscillations using low order controllers'. In: Power and Energy Society General Meeting - Conversion and Delivery of Electrical Energy in the 21st Century, IEEE, 2008, pp. 1 –7

[31] Mithulananthan N., Canizares C.A., Reeve J., Rogers G.J.: 'Comparison of PSS, SVC, and STATCOM controllers for damping power system oscillations', IEEE Trans. Power Syst., 2003, 18, (2), pp. 786 – 792

[32] Larsen E.V., Sanchez-Gasca J.J., Chow J.H.: 'Concepts for design of FACTS controllers to damp power swings', IEEE Trans. Power Syst., 1995, 10, (2), pp. 948–956

A.6 Paper VI

Thyge Knüppel, Sathees Kumar, Patrik Thuring, Michael Støttrup, and Johan Friman. Towards a reactive power oscillation damping controller for wind power plant based on full converter wind turbines. In *2012 IEEE PES General Meeting* (accepted for panel presentation in the session: "Advanced Power Controls in Wind Parks"), pages 1 – 8, San Diego, CA, USA, July 2012. IEEE Power & Energy Society.

Towards a Reactive Power Oscillation Damping Controller for Wind Power Plant Based on Full Converter Wind Turbines

Thyge Knüppel, Sathees Kumar, Patrik Thuring, Michael Støttrup, Johan Friman

***Abstract*—In this paper a power oscillation damping controller (POD) based on modulation of reactive power (ΔQ POD) is analyzed where the modular and distributed characteristics of the wind power plant (WPP) are considered. For a ΔQ POD it is essential that the phase of the modulated output is tightly controlled to achieve a positive damping contribution. It is investigated how a park level voltage, reactive power, and power factor control at different grid strengths interact with the ΔQ POD in terms of a resulting phase shift. A WPP is modular and distributed and a WPP ΔQ POD necessitate that each WT contributes to a collective response. This ability is shown with a 150 wind turbine (WT) WPP with all WTs represented, and it is demonstrated that the WPP contributes to the inter-area damping. The work is based on a nonlinear, dynamic model of the 3.6 MW Siemens Wind Power WT.**

***Index Terms*—wind turbines, wind power plant, wind power plant controller, power oscillation damping controller (POD), power systems, small-signal stability**

I. Introduction

With increased penetration of wind turbines (WT) and wind power plants (WPP) it is important to understand how these units interact with and affect phenomena associated with power system stability. Regarding power system oscillations, several studies have investigated the impact of wind power on power system oscillations [1]–[4].

The controllable active and reactive power output of a WPP based on converter interfaced WTs means that by proper control, the WPP output can be modulated to increase the system damping to power oscillations. It has been suggested in a number of recent publications to equip WTs with a power oscillation damping controller (POD) for either active power modulation (ΔP POD) [5]–[9], reactive power modulation (ΔQ POD) [8], [10], [11], or a combination of both [12]. The impact of reduced inertia is studied in [13] and it is found that a control proportional to frequency deviation had a positive damping contribution. In [8], the torsional drive train mode is analyzed for a doubly fed induction generator (DFIG) for both ΔP and ΔQ POD and it is found that the ΔP POD can destabilize this mode, while this mode seemed immune to the ΔQ POD. The presence of WT mechanical resonance frequencies within the typical range for power system oscillations may limit the frequency range in which a particular WT can participate with ΔP modulation, since the feasibility of a ΔP POD requires that it can be operated without exciting oscillations at mechanical resonance frequencies.

In [14] the modular and distributed characteristics of a WPP were included and the results indicate that a central WPP POD is possible for both active and reactive power modulation.

It is well-known that power oscillation damping may be increased from proper reactive power modulation of FACTS devices [15] and this ability is in practice utilized by transmission system operators [16]. It is, however, also recognized that FACTS devices are generally less robust against changes in the operating condition than synchronous machine power system stabilizers (PSS) [15]. Therefore, optimal siting for FACTS units and optimal choice of control signals are tasks that have been widely treated in the literature as e.g. [17]–[20]. Robust control and optimization methods have also been proposed to enhance the robustness towards changing operating conditions, control interactions, time delay uncertainties, e.g. [21]–[23]. A comprehensive review of robust control applications for power system studies is presented in [24]. In [25], [26] a combination of a discontinuous bang-bang control and a low gain continuous controller are proposed to avoid interactions with other stabilizing controllers. For a WPP ΔQ POD many of the considerations for FACTS devices would also apply, although the siting may already be decided by other factors such as wind resources and access to the transmission grid.

Although it has previously been shown that a WPP equipped with a ΔQ POD can contribute positively to the damping of power system oscillations, many aspects of a ΔQ POD still remain to be understood. The published studies have dealt with very simplified WPP models using an aggregate WT model, which do not consider that the WTs within a feeder do not necessarily have the same reactive capacity available for reactive power modulation. Large WPPs are routinely equipped with park level voltage, reactive power, or power factor controllers that coordinate the response of the WTs to regulate at a specific bus, and the interaction between these park level controllers and the ΔQ POD remains to be analyzed.

First in section II, factors influencing the resulting phase shift of a ΔQ POD in a WPP are investigated. Secondly in section III, a WPP including a ΔQ POD is simulated where all the WTs are represented individually to assess the capability of the WTs to execute the commanded reactive power modulation. Finally, the discussion and the conclusion are found in section IV and V, respectively.

T. Knüppel is with Siemens Wind Power A/S, DK-7330 Brande, Denmark and Centre for Electric Technology, Department of Electrical Engineering, Technical University of Denmark, DK-2800 Lyngby, Denmark (thyge.knuppel@siemens.com)

S. Kumar, P. Thuring, M. Støttrup, and J. Friman are with with Siemens Wind Power A/S, DK-7330 Brande, Denmark

II. Phase Control of ΔQ POD

The damping of a selected eigenvalue is improved by modulation of the WPP reactive power output where the modulated output power has a certain phase shift with respect to the input signal that contains the oscillation. To have a positive damping contribution it is, thus, necessary to tightly control the phase of the oscillating reactive power. The ability of the WPP to track this phase depends among other things on *1)* the interaction between the ΔQ POD and WPP level voltage, reactive power, and power factor controls, *2)* the speed of WPP and WT responses, and *3)* the strength of the grid. To evaluate the need for phase compensation for a typical WPP, the phase shift induced from the WT voltage control and from the WPP voltage, reactive power, and power factor controls are considered in section II-C and II-D, respectively.

A. Wind Power Plant Model

An aggregate WPP model is used for this part of the study, since the scope is the interaction between the grid and the WPP. A single-line diagram of the system is shown in Fig. 1 where an equivalent collector grid connects the upscaled WT to the park transformer, and where the external grid is modeled as a voltage source and an impedance with a given short-circuit ratio (SCR).

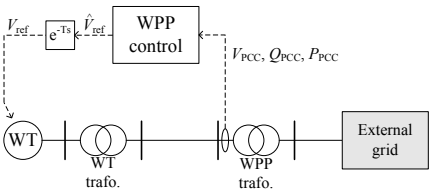

Fig. 1. Single-line diagram of the single machine infinite bus system used for the analysis in section II

The WPP is equipped with a park level controller for voltage, reactive power, or power factor control, which at the point of common connection (PCC) measures the voltage, V_{PCC}, the reactive power flow, Q_{PCC}, and the active power flow, P_{PCC}. In Fig. 1 the PCC is placed on the low voltage side of the WPP transformer but could also have been placed elsewhere, as e.g. the high voltage side of the transformer. For this study a continuous time park level controller is used and issues related to the speed of the controller have, thus, not been considered. However, for a digital controller with a certain sample rate, it is important to evaluate the frequencies at which a meaningful control can be designed.

A transmission delay of 50 ms is considered between the WPP controller and the WTs to account for processing time at both WPP and WT level as well as the actual transmission time from the WPP to the WTs.

B. Wind Turbine Model

The WPP is represented by a single upscaled WT model that is operated in voltage control mode. The WT concept for this study is a variable-speed, pitch controlled, full converter interfaced WT. The WT is represented with a reduced order model suitable for transient and dynamic power system studies. The model represents a 3.6 MW Siemens Wind Power WT [27]. The model includes a variable wind speed aerodynamic model, a two-mass model of rotor, gearbox, and generator, machine and grid side converter, DC-link, and a generic reduced order control scheme.

C. Phase Shift by Grid Strength

The voltage control of the WT tracks the desired terminal voltage reference by control of the reactive current output. Intuitively, the strength of the grid at the PCC determines the amount of required reactive current to track the voltage reference, where a higher current is needed for the same change in terminal voltage for the stronger grid. For ΔQ POD operation, where the WT voltage controller receives an oscillating reference, the inability of the voltage controller to track the reference results in the terminal voltage that is lagging the reference.

To illustrate this, consider the circuit diagram in Fig. 2, which is a simplified representation of the setup in Fig. 1 with the ΔQ POD being the only WPP control in service. For simplicity only the top level WT voltage control, $C(s)$, is shown.

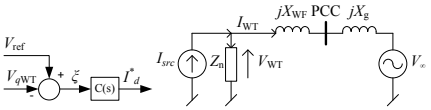

Fig. 2. Simplified circuit of the WPP with only the reactive WT control considered.

The ability of the voltage controller, $C(s)$, to track the voltage reference, V_{ref}, is analyzed by means of the transfer function between the voltage reference, V_{ref}, and infinite bus voltage, V_∞, to the terminal voltage, V_{WT}, which is shown in (1). The transfer function is given by the network equations and the block diagram in Fig. 2. If the q axis of the dq coordinate system is aligned with V_{WT}, the transfer function may be derived as

$$V_{q\text{WT}} = T_1(s)V_{\text{ref}} + T_2(s)V_{q\infty} \tag{1}$$

$$= \frac{C(s)}{\frac{1}{X_{\text{WF}}+X_g} + \frac{X_n}{|Z_n|^2} + C(s)}V_{\text{ref}} + \frac{1}{(X_{\text{WF}}+X_g)\left(C(s)+\frac{X_n}{|Z_n|^2}\right)+1}V_{q\infty}. \tag{2}$$

Ideally $T_1(s) = 1$ in (1) which would imply perfect tracking of V_{ref} for all frequencies, and from the derived expression in (2) it is, thus, possible to investigate factors that influence the tracking ability of the WT voltage control. For a common WPP installation $X_g \gg X_{\text{WF}}$ and from (2) it is clear that as the SCR increases, i.e. X_g decreases, the ability to track the reference reduces.

In Fig. 3 the expression in (2) is compared with a detailed model of the system in Fig. 1 for a sweep of network SCRs.

From the comparison it is seen that the simple representation in (2) captures the dominant dynamics of the system, although the results are seen to be more conservative than the detailed model. For frequencies above 1 Hz the phase response for the simple representation starts to deviate from the phase response of the detailed model.

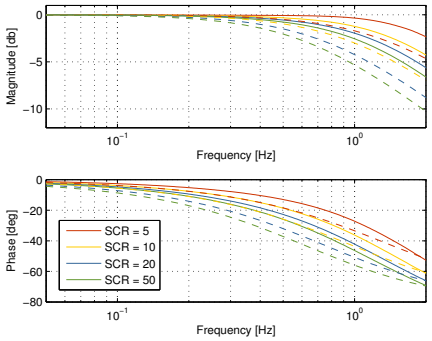

Fig. 3. Dependency of phase shift induced by WT voltage controller to the strength of the grid. Solid lines: detailed model, dashed lines: simplified model.

D. Phase Shift by Park Level Voltage, Reactive Power, and Power Factor Control

The objective of a WPP voltage, reactive power, and power factor control is to coordinate the response of the individual WTs to achieve a certain condition at a remote bus, i.e. typically at the PCC, as schematically illustrated in Fig. 1. For a ΔQ POD this adds an additional feedback path from the modulated reactive power output at the WT, through the collector grid, the WPP voltage, reactive power, or power factor control, and an updated voltage reference signal. Evidently, this feedback has the potential of changing the phase of the modulated reactive power output if the bandwidth of the controllers overlap. The speed of the WPP voltage control is determined by the grid code requirements where the UK grid code requires that 90 % of the pre-disturbed value is delivered within 1 second [28]. Such response time is clearly within the range of the low frequency power system oscillations.

As an example, the block diagram of a WPP voltage control is shown in Fig. 4 where also two input candidates for the ΔQ POD reference signal are shown. For the WPP voltage controller, input 1, V_{POD1}, corresponds to a tracking problem whereas input 2, V_{POD2}, corresponds to a disturbance that should be rejected. The general structure in Fig. 4 is also used for the WPP reactive power control and the power factor control where the error calculation, ξ, in each case have been appropriately modified.

The transfer function between the ΔQ POD output and the voltage reference received at the WT, $\frac{V_{\text{ref}}(s)}{V_{\text{POD}}(s)}$, is in Fig. 5 and 6 evaluated for, respectively, V_{POD1} and V_{POD2} as input. Frequency responses are shown for both WPP voltage control, reactive power control, and power factor control, and the responses have been evaluated for a sweep of SCRs. The

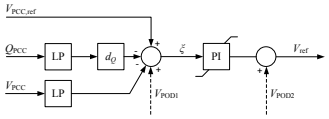

Fig. 4. Block diagram of WPP voltage droop controller with two possible input connections for the ΔQ POD.

frequency responses are only shown for a single parameter set for each controller, but it is clear that the tuning of the controllers will impact the resulting frequency responses. In both Fig. 5 and 6 the frequency responses for reactive power and power factor control overlap and it is not possible to distinguish between the curves for these controllers. The frequency response for the voltage control is fundamentally different from that of the reactive power and power factor control. For frequencies below 1 Hz, reactive power control and power factor control show a response that varies for different SCRs, whereas much less variation is noted using voltage control. For higher frequencies, i.e. $>$ 1 Hz, the transmission delay dominates the phase response with an increasing phase lag.

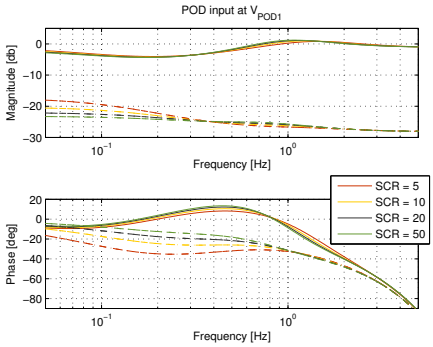

Fig. 5. Induced phase shift in WT voltage reference signal by WPP voltage or reactive power control for an input at V_{POD1}. Solid: voltage control, dashed: reactive power control, dash dotted: power factor control. Note that the curves for reactive power and power factor control overlap.

For the tracking control in Fig. 5 it is seen that the phase response for the voltage control has a variation of $\pm 15^{\text{o}}$ around 0^{o}. The reactive and the power factor control has for SCRs ≥ 10 a constant and increasing phase lag for increasing frequencies of oscillation. The large difference in magnitude is due to the different units used internally in the controllers.

A similar response is found for all three WPP controllers when the V_{POD2} input is used, cf. Fig. 6. For low frequencies the WPP control is sufficiently fast to cancel much of the ΔQ POD response with a resulting large phase shift and a low gain.

III. Case Study With Detailed WPP

Successful operation of the WPP ΔQ POD requires that the WTs within the unit are capable of executing the commanded reactive power modulation and that the WTs respond to give

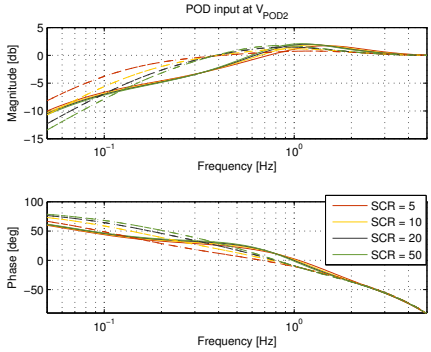

Fig. 6. Induced phase shift in WT voltage reference signal by WPP voltage or reactive power control for an input at V_{POD2}. Solid: voltage control, dashed: reactive power control, dash dotted: power factor control. Note that the curves for reactive power and power factor control overlap.

a collective WPP response. The distributed nature of a WPP means that the control of one WT interacts with the control of the other WTs and it is important to evaluate how this interaction affects the collective WPP response. Additionally, the distributed nature means that the WTs might be in different steady state operating points.

Clearly, an analysis as indicated above requires the use of a detailed WPP model with the WTs represented individually. The study is performed with PSS®NETOMAC [29].

A. Network Model

This part of the study is based on the benchmark power system developed by Gibbard and Vowles [30] to have a system with a complex oscillatory pattern. The synchronous generators within the 14 power stations are here represented individually and all generators are equipped with standard IEEE STAB1 PSSs that have been tuned for weakly damped oscillations between the five areas. The single-line diagram is given in Fig. 7.

In area 2 a 540 MW WPP is connected at bus 212 through a 100 km transmission line. A short-circuit analysis showed a SCR $\simeq$ 10 at bus 212. The load and the generator dispatch are given by the "heavy load" scenario in [30] with a total demand of 22 300 MW and a combined generation of 23 030 MW. The production from the WPP is compensated locally in area 2 to maintain the power flow between the areas as described in this scenario.

B. Wind Power Plant Model

The WPP consists of 150 3.6 MW WTs that are represented individually and distributed over 19 feeders, three park transformers, and where the PCC is defined as the high voltage side of the park transformers. The interconnection to the network is shown in Fig. 7 and the single-line diagram of the WPP layout in Fig. 8. A more detailed description of the WPP model with cable and transformer parameters are given in [14].

Each WT is represented by the model described in section II-B and a WPP voltage controller as shown in Fig. 4 is

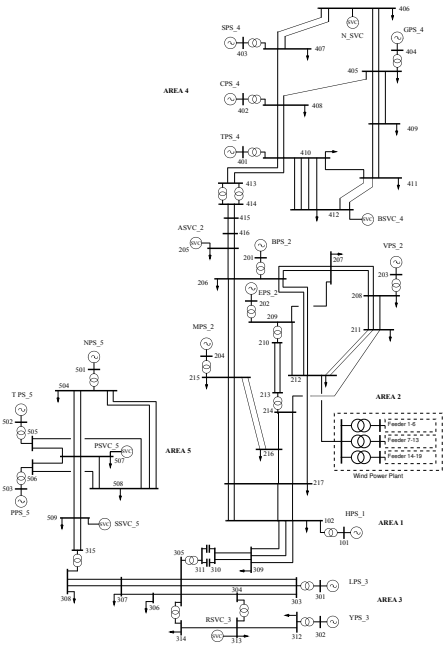

Fig. 7. Single-line diagram of the studied power system [30]

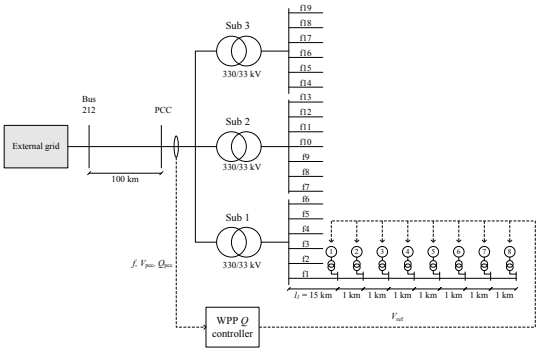

Fig. 8. Single-line diagram of the WPP layout used in the analysis.

connected to the unit, to which a ΔQ POD is interfaced at input V_{POD1}. In Fig. 8, the block "WPP Q controller" includes both WPP voltage control, WPP ΔQ POD, and a transmission and processing delay as discussed in section II-A. The ΔQ POD loop is defined as

$$G_{\text{POD}}(s) = K \frac{s\,T_{wo}}{s\,T_{wo}+1} \frac{1}{s\,T_{lp}+1} G_{pc}(s) \qquad (3)$$

where K is the gain, T_{wo} is the wash-out filter time constant, T_{lp} the low-pass filter time constant, and where $G_{pc}(s)$ is the transfer function for the phase compensation. The ΔQ POD is driven by the PCC frequency, which is here synthesized by the

time derivative of the PCC voltage angle using $\frac{s}{s\,0.03+1}$, and the output is limited to $\Delta V_{\text{POD}} = 0.05$ pu and the transmitted voltage reference is here limited to $V_{\text{ref}} = 1.08$ pu.

C. Simulation Results

A distant 50 ms three-phase short-circuit at bus 307 is used to excite oscillations between the five system areas. A base case is, furthermore, simulated where the ΔQ POD is disabled. The transfer function for the phase compensation, $G_{pc}(s)$, is designed with classical residue analysis and is designed for a PCC voltage of 0.99 pu, which corresponds to nominal terminal voltage of the WTs, i.e. 1.00 pu.

1) WPP Characteristics: The modal characteristics of the analyzed system in terms of the frequency, f, and the damping ratio, ζ, of the dominant oscillations are shown in TABLE I and plotted in Fig. 9. The frequencies and damping ratios in TABLE I have been computed with Prony analysis of the speed of G_1 at the NPS_5 power station in area 5. The oscillations described by λ_{1-2} are global with all the areas participating, whereas λ_3 is contained mainly within area 3 and λ_4 mainly has participation from area 1 and 2. From TABLE I and Fig. 9 it is seen that the damping ratios for $\lambda_{1,2,4}$ increase with the ΔQ POD in operation, whereas the damping ratio for λ_3 is unchanged.

TABLE I
MODAL CHARACTERISTICS OF THE DOMINANT OSCILLATIONS, λ_{1-4}, COMPUTED WITH PRONY ANALYSIS. THE INDEX OF f AND ζ REFERS TO THE FOUR SELECTED EIGENVALUES.

	no POD	ΔQ POD
f_1 [Hz]	0.524	0.527
ζ_1 [-]	0.019	0.022
f_2 [Hz]	0.346	0.347
ζ_2 [-]	0.063	0.102
f_3 [Hz]	1.056	1.065
ζ_3 [-]	0.013	0.013
f_4 [Hz]	1.561	1.571
ζ_4 [-]	0.021	0.023

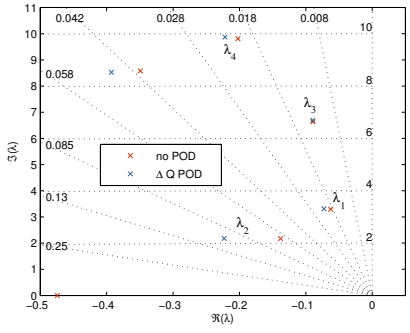

Fig. 9. Complex plane with eigenvalues extracted by Prony analysis of the speed response of G_1 at the NPS_5 power station.

The control action of the ΔQ POD is shown in Fig. 10 together with the synthesized frequency measurement and the resulting voltage reference, which is finally transmitted to the WTs. From the frequency measurement and from the speed of a dominant generator in each area, shown in Fig. 11, an increased mode damping is noted when the ΔQ POD is in operation.

When no POD is in operation only minor oscillations are noted in V_{ref}, which stem from the response of the WPP voltage controller to the voltage oscillations induced by the applied disturbance.

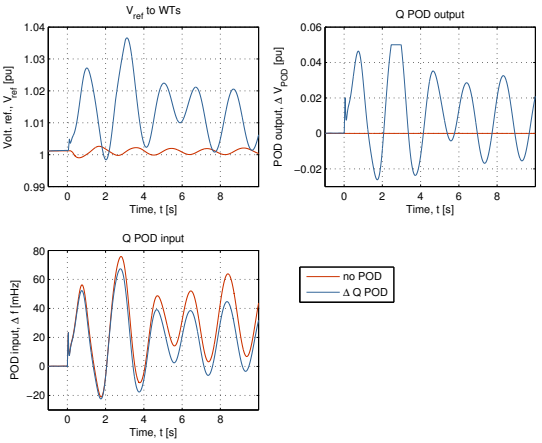

Fig. 10. Input and output signals of the WPP control during a distant tree-phase short-circuit.

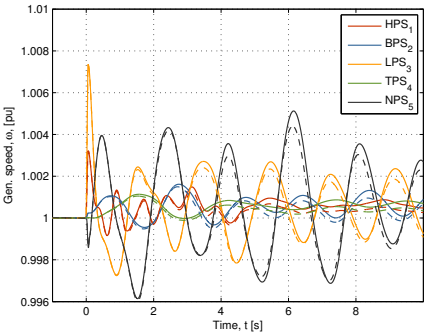

Fig. 11. Impact of ΔQ POD operation during a distant three-phase short-circuit on the speed of selected synchronous generators. The results are shown for different PCC steady state voltages. Solid: no WPP POD, dotted: ΔQ POD.

The reactive power transfer and the bus voltage at the PCC are shown in Fig. 12 for the applied disturbance. It is interesting to observe that the PCC voltage oscillates in almost counter phase when comparing the case with and without the ΔQ POD in operation.

2) WT Characteristics: The terminal voltage and the reactive power output are shown for eight WTs in Fig. 13 and 14,

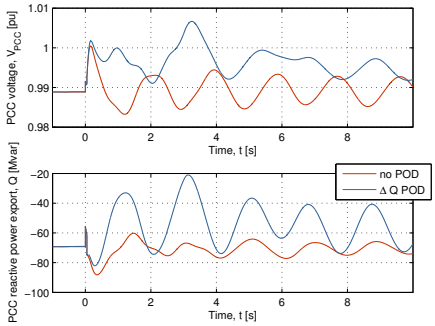

Fig. 12. Impact of ΔQ POD operation during a distant three-phase short-circuit on the PCC voltage and reactive power transfer.

respectively. The WTs are the first and the last WT in three selected feeders, which are characterized by the distance of the first WT to the PCC, l_1, and number of connected WTs, N_{WT}

1) short distance: $l_1 = 1$ km, $N_{\text{WT}} = 9$, WT_{80-88}, and
2) medium distance: $l_1 = 15$ km, $N_{\text{WT}} = 8$, WT_{1-8},
3) long distance: $l_1 = 20$ km, $N_{\text{WT}} = 7$, $\text{WT}_{127-133}$.

From the WT terminal voltages shown in Fig. 13, it is seen that the responses of the individual WTs are very similar in both magnitude and phase. In the presented simulation, the interaction between the WTs within the WPP therefore does not hinder the WTs in tracking the received voltage reference.

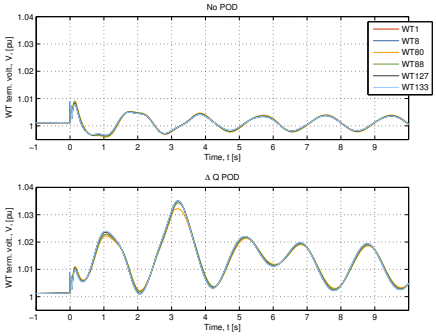

Fig. 13. Selected WT terminal voltage magnitude during a distant three-phase short-circuit with and without the ΔQ POD in operation.

The reactive power output of the selected WTs is shown in Fig. 14 with and without the ΔQ POD in operation. The different steady state starting points for the WTs are clearly noted from Fig. 14 where WT_{80} is exporting reactive power, $\text{WT}_{8,133}$ are importing reactive power, and $\text{WT}_{1,88,127}$ are close to unity power factor. With the ΔQ POD in operation, an increased reactive power modulation is noted at a lagging phase compared to the pure voltage control response. This is as demanded by the ΔQ POD.

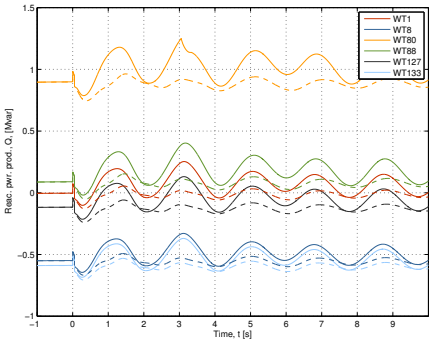

Fig. 14. Selected WT reactive power outputs during a distant three-phase short-circuit with and without the ΔQ POD in operation. Dashed: no ΔQ POD, solid: ΔQ POD.

IV. Discussion

A continuous power oscillation damping controller (POD) induces a damping torque by demanding a scaled and phase shifted response with respect to a measured input signal with good observability of the eigenvalue(s) to be damped. This study has analyzed the potential use of a park level reactive power POD (ΔQ POD) for wind power plants (WPP) with full converter wind turbines (WT).

On both WT and WPP level it is analyzed how existing control structures respond to an oscillating voltage reference to assess the frequency dependency of the resulting phase shift of the oscillation through a WPP.

Today, WPPs are routinely fitted with park level voltage, reactive power, or power factor controllers that coordinate the responses of the WTs to give a combined WPP response. With current requirements for voltage control, the bandwidth of a typical WPP voltage control is within the frequency range of interest for power system oscillations, which means that the interaction between the controllers needs to be considered. The ΔQ POD is analyzed where it is considered as either a reference tracking problem or a disturbance rejection problem as presented in Fig. 5 and 6, respectively. The analysis showed that the reference tracking input had the most steady characteristic in terms of both magnitude and phase and this input was subsequently used when the ΔQ POD was analyzed with time domain simulations.

The short-circuit ratio (SCR) at the point of common connection (PCC) is important with respect to both the stiffness of the voltage and the ability of the WT voltage controller to track a given oscillating voltage reference. A low SCR increases the voltage and reactive power oscillations that the WPP can induce when subject to an oscillating voltage reference and therefore increases the feedback gain through the WPP voltage controller to the ΔQ POD output. For a WPP voltage controller the impact of the SCR is found to be small, whereas a larger impact is found for the analyzed reactive power and power factor controller for frequencies below 1 Hz. A high SCR on the other hand, implies that the terminal voltage of the WT is difficult to change and,

hence, that the WT voltage controller has difficulties tracking the oscillating voltage reference, which results in a phase lag with respect to the reference, cf. Fig. 3.

Based on frequency analysis, a WPP ΔQ POD was designed for a 150 WT WPP with all WTs represented individually. Generally, a ΔQ POD necessitate that sufficient margin is available for the reactive power modulation if a two sided response is requested. The simulations presented in section III-C were performed under this condition, although it is clear that the WTs in a WPP for various reasons may not always be in an operating point where such condition is satisfied. However, many measures do exist to keep the WT terminal voltage close to nominal, e.g. operation of the park transformer tap-changer, components for static or dynamic reactive power compensation, etc. Therefore, the authors consider it a reasonable assumption to perform the study at nominal WT terminal voltage. It is, however, clear that it is necessary to include the ΔQ POD in the operational planning and design of the WPP.

The time domain simulations showed that the WTs were capable of tightly following the received voltage reference to produce a collective WPP response as shown in Fig. 13 and 14. In the analyzed cases, the interaction between the WTs was not found to have any adverse impact on the ability of the WTs to respond to the commanded voltage reference. Prony analysis of the speed of a dominant generator showed that a positive damping contribution was achieved when adding the ΔQ POD to the WPP control. Time traces of generator speeds and results of the Prony analysis are shown in Fig. 12 and TABLE I, respectively.

V. Conclusion

A reactive power, power oscillation damping control (ΔQ POD) requires that tight phase control of the modulated reactive power is possible. For a simple wind power plant (WPP) system, the induced phase shift at both WPP and wind turbine (WT) level was analyzed for frequencies of interest for power system oscillations. It was found that the analyzed elements all contribute to the resulting and not insignificant phase shift through the WPP and that they should be considered when phase compensation filters are designed for a ΔQ POD.

Next, such control was designed for a 150 WT, 540 MW WPP where all WTs were represented individually and the ability of the designed ΔQ POD to contribute to the damping of weakly damped dominant eigenvalues was demonstrated. Time domain simulations with the 150 WT WPP showed that a tight coordination between the WTs was possible such that the WTs contributed to a collective WPP response. The ability to produce a collective WPP response is very important, since a positive damping contribution necessitate a certain phase characteristic of the modulated reactive power as found from e.g. modal analysis. Prony analysis showed an increased damping of the dominant power system oscillations with the WPP ΔQ POD in operation.

References

[1] E. Hagstrom, I. Norheim, and K. Uhlen, "Large-scale wind power integration in norway and impact on damping in the nordic grid," *WIND ENERGY*, vol. 8, no. 3, pp. 375–384, JUL-SEP 2005.

[2] J. Slootweg and W. Kling, "The impact of large scale wind power generation on power system oscillations," *Electric Power Systems Research*, vol. 67, no. 1, pp. 9 – 20, 2003.

[3] T. Knüppel, J. N. Nielsen, K. H. Jensen, A. Dixon, and J. Østergaard, "Small-signal stability of wind power system with full-load converter interfaced wind turbines," *Accepted for publication by IET Renewable Power Generation*, 2011.

[4] G. Tsourakis, B. Nomikos, and C. Vournas, "Effect of wind parks with doubly fed asynchronous generators on small-signal stability," *Electric Power Systems Research*, vol. 79, no. 1, pp. 190 – 200, 2009. [Online]. Available: http://www.sciencedirect.com/science/article/B6V30-4T0FHRM-1/2/3b6ac71f22cac8ff81670dcc6944a0f9

[5] T. Knüppel, J. N. Nielsen, K. H. Jensen, A. Dixon, and J. Østergaard, "Power oscillation damping controller for wind power plant utilizing wind turbine inertia as energy storage," in *2011 IEEE PES General Meeting*. Detroit, MI, USA: IEEE Power & Energy Society, July 2011, pp. 1–8, iSBN: 978-1-4577-1001-8.

[6] K. Elkington, "Modelling and control of doubly fed induction generators in power systems: Towards understanding the impact of large wind parks on power system stability," PhD Thesis, KTH, Electric Power Systems, SE-100 44, Stockholm, Sweden, April 2009, ISBN: 978-91-7415-264-7. [Online]. Available: http://urn.kb.se/resolve?urn=urn:nbn:se:kth:diva-10206

[7] F. Hughes, O. Anaya-Lara, N. Jenkins, and G. Strbac, "A power system stabilizer for dfig-based wind generation," *Power System, IEEE Transactions on*, vol. 21, no. 2, pp. 763–772, 2006.

[8] L. Fan, H. Yin, and Z. Miao, "On active/reactive power modulation of dfig-based wind generation for interarea oscillation damping," *Energy Conversion, IEEE Transactions on*, vol. 26, no. 2, pp. 513 –521, June 2011.

[9] G. Tsourakis, B. Nomikos, and C. Vournas, "Contribution of doubly fed wind generators to oscillation damping," *Energy Conversion, IEEE Transactions on*, vol. 24, no. 3, pp. 783 –791, Sept. 2009.

[10] D. Gautam, V. Vittal, R. Ayyanar, and T. Harbour, "Supplementary control for damping power oscillations due to increased penetration of doubly fed induction generators in large power systems," in *2011 IEEE/PES Power Systems Conference and Exposition (PSCE 2011)*. Department of Electrical Engineering Arizona State University Tempe, AZ 85287, 2011, pp. 1 – 6, ISBN: 9781612847870.

[11] A. Adamczyk, R. Teodorescu, and P. Rodriguez, "Control of full-scale converter based wind power plants for damping of low frequency system oscillations," in *PowerTech, 2011 IEEE Trondheim*, June 2011, pp. 1–7.

[12] R. Fernandez, R. Mantz, and P. Battaiotto, "Contribution of wind farms to the network stability," in *Power Engineering Society General Meeting, 2006. IEEE*, 2006, pp. 1–6.

[13] D. Gautam, L. Goel, R. Ayyanar, V. Vittal, and T. Harbour, "Control strategy to mitigate the impact of reduced inertia due to doubly fed induction generators on large power systems," *Power Systems, IEEE Transactions on*, vol. 26, no. 1, pp. 214 –224, Feb 2011.

[14] T. Knüppel, J. N. Nielsen, K. H. Jensen, A. Dixon, and J. Østergaard, "Power oscillation damping capabilities of wind power plant with full converter wind turbines considering its distributed and modular characteristics," in *Proceedings of IET Renewable Power Generation Conference 2011*, The Institution of Engineering and Technology. Radisson Blu, Edinburgh, UK: IET RPG, September 2011.

[15] G. Rogers, *Power System Oscillations*, 1st ed., ser. Power Electronics and Power Systems. Kluwer Academic Publishers, 2000, ISBN-10: 0792377125.

[16] M. Lahtinen, T. Rauhala, H. Kuisti, J. Peltola, and P. Halonen, "Static var compensator enhancing the operational reliability of finnish transmission network," in *Proceedings of CIGRE Session 2010*, Paris, France, August 2010, paper B4-206.

[17] S. Ray, B. Chaudhuri, and R. Majumder, "Appropriate signal selection for damping multi-modal oscillations using low order controllers," in *Power and Energy Society General Meeting - Conversion and Delivery of Electrical Energy in the 21st Century, 2008 IEEE*, July 2008, pp. 1 –7.

[18] N. Mithulananthan, C. Canizares, J. Reeve, and G. Rogers, "Comparison of pss, svc, and statcom controllers for damping power system oscillations," *Power Systems, IEEE Transactions on*, vol. 18, no. 2, pp. 786 – 792, May 2003.

[19] E. Larsen, J. Sanchez-Gasca, and J. Chow, "Concepts for design of facts controllers to damp power swings," *Power Systems, IEEE Transactions on*, vol. 10, no. 2, pp. 948–956, May 1995.

[20] S. Wang, J. Chow, K. Minto, and R. Rajamani, "Low-order controller design for model matching optimization using coprime factors and lmi,"

in *American Control Conference, 1999. Proceedings of the 1999*, vol. 3, 1999, pp. 1871 –1875 vol.3.

[21] R. Ramos, L. Alberto, and N. Bretas, "A new methodology for the coordinated design of robust decentralized power system damping controllers," *Power Systems, IEEE Transactions on*, vol. 19, no. 1, pp. 444 – 454, Feb. 2004.

[22] A. R. Messina, O. Begovich, J. H. López, and E. N. Reyes, "Design of multiple facts controllers for damping inter-area oscillations: a decentralised control approach," *International Journal of Electrical Power & Energy Systems*, vol. 26, no. 1, pp. 19 – 29, 2004. [Online]. Available: http://www.sciencedirect.com/science/article/B6V2T-49DN6VC-1/2/ab5a3d7c05115434bad4c6a5453df94c

[23] N. R. Chaudhuri, S. Ray, R. Majumder, and B. Chaudhuri, "A new approach to continuous latency compensation with adaptive phasor power oscillation damping controller (pod)," *Power Systems, IEEE Transactions on*, vol. 25, no. 2, pp. 939 –946, May 2010.

[24] L. Fan, "Review of robust feedback control applications in power systems," in *Power Systems Conference and Exposition, 2009. PSCE '09. IEEE/PES*, March 2009, pp. 1–7.

[25] E. Lerch, D. Povh, and L. Xu, "Advanced svc control for damping power system oscillations," *Power Systems, IEEE Transactions on*, vol. 6, no. 2, pp. 524 –535, May 1991.

[26] H. Nguyen-Duc, L.-A. Dessaint, A. F. Okou, and I. Kamwa, "A power oscillation damping control scheme based on bang-bang modulation of facts signals," *Power Systems, IEEE Transactions on*, vol. 25, no. 4, pp. 1918–1927, Nov. 2010.

[27] J. N. Nielsen, V. Akhmatov, J. Thisted, E. Grøndahl, P. Egedal, M. N. Frydensbjerg, and K. H. Jensen, "Modelling and fault-ride-trough tests of Siemens Wind Power 3.6 MW variable-speed wind turbines," *Wind Engineering*, vol. 31, pp. 441–452(12), December 2007.

[28] N. G. plc, "The grid code," National Grid Electricity Transmission plc, National Grid House, Warwick Technology Park, Gallows Hill, Warwick, CV34 6DA, UK, Tech. Rep. Issue 4 Revision 2, March 2010.

[29] X. Lei, E. Lerch, D. Povh, and O. Ruhle, "A large integrated power system software package-netomac," in *Power System Technology, 1998. Proceedings. POWERCON '98. 1998 International Conference on*, vol. 1, Aug. 1998, pp. 17 –22 vol.1.

[30] M. Gibbard and D. Vowles, "Simplified 14-generator model of the SE Australian power system," School of Electrical & Electronic Engineering, The University of Adelaide, South Australia, Tech. Rep. 2, May 2008. [Online]. Available: http://www.eleceng.adelaide.edu.au/Groups/PCON/PowerSystems/IEEE/BenchmarkData/index.html

www.elektro.dtu.dk

Department of Electrical Engineering
Technical University of Denmark
Ørsteds Plads
Building 348
DK-2800 Kgs. Lyngby
Denmark
Tel: (+45) 45 25 38 00
Fax: (+45) 45 93 16 34
Email: info@elektro.dtu.dk

ISBN: 978-87-92465-79-5